UNIVERSITY OF LIVERPOOL

Molecular genetic analysis of the *Drosophila* MRL adapter protein in hyperplastic growth and experimental metastasis

Thesis submitted in accordance with the requirements of the University of Liverpool for the degree of Doctor in Philosophy by

Nada Ali Alqadri

April 2016

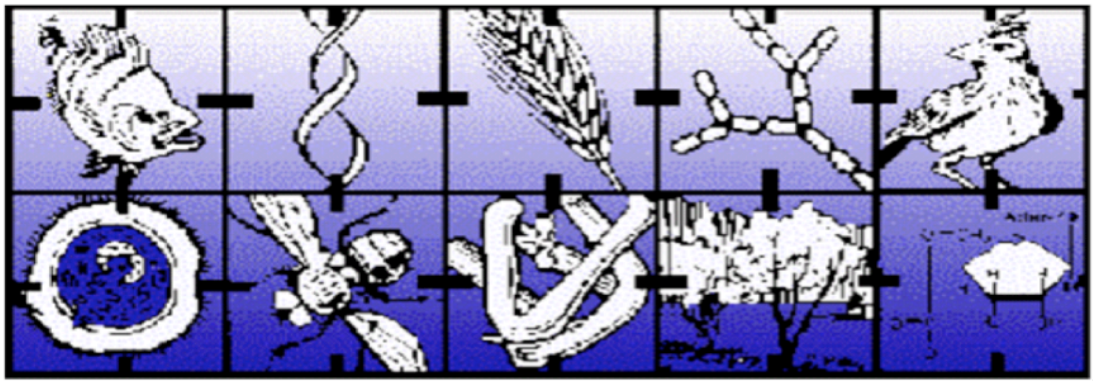

Declaration

This thesis is the result of my own work unless otherwise stated, and is based upon results from experimental and theoretical work performed as a PhD student between March 2012 and April 2016 within the Institute of Integrative Biology at the University of Liverpool.

Neither this thesis nor any part of it has been submitted in support of an application for another degree or qualification at this or any other University or Institute of Learning.

Nada Ali Alqadri

April 2016

Abstract

Members of the Mig-10/RIAM/Lamellipodin (MRL) family of adapter proteins transduce signals derived from growth factor receptors, via interactions with Ras GTPases and/or phospholipids, to changes in the actin cytoskeleton, increased cell motility, and altered cell adhesion properties. MRL proteins have roles in normal development and their overexpression is implicated in tumour development and cancer progression. The focus of this thesis has been to explore signalling upstream and downstream of the *Drosophila* MRL protein, encoded by *pico*, to better understand the effects of manipulating its function. This has been done both in the developing wing, where overexpressed *pico* is capable of driving hyperplastic overgrowth, and in the larval CNS, where *pico* cooperates with oncogenic *Ras* to promote both hyperproliferation and cell invasion. An important downstream consequence of *pico* overexpression is thought to be activation of the Serum Response Factor (SRF), which responds to changes in actin dynamics through the action of its cofactor Mal. An SRF-responsive reporter gene, whose expression recapitulates the distribution of SRF protein in the developing wing, has been used to provide the first *in vivo* evidence that *pico*, and its associated actin regulatory proteins, promote SRF signalling. This work has also helped to identify *deterin*, which encodes *Drosophila* Survivin, as an SRF target that is necessary for *pico*-mediated overgrowth of the wing by suppressing proliferation-associated cell death. SRF is also likely to be a key effector of *pico* in the brain, based on genetic evidence and the observation that cooperation between *pico* and oncogenic Ras is restricted to two populations of Repo-positive glial cells, which are enriched for SRF expression. This work has also explored the involvement of a potential cascade of protein phosphorylation upstream of *pico* using a panel of site-directed mutants in *pico* designed to abolish binding to specific MRL-associated proteins and/or mimic its phosphorylation state. Importantly, these findings are consistent with the known roles of MRL proteins in promoting growth via changes in the actin cytoskeleton, and support the potential involvement of MRL gain-of-function in tumour cell invasion and metastasis.

Table of Contents

Abbreviations

Ab1	Abelson tyrosine kinase
ACS	The American Cancer Society
APS	Adapter protein with PH and SH2 domains
ATP	Adenosine Triphosphate
Arp	Actin-Related Proteins
bp	Base pair
bs	Blisterd
bsk	*Basket*
BPS	Between the PH and SH2
CAN	Canal-associated neurons
cDNA	Complementary DNA
chic	Chickadee
ChIP	Chromatin Immunoprecipitation
CNS	Central Neurolal System
Co-IP	Co-immunoprecipitation
CyO	Curly Oster
da	Daughterless
DGRC	*Drosophila* genomics resource centre
DNA	Deoxyribo Nucleic Acid
ECM	Extracellular matrix
EDTA	Ethylene-diamine-tetraacetic acid
EGF	Epidermal growth factor
EGFR	Epidermal growth factor receptor

eIF	Eukaryotic translation initiation factor
EMS	Ethyl methanesulfonate
ena	Enabled
ey	eyeless
en	Engrailed
Ena	Enabled
ERK	Extracellular signal-regulated kinases
EVH1	Ena/VASP homology 1
FA	Focal Adhesion
F-actin	Actin filaments
FACS	Fluorescence-activated cell sorter
FAK	Focal adhesion kinase
FCS	Fetal Calf Serum
FDG	Fluorodeoxyglucose
Flp	flippase
FRET	FLP recombinase target
G-actin	Actin monomers
GAP	GTPase-Activating Protein
GDP	Guanosine Dephosphate
GEF	Guanine nucleotide exchange factors
GFP	Green Fluorescent Protein
GO	Gene Ontology
Grb	Growth Factor Receptor-Bound
HER2	Human Epidermal Growth Factor Receptor type 2

hh	Hedgehog
HRP	Horseradish Peroxidase
hs	Heat shock promoted
IR	Insulin receptor
IGFR	Type I insulin-like growth factor receptor
JNK	Jun N-terminal Kinase
kDa	KiloDaltons
Lpd	Lamellipodin
MADS	MCM1, Agamous, Deficiens, SRF
MARCM	Mosaic analysis with a repressible cell marker
MAPK	Mitogen-activated protein kinase
MEK	MAP kinase/Erk kinase
Mig-10	Abnormal cell migration protein 10
MMP1	Matrix Metalloproteinases
MRL	Mig-10/RIAM/Lamellipodin
MRTF	Myocardin-Related Transcription Factor
ORF	Open reading frame
PC	Principal Component Analysis
PCR	Polymerase Chain Reaction
PDGF	Platelet-derived growth factor
PDGFR	Platelet-derived growth factor receptor
PDK- 1	Pyruvate dehydrogenase kinase-1
PH	Pleckstin homology
PI	Phosphoinositide

PIC	
PI3K	Phosphoinositide 3-kinase
PKC	Protein Kinase A
PKA	Protein Kinase C
PLC-γ	Phospholipase C-γ
PMSF	Phenylmethane sulfonyl fluoride
PP1	Protein Phosphatase 1
RA	Ras- association
Ras	Rat Sarcoma
Rap	Ras-related proteins
RFP	Red Fluorescent Protein
Rho	GTPase activating protein
RIAM	Rap-1-GTP- Interacting Adapter Molecule
RNA	Ribo Nucleic Acid
RNAi	RNA interference
scrib	*Scribble*
SDS	Sodium Dodecyl Sulfate
SH2	Src Homology 2
S2R+	S2 Receptor +
SRE	Serum response element
SRF	Serum response factor
srGAP3	SLIT-ROBO
TCF	Ternary complex factor
Tft	Tufted

TNF	Tumor necrosis factor
TSS	Transcription start site
UAS	Upstream Activating Sequence
VASP	Vasodilator-Stimulated Phosphoprotein
VNC	Ventral Nerve Cord
WASP	Wiskott-adrich syndrome protein
WHO	The World Health Organization
WT	Wild Type
YAP	Yes-associated protein
YFP	Yellow Fluorescent Protein

Acknowledgments

Though only my name appears on the cover of this thesis, a great many people have contributed to its production. I owe my gratitude to all those people who have made this thesis possible and because of whom my graduate experience has been one that I will cherish forever.

My deepest gratitude is to my supervisor, Dr. Daimark Bennett. I have been amazingly fortunate to have an advisor who gave me the freedom to explore on my own and at the same time the guidance to recover when my steps faltered. Dr. Daimark taught me how to question thoughts and express ideas. His patience and support helped me overcome many critical situations and obstacles to finish this work. He has been always there to listen and give advice. I am deeply grateful to him for the long discussions that helped me sort out the technical details of my work and for carefully reading and commenting on countless revisions of this report. Additionally, for holding me to a high research standard and enforcing strict validations for each research and experimental result.

I am also grateful to the staff at University of Liverpool, for their various forms of support during my study and specifically to the technical staff who maintained all the equipment in my lab so efficiently that I never had to worry about my experiments.

Many friends and colleagues have helped and encouraged me through these difficult years of my studies. Their support and care helped me overcome setbacks and stay

focused on my research. I greatly value their friendship and I deeply appreciate their belief in me.

Most importantly, none of this would have been possible without the love and patience of my family to whom this work is dedicated to, has been a constant source of love, concern, support and strength all these years. I would like to express my heart-felt gratitude to them for their support and encouragement throughout this endeavor.

I would like to extend my profound gratitude with love and give a special mention to:

My beloved husband Mazen Gadri who accompanied me during the years of my stay in UK for his affection, encouragement, caring for me and our four children.

My two well behaved and smart sons Mohammed and Tariq who I am so proud of their dedication and understanding.

My adorable twin daughters who accompanied me since they were three months old, enlightening and delighting our stay in UK.

My mother Fareedah, my father Ali, my brother Dr. Tariq and my sisters Dania, Nouf, Sarah and Rewf for their encouragement and spiritual support and for visiting me every summer.

Finally, I appreciate the financial support from the government of Saudi Arabia and the Saudi cultural attaché in London that funded my overall post-graduate studies and living expenses for my family and me.

1 Introduction

1.1 Introducing cancer and the characteristics of tumourigenesis

Statistics point to an alarming rate of cancer incidence in the future. The American Cancer Society, ACS, 2010, has predicted that the number of death cases caused by cancer will increase to 12 million per year by 2030. Consequently, cancer is considered as an enormous health problem worldwide (The American Cancer Society, ACS, 2010). The largest percentage of cancer deaths has been dicovered in the countries with low- and medium- income due to the unavailability of the treatments. Nowadays, number of death cases caused by cancer has exceeded the number of deaths due to other major diseases, such as heart disease and stroke. The increase of this disease worldwide leads to an urgent need for new medical discoveries and inventions in order to prevent and treat this disease. Primarily, important discoveries that unravelled the many facets of cancer have been discovered due to the biological studies of the disease occurrence and progression.

Amongst the most important of these discoveries has been the identification of genes, called tumour suppressor genes, that can act as molecular brakes, preventing the onset of tumour formation (Lodish et al., 2000), and genes that act as accelerators, acting to promote cancer progression, called oncogenes (Lodish et al., 2000). Many of these genes encode components of signalling pathways, normally acting inside the cell, to transduce extracellular cues, such as growth factors or hormones, into the appropriate biological responses. Mutation of tumour suppressors or overexpression of oncogenes often leads to aberrant cell signaling events,

ultimately triggering a range of inappropriate cellular behaviours, such as uncontrolled proliferation or cell invasion, which underpin cancer development (Pitot et al., 1981, Schmidt, 2007).

Intensive cancer research over the past decade has highlighted the varied dynamics of the disease- its initiation and progression. According to early experiments on animal models, cancer was primarily categorised into three stages: Initiation, Promotion and Progression (Yamagiwa and Ichikawa, 1977). Initiation might be caused for example when a subject is exposed to a DNA reactive agent, causing irreversible mutations in the DNA (Pitot, 1993). The cells then proliferate leading to formation of daughter cells that also contain the same mutations. This step predisposes the cell towards cancer. Promotion was proposed to be the step when a non-reactive agent acts on the affected cells through receptors and instigates tumour development (Troll and Wiesner, 1985). Progression is the term coined initially by Rous, but later extended and applied by a British pathologist Leslie Foulds in 1958, to define the development of tumors by multiple, stepwise changes in several "unit characteristics". Foulds described cancer as "a dynamic process advancing through stages that are qualitatively different" (Foulds, 1958).

Over the years, based on accumulated knowledge on biochemical and cellular processes, Clark (1991) classified the progression of cancer in 4 stages (Clark, 1991). According to this classification, the first stage is when the effects of carcinogens cause lesions that are temporally restricted in growth. These proliferations are considered to be uniform and are termed as "Benign tumours". These benign tumors can sometimes take almost half a life span of an individual

before symptoms develop and grow into primary cancers. The second stage shows abnormal differentiation in the lesion leading to disorganisation of cell growth and cytological abnormalities of the neoplasm. The cells do not remain temporally constricted but still remain within the tissue of origin and are generically termed as carcinoma *in situ* or *in situ* malignancy (Chang, 2006). The stage when the proliferative lesions are not temporally restricted and move to nearby tissue is the third stage and called as the invasive stage. Fourth stage is the final stage when cancerous cells can grow over surrounding tissues and sometimes travel from the site of origin to various other organs; this stage is known as "metastases."

Interestingly, studies (Chang, 2006) have shown that every stage is unique in regard to its biochemistry and morphology. Each stage is marked by a set of abnormal genetic information triggering dysregulated signalling events. Signalling by the Ras GTPase, for example, is known to play important roles in cancer initiation, invasion and metastasis (Hanahan and Weinberg, 2000), as discussed in more details in Section 1.2.

The hallmarks of cancer involve of six biological capabilities that are acquired during a multi-step process of tumor development (Figure 1.1) (Hanahan and Weinberg, 2000). The six hallmarks of cancer include sustaining proliferative signalling, resisting cell death, enabling replicative mortality, inducing angiogenesis, evading growth suppressors and activation invasion and metastasis (Hanahan and Weinberg, 2011). These hallmarks of cancer are complementary capabilities that enable tumor growth and metastasis and they also provide a foundation for understanding the biology of cancer (Hanahan and Weinberg, 2011).

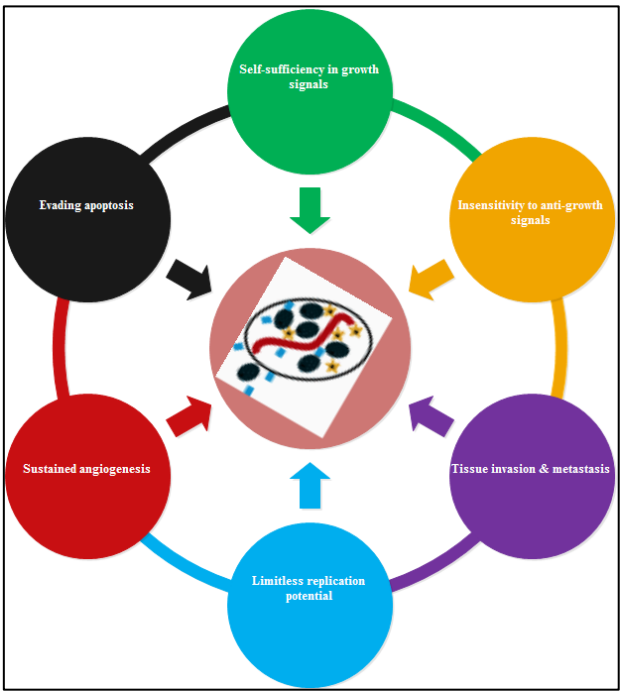

Figure 1.1. The hallmarks of cancer. The traits cancer cells acquire, contributing to their growth advantage over neighbouring healthy cells. Figure redrawn after Hanahan and Weinberg, 2011.

As the comprehension of biological pathways and cellular processes driving cancer progression increases, so too do treatment options for patients (Hudis, 2007). Surgery, radiotherapy and chemotherapy are the most common forms of cancer treatments. Surgery can be used as a treatment of non-haematological neoplasms that have not reached metastatic stages. Surgery is also useful in palliative treatment to regulate symptoms of bowel and spinal cancers (Nelson et al., 2001).Depending on the stage of the tumour, surgery can be used either before or after the other treatments with the goal of shrinking the tumour.

Radiotherapy entails the shrinking of tumours and killing of tumourigenic cells though irradiation with ionizing radiation (Ettinger et al., 2006, Sheehan et al., 2010). This form of treatment is localised to the target region, it destroys the

malignant genetic composition preventing further division and growth and triggers cell death. It is administered in fractions to prevent the extensive damage of normal cells. This however depends on the specific radio- sensitivity of the target region and its adjacent organs/tissues' sensitivity (Bange et al., 2001).

Chemotherapy involves the administration of anti-cancer drugs that are either cytotoxic or targeted therapies (Bild et al., 2006a). The former inhibit the cell division while the latter deregulate cancer-promoting proteins. The combination of these drugs is a common undertaking and may have synergistic effects (Hirsch, 2006). This form of treatment however causes the damage of non-cancerous tissues making treatment often hard to tolerate.

The use of genomic technologies has achieved the goal of personalised cancer therapies. These therapies have been aided in the identification of targets for new drug development that can exclusively attack a given tumor (Garman et al., 2007). Imatinib mesylate (Gleevec) and trastuzumab (Herceptin), that have achieved therapeutic successes, are examples of drug developments in cancer whereby the drug is matched to a specific target, for which assays are available (Fischer et al., 2003).

Gene expression patterns which reflect the activation status of a number of well-defined oncogenic pathways, such as the Ras pathway, have now been identified (Bild et al., 2006b). This has aided the identification of cell-based model systems in which to test the potential efficacy and specificity of therapeutic agents (Bild et al., 2006b). It is hoped that the increased specificity of targeted treatments will improve

disease outcome and may also reduce the number of side affects that are experienced with traditional treatments. However, it is likely that the most effective treatment regimes will involve a combination of targeted agents and carefully chosen cytotoxic compounds.

1.2 Oncogenic Ras signalling

Ras (whose name is derived from the Rat Sarcoma) was one of the first proto-oncogenes identified (Harvey, 1964), and has since been implicated in the development of many different types of cancer.

Ras proteins belong to a superfamily of GTPases that can be categorised into several sub-families including- Ras (H, K, M and R), Rap (1 and 2) and Ral, with these three types sharing more than 50% sequence identity (Matozaki et al., 2000). The *Ras* gene product is a 21 kDa monomeric membrane-bound protein that acts as an interlinking switch between receptors and intracellular kinases that form the signalling pathway. The Ras proteins have two interconvertible forms: GDP-bound inactive and GTP-bound active forms (Figure 1.2).

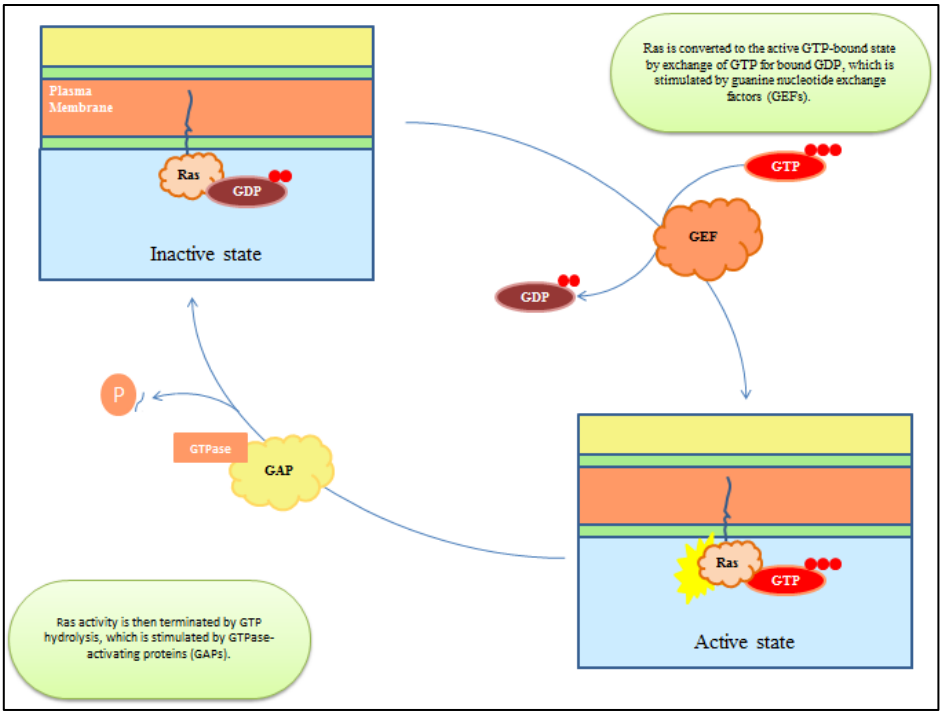

Figure 1.2. The active and inactive forms of Ras proteins. The Ras proteins alternate between inactive GDP-bound and active GTP-bound states, reproduced from (Cooper, 2000).

When Ras protein is bound to GDP it is in an inactive/neutral state. Upon signalling, cell surface receptors transmit information to Ras through Guanine nucleotide exchange factors (GEFs) that remove GDP, and promotes GTP binding, which is vital for Ras GTPase activation. A cascade of Mitogen activated kinases is activated in response to Ras, ultimately leading to phosphorylation of transcription factors that trigger the expression of genes that promote cell proliferation, growth and cell survival. This is identified as a self-limiting process, wherein activated Ras turns off immediately with the help of GTPase activating proteins (GAPs) that stimulate hydrolysis of GTP to GDP bringing back Ras to its inactive/neutral state. Studies have shown that mutations in the *Ras* gene allow the Ras signalling pathway to be

continuously switched “on” giving the cell unchecked permission to continuously proliferate, leading to the formation of tumours (Bos, 1989, Ehrhardt et al., 2002).

In addition to promoting tissue growth and tumourigenesis, Ras has been linked to metastasis. To define the role of Ras signalling cascades in metastasis, researchers have utilised the fruit fly *Drosophila melanogaster*, which is a genetically tractable *in vivo* model (Miles et al., 2011).

1.3 Using *Drosophila melanogaster* to Model Tumourigenesis

The fruit fly *Drosophila melanogaster* is a model organism that has been widely used in research for over a century; more recently, it has proven to be an effective system for modelling cancer in *vivo.* There are several reasons for it being an appealing system with which to work, not least the ease of rearing fly stocks in the laboratory, its short generation time and the plethora of powerful genetic techniques that have been developed over time, thereby allowing the efficient identification of genes that give a desired phenotype and their subsequent characterisation. Furthermore, both human and flies shared conserved pathways that control the cellular biological processes and most of the cancer causing genes found in humans are conserved in flies (Miles et al., 2011). For instance, Ras plays a conserved role in promoting cell proliferation, growth and survival in flies and human (Legg and Machesky, 2004).

A wide variety of *in vivo* experiments can be performed according to the development of the powerful genetic tools in the *Drosophila* system. For identifying

genes involved in the regulation of specific biological processes, such as migration, development or growth, large- scale forward genetic screens can be used. In *Drosophila* genome, multiple independent gene mutations can be generated through either exposure to mutagens such as EMS (ethyl methanesulfonate) followed by chemical mutagenesis, or transposable element insertion using *P*-elements (St Johnston, 2002, Adams and Sekelsky, 2002). Although, this allows screening of a large number of genes for a specific phenotype of interest, genes with redundant functions often fail to produce a visible phenotype when mutated (St Johnston, 2002, Brumby and Richardson, 2005).

Performing mis-expression screens that exploit the yeast *GAL4-UAS* bipartite expression system for inducing tissue specific ectopic gene expression can help to avoid the above issue (St Johnston, 2002, Adams and Sekelsky, 2002). In brief, *P*-elements carrying the yeast upstream activating sequence (*UAS*) element and a gene of interest are initially inserted into the *Drosophila* germline. Progeny that have incorporated the *UAS* construct into their genome are consequently crossed to flies, which under the control of an endogenous promoter, express the yeast transcriptional activator *GAL4* in a defined spatial and temporal pattern. Large numbers of transgenic *GAL4* strains, each under the control of different regulatory elements, are publicly available, making this a very flexible technique. Once expressed, GAL4 binds to the *UAS* site leading to expression of any gene that lies immediately downstream of the activating sequence in the same tissue/temporal specific pattern (Figure 1.3) (Adams and Sekelsky, 2002, St Johnston, 2002, Duffy, 2002).

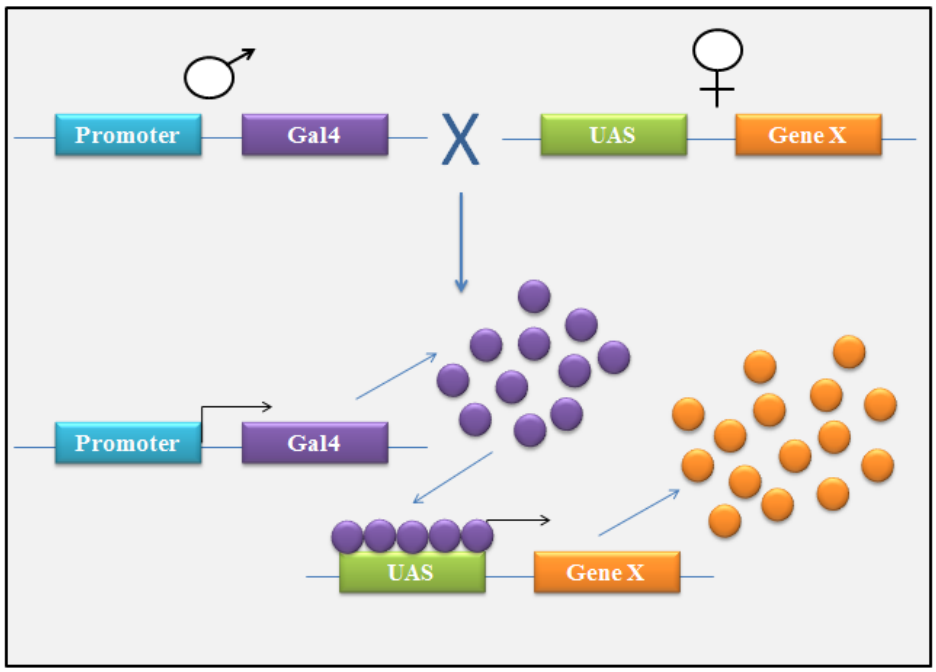

Figure 1.3. The *Gal4-UAS* bipartite expression system. *GAL4* gene expression is controlled by nearby genetic enhancers. A range of *GAL4* enhancer lines are available, which express the transcription activator in tissue- and temporal-specific patterns. The GAL4 protein binds to any *UAS* sites present in the *Drosophila* genome and any gene that lies immediately downstream of the activating sequence will be expressed in the same spatial and temporal pattern as the *GAL4* gene (Adams and Sekelsky, 2002, St Johnston, 2002, Duffy, 2002).

The *GAL4-UAS* system can also be used to knock down expression of genes by utilising inverted-repeat constructs that express double-stranded hairpin RNA resulting in sequence-specific post-transcriptional silencing of the targeted gene through RNA interference (RNAi) (Duffy, 2002). Any phenotype of interest that has produced by any gene can be used to identify further genes acting in the same pathway. This is achieved by analysing the ability of other genes to enhance or suppress the original phenotype (Adams and Sekelsky, 2002, St Johnston, 2002). Similarly, known homologues of the genes of interest can be ectopically expressed to determine if they can produce similar phenotypes. Lastly, modified proteins produced by *in vitro* genetic alterations can be expressed, enabling the role of

various binding domains and post translational modification sites in a given protein to be determined.

Mutational analysis using classical mutants has been the mainstay of *Drosophila* genetics. However, analysis of gene function using mutations can be problematic if the gene is essential for viability and insects die before the stage of development under investigation. The FLP recombinase/FLP recombinase target (FLP/*FRT*) system has been developed to overcome this limitation, by enabling clones of homozygous mutant cells to be created in otherwise heterozygous insects (Theodosiou and Xu, 1998). This approach is also of particular relevance to cancer studies, since it is possible to recapitulate the kind of genetic changes that occur in tumour cells residing in otherwise wild type tissue in humans. The FLP/FRT system can also be exploited to allow homozygous mutant clone (Golic, 1991). Briefly, mitotic recombination between two *FRT* sites present on homologous chromosome arms is driven by tissue or developmental-specific expression of the yeast FLP recombinase. Clones of homozygous mutant cells can be produced only when one chromosome arm contains a mutant allele of the gene of interest, (Figure 1.4.A) (Theodosiou and Xu, 1998). On the other hand, coupling the FLP/*FRT* recombination system with the *UAS-GAL4* system results in generating mis-expression clones. In this instance, induction of FLP recombinase induces recombination between two *FRT* sites flanking a reporter/silencer cassette. The removal of this cassette brings the *GAL4* gene under the control of a constitutive promoter driving its expression of *GAL4*, which in turn drives the expression of any *UAS*-linked genes (Figure 1.4.B) (Theodosiou and Xu, 1998).

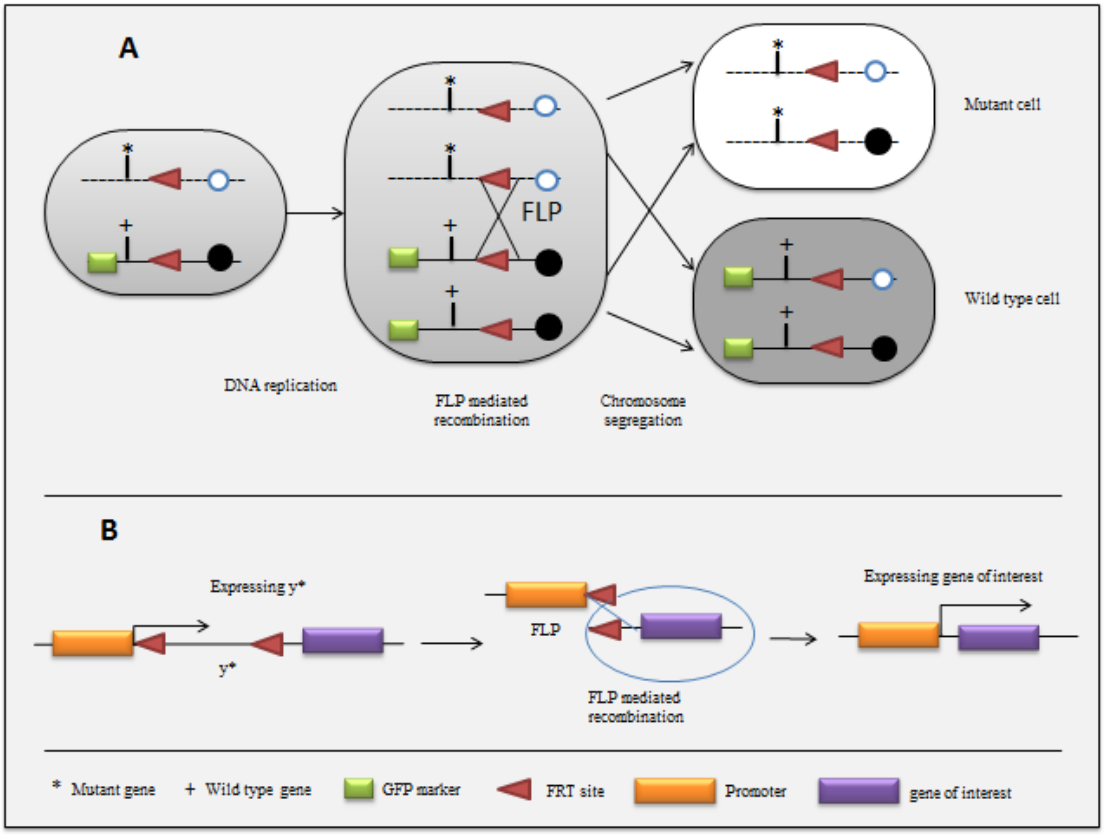

Figure 1.4. Generating mosaic clones using FLP/*FRT*-mediated mitotic recombination. (A) FLP enzyme expression induces recombination between *FRT* sites on homologous chromosomes, allowing generating of daughter cells that homozygous for a mutant allele. (B) Conversely, activation of FLP can initiate recombination between two *FRT* sites flanking a reporter/silencer cassette leading to its excision (Theodosiou and Xu, 1998).

1.4 Metastasis at the cellular level

Tumour cells disseminate either as single cells, using mesenchymal- or amoeboid-type movement, or as sheet, chains and cluster using collective movement mechanisms when leaving the primary mass (Friedl and Wolf, 2003). All these different migration strategies are similar or identical to those that are observed when normal cells migrate during physiological processes such as wound healing and embryo morphogenesis (Friedl and Wolf, 2003). It is assumed that pro-migratory signalling pathways are stimulated by genetic changes that occur in tumour cells,

causing inappropriate activation of the cell's normal migration machinery. *In vivo* experiments indicated that there are a number of interdependent steps that occur in a continuous cycle to drive movement of cell migration (Friedl and Bröcker, 2000). The initial step is when a quiescent, non-motile cell becomes polarized, responding to extracellular signals, and reorganises its cytoskeleton into a front 'moving portion' and a rear 'retracting portion'. Cellular protrusions, known as lamellipodia and filopodia, subsequently form at the leading edge of the cell; the extension of these protrusions is driven by actin polymerisation involving both the formation of new actin filaments (F-actin) via actin nucleation and the addition of actin monomers (G-actin) to the fast-growing, barbed ends of pre-existing filaments (Pollard and Borisy, 2003, Small et al., 2002). This rapid increase in F-actin is restricted to the tips of the cellular protrusions where the Arp2/3 complex, which drives actin nucleation, and other modulatory factors, such as the Ena/VASP family proteins, are localised (Bear et al., 2002, Pollard and Borisy, 2003). The extended protrusions subsequently adhere to the substrate over which the cell is moving, thereby providing the traction required for the cell to pull itself forward. It is the presence of actin-linked adhesion molecules, such as integins, on the outer membrane of the cellular protrusions that enable cell-substrate interactions to occur (Hynes, 2002). Finally, adhesions linking the trailing edge of the cell to the substrate are disassembled and myosin-driven retraction of the cell rear occurs (Hynes, 2002). It is thought that all the migration strategies used by motile tumour cells are variations on this basic 4-step model of the cell migration (Friedl and Wolf, 2003).

In addition to promoting cell motility, proteolytic degradation mediated by extracellular protease activity is required for tumour cell penetration of the basement

membrane and other tissue barriers. Protease genes are typically upregulated, whereas protease inhibitor genes are typically downregulated in mammalian cancer. However, as the production of proteases is also involved in growth signaling and angiogenesis it cannot be described as a unique characteristic of metastatic tumour cells (Hanahan and Weinberg, 2000).

In *Drosophila* there are two different approaches that have been adopted to model cell migration. Firstly, to identify groups of proteins that could potentially drive metastasis if misregulated, researchers have exploited the stereotypical cell migration patterns that occur normally during *Drosophila* development (Jang et al., 2007). Secondly, to identify genes that can cause inappropriate migration when deregulated, researchers have studied the effects of perturbing the function of specific tumour suppressors and oncogenes, triggering the acquisition of transformation in otherwise non-motile cells.

During *Drosophila* embryogenesis and oogenesis, single cells and groups of cells migrate in a predictable pattern, at a predictable stage. For instance, during gastrulation, germ cells actively migrate across the epithelium of the posterior midgut before assembling into the gonads (Santos and Lehmann, 2004). Proteins that possess the capacity to regulate cell migration can be identified by overexpressing and knocking down genes in the motile cells; this is typically achieved by screening for migration events that do not occur, do not reach completion, that occur at a different stage to that expected or do not occur on the expected trajectory. The main advantage of these models is that the migration process occurs *in vivo* and the entire event can be observed and recorded.

In addition to elucidating the mechanisms underlying naturally-occuring forms of cell migration, it is also possible to screen for genes that can promote the acquisition of motile behaviours in stationary cells. For example, loss of Moesin function in a subset of wing imaginal disc epithelial cells results in a loss of apical-basal polarity and the adoption of mesenchymal characteristics, with mutant cells exhibiting motile behaviour by migrating between wild type epithelial cells (Speck et al., 2003). This behaviour has been found to be dependent on the activity of a well-known regulator of cell migration, Rhol (Raftopoulou and Hall, 2004). Moreover, for screening of genes that can promote invasive cell behaviour when misexpressed, benign tumours in *Drosophila* tissues can be induced through overexpressing/knocking down genes that induce overproliferation but not migration (Xu et al., 1995). It is hoped that by insights such as these in *in vivo* models of migration will lead to the indentification of genes that could potentially regulate tumour cell invasion and metastasis in humans and pave the way for the development of novel anti-metastasis therapies.

1.5 The RA-PH family of adapter proteins

Adapter proteins play an essential role in the regulation of diverse range of cellular activities through the coupling of extracellular signalling events with intracellular signal transduction pathways. Although these proteins do not possess any intrinsic enzymatic activity themselves, they contain multiple protein and lipid binding domains that determine their function through facilitating the formation of various protein complexes. These adapter-protein recruited complexes can respond to physical/behavioural changes in cell surface receptors and regulate intracellular

activity, leading to a diverse array of outcomes, such as changes in cell proliferation, cell metabolism and cell motility (Samelson, 2002).

One class of molecular adaptors are the RA (Ras-association) and PH (Pleckstrin homology) domain containing proteins. This class of proteins are sub-divided into two small but distinct families; the Grb (**G**rowth Factor **R**eceptor-**B**ound) 7/10/14 family and the MRL (**M**ig-10/**R**IAM/**L**amellipodin) family (Figure 1.5) (Shen and Guan, 2004, Lafuente et al., 2004). While the MRL proteins can be found in *Caenorhabditis elegans* (*C. elegans*) and *Drosophila melanogaster*, Grb proteins are only found in higher multicellular organisms; with no orthologues identified in either *Caenorhabditis elegans* (*C. elegans*) or *Drosophila melanogaster*, which indicates that the acquisition of Grb7/10/14 structure and function has been relatively late in evolutionary term (Holt and Siddle, 2005).

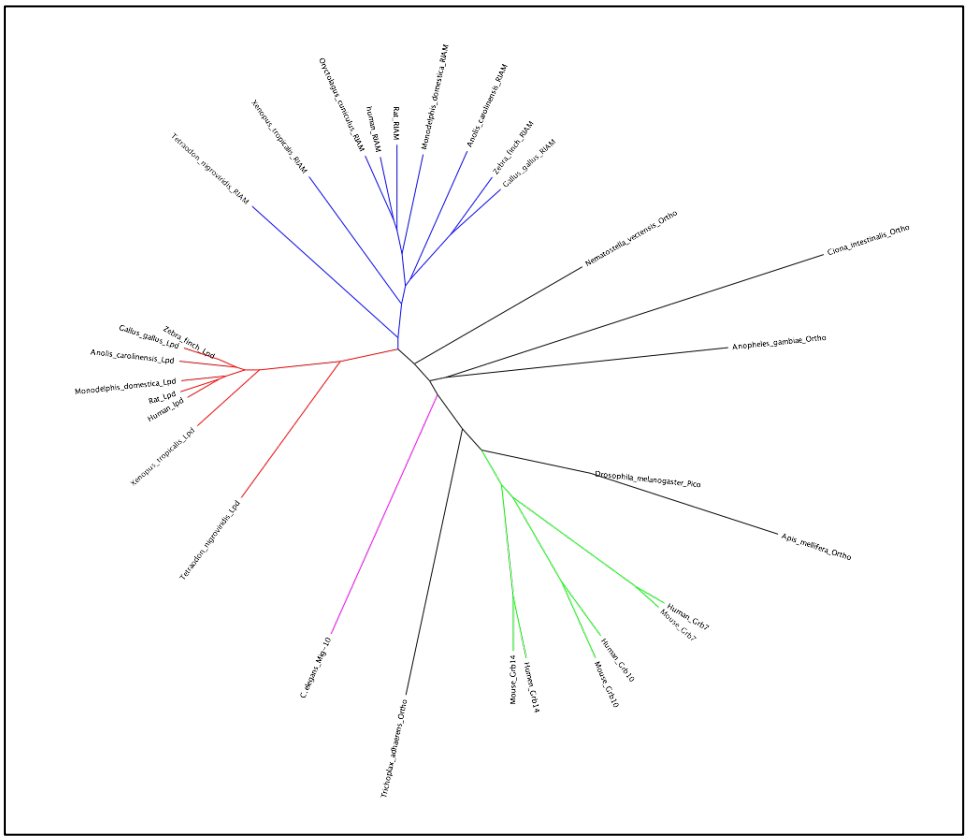

Figure 1.5. Dendrogram of the full-length proteins of the Grb7/10/14 and MRL families. The MRL family (Lpd in red, RIAM in blue, Mig-10 in pink and Pico in blak) and the Grb7/10/14 family(in green) represent two distinct sub-groups of the RA- PH superfamily. No Grb7/10/14 orthologues are found in *C. elegans* or *Drosophila melanogaster*. Basic Local Alignment Search Tool (BLAST) algorithms were used to identify MRL and Grb homologues in a wide variety of species. Sequence alignments and a phylogenetic tree were then performed using Clustal Omega. Finally, the tree was visualised using Figtree program.

1.5.1 The Grb7/10/14 family

Grb7, Grb10 and Grb14 constitute the Grb7/10/14 family of adapter proteins and they all share a common domain structure; in addition to the central RA and PH domains mentioned previously, these proteins also possess an N-terminally located proline-rich region, a C-terminal SH2 (Src homology 2) domain and a BPS (**B**etween the **P**H and **S**H2) domain (Figure 1.6) (Han et al., 2001).

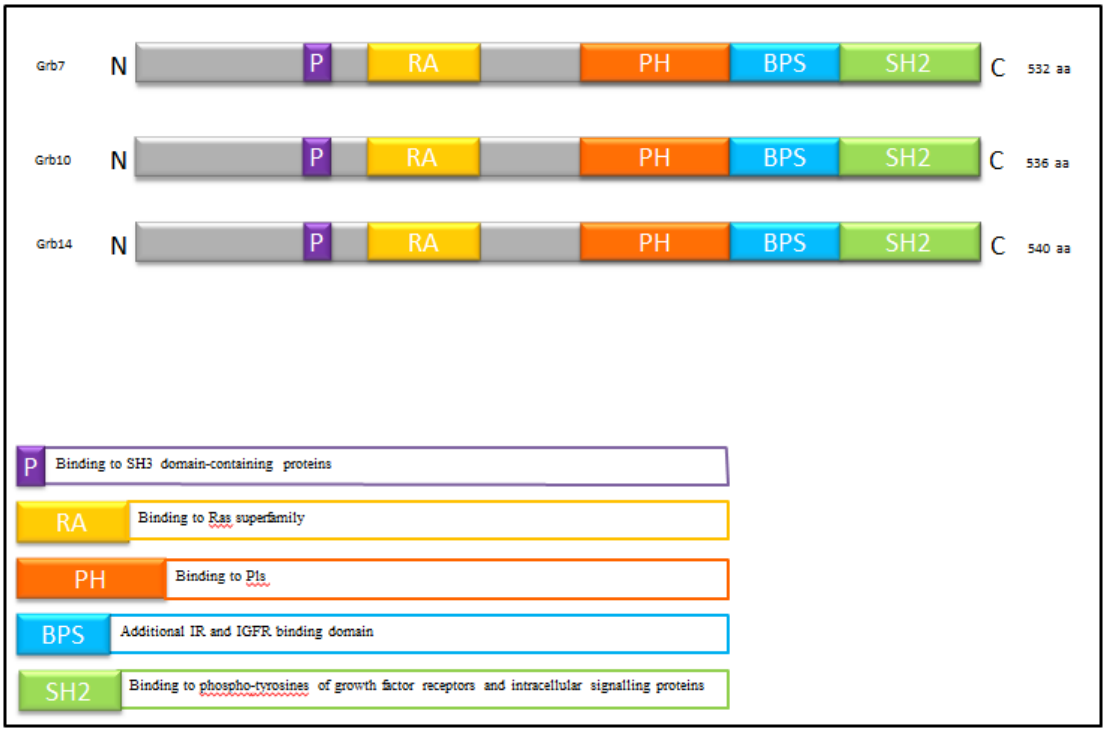

Figure 1.6. A schematic representation of the Grb7/10/14 family of proteins. The Grb7/10/14 all possess central RA and PH domains in addition to an N-terminal proline rich region and a C-terminal SH2 domain. The BPS domain appears to be unique to the Grb7/10/14 family.

The Ras superfamily of proteins is prolific signal-transducing GTPases that cycle between inactive GDP-bound and active GTP-bound forms as mentioned previously. They have been shown to interact with a spectrum of effector molecules enabling them to act through various signalling pathways; most notably those involved in cell proliferation, cellular adhesion, and membrane trafficking (Bourne et al., 1990, Wennerberg et al., 2005). A number of effector molecules can be identified by the presence of a Ras-Association (RA) domain, which facilitates the interaction between Ras and components of the downstream signalling cascade (Ponting and Benjamin, 1996). Accordingly, it has been reported that the RA domains present in the Grb7/10/14 facilitate interactions with members of the Ras superfamily. Grb7 has been shown to bind to N-Ras, K- Ras and R-Ras3 in addition to activated Rap1

and Rap2, albeit with a much weaker affinity (Rodriguez-Viciana et al., 2004, Depetris et al., 2009). Grb10 and Grb14 have only been found to bind to N-Ras, but not Rap1 or Rap2 so far, suggesting that further experimentations are required to determine if other Ras family GTPases can interact (Depetris et al., 2009).

PH domains can be found in numerous proteins involved in cellular signalling, they are small protein modules typically around 120 amino acids in length (Haslam et al., 1993, Mayer et al., 1993, Lemmon and Ferguson, 2000). It is thought that these domains predominantly function in targeting proteins to the plasma membrane through direct interactions with phospholipids (Lemmon, 2007, Rameh et al., 1997). In addition to their role in membrane localisation, they have also been shown to interact with a small number of proteins, such as isoforms of PKC (protein kinase C) and heterotrimeric G-proteins (Wang et al., 1994, Yao et al., 1994).

As expected, the PH domains of the Grb7/10/14 proteins have been shown to interact with a range of specific phosphoinositides. Grb7 has been reported to interact strongly with PI(3)P and PI(5)P, while only moderate or weak binding was observed with PI(4)P, PI(3,5)P_2, PI(3,4)P_2 and PI(3,4,5)P_3 (Depetris et al., 2009, Shen et al., 2002). The PH domain of Grb10 was reported to have a fairly high affinity association with PI(5)P, PI(4,5)P_2, PI(3,4)P_2 and PI(3,4,5)P_3, whereas Grb14 has been found to interact weakly with PI(3,4,5)P_3 (Depetris et al., 2009).

The most highly conserved region amongst the Grb7/10/14 family is the SH2 domain that acts as a phosphotyrosine-binding module, allowing interactions with

receptor tyrosine kinases and other intracellular signalling proteins (Holt and Siddle, 2005).

Despite the high degree of sequence similarity between members of the Grb family, the binding preferences of the SH2 domain vary between the proteins. The SH2 domains have been shown to interact with the activated IP, insulin receptor, in the all three Grb7/10/14 members, nevertheless, the affinity association significantly differs and may be important in influencing the outcome of IR-dependent signalling (Kasus-Jacobi et al., 2000, Kasus-Jacobi et al., 1998, Hansen et al., 1996). The SH2 domain of Grb7 associates with the cytoplasmic tyrosine kinase FAK (focal adhesion kinase) and the receptor tyrosine kinase ErbB2, however both Grb10 and Grb14 do not (Frantz et al., 1997, Han and Guan, 1999, Janes et al., 1997).

The BPS domain is unique to Grb7/10/14 proteins and named due to its location between the PH and SH2 domains, it is short region approximately 80 amino acids long (He et al., 1998). It appears to be intrinsically unstructured yet the isolated domain retains physiological activity by interacting with activated IR and IGFR, and inhibiting IR catalytic activity (Moncoq et al., 2003, Stein et al., 2001, Béréziat et al., 2002). The BPS domain cooperates with the SH2 domain to facilitate interactions with tyrosine-phosphorylated signalling molecules, involving receptor tyrosine kinases (He et al., 1998). Additionally, despite its high sequence conservation among the Grb7/10/14 proteins, it is believed that the BPS domain acts as an important receptor-binding determinant to impart specificity amongst the family (Holt and Siddle, 2005).

Lastly, the N-terminal regions of the Grb7/10/14 proteins contain a conserved proline rich sequence in addition to a number of PXXP motifs, enabling interaction with Src homology 3 (SH3) domains, such as the SH3 domain of c-Abl (Abelson) has been reported to interact, *in vitro*, with the proline rich region of Grb10 (Frantz et al., 1997). Grb10 proline rich regions in the N-terminus have also been shown to interact with GIGYF-1 and GIGYF-2 (Grb10-interacting GYF proteins 1 and 2); two proteins implicated in EGFR mediated Akt activity regulation, via GYF motifs rather than SH3 domains (Giovannone et al., 2003, Ajiro et al., 2010). In addition, the N-terminal region of Grb14 associate with Tankyrase 2, an ankyrin repeat region of the poly (ADP-Ribose) polymerase, *in vivo*; however, neither the functional significance or exact site of this interaction have yet been determined (Lyons et al., 2001). So, far no N-terminal binding partners have yet been identified for Grb7.

The three Grb7/10/14 family proteins share significant structural and sequence homology, but have been found to regulate distinct cellular activities (Holt and Daly, 2005), with only some functional overlap existing between Grb10 and Grb14 due to their different binding partners (Figure 1.7).

It is thought that Grb7 acts as a positive regulator of cell migration and plays a role in tumourigenesis (Holt and Daly, 2005). Overexpression of *Grb7* has frequently been observed in metastatic cell lines and in clinical tumour samples, usually in association with FAK or ErbB2 overexpression (Holt and Daly, 2005, Siamakpour-Reihani et al., 2009). Particularly, in a range of breast carcinoma cell lines as well as in tissue samples taken from primary breast tumours, *Grb7* has been reported to be upregulated in conjunction with ErbB2 (also known as HER2) (Stein et al., 1994). In

addition, Grb7 and FAK are required for integrin-stimulated cell migration and that Grb7/FAK complex formation correlated with the metastatic behaviour of esophageal carcinoma cells (Tanaka et al., 2000). Furthermore, expression of a peptide inhibitor, which binds to the SH2 domain of Grb7, has been shown to significantly reduce the migratory behavior exhibited by pancreatic cancer cells (Tanaka et al., 2006). Recently, it has been proposed that the rate of tumour cell proliferation can be influenced by Grb7. In addition, it has been found that the proliferation of breast cancer cells can be suppressed by the expression of the aforementioned Grb7-specific peptide inhibitor (Pero et al., 2007). However, the ability to regulate cell migration is not shared by Grb10 and Grb14.

Grb10 and Grb14 have been shown to play a key role in the control of cellular growth, proliferation and metabolism by directly associating and inhibiting the activated insulin receptor (IR); this prevents insulin-induced activation of signalling cascades involved in metabolic and mitogenic pathways (Wick et al., 2003, Kairouz et al., 2005, Kasus-Jacobi et al., 1998). It has been thought that Grb10 and Grb14 binding can inhibit the catalytic activity of the IR, and also block access of substrates to the activated receptor (Béréziat et al., 2002, Wick et al., 2003, Langlais et al., 2004). Contradicting this, some studies have indicated that Grb10/14 positively regulates insulin signalling. Grb10 reportedly associates with and increases the activity of the insulin signalling pathway molecule Akt (Holt and Siddle, 2005). Grb14 has been shown to constitutively interact with PDK-1 leading to recruitment of the activated IR, Akt phosphorylation and insulin signal transduction (Holt and Siddle, 2005, Jahn et al., 2002, King and Newton, 2004)

Grb10 has been shown to be involved in controlling cell growth and proliferation, in addition to apoptosis. Genomic imprinting and inheritance of a maternal regulate *Grb10*, loss-of-function of *Grb10* allele can promote placental and embryonic growth, leading to neonates that are 30% larger than wild type progeny (Charalambous et al., 2003, Charalambous et al., 2010, Wang et al., 2007). Moreover, overexpression of *Grb10* results in growth retardation; it has been found that transgenic mice with elevated levels of Grb10 are significantly smaller than sibling control mice when compared at 3 weeks old (Shiura et al., 2005).

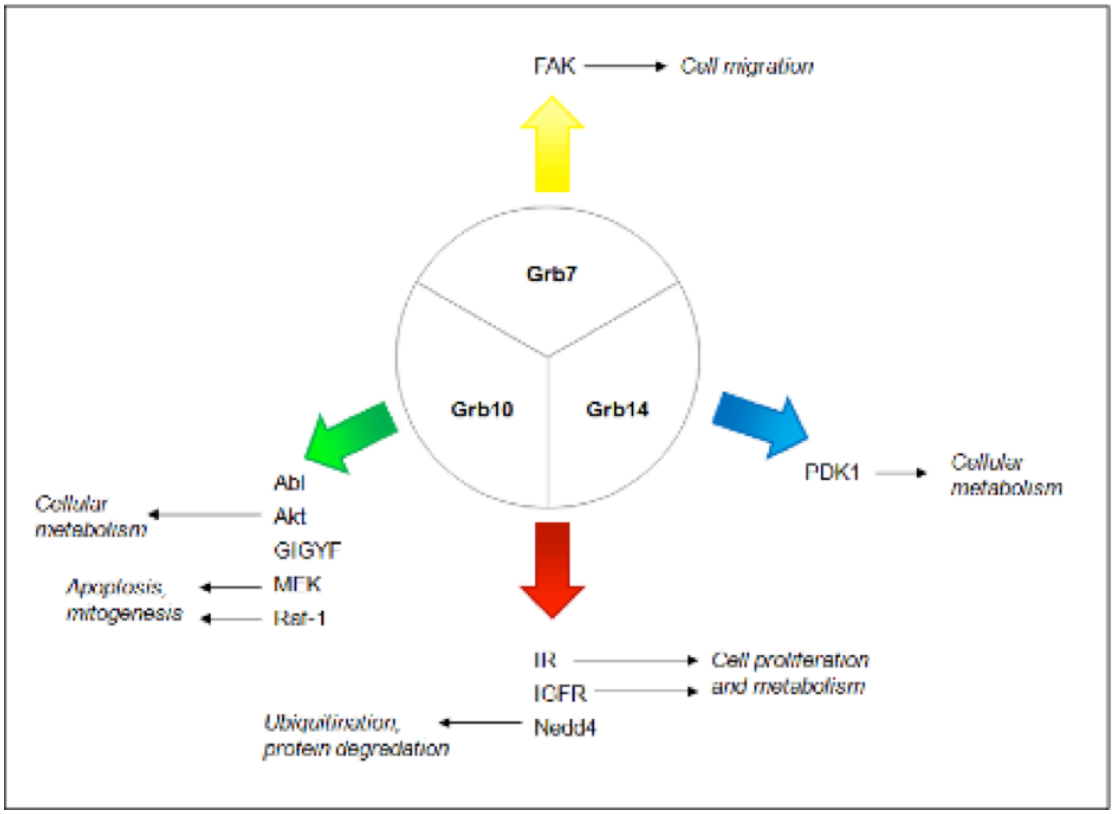

Figure 1.7. The different functions of the Grb7/10/14 family. Grb7/10/14 interactions play a key role in their functionality (Holt and Siddle, 2005).

1.5.2 The MRL family of adapter molecules

The MRL family of adapter proteins consists of the *C. elegans* orthologue Mig-10 (abnormal cell migration protein 10), as well as two mammalian paralogues RIAM (Rap1-GTP-interacting adapter molecule) and Lpd (Lamellipodin), and the most recently characterised *Drosophila* orthologue, Pico (CG11940) (Figure 1.8) (Manser and Wood, 1990, Lafuente et al., 2004, Lyulcheva et al., 2008, Krause et al., 2004). It has been proposed that members of this recently identified family facilitate in transducing signals derived from membrane receptors to changes in the actin cytoskeleton allowing regulation of actin dynamics, cell adhesion, migration and growth (Krause et al., 2004, Lafuente et al., 2004, Lyulcheva et al., 2008, Coló et al., 2012). Much like the Grb7/10/14 family members, the MRL proteins all contain a well-defined central RA domain and PH domain; in addition they possess a number of proline-rich regions. While these regions are located at the N-terminus in the Grb7/10/14 protein, they are predominatly found in the to C-terminal region of MRL proteins, with the exception of RIAM, which contains an N-terminal proline rich region. Unlike the Grb7/10/14 proteins none of the MRL protein contains BPS and SH2 domains (Figure 1.8). The RA domain is approximately 90 amino acids long, it directly interacts with specific Ras-like GTPases, potentially playing a critical role in activation of the protein and/or its other associated factors (Holt and Daly, 2005). The PH domain has been found to target the MRL proteins to the plasma membrane via direct interactions with phosphoinositides, and spans roughly 100 amino acid residues (Holt and Daly, 2005, Krause et al., 2004).

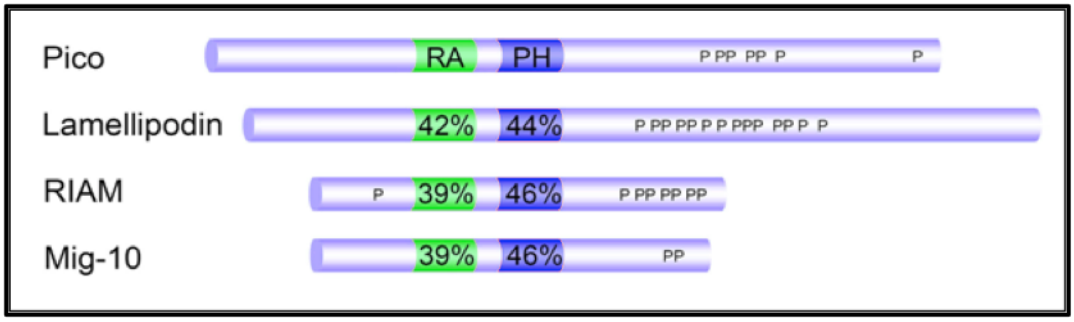

Figure 1.8. Common structural domains of the MRL proteins. *Drosophila* Pico, human Lamellipodin, human RIAM and *C.elegans* MIG-10. RA = *Ras*-association domain, PH = Pleckstrin homology domain, P = Proline rich regions. The % refers to the identity between the members of the MRL proteins (Lyulcheva et al., 2008).

The MRL proteins also possess a highly charged N- terminal region around 55 amino acids in length in addition to the RA and PH domains. Amphipathic helical structured talin binding sites have been identified within the first 100 amino acids of RIAM and Lpd (Lafuente et al., 2004, Krause et al., 2004, Lee et al., 2009). MRL proteins also contain a characteristic 25 amino acid putative coiled-coil motif adjacent to the N-terminus of the RA domain, and may function in promoting either homodimeric or heterodimeric interactions (Legg and Machesky, 2004, Lupas, 1996). Finally, proline-rich C-termini have been found in all MRL proteins containing multiple FPPPP motifs enabling interactions with EVH1 (Ena/VASP homology 1) domains that can be found in the actin regulatory proteins Enabled and VASP; together with XPPPP motifs that bind to profilin and other SH3-binding motif containing proteins (Coló et al., 2012, Krause et al., 2004, Lafuente et al., 2004).

The two mammalian MRL proteins, RIAM and Lpd, have well conserved RA and PH domains, however, the C-terminal and N-terminal regions of these proteins show considerable divergence pointing to there being both overlapping and distinct functions (Lafuente et al., 2004). RIAM possesses an additional proline- rich region with two putative EVH1 binding sites and an extra coiled-coil motif at its N-terminus that have not found in the other MRL members (Figure 1.8) (Lafuente et al., 2004). At its C-terminus, RIAM contains a proline-rich motif including five profilin-binding sites and five EVH1 binding motifs, whereas Lpd contains the larger C-terminal proline rich region that consists of eight potential SH3 binding sites, six EVH1 domain binding regions and three profilin interacting motifs (Lafuente et al., 2004, Krause et al., 2004).

Profilin and Ena/VASP bind profilin and EVH1 sites respectively; potentially facilitating their recruitment towards the leading edge to enable regulation of the actin cytoskeleton (Lafuente et al., 2004, Krause et al., 2004). Indeed, RIAM and Lpd co-localise with Ena/VASP proteins as well as F-actin at lamellipodia and filopodia tips (Krause et al., 2004, Lafuente et al., 2004). In addition, they have been found to regulate actin dynamics in an Ena/VASP dependent manner (Lafuente et al., 2004, Krause et al., 2004, Jenzora et al., 2005). When overexpressed, RIAM induces cell spreading and lamellipodia formation whilst Lpd increases lamella protrusion velocity (Krause et al., 2004). Blocking Ena/VASP functionality can suppress the increased lamellipodial protrusion velocity that resultd from Lpd overexpression (Krause et al., 2004). Contrastingly, lamella formation is reduced when knocking down Lpd in addition to reducing actin branching density and F-actin levels within the lamellipodium; while F-actin quantities is decreased when

silencing RIAM (Krause et al., 2004, Lafuente et al., 2004). RIAM and Lpd have been shown to bind to Talin through their N-terminal amphipathic helices, leading to integrin activation and promotion of cell adhesion (Lafuente et al., 2004, Lee et al., 2009, Han et al., 2006, Watanabe et al., 2008). Moreover, it has been found that RIAM co-localise with Vinculin and actin in early focal adhesions during initial cell spreading but is absent in more mature formations (Han et al., 2006). In addition to the role of RIAM in controlling actin dynamics and integrin mediated adhesion, it has also been shown to regulate the directionality of cell migration and play a role in FA disassembly through an integrin-RIAM dependent MEK/Erk activated feedback-loop (Hernández-Varas et al., 2011, Coló et al., 2012).

RIAM and Lpd also show differences with respect to the binding preferences. RIAM has been reported to interact predominantly with active Rap-1, which is a well-known regulator of integrin activation; it can also bind to active Ras at a lower affinity (Lafuente et al., 2004, Bos, 2005). This interaction requires both the RA and PH domains, and is enhanced by the RIAM N-terminus (Lafuente et al., 2004c). Contrastingly, interaction of Lpd with Rap-1 has not been observed yet, however it has been found to associate with active H-Ras, K-Ras, N-Ras, R-Ras and Rac (Rodriguez-Viciana et al., 2004, Jenzora et al., 2005, Krause et al., 2004). RIAM and Lpd display differential PH domain binding preferences, with RIAM interacting with the more common PI(3)P and PI(5)P, whilst Lpd associates with the relatively rarer $PI(3,4)P_2$ (Krause et al., 2004, Jenzora et al., 2005, Lemmon, 2008). Since PIs represent early polarising molecules during cell activation, the differential binding capacities of the Lpd and RIAM PH domains may contribute to the characteristic

temporal and spatial localisations observed in these proteins (Lemmon, 2003, Coló et al., 2012b). At the cellular level, Lpd is mostly located at the plasma membrane, while RIAM is found both in the cytoplasm and in lamellipodia at the leading edge of the cell membrane (Lafuente et al., 2004, Jenzora et al., 2005, Krause et al., 2004).

It is thought that RIAM and Lpd are also regulated by further protein interactions and post-translational modifications that lead to tight control over their divergent downstream functions. RIAM has been found to be a substrate for the tyrosine kinases Fyn, Lck and ZAP-70, in stimulated T cells, enabling the C-terminal proline-rich region to bind to the SH3 domain of PLC-γ1 (Patsoukis et al., 2009). RIAM then assists in the translocation of PLC- γ1 to the actin cytoskeleton where, through interactions with $PI(4,5)P_2$, a signalling cascade is initiated by PLC- γ1 that increases Ras-GTP formation, MEK/Erk activation, and changes in gene expression (Patsoukis et al., 2009). Following phosphorylation of key tyrosine residues within Lpd, it can then bind the SH2 domain of c-Abl tyrosine kinase (Michael et al., 2010). Abl family kinases are critical regulators of cytoskeletal dynamics they have been also implicated in axon guidance in both *Drosophila* and mammals (Lanier and Gertler, 2000). In fibroblasts, phosphorylation of Lpd by c-Abl downstream of PDGF regulated formation of dorsal ruffle via recruiting Ena/VASP proteins (Michael et al., 2010). Cooperation of Lpd with c-Ab1 has been reported to mediate the regulation of axon morphogenesis in primary hippocampal neurons (Michael et al., 2010). Lastly, interactions of Lpd with the SH3 domain of srGAP3 (SLIT-ROBO Rho GTPase activating protein) in primary fibroblasts can negatively regulate

lamellipodial dynamics. It is believed that srGAP3 interacts with Lpd close to the membrane, leading to release the binding between Lpd and Rac1, causing inhibition of membrane protrusions associated with a reduction in the local Rac1-GTP levels (Endris et al., 2011).

Although RIAM and Lpd have both been implicated in cell growth and proliferation, the mechanisms by which they act are thought to be different. It has been shown that the reduction in integrin-dependent adhesion in RIAM silenced cells is correlated with the reduction in Erk1/2 and PI3K activation, two central molecules controlling cell growth and survival (Hernández-Varas et al., 2011). In addition to inhibition of anchorage-independent growth, RIAM depleted cells showed reduced tumour growth as well as delayed metastasis, suggesting that RIAM mediated activation of Erk1/2 and PI3K contributes to cellular proliferation (Hernández-Varas et al., 2011, Coló et al., 2012b). Lpd, on the other hand, has been implicated in proliferation of mammalian cells by regulation of the Serum Response Factor (SRF), see also Section 1.6 below. F-actin levels increased by Lpd leads to depletion of G-actin. Consequently, the co-factor MAL is released from G-actin and is transported into the nucleus where associated with SRF and induces gene expression.

(Coló et al., 2012b, Lyulcheva et al., 2008, Pinheiro et al., 2011). The regulation of SRF activity via Lpd is also implicated in directing pyramidal neurons to select a radial migration pathway along glia rather than a tangential migration mode (Pinheiro et al., 2011).

Mig-10, the only *C. elegans* MRL homologue, like all MRL proteins, contains the characteristic central RA and PH domains, C-terminal proline rich regions and N-terminal coiled-coil motif (Manser and Wood, 1990, Coló et al., 2012b). Studies have been shown that Mig-10 is required for processes requiring well controlled directional migration including long-range antero-posterior migration of embryonic CAN (canal- associated neurons), ALM (anterior lateral microtubule cells) and HSN (hermaphrodite-specific neurons), as well as efficient development of excretory canals used in osmoregulation (Coló et al., 2012b, Manser et al., 1997, Manser and Wood, 1990, Chang et al., 2006). However, unlike the other members of the MRL family, Mig-10 has not yet been found to play a role in cellular growth and proliferation (Coló et al., 2012b).

MIG-10 shares significant homology with Lpd, it contains consensus EVH1 binding sites thought to facilitate interactions with members of the Ena/VASP family which can then assist in their recruitment to the leading edge, enabling cytoskeletal changes and enhancement of migration (Holt and Daly, 2005, Drees and Gertler, 2008). Indeed, disrupted embryonic cell migration responses instigated by *mig-10* mutants resemble those of mutants for *unc-34*, the *C. elegans* Ena/VASP orthologue (Forrester and Garriga, 1997). Moreover, during neuronal development, MIG-10 and UNC-34 act in conjunction to guide the migration of axons toward UNC-6 (Netrin), an attractive guidance cue, and away from SLT-1 (Slit), a repulsive guidance cue, with UNC-34 required for the formation of filopodia and MIG-10 enhancing their numbers (Chang et al., 2006, Quinn et al., 2006).

However, double mutants of *unc-34* and *mig-10* cause much more severe defects than either mutant separately, while in *unc-34* mutants alone, developing axons that lack filopodia are still guided to UNC-6 through MIG-10 mediated lamellipodial growth. This suggests that the two proteins may act in overlapping functional pathways (Chang et al., 2006). In particular, it is thought that MIG-10 is likely to interact with actin polymerisation machinery through additional partner molecules, however interactions with UNC-34 through a common pathway are still probable (Chang et al., 2006, McShea et al., 2013).

1.6 *pico* encodes the *Drosophila* MRL homologue

Pico is a *Drosophila* MRL orthologue (CG11940), it is the most recently characterised MRL family member (Lyulcheva et al., 2008). *pico* encodes two major transcripts generated from alternative transcription start sites, *pico* and *pico-L*. *pico-L* encodes a 1159 amino acid protein identical to the shorter form, except for the presence of additional 128 N-terminal amino acids (Lyulcheva et al., 2008).

Previous experiments showed that knocking down *pico* in *Drosophila* wing discs caused a significant reduction in tissue growth through reduced cellular proliferation rather than induced apoptosis (Lyulcheva et al., 2008). Further investigations demonstrated that homozygous *pico* mutant clones generated in *Drosophila* imaginal discs also showed severe growth and proliferation defects and were gradually extruded from the otherwise wild type tissue (Lyulcheva et al., 2008). Conversely, overexpression of *pico* induced growth at both the tissue and whole organism level,

owing to co-ordinated increases in both cell number and size (Lyulcheva et al., 2008, Lyulcheva, 2006).

Reduction in *pico* levels is accompanied by reduction of monomeric (G)-actin levels and a concomitant increase in filamentous (F)-actin (Lyulcheva et al., 2008). Conversely, when *pico* is overexpressed, it leads to an increase in G:F actin ratios and promotes tissue overgrowth (Lyulcheva et al., 2008). This has led to the suggestion that pico induces serum response factor (SRF) signalling, which responds to reduced levels of G: F- actin ratios through its co-factor Mal (Miralles et al., 2003). Overexpression of *mal* also stimulated tissue growth leading to the suggestion that Pico promotes growth via Mal-SRF signalling, (Figure 1.9) (Lyulcheva et al., 2008). Unpublished data from the Bennett laboratory has also revealed that Pico functionally interacts with constitutively active Ras to promote tumour growth and invasion (Taylor, 2010). SRF signalling is also implicated in this process, see Chapter 4.

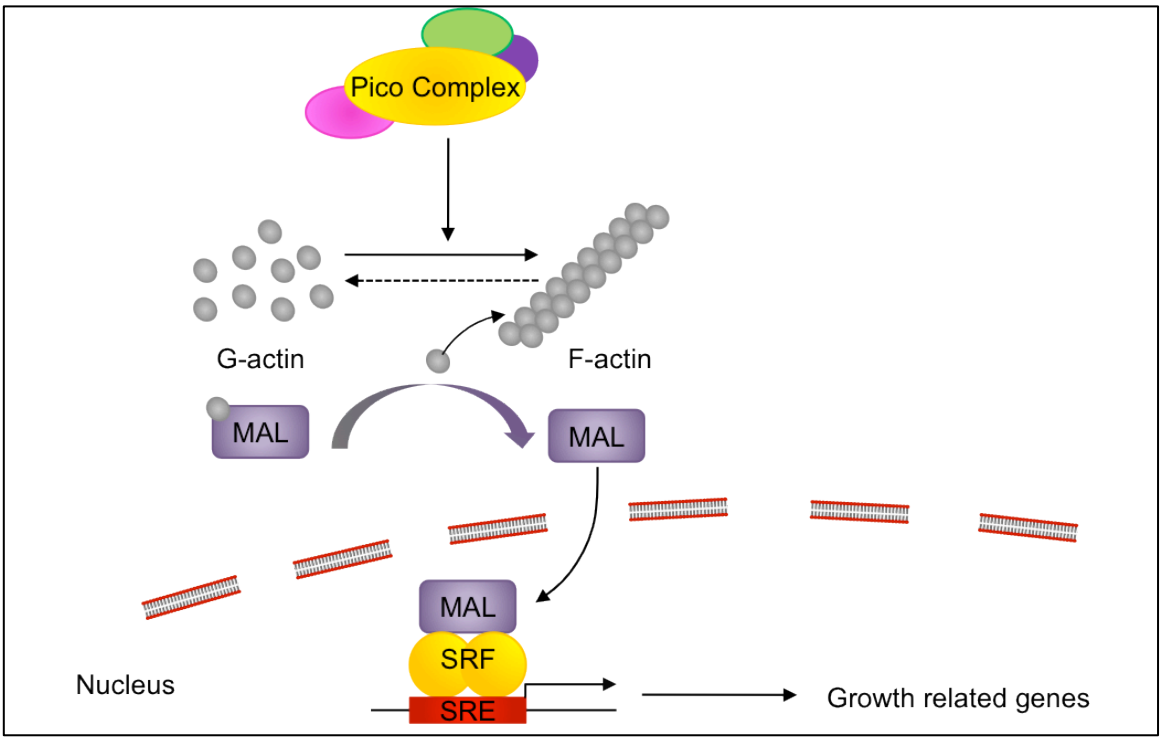

Figure 1.9. Model of Pico signalling mediating tissue growth. Pico and its associated proteins enhance F-actin formation leading to release of G-actin bound to MAL. Unbound MAL translocates to the nucleus where it complexes with SRF enabling transcription of a subset of SRF Responsive Element (SRE)-containing growth-related genes. The figure is adapted from (Lofthouse, 2013).

Sequence analysis has revealed that Pico contains all the characteristic domains found in the MRL proteins, namely an N-terminal coiled motif, the consecutive RA and PH domains, and numerous proline-rich regions (Figure 1.8). In addition, currently unpublished work performed within the laboratory has identified a highly conserved Mitogen Activated Protein Kinase (MAPK) binding site N-terminal to the RA domain, which has been shown to interact with the MAPK Erk1/2 in both full-length Pico and Lpd, and a short fragment of RIAM. Preliminary work has shown that bound MAPK may phosphorylate Pico at Serine 819 (a phosphorylation site initially identified in a high-throughput proteomics screen), which in turn enables

Protein Phosphatase 1 (PP1) to bind at a putative binding site located at residues 810-817.

1.7 Project aims

The focus of this project has been to interrogate signalling upstream and downstream of *pico*, to better understand the effects of manipulating its function. This has been done both in the developing wing, where overexpressed *pico* is capable of driving hyperplastic overgrowth (Chapter 3), and in the larval CNS, where pico cooperates with oncogenic Ras to promote both hyperproliferation and cell invasion (Chapter 4). A key focus has been to explore the involvement of SRF signalling, making use of a range of genetic tools including an *in vivo* reporter for SRF, which is characterised here for the first time. In addition, a panel of site-directed mutants in pico, including a Protein Phosphatase 1 binding site mutation, non-phosphorylatable and phosphomimetic (SD) mutations of S819 and mutation of the MAPK binding site, have been used to test the effect of specific regulatory interactions on *pico* function. (Chapter 5). Insights gained from this work are likely to feed into studies being conducted in more complex organisms, including mammals, and may have relevance to our understanding of cancer development or progression. Furthermore, a better understanding of the regulation of MRL signalling may make the affected pathways open to pharmacological manipulation.

2 Materials and methods

2.1 Commonly used media and solutions

2.1.1 Lysogeny broth (LB) Media

LB medium essential for growth of bacterial strains. It is composed of 1.0% (w/v) Tryptone, 0.5% (w/v) Bacto-yeast Extract and 1.0% (w/v) NaCl dissolved in pure deionised water with a pH of 7.0. The solution has to be autoclaved before use.

2.1.2 LB Agar

LB agar Required for growth of bacterial strains on solid plates. It is comprised of 1.0% (w/v) Tryptone, 0.5% (w/v) Bacto-yeast Extract, 1.0% (w/v) NaCl and 1.6% (w/v) agar dissolved in in pure deionised water with a pH of 7.0. The mixture has to be autoclaved and left to cool to 55°C before pouring the mixture into plates to set, an appropriate antibiotic has to be added. Plates can be stored at 4°C.

2.1.3 Complete Schneider's Insect Medium (S2)

Drosophila Medium ((with L-glutamine and sodium bicarbonate, Sigma) modified with 10% (v/v) heat-inactivated Foetal Calf Serum (FCS, Gibco) and Penicillin-Streptomycin (Invitrogen) to a final concentration of 50 units Penicillin G and 50 µg Streptomycin sulphate per millilitre of medium.

2.1.4 Tris-EDTA (TE) Buffer (Sigma)

Using For resuspension of DNA: 10mM Tris-Cl pH 7.5 and 1mM EDTA (Ethylenediaminetetraacetic acid).

2.1.5 ChromoTek lysis buffer

ChromoTek lysis buffer contains 10 mM Tris- Cl pH 7.5, 150 mM NaCl, 0.5 mM EDTA, and 0.5% (v/v) NP-40.

It has been optimised by the manufacturer for GFP-Trap co- immunoprecipitation and enables efficient cell lysis and protein solubilisation while avoiding protein degradation and interference with the proteins immunoreactivity and biological activity.

2.1.6 2x SDS-Sample Buffer

Laemmli sample buffer (Sigma) was used for preparation and loading of protein samples onto an SDS- polyacrylamide gel for SDS-PAGE and Western Blotting. It is composed of 4% SDS, 20% glycerol, 10% (v/v) 2-mercaptoethanol, 0.004% (w/v) bromophenol blue and 0.125M Tris-HCl, pH 6.8.

2.1.7 1x SDS-PAGE Running Buffer

1x SDS-PAGE running buffer allows protein separation by SDS-polyacrylamide gel electrophoresis to occur and is comprised of 25 mM Tris (Anachem), 250 mM glycine (Anachem) pH 8.3 and 0.1% (v/v) SDS dissolved in pure deionised water.

2.1.8 Tris-glycine Transfer Buffer

Tris-glycine transfer buffer enables protein transfer from SDS-polyacrylamide gels to nitrocellulose membrane. The solution is comprised of 25 mM Tris, 193 mM glycine and 20% (v/v) methanol in pure deionised water.

2.1.9 PBS (Phosphate Buffered Saline)/PBST

PBS is a buffer solution designed to replicate the osmolarity and ion concentrations of normal cells and is composed of 137 mM NaCl, 2.7 mM KCl, 8 mM Na_2HPO_4, and 1.46 mM KH_2PO_4. PBST is made up of 1 x PBS with 0.1% (v/v) Tween-20.

2.1.10 Tris-buffered saline with Tween (TBST)

For washing nitrocellulose membranes for during western blotting: 150mM NaCl, 10mM Tris-HCl and either 0.1% or 0.05% (v/v) Tween-20 (Sigma) diluted in pure deionised water.

2.1.11 Blocking buffer (Western Blots)

5% (w/v) Marvel skimmed milk powder in PBST or 5% (w/v) Bovine Serum Albumin (BSA, Sigma Aldrich) in 0.05% TBST.

2.1.12 3.7% (w/v) Paraformaldehyde (Sigma)

A 37% stock was made by dissolving 0.185g in 500μL 1 x PBS (+7μL 1M NaOH to aid solubilisation) at 95°C for 5 minutes before diluting in 1X PBS to make a 3.7% solution for fixation of *Drosophila* tissue.

2.1.13 Blocking solution (*Drosophila* tissues)

1 x PBS, 5% (w/v) Fetal Bovine Serum, 0.1% (v/v) Triton X-100.

2.1.14 PBST (*Drosophila* tissues)

1 x PBS, 0.1% (v/v) Triton X-100.

2.2 Commonly used strains

2.2.1 Bacterial lines utilised

One Shot® Top 10 chemically competent E. coli (Life Technologies) F- mcrmrr-hsdRMS-mcrlaclacX74 recA1 araara-leu) 7697 galU galK rpsL (StrR) endA1 nupG.

2.2.2 Cell lines used

- *Drosophila* Schneider Receptor + (S2R+) Cells

Drosophila Schneider Receptor + (S2R+) cells are a line derived from the Schneider laboratory, which possess the wingless receptors Dfrizzled-1 and Dfrizzled-2 and formed a highly adherent monolayer in tissue culture flasks (Yanagawa et al., 1998).

- Initiating cultures from frozen stocks

To initiate cultures from a frozen stock, cells need to be quickly thawed at 30^{o}C then transferred to a 25cm^{2} flask containing 5 ml of room temperature complete Schneider's Medium. The cells were resuspended in and centrifuged at 1000 x g for 5 minutes then incubated at 28^{o}C for 30 minutes the supernatant was discarded to remove DMSO present in the storage medium. The cells were resuspended in 10ml fresh complete Schneider's medium and split into 2 25cm^{2} tissue culture flasks (5ml each). Next, cells were incubated at 28^{o}C for 3-4 days until they reached a density of 6-20 x10^{6} cells/ml.

- Passaging S2 cells

When cells reached an optimum density of 6-20 x 10^6 cells/ml, the most adherent cells were selected for by gently tapping the flask to remove the least adhered cells and discard the excess. Then, 10 ml was added of fresh complete medium and by pipetting up and down the conditioned medium several times the clumps of cells will be broken and wash the surface of the flask to remove adherent cells. The cells were split at a 1:2 to 1:5 dilutions into new culture vessels and fresh Complete S2 Medium added to create a final density of 2-4 x 10^6 cells/ml. The cells were then incubated at 28^{o}C until an optimum density was reached.

- Freezing S2 cells

To create a frozen stock, cells were grown to a density of 1-2 x 10^7 cells/ml and pelleted by centrifuging at 1000 x g for 5 minutes. The cells were then washed in 10 ml PBS and pelleted again before being resuspended at a density of 1.1 x 10^7 cells/ml in Freezing Medium (45% (v/v) conditioned Complete S2 Medium, 45% (v/v) fresh Complete S2 Medium, and 10% (v/v) DMSO). 1 ml of the cell suspension was aliquoted per vial and the cells were frozen in a control rate freezer to - 80^{o}C for 24 hours before being transferred to liquid nitrogen for long term storage.

2.3 Growth and maintenance of *Drosophila*

Fly stocks were kept at 18°C, 22°C or 25°C on standard yeast/dextrose medium (1% (w/v) agar, 7.3% (w/v) dextrose, 5% (w/v) yeast, 6.7% (w/v) organic wholemeal flour, 0.25% (v/v) nipagin, 0.3% (v/v) propionic acid) in 30/50ml vials or 250ml

bottles as appropriate. Flies were anaesthetised with CO_2 and examined using Nikon SMZ-645 or Nikon SMZ-800 microscopes and Photonics 200 light sources using standard fly-pushing techniques (Roberts, 1998, Greenspan, 2004). Fly stocks were ordered from the Vienna *Drosophila* RNAi Centre (VDRC, Austria), The National Institute of Genetics (NIG-FLY, Japan) and The Bloomington Stock Centre (Indiana, USA). Crosses were kept at 25°C and transferred to fresh vials every 2-3 days.

2.3.1 *Drosophila GAL4* stocks employed

- *da-GAL4*

w; 13B/CyO; *da-GAL4*/MKRS Ubiquitous expression of GAL4 under the control of daughterless.

- *en-GAL4*

w; *enGAL4*/CyO Expresses GAL4 in the posterior compartment of embryonic segments in the pattern of the *engrailed* gene.

- *hs-GAL4*

w; *hsp70-GAL4*/ *hsp70-GAL4* Heat shock inducible ubiquitous expression of GAL4.

- *MS1096-GAL4*

MS1096-Gal4 on X Expresses GAL4 across the wing pouch in early third instar larval wing discs and predominantly in the in dorsal half of the wing disc in mid-late third instar larvae.

2.4 Polymerase Chain Reaction (PCR)

2.4.1 Taq Polymerase (Qiagen)

The *Taq* PCR Master Mix Kit (Qiagen) was used for all PCR reactions where not specified. Reactions were set up in a final volume of 20µl as shown in (Table2.1) . Conditions for most PCR reactions are shown in (Table2.2).

Table 2.1. PCR reaction components

Component	Volume (µl)
Mastermix	10
Forward Primer (10µM)	1
Reverse Primer (10µM)	1
cDNA (~2µg)	-
H_2O	to 20

Table 2.2. PCR reaction conditions

Temperature (°C)	Time	No of Cycles
94	3 min	1
92	30s	
54	30s	30
72	40s	
72	40s	1
4	∞	-

2.4.2 Pfx PCR

Pfx amplification was done using the Platinum® *Pfx* DNA Polymerase Kit (Invitrogen). Reactions were set up in a 20µl volume. Reaction components (Table2.3) and reaction conditions (Table2.4) are shown below.

Table 2.3. *Pfx* amplification reaction components

Component	Amount
10 × *Pfx* amplification buffer	2µl
50mM $MgSO_4$	0.4µl
10mM dNTPs (Qiagen)	0.6µl
10µM Forward Primer	1µl
10µM Reverse Primer	1µl
Pfx enzyme	0.25µl
Vector clone DNA	50ng
H_2O	to 20µl

Table 2.4. *Pfx* reaction conditions

Temperature (°C)	Time	No of Cycles
94	3 min	1
92	20s	
55	30s	30
68	2min/kb	
68	10min	1
4	∞	-

2.5 List of oligonucleotides

All oligonucleotides were designed using primer3 and synthesised by MWG Biotech. The primers were diluted in TE buffer (Sigma, pH 8.0) according to the manufacturer's recommendations to make 100 µM stock and stored at -20 ^{o}C. A dilution of 10 µM was made with ultrapure water to use for PCR and sequencing reactions. Sequencing was performed by GATC Biotech.

- Making double mutation

-F816A+: 5'- CAGAAGAAGGTCTCCGCCGCCGATGACCCCGTG -3'

-F816A-: 5'- ACGGGGTCATCGGCGGCGGAGACCTTCTTCTGGG - 3'

- Primers for testing pico insertion

-M13-fwd: 5'- TTGTAAAACGACGGCCAGTC - 3'

-M13-rev: 5' -TGCCAGGAAACAGCTATGAC -3'

- Sequencing primers for *pico* constructs

-Pico_Seq1: 5'- GGCATGATGGTCCAACCGC -3'

-Pico_Seq2: 5'- GGGCTGCGGACACGTGACC -3'

- Pico_Seq3: 5'- CTGTTCCACGGCCACAACGTG -3'

- Pico_Seq4: 5'- ACGCCTTCGATAGCGAGTTC -3'

- Pico_Seq5: 5'- GCTGTCGCTGGCCTCCCTG -3'

- Pico_Seq6: 5'- TGAGCAGCCTGTCCAACGGC -3'

2.6 Agarose gel electrophoresis

DNA molecules were separated by size using agarose gel electrophoresis. According to Sambrook, 2001, agarose gels were prepared and run. Ethidium bromide (Sigma) was added to the gel at a final concentration of 0.2-0.5 μg/ml. 1 X loading buffer (10 X agarose loading buffer, 30% (v/v) glycerol, 0.35% (v/v) bromophenol blue) were added to samples before being loaded on the gel. The samples were electrophoresed in 1 x TAE at 100 volts for 30-45 minutes, using a GIBCO BRL electrophoresis power supply and Fisher Brand gel tank. To determine DNA concentration as well as fragment size, 5μl SmartLadder I (Eurogentec), a molecular weight marker, or Hyperladder I (bioline) was loaded. An ultraviolet light source (UVi-tech) was used to visualise the DNA fragments and documented with a PULNiX TM-300 video camera system and Syngene UP-895MD video graphic printer.

2.7 Gel extraction

DNA fragments were cut from the gel using a scalpel blade under a UV light then purified using the QIAquick Gel Extraction Kit (Qiagen) according to manufacturer's instructions. Briefly, agarose was dissolved in an optimised buffer containing a pH indicator, to determine the optimal pH for DNA binding. DNA is purified by binding to an anion-exchange membrane, washed and eluted in an

appropriate volume of TE buffer. DNA could only be semi-quantified by gel electrophoresis because of the nature of the protocol.

2.8 Restriction digestion

Restriction digests were performed using enzymes and compatible buffers (New England Biolabs) as per the manufacture's guidelines. Typically, 20 µl reactions were carried out using 1×enzyme buffer, 0.4-1µl (3 units) of each enzyme, 0.2µl BSA and 0.3/0.4µg DNA for diagnostic digests or 1µg DNA for gel purification. For double or triple digests, buffers compatible with all enzymes were used. Reactions were incubated at 37°C in a hot block or water bath for 2-3 hours or at 25°C (room temperature) overnight.

2.9 DNA ligation

Products produced from the digestion step were run on an appropriate percentage agarose gel and the gel extraction protocol was used for fragments extraction. Complementary linear DNA fragments formed from digestion and extraction were ligated into circular plasmids using a T4 DNA ligase Kit (Roche). For ligation, two fragments totalling an approximate 3:1 molar ratio of insert:vector were used The following equation was used to calculate appropriate amounts of DNA to use for a 3:1 molecular ratio:

$$\frac{ng\ of\ vector \times kb\ size\ of\ insert}{kb\ size\ of\ vector} \times \text{Insert: vector molar ratio= ng of insert}$$

Depending on experimental success, molecular ratios could be altered. One unit of T4 DNA ligase was incubated with a total of 100 ng of DNA in T4 reaction buffer (Roche). Reaction volumes were kept at 20 µl as per manufacturer's guidelines. Reaction mixtures were incubated at 16°C for 20 hours before 2-4µl of the ligation

reaction was transformed into One Shot® Top 10 chemically competent *E. coli* (Life technologies). Ligations were screened by PCR and restriction digestion before sequencing was carried out.

2.10 Gateway LR Recombination Reaction

The Gateway LR Clonase™ II Enzyme Mix (Life Technologies) was performed to shuttle the Pico wild type and mutant construct from the entry vector pDONR^{TM}221 into the desired destination vectors pTVW (*Drosophila* Genomics Resource Center). Giving a final volume of 8 µl, 50 -150 ng of the entry clone containing the gene of interest was mixed with 1µl (150ng/µl) of the destination vector and TE buffer pH 8.0. Before adding 2 µl of the LR Clonase™ II Enzyme Mix to the reaction, the enzyme mix was thawed on ice for 2 minutes then vortexed briefly. Reactions were incubated at 25^{o}C for a minimum of 1 hour, although overnight incubation is recommended for large plasmids (over 10 kb). Following incubation, the reaction was stopped by adding 1 µl of Proteinase K (Invitrogen) solution and incubated at 37^{o}C for 10 minutes. 1 µl of the reaction mix was then transformed into One Shot® Top10 Chemically Competent Cells (Life Technologies). The transformed cells were plated onto ampicillin-LB agar plates and incubated at 37^{o}C overnight. Colonies were screened by restriction digestion.

2.11 Transformation of TOP10 chemically competent cells

For every two transformations, one vial (50µl) of One Shot® Top10 Chemically Competent Cells (Life Technologies) was thawed on ice split between two fresh microcentrifuge tubes and 1-5 µl of the DNA added and mixed gently, incubating the cells on ice for 30 minutes, then heat shock at 42^{o}C for exactly 30 seconds. Following, the cells were placed on ice for two minutes and 200 µl of pre-warmed

S.O.C Medium (Life Technologies) was added to each reaction. In a shaking incubator the microcentrifuge tubes were placed horizontally at 225 rpm for 1 hour at 37^{o}C before spreading each transformation reaction on pre-warmed selective LB agar plates using sterile technique. The plates were inverted and incubated overnight at 37^{o}C. 24 hours later colonies were picked using sterile technique and propagated in 6ml LB broth plus selective antibiotic overnight at 37°C with shaking at 225rpm. Plasmid DNA was purified as in 2.12.

2.12 DNA extraction from culture

Small-scale plasmid purification (≤20 μg) was carried out using QIAprep Spin Miniprep Kits (Qiagen), while medium (≤100 μg) and large-scale (≤2.5 mg) plasmid purification was carried out using QIAfilter Plasmid Midi kits or Mega kits (Qiagen) respectively according to the manufacturer's instructions. Briefly, in selective LB media cells were grown overnight then, were pelleted at approximately 4500rpm for 5 minutes and the supernatant removed. Cells were then lysed under alkaline conditions and debris removed by centrifugation (mini) or filtering (midi). Clear cell lysates were applied to columns containing a silica gel membrane capable of binding DNA, yet allowing contaminants to be washed away. DNA was eluted from the columns with an appropriate volume of Qiagen Elution Buffer or TE buffer. The concentration of DNA obtained was then measured using a NanoDrop (see section 2.13). DNA was stored at -20°C until use.

2.13 DNA quantification

A Thermo scientific NanoDrop^{TM} 1000 Spectrophotometer was used for quantifying DNA concentrations according to the manufacturer's instructions. The NanoDrop uses a 1-2 μl sample held in place by surface tension of the liquid and measures

absorbance of the sample over a 220nm-750nm spectrum, reporting DNA concentration and relative purity of the sample with 230/260 and 260/280 ratio measurements. DNA could also be semi-quantified by analysing the intensity of DNA run on an agarose gel compared to reference ladder of known concentration.

2.14 Vector storage

Working purified DNA stocks were stored at -20°C. A frozen bacterial stock of each vector was prepared by adding glycerol to cultures to a final concentration of 15% and stored at -80°C.

2.15 DNA sequencing

DNA sequencing was carried out by GATC Biotech (Germany), (http://www. gatc-biotech.com/en). DNA was provided for a total of 6 reactions at a concentration of 30- 100 ng/µl (typically 50ng/µl) in a total volume of 20 µl DNA diluted in ultra pure ddH_2O.

2.16 Insertion of constructs into flies

Transgenic flies expressing the Venus tagged Pico constructs under the control of the upstream activator sequence (*UAS*) were generated through *P*-element mediated germline transformation by Genetic Services Inc (Cambridge, MA, USA) (Rubin and Spradling, 1982, Sentry and Kaiser, 1992). The Pico constructs were injected into w^{1118} embryos along with the helper plasmid pUC*hs*Delta2-3, which provided a source of *P*-element transposase. The progeny were screened for non-white eyes indicating that the constructs, which carried a $white^{+}$ minigene, had successfully been transformed into the germline cells. The chromosome harbouring each independent insert was determined by crossing individual transgene-carrying males

to *w; Tft/CyO* and then crossing the progeny to *w; Tft/CyO; MKRS/TM6B*. Each insert was then balanced with an appropriate, dominantly marked, balancer chromosome (Greenspan, 2004). Verification and analysis of ectopic protein expression was carried out by visualisation of fluorescent Venus in larvae carrying the *engrailed-GAL4* driver and one copy of the transgene of interest or by western blot using GFP antibody.

2.17 Transfection of S2 and S2R+ cells

2.17.1 Transient transfection with Effectene®

For transient transfection in 6 well dishes, S2R+ cells were plated at 2×10^6 cells in 4ml complete Schneider's medium (approximately 60% confluency) and allowed to adhere for a minimum of 2 hours under normal conditions. Before transfection, the Schneider's medium was removed and replaced with 1.6ml of fresh medium. The cells were then transfected using the Effectene® Transfection Reagent as per manufacturer's instructions (Qiagen). Briefly, 0.8 μg of total plasmid DNA was diluted with EC buffer to a volume of 100μl and condensed by adding 6.4μl of Enhancer. The mixture was vortexed for 1s, incubated for 5 minutes at room temperature and then centrifuged briefly. 20μl of Effectene transfection reagent was added to the DNA-enhancer mixture, mixed by gently pipetting up and down then incubated for 15-20 minutes at room temperature to allow complex formation. 600μl of fresh complete Schneider's medium was added to the transfection tube, mixed by pipetting up and down twice and directly added drop-wise onto the cells in the 6-well plates. Swirling the plates gently to ensure the transfection solution was

properly diffused. Cells were incubated for 48-72 hours following transfection to enable suitable gene expression.

2.18 Immunoprecipitation

2.18.1 GFP-Trap immunoprecipitation of GFP tagged proteins

Cells were pelleted by centrifugation at 4000 rpm for 3 minutes and the supernatant removed. For immunoprecipitate GFP tagged proteins, the magnetic GFP-Trap®_M kit (Chromotek) was used. 125 µl of ChromoTek lysis buffer (plus 1mM PMSF [SIGMA] and 1×Protease Inhibitor Cocktail) was added to each sample for resuspening the cells. The samples were placed on ice for 30 minutes with extensive pipetting every 10 minutes. The lysate was then centrifuged at 13,000 rpm for 10 minutes at 4°C to pellet the cells before the supernatant was carefully removed using a pipette, transferred to a pre-cooled 1.5 ml labelled eppendorf tube and set on ice. The supernatant was diluted to 500 µl with ice-cold Chromotek dilution buffer (plus 1mM PMSF and PIC). 50 µl samples were removed to act as a positive control. Next, 20 µl of GFP-Trap magnetic beads were equilibrated by washing three times in 500 µl ice cold ChromoTek dilution buffer. Between each wash step the beads were pulled down using a DiaMag1.5 magnetic separator (Diagenode) and the buffer removed. Once equilibrated, the *Drosophila* lysate was added to the beads and subjected to over-end mixing for 2 hours at 4°C. Following the 2 hour incubation, the GFP-Trap beads were pelleted using the magnetic separator and the supernatant removed. The beads were then washed two times with 500 µl ice cold ChromoTek dilution buffer before being boiled for 20 minutes in 100 µl 2x SDS-Sample buffer at 95°C. The beads were once again pulled down using the magnetic separator and the

remaining supernatant transferred to a 1.5ml tube and loaded onto a polyacrylamide gel for SDS-PAGE (see section 2.19) or stored at -20°C until use.

2.19 SDS-PAGE

Proteins were separated on the basis of molecular weight on SDS-polyacrylamide gels as described in Sambrook, 2001. In brief, The protein extracts were run on Tris-buffered SDS-polyacrylamide gels, made according to Table 2.5 or purchased from Bio-Rad (7.5% or 12% Mini-PROTEAN® TGX™ Precast Gels), in 1 x Running Buffer, with the acrylamide concentration of the separating gel varying depending on the size of the proteins being separated. 5µl Precision Plus Protein™ WesternC™ prestained protein standards (Bio-Rad) was employed to allow the size of separated proteins to be estimated. Mini-Protean II Vertical Electrophoresis apparatus (Bio-Rad) was used according to manufactuer's instructions. Samples were run at approximately 100 volts with time varying depending on the size and level of separation required.

Table 2.5. Components for SDS-PAGE gels

Component	Separating Gel (10ml)					Stacking gel
	6%	8%	10%	12%	14%	(5ml)
40% Acrylamide (Sigma)	1.5ml	2.0ml	2.5ml	3.0ml	3.5ml	0.625ml
1.5M Tris-HCl pH 8.8.	2.5ml	2.5ml	2.5ml	2.5ml	2.5ml	2.5ml
1M Tris-HCl pH 6.8	-	-	-	-	-	0.63ml
10% SDS	0.1ml	0.1ml	0.1ml	0.1ml	0.1ml	0.1ml
DdH_2O	5.9ml	5.3ml	4.8ml	4.4ml	3.9ml	3.6ml
10% APS	0.1ml	0.1ml	0.1ml	0.1ml	0.1ml	0.1ml
TEMED	5µl	5µl	5µl	5µl	5µl	5µl

2.20 Western blotting

Following sufficient separation of proteins by SDS-PAGE, proteins were transferred overnight at 25 volts and 4^{o}C onto a nitrocellulose membrane (Amersham Hybond ECL, GE Healthcare). Before setting up the transfer apparatus the membrane was pre-wetted in Tris-Glycine transfer buffer, using Bio- Rad electrophoretic transfer apparatus as per manufacturer's instructions. After blotting, membranes were stained briefly with Ponceau S solution (Sigma Aldrich) to determine adequate

electrophoretic transfer and to label the lanes with a pencil. Membranes were rinsed with water and 0.1% PBST or TBST to remove the stain.

Membranes were incubated in blocking buffer (PBST or TBST + 5% w/v Marvel skimmed milk powder) for 90 minutes, at room temperature, to reduce non-specific binding of the antibody before being incubated for overnight at 4°C with a suitable primary antibody, diluted in blocking buffer, under optimised conditions detailed in Table 2.6 Membranes were then washed three times in PBST or TBST for 10 minutes and incubated with an appropriate horseradish peroxidase (HRP)-conjugated secondary antibody (Table 2.7), plus StrepTactin-HRP conjugate (1:10,000, Bio-Rad) for detection of the protein standards in blocking buffer for 2 hours at room temperature on a roller. Next, membranes were washed three times in PBST or TBST for 10 minutes and once in PBS for 10 minutes. SuperSignal® West Pico chemiluminescent substrate (Pierce) was used to detect the HRP-conjugated secondary antibodies on the membrane. The chemiluminescent signal was detected and imaged using the ImageQuant™ LAS 4000 Biomolecular Imager (GE Healthcare) or by exposure to Amersham Hyperfilm ELC (GE healthcare) for a length of time dependent on the signal intensity and then developed and fixed using Kodak GBX developer and fixer according to the manufacturer's instructions.

Table 2.6. Primary antibodies used in western blots

Primary Antibody	Supplier	Species	Concentration
MAPK	Cell Signalling	Rabbit	1:2000
RFP	Chromotek	Rat	1:1000
SRF	Active Motif	Mouse	1:200
GFP	Life technologies	Rabbit	1:1000
β -Actin	Merck Millipore	Mouse	1:1000000

Table 2.7. Secondary antibodies used in western blots

Secondary Antibody	Supplier	Species	Concentration
Anti-mouse HRP	Cell Signalling	Goat	1:2000
Anti-rabbit HRP	Cell Signalling	Goat	1:2000
Anti-rat HRP	Cell Signalling	Goat	1:2000

2.21 Western blot analysis

A membrane was scanned and intensity was computed using Image Studio Lite software V5.2 (LiI-COR Biotechnology, UK Ltd). For relative quantification, equal sized rectangular boxes for each antibody were drawn around images of the bands and the mean value for each protein band was calculated. To correct for slight loading differences, the intensity of each band was divided by that of actin. Finally the mean values of three separate experiments ± SE were recorded.

2.22 Dissection and Immunofluorescence

2.22.1 Dissection and staining of wing and eye discs for fluorescence microscopy

Tissues were dissected from wandering third instar larvae in cold 1× PBS, transferred to a watchglass, and fixed with 3.7% (v/v) paraformaldehyde in PBS for 20 minutes at room temperature. Tissues were subjected to three 10-minute washes with 1× PBS and then blocked with PBST + 5% (v/v) FCS for 30 minutes at room temperature or a minimum of 2 hours at 4°C. tissues were then incubated with primary antibodies diluted in PBST + 5% (v/v) FCS (Table 2.8) overnight at 4^{o}C and then washed a further three times((10 minutes per wash) in PBST. Secondary antibodies diluted in PBST + 5% FCS (Table 2.9) added to the tissues and incubated at room temperature in the dark for two hours. The tissues were then subjected to a further two 15 minutes PBST washes and one 15 minutes wash in PBS. Lastly, tissues were mounted in 17.5µl of Vectashield mounting medium (Vector Laboratories) on a standard glass microscope slide and covered with a coverslip (22mm × 22mm). The slides were sealed with clear nail polish and slides stored in the dark for no longer than a week at 4^{o}C.

Table 2.8. Primary antibodies used in wing and eye discs staining

Primary Antibody	Supplier	Species	Concentration
Anti-MMP	DSHB	Mouse	1:10
Anti-RFP	Chromotek	Rat	1:1000
Anti- pJNK	Cell Signalling Technology	Rabbit	1:1000
Anti-Repo	DSHB	Mouse	1:10
Anti-SRF	Active motif	Mouse	1:200
Anti-cleaved caspase- 3	Cell Signalling Technology	Rabbit	1:100

Table 2.9. Secondary antibodies used in wing and eye discs staining

Secondary Antibody	Supplier	Species	Concentration
Anti-mouse AF555	Invitrogen	Goat	1:500
Anti-mouse AF633	Invitrogen	Goat	1:500
Anti-rabbit AF488	Invitrogen	Goat	1:500
Anti-rabbit AF555	Invitrogen	Goat	1:500
Anti-rabbit AF633	Invitrogen	Goat	1:500
Anti-Rat AF555	Invitrogen	Goat	1:500
Anti Rat AF633	Invitrogen	Goat	1:500

2.23 Generation of clones by FLP/FRT mediated recombination

Crosses were allowed to lay for 48 hours. Embryos were left to develop for a further 48 hours and then heat shocked in a 37°C water bath for 1 hour. Wing discs were dissected from third instar larvae at 48 hours post heat shock.

2.24 Confocal microscopy

Tissues prepared using the above immunostaining protocols were examined using an LSM 710 or LSM 780 confocal microscope (Zeiss) and Zen 2011 confocal software (Zeiss) equipped with 405nm, 488nm, 561nm and 633nm lasers. GFP and Venus fusion proteins were excited at 488nm using an argon laser. Fluorescence was measured by the 32-channel internal detector and images visualised using Zen 2011 Lite (Zeiss). Wing and eye discs were assessed by multiple 2.5μm slides z-stacks.

Table 2.10. Antibodies and stain used for confocal microscopy

Name	Type	Supplier	Concentration	Laser (nm)
TO-PRO®-3	Fluorescent stain	Life Technologies	1:1000	633
Alexa Fluor® 555 Phalloidin	Fluorescent dye	Life Technologies	1:500	561
Alexa Fluor® 633 Phalloidin	Fluorescent dye	Life Technologies	1:500	633
Alexa Fluor® 488	Secondary antibody (Goat)	Life Technologies	1:500	488
Alexa Fluor® 555	Secondary antibody (Goat)	Life Technologies	1:500	561
Alexa Fluor® 633	Secondary antibody (Goat)	Life Technologies	1:500	561

2.25 Image analysis

Images were prepared using Fiji (ImageJ). Then, Images were imported to Adobe Photoshop and adjusted for brightness and contrast uniformly across entire fields. Omero figures were also used.

2.26 Wing size analysis

For wing preparations, appropriate adult flies were stored in 70% (v/v) ethanol for at least 24 hours to dehydrate and preserve the wings. Wings were removed from flies using dissection tweezers (Dumont Medical) and placed on a microscope slide to dry. Twenty-five wings, from individual flies, were dissected per genotype. Once dry, the wings were transferred to a small drop of mounting medium (1:1 methylsalicylate/ Canada balsam) where air bubbles could be removed. The wings were then transferred to a fresh 15µl drop of mounting medium on a new slide and covered with a coverslip. The slides were examined using a Leica MZ10F microscope. A Leica DFC420 digital camera and Leica application suite software (Version 2.8.1) were used to take images of the tissues. Wing areas were measured using the polygon tool within ImageJ to mark the area of the wing to be measured, and the area calculated using the measurement function.

3 Monitoring SRF-dependent gene expression *in vivo*

3.1 Introduction

3.1.1 Reporter genes

Reporter gene technology is used for monitoring the cellular events and transcriptional responses associated with signal transduction. The term reporter gene is used to define a gene with a readily measurable phenotype that can be distinguished easily over a background of endogenous proteins (Alam and Cook, 1990). Generally, reporters can be selected according to their sensitivity, dynamic range, convenience, and reliability of their assay (Alam and Cook, 1990, Bronstein et al., 1994, Wood et al., 1995, Suto et al., 1997). Reporter gene technology involves alteration in gene activity by defined *cis* regulatory sequences (response elements), which are responsive to alterations in gene expression and regulation inside the cells. There are several hormones and growth factors that have been shown to stimulate target cells through activating second messenger pathways that regulate the phosphorylation of specific nuclear factors to alter gene transcription (Karin, 1994).

lacZ-encoded β-galactosidase is one of the reporter genes that has been used as a valuable tool for cell and developmental biologists (Naylor, 1999). The activity of β-galactosidase, which is comprised of a homotetramer of 116-kDa subunits, in a cell or fixed tissue, can be monitored colorimetrically with its substrate 5- bromo-4-chloro-3-indolyl-β-D-galactopyranoside (X-gal), which produces a blue precipitate upon cleavage. In live cells, the enzyme's activity can also be detected fluorometrically with the synthetic substrate, fluorescein-β-digalactopyranoside

(FDG) (Rotman et al., 1963). By cleaving FDG, free fluorescein is produced which can be then detected in live cells using epifluorescence microscopy or flow cytometry. Although the combination of β-galactosidase/FDG has been used in FACS, it has some shortcomings (Nolan et al., 1988). Firstly, the FDG cannot readily cross the plasma membrane, because it is polar. Cells must be exposed to a harsh hypotonic shock procedure to introduce FDG inside them, which leads to uneven substrate loading. This uneven substrate loading affects the fluorescence signal intensity from the cells that depends on both enzyme and substrate concentrations. Secondly, the free fluorescein produced by cleavage of FDG rapidly diffuses out of the cell. To reduce this efflux, cells must be kept on ice during the entire loading period. Although there are several problems associated with the β-galactosidase/FDG system, it has been used as a tool for studying protein-protein interactions in live cells (Rossi et al., 2000).

Green fluorescent protein (GFP) is another commonly used reporter (Tsien, 1998). GFP is a protein that was originally isolated from the jellyfish *Aequorea victoria* and fully characterised by Cody et al (Cody et al., 1993). The value of GFP lies with its unique autofluorescence properties, as it does not require the presence of any cofactors or substrates to generate its green light (510 nm); thus, intracellular events can be studied in intact living cells easily. In 1991, the gene for GFP was cloned (Prasher et al., 1992), and numerous GFP mutants are now available, which exhibit improved fluorescence properties over wild-type GFP (Misteli et al., 1997, Welsh et al., 1997).

The main advantage of the green fluorescence protein is that it is noninvasive and inherently fluorescent so it does not require substrate for detection. In addition, two or more genes in the same cell can be tracked by an investigator using different spectrally-resolved mutants of GFP. Since GFP is a non-enzymatic reporter, its limit of detection is approximately 10^5 molecules/cell. The low sensitivity of GFP undermines its effectiveness as a good reporter system.

3.1.2 Serum reponse factor signalling is induced by two key pathways

Serum response factor (SRF), a ubiquitously expressed member of the MADS box family of transcription factors, is considered as the master regulator of the actin cytoskeleton (Miano et al., 2007). It plays essential functions in multiple cellular processes, for example, cell contractility, migration, cell growth, and cell differentiation in several tissues and cell types (Miano et al., 2007).

In the human proteome, SRF is considered to be one of the best-understood DNA-binding proteins. The laboratory of Richard Treisman was the first to define the DNA-binding properties of SRF (Treisman, 1986, Norman et al., 1988); while SRF has relatively low intrinsic transcriptional activity, its interaction with over 60 cofactors confers strong transactivation potential in a cell- and context-specific manner.

There are at least two major signalling pathways that converge on SRF to direct SRF-dependent gene expression, Figure 3.1 (Posern et al., 2006, Pipes et al., 2006). The classic pathway involves stimulation of growth factor and mitogen-activated protein kinase signalling leading to the phosphorylation of the SRF cofactor, and the

activation of growth-related genes (Shaw et al., 1989, Janknecht et al., 1993). Rho-dependent changes in actin dynamics is a second regulatory pathway (Sotiropoulos et al., 1999b). In this pathway, the ratio of globular actin (G-actin) to fibrillar actin (F-actin) is lowered by the signal inputs, releasing the binding of myocardin-related transcription factor-A (MRTF A)/MAL to G-actin, leading to nuclear accumulation of MAL and subsequent SRF-dependent gene expression (Miralles et al., 2003). SRF binds as a dimer to at least 1216 permutations of a 10-bp segment of DNA known as the CArG box. CArG boxes can be found mostly in the first intron of hundreds of experimentally validated or hypothesized target genes and in the proximal promoter (Philippar et al., 2004, Sun et al., 2006, Balza and Misra, 2006, Niu et al., 2007, Verdoni et al., 2008, Selvaraj and Prywes, 2004, Zhang et al., 2005, Cooper et al., 2007). Bioinformatics and Microarrays studies have revealed a disproportionate number of SRF-target genes encoding for elements of the actin cytoskeleton (Philippar et al., 2004, Sun et al., 2006, Balza and Misra, 2006, Verdoni et al., 2008).

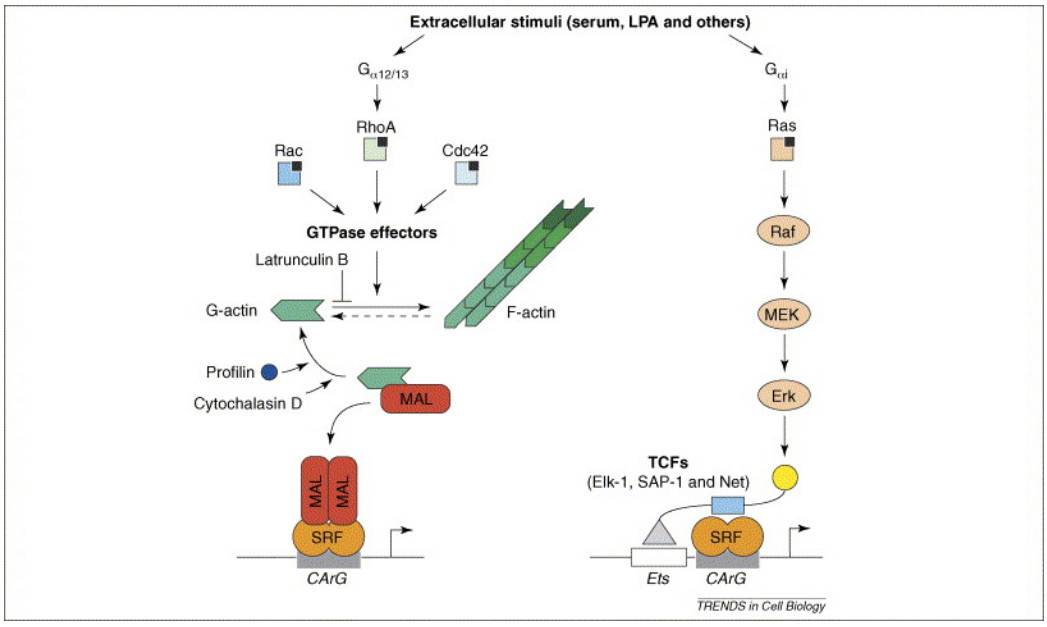

Figure 3.1. Model of two pathways regulating Serum Response Factor (SRF) activity. Both Rho-dependent (left) and Ras-dependent (right) signaling are activated by extracellular inputs. MAP kinase pathway is activated through Ras, Raf, MEK and ERK leading to phosphorylation of TCFs. TCFs then bind to their own sequence-specific target sequence (Ets motif, depicted) and to SRF. Activation of signalling through Rho family GTPases results in dissociation of MAL from G-actin, and accumulation of MAL in the nucleus where it binds and activates SRF (Posern and Treisman, 2006).

Mammalian tissue culture cells have been used to confirm that SRF activity is regulated by changes in actin dynamics (Sotiropoulos et al., 1999). Experiments using latrunculin and C2 toxin, which are actin polymerization inhibitors, have been shown to inhibit the expression of SRF reporter genes (Sotiropoulos et al., 1999). In contrast, preventing F-actin disassembly by jasplakinolide or promoting *de novo* actin polymerization by VASP and WASP can induce the activation of SRF (Grosse et al., 2003, sotiropoulos et al., 1999). Importantly, it was also found that SRF is strongly activated by promoting G-actin dimerization using swinholide A and cytochalasin D but not by inducing polymerization *per se*. This indicates that SRF dependent-transcription occurs particularly as a result of G-actin depletion rather than as a response to increased levels of F-actin (Sotiropoulos et al., 1999).

3.1.3 Mal/MRTF regulates the response of SRF to altered actin dynamics

SRF activation that results from decreasing G-actin levels has been found to be mediated by myocardin and myocardin-related transcription factor (MRTFs), which are transcriptional co-activators of SRF (Miralles et al., 2003) Wang et al., 2001, Wang et al., 2002). MRTFs associate with G-actin via their N-terminal RPEL domains (Miralles et al., 2003), which then continuously cycle between the cytoplasm and the nucleus depending on their bound state. MRTFs are transferred

from the nucleus and remain cytoplasmic when bound to G-actin. MRTFs are imported back into the nucleus when separated from the actin monomers (Posern et al., 2004, Posern et al., 2002). Increasing the actin polymerization rates reduces the G-actin levels in the cytoplasm and nucleus leading to increases of unbound MRTFs, which then become predominantly nuclear (Miralles et al., 2003, Posern et al., 2004, Posern et al., 2002). It has been found that increasing the rates of protein translocation into the nucleus and reducing the rates of MRTF nuclear export result in the relocalisation of MRTFs to the nucleus (Vartiainen et al., 2007). Nuclear MRTF is able to interact with SRF at the promoter of a range of target genes and allow SRF-mediated transcription (Miralles et al., 2003, Wang et al., 2002) (Figure 3.2.).

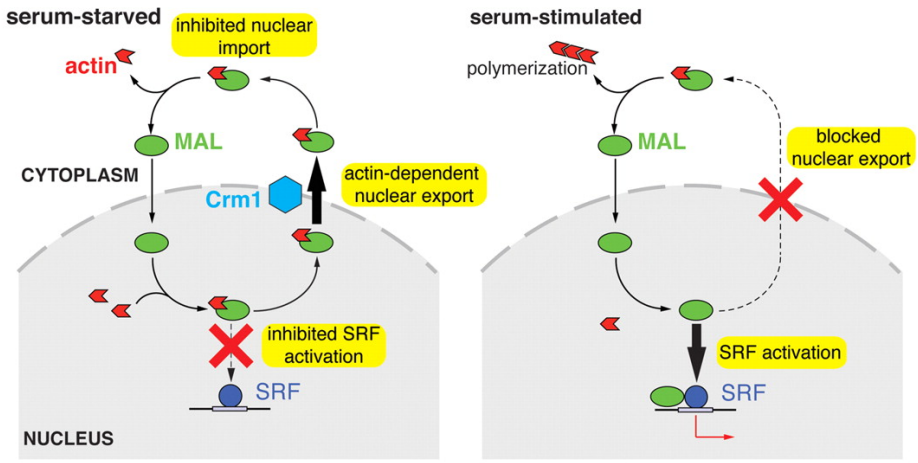

Figure 3.2. MAL interacts with actin in both cytoplasm and nucleus. Multiple roles for actin in MAL regulation. MAL is mainly located in the cytoplasm in unstimulated cells (left), whereas SRF activation is prevented by nuclear actin. Upon stimulation (right), decreased export leads to MAL accumulation in the nucleus, and reduced interaction with actin allows SRF activation (Vartiainen et al., 2007).

3.1.4 MRL proteins and SRF signalling

Studies using a range of species have determined that MRL (Mig-10; RIAM; Lamellipodin) proteins act as scaffold molecules linking upstream growth factor

signalling with downstream effects on the cytoskeleton (Krause et al., 2004, Lafuente et al., 2004, Lyulcheva et al., 2008). For instance, both RIAM and Lpd bind with Ena/VASP proteins and Profilin through their EVH1- and Profilin- binding sites respectively; potentially enabling their recruitment towards the leading edge to facilitate regulation of the actin cytoskeleton (Lafuente et al., 2004, Krause et al., 2004). RIAM and Lpd have been shown to control actin dynamics in an Ena/VASP dependent manner by co-localising with Ena/VASP proteins and filament actin at lamellipodia and filopodia tips (Jenzora et al., 2005, Lafuente et al., 2004, Krause et al., 2004).

Recent studies suggest that MRL proteins play a role in growth control. Overexpression of Pico induced hyperplastic growth at both the tissue and whole organism level in a dose-dependent manner, owing to co-ordinated increases in both cell number and size (Lyulcheva, 2006, Lyulcheva et al., 2008). Knock-down of *pico* in *Drosophila* wing discs led to a reduction in tissue growth by reducing cellular proliferation without an increase in apoptosis (Lyulcheva et al., 2008). Remarkably this growth phenotype seems to be closely linked to the actin/MAL/SRF proliferative pathway. Results from an earlier study indicated that the expression of an SRF-responsive reporter gene in mammalian cell cultures can be increased by overexpression of Pico, whereas a hypomorphic mutation in *blistered* (*bs*), the *Drosophila* SRF homologue, decreased *pico*-mediated wing overgrowth (Lyulcheva et al., 2008). The ability of pico to increase the cellular F:G actin ratio provides an explanation for SRF activation through release of its cofactor MAL bound G- actin (Lyulcheva et al., 2008, Miralles et al., 2003, Settleman, 2003).

3.2 Results

This chapter describes the use of a transcriptional reporter to monitor SRF-dependent gene expression *in vivo*. Results of this work and other work related to this study are reported in the submitted manuscript reproduced below.

3.2.1 Paper summary

Jonchère.V., Alqadri.N., Herbert.J., Dodgson.L., Mason.D., Messina.G., Falciani.F., Bennett.D. (2015). Transcriptional responses to hyperplastic MRL signalling in *Drosophila*

Contributions of Authors:

Jonchère.V: Generated all RNA-Seq data, performed validation by q-RTPCR and performed initial bioinformatics analysis using GO descriptors (Fig.1). Generated the SRE-mCherry reporter construct used in Figure 3. Performed comparative analysis of growth literature and screen of RNAi lines (Fig.7A-B). Performed ChIP (Fig.8A). Contributed to writing and editing the paper.

Alqadri. N: Analysed wing discs of different genetic backgrounds to determine effect on expression of an *in vivo* SRF-responsive reporter gene (Fig.3B) and (fig.5A). Dissected and mounted adult wings to examine whether genes induced by ectopic *pico* were required for *pico*-mediated tissue growth (Fig.7C). Analysed wing discs to determine the role of *deterin* in suppressing proliferation-induced apoptosis during pico-mediated tissue overgrowth (Fig. 8B). Contributed to writing and editing the paper.

Herbert.J*:* Performed PCA bioinformatics analysis on RNA-Seq data (Fig 3A-B-C). Contributed to writing and editing the paper.

Dodgson.L*:* Generated expression construct and transgenic flies for FLAG-SRF. Performed initial experiments validating the use of this reagent for ChIP as done in Fig.8. Contributed to writing and editing the paper.

Mason.D: Developed the image analysis pipeline for quantification of SRE-mCherry expression presented in Figs. 4-5.

Messina.G: Analysed the effect of knocking down pro-survival genes and contributed data to Fig. 7B.

Bennett.D: Conceived and designed the experiments; secured funding for the work; analysed the data; contributed to writing and editing the paper.

3.2.2 – Submitted manuscript

Transcriptional responses to hyperplastic MRL signalling in *Drosophila*

Vincent Jonchère[1,4], Nada Alqadri[1], John Herbert[3], Lauren Dodgson[1,5], David Mason[2], Giovanni Messina[1], Francesco Falciani[3], Daimark Bennett[1,2,*]

1 Department of Biochemistry, Institute of Integrative Biology, University of Liverpool, Crown Street, Liverpool, L69 7ZB, UK

2 Centre for Cell Imaging, Institute of Integrative Biology, University of Liverpool, Crown Street, Liverpool, L69 7ZB, UK

3 Centre for Computational Biology and Modelling (CCBM), Institute of Integrative Biology, University of Liverpool, Crown Street, Liverpool, L69 7ZB, UK

4 Current address: INSERM, UMRS 938-Research Center Hospital Saint-Antoine, Paris, 75012 FR.

5 Current address: North Western Deanery, Salford Royal NHS Foundation Trust, Salford, UK

* E-mail: daimark.bennett@liverpool.ac.uk

Abstract

Recent work has implicated the actin cytoskeleton in tissue size control, but how changes in actin dynamics contribute to hyperplastic growth is still unclear. Overexpression of Pico, the only member of the MRL adapter protein in *Drosophila*, has been linked to tissue overgrowth via its effect on the F-actin sensor Mrtf, and consequently Mrtf's DNA-binding factor SRF, providing a model for mechanistic investigation. Whilst Mal/SRF-induced transcriptional changes have been largely linked to actin biosynthesis and cytoskeletal regulation, we report here that RNA profiling of *Drosophila* wing discs overexpressing *pico* or *mrtf* did not reveal a cytoskeletal gene signature. Indeed, prominent among the common response to *mrtf* and *pico* overexpression was upregulation of ribosome protein and mitochondrial genes, which are known growth drivers and are conserved Mrtf/SRF targets in flies and human cells. Consistent with their ability to induce a common transcriptional response and activate SRF signalling *in vitro*, both *pico* and *mrtf* stimulate expression of an SRF-responsive reporter gene in wing discs. Multiple transcriptional targets are likely to be important for *pico*-mediated overgrowth, but in a functional genetic screen, we also identified *deterin*, which encodes *Drosophila* Survivin, as a Mrtf/SRF target that is necessary for *pico*-mediated tissue overgrowth by suppressing proliferation-associated cell death. Taken together, these data point to an unappreciated effect of Mrtf/SRF on protein biosynthesis and proliferation control under conditions of chronic MRL or Mrtf overexpression, with potential implications for the understanding of growth control during normal development and tumourigenesis.

Introduction

1. Actin cytoskeleton and transcriptional regulation

The actin cytoskeleton has emerged over the last few years as an important regulator of gene expression, with actin being involved both in the direct regulation of transcription complexes but also in the transduction of signals to downstream transcriptional responses via the Serum Response Factor (SRF) and Hippo signalling pathways (Rajakyla and Vartiainen, 2014). In actin-induced SRF signalling, the SRF cofactor Mrtf (Myocardin-Related Transcription Factor) responds to levels of monomeric (G)-actin, which inhibits nuclear import and enhances nuclear export of Mrtf and represses transcriptional activation of SRF target genes (Vartiainen et al., 2007). Correspondingly, actin regulators that drive F-actin formation, including Ena/VASP (Grosse et al., 2003), release the inhibition of Mrtf by G-actin and activate SRF. Increased levels of F-actin, e.g. mediated by anti-Capping protein or by the nucleation factor Diaphanous, also stimulate Hippo target gene expression (Sansores-Garcia et al., 2011, Fernandez et al., 2011) via the transcriptional coactivator Yorkie/YAP/TAZ, which is normally inhibited by Hippo signalling. Correspondingly, disruption of F-actin has been shown to exclude YAP from the nucleus and suppress its transcriptional activation (Dupont et al., 2011, Aragona et al., 2013, Wada et al., 2011). Despite similarities between the regulation of Yorkie/YAP/TAZ and Mrtf-SRF by the actin cytoskeleton, expression of a mutant actin that cannot polymerise inhibits Mrtf signalling (Miralles et al., 2003b, Posern et al., 2002) but has no effect on YAP/TAZ (Dupont et al., 2011), suggesting that the Hippo pathway is not affected by G-actin, but rather might respond to changes in a particular F-actin structure (Aragona et al., 2013, Dupont et al., 2011).

Results obtained in a range of species support the idea that MRL (Mig-10; RIAM; Lamellipodin) proteins act as molecular scaffolds for Ras-like GTPases and actin regulators, including Ena/VASP and the Scar/WAVE complex, to remodel the actin cytoskeleton, linking extracellular signalling to changes in cell adhesion and migration (Lafuente et al., 2004, Krause et al., 2004, Law et al., 2013). Recent evidence suggests that MRL proteins also

play a role in growth control. For instance, in mammalian cells, Lpd knockdown abrogates the effect of EGF on proliferation (Lyulcheva et al., 2008) and abolishes Rac-induced cyclin D accumulation and mechanosensitive cell cycling (Bae et al., 2014). In *Drosophila*, the MRL orthologue, encoded by *pico*, is capable of driving growth of the developing wing, by inducing a coordinated increase in cell size and number (Lyulcheva et al., 2008, Jonchere and Bennett, 2013). Genetic experiments in *Drosophila* have linked *pico*-mediated tissue overgrowth to activation of Mrtf/SRF since overexpression of *mrtf* or *blistered*, which encodes *Drosophila* SRF, induced tissue overgrowth and loss of function in *blistered*, suppressed the effect of *pico* on wing size (Lyulcheva et al., 2008, Han et al., 2004). However, the Mrtf/SRF pathway has predominantly been associated with the expression of cytoskeletal- rather than growth-promoting genes in other contexts (Cenik et al., 2016, Esnault et al., 2014). Consequently, it is not clear which genes might be induced to drive hyperplastic tissue growth and to what extent the transcriptional response to MRL protein overexpression is elicited by the Mrtf-SRF pathway.

Here we have used digital transcriptomics to determine the transcriptional responses to hyperplastic MRL signalling in the *Drosophila* wing imaginal disc. We found little evidence for involvement of the Hippo pathway in *pico*-induced overgrowth, based on minimal effect on the genes used as readouts of pathway activation. Through analysis of the Mrtf-induced transcriptome in wing discs, we identify a common signature representing possible targets of a Pico-Mrtf signalling pathway, with an *in vivo* reporter confirming the ability of *mrtf* and *pico* to drive SRF activation. Although there were clear differences in the transcriptional responses to *pico* and *mrtf* overexpression, notably, we did not see an enrichment of cytoskeletal genes in either condition. Instead, the common transcriptional signature, associated with *mrtf* and *pico*-mediated hyperplastic growth, includes ribosomal protein and mitochondrial genes that are known to be associated with Mrtf/SRF in mammalian cells, but whose significance to Mrtf/SRF function had not established. Functional analysis supports the involvement of a selection of

these genes in growth control including the *Drosophila* Survivin orthologue, encoded by *deterin*, which is required for suppressing apoptosis in discs overexpressing *pico*.

Results

Genome-wide transcriptional changes observed in *Drosophila* wing discs with *pico* overexpression

Overexpression of *pico* with *MS1096-GAL4* (*MS1096>pico*) in the developing larval wing imaginal disc leads to a significant overgrowth of the adult wing (Lyulcheva et al., 2008). To identify molecular signatures of ectopic *pico* expression, we micro-dissected wing imaginal discs from *MS1096>pico* and control (w^{1118}) third instar larvae and determined their mRNA profiles by RNA-Seq. For these experiments four biological replicates were prepared from each strain. A comparison of the overall gene expression profiles of the *MS1096>pico* and control lines is shown in **Fig.S1**. Hierarchical clustering of the replicates, shows close agreement between the different samples of each line **Fig.S1**. Using Cufflinks (see Materials and Methods) we identified a total of 1490 differentially expressed genes (10.7% of 13,895) in wing discs ectopically expressing *pico* (P<0.05, **Table S1**), with 691 and 799 genes under- and over-expressed, respectively.

To identify biological processes that might be affected by ectopic *pico*, we compared the frequency of GO terms (GO) amongst differentially expressed genes using DAVID (Huang et al., 2009). A large number of terms (193) were enriched amongst the underexpressed genes, making it hard to interpret the functional significance of these descriptors. In constrast, only 23 GO terms for biological functions were enriched amongst genes over-expressed in *MS1096>pico* wing discs belonging to 5 main categories (**Fig.1A**), with translation and chromosome organisation being the most significant (P=3.6 e10^{-3} and P=8.4 e10^{-3}, respectively). *Drosophila* specific searches with Flymine also revealed enrichment of ribosome pathways (P=2.7 e10^{-6}, Holm-Bonferroni). We used STRING (Franceschini et al., 2013) to help visualise over-expressed protein networks, which revealed 6 key network hubs genes overexpressed in response to ectopic *pico* (**Fig.1B**): ribosomal proteins, eukaryotic initiation factors (eIFs), heat shock proteins, tubulins, mitochondrial proteins and proteins involved in glycolysis. These

patterns of transcriptional change are consistent with the wing overgrowth phenotype exhibited by animals with ectopic *pico*. To confirm our RNA-Seq results, we selected genes representative of enriched GO categories for quantitative real-time qRT-PCR analysis. Measurements of relative mRNA expression level determined using this method were in close agreement with RNA-Seq data. Indeed, even genes that that were only modestly overexpressed (~1.5 fold) by RNA-Seq were found to be significantly increased when assessed by qRT-PCR (P<0.05, **Fig.2**). The transcriptome dataset therefore accurately captures the expression profile of hyperplastic tissues and contains genes that promote overgrowth induced by ectopic *pico*.

Pico is capable of inducing SRF-responsive gene expression *in vivo*

Actin dynamics have been reported to induce Hippo signalling, a tumour suppressor network regulating growth (Esnault et al., 2014, Sansores-Garcia et al., 2011). However, the absence of any induction of canonical Hippo targets in response to ectopic *pico* suggests that the *pico*-mediated growth is unlikely to be driven by engagement of the Hippo pathway (**Fig.S2**). We previously reported that *mrtf* overexpression phenocopied the effect of ectopic *pico* in the wing and *pico*-mediated overgrowth was sensitive to the levels of *blistered*, suggesting that tissue overgrowth might require SRF-dependent gene expression (Lyulcheva et al., 2008). To test the ability of *pico* overexpression to induce SRF signalling in the wing disc, we generated transgenic flies harbouring an *in vivo* SRF reporter, consisting of an SRF-responsible element (SRE), containing 9 CArG binding motifs ($CC[A/T]_6GG$), upstream of the coding sequence for mCherry (SRE-mCherry) (**Fig.3A**). In wing discs from 3rd instar larvae, expression of SRE-mCherry was often very weak, but recapitulated the expression pattern of SRF protein, which is restricted to intervein cells (**Fig.3B**). Although relatively few SRF-expressing cells expressed the mCherry reporter, 93.1% ±10.6 (mean ±SD, n=5 discs) of cells with detectible SRE-mCherry expressed SRF. Stronger expression of the reporter was detected as the wing disc matured; by pupariation, in animals with two copies of the reporter, mCherry was clearly visible in the pupal wing but not other tissues.

To test the effect of *pico* on the expression of our reporter gene, we overexpressed *UAS-pico* in the posterior half of the wing disc, together with UAS-GFP, under the control of *hh-GAL4*, and measured the ratio of mCherry fluorescence in anterior (GFP-negative):posterior (GFP-positive) cells (**Figures 4, 5**). To ensure signal intensities were in the linear range, laser power was adjusted so that the maximum intensity signal was below the level of saturation for the detectors. Cells in control discs from 3rd instar larvae showed a mean anterior:posterior mCherry ratio of 1:1.4, reflecting the fact there are more intervein cells in the posterior half of the disc. There was a 1.5 fold increase in the mean ratio of mCherry intensity (to 1:2.1) in wing discs overexpressing *pico* compared to the controls (P=0.001). A similar induction (of 1.5 fold) in SRE-mCherry expression was seen in wing discs from white pre-pupae, indicating this effect was not stage specific (**Figure 4**). We also confirmed this effect by pooling intensity measurements from multiple discs and comparing the intensity bias in GFP and non-GFP compartments (**Figure 5B**). This revealed a 1.4 fold increase in the mean intensity of mCherry in the presence of overexpressed *pico* compared to controls (x^2 <0.001). A similar effect was observed for overexpressed *mrtf* (mean fold change 1.9, x^2 <0.001). These data indicate that both *mrtf* and *pico* are capable of inducing the SRE-mCherry reporter gene in the wing imaginal disc, consistent with their reported effects on SRF signalling in mammalian cells (Lyulcheva et al., 2008, Pinheiro et al., 2011).

Upregulation of ribosome and mitochondrial genes is a common response to overexpressed *pico* and *mrtf*

To identify potential targets of Mrtf/SRF signalling that might be subject to regulation by *pico*, we analysed the mRNA expression levels of wing discs overexpressing wild type *mrtf* (*MS1096>mrtf*) by RNA-seq. This revealed a total of 1526 differentially expressed genes (11% of 13,895) in wing discs ectopically expressing *mrtf* compared to w^{1118} controls (*P*<0.05, **Table S1**), with 820 and 706 genes under- and over-expressed, respectively. A comparison of the overall gene expression profiles of the *MS1096>mtrf* lines

and hierarchical clustering of the replicates is shown in **Fig.S1**. Interestingly, we did not observe a significant induction of Actin5C, which has been proposed to be a homeostatic target of Mrtf/SRF in ovaries (Salvany et al., 2014), nor did we see enrichment of GO categories corresponding to cytoskeletal genes amongst the overexpressed genes in DAVID or Flymine (**Table S2**).

To determine the relationship between the effects of *mrtf* and *pico*, we subjected our RNA-Seq datasets to Principal component analysis, which is not subject to thresholding and therefore has the ability to scrutinise all the available transcriptomics data in a non-biased fashion. We took this approach because we reasoned that Mrtf-SRF responsive genes might show modest changes in transcript levels (similar to our reporter gene), but be biologically relevant when individual genes belong to a cohort of genes with related functions that show a consistent change in expression. Principal component analysis identified a divergent (PC1) and common (PC2) response to overexpressed *pico* and *mrtf*, respectively, which together explain approximately 70% of the variance in gene expression (**Figure 6A**). Clustering of the biological replicates for each genotype indicated these responses are highly reproducible.

To determine whether there was any enrichment of genes belonging to functionally-related biological processes, we analysed the distribution of GO terms in the PC1 and PC2 loadings. The signatures associated with the divergent response related to broad GO terms such as morphogenesis, transcription and regulation of cell development (**Figure 6B**). Literature mining of PC1 components identified a significant enrichment in circadian clock genes (*P*=3.3e-8), with 76 Clock target genes (Abruzzi et al., 2011) being associated with the divergent response. Correspondingly, we found differential expression of mRNA for core clock components *timeless* and *clock*, but not *period*, whose human orthologue is a target of Mrtf (Esnault et al., 2014). This suggests that part of the divergent response might be explained by alterations in phasing of the circadian clock.

Strikingly, the overexpression of ribosome protein and mitochondrial protein genes were highly significant common responses to *pico* and *mrtf* overexpression (**Figure 6C**). We wondered whether ribosome genes representing part of the common transcriptional signature (PC2) for *mrtf* and *pico* may be direct targets of Mrtf. To assess this we referred to a dataset of genes known to be bound by Mrtf in *Drosophila* adult ovaries based on ChIP-Seq (Salvany et al., 2014). We examined the overlap between the top 10% of Mrtf-binding sites ranked according to their *P*-value score (Salvany et al., 2014), and the top 10% of upregulated genes in PC2. Contained in this dataset are a total of 19 ribosome protein genes representative of the enriched GO category in PC2. Since ribosome protein genes are highly conserved, we were also able to ask whether these genes represent targets of Mrtf in mammalian cells. 90% of homologous genes were found to be experimentally associated with both SRF and Mrtf in fibroblasts (Esnault et al., 2014).

Identification of differentially expressed genes contributing to *pico*-mediated overgrowth by directed screening

To identify potential effectors of *pico*-mediated tissue overgrowth, we compared the overlap of our transcriptomics data with functional information from three publications (Bjorklund et al., 2006, Schertel et al., 2013, Guest et al., 2011) describing 651 genes involved in cell cycle progression or growth in *Drosophila* (**Figure 7A**). This identified 42 *pico*-responsive genes previously demonstrated to regulate cell cycle progression or cell growth. Of these proteins, 45% (19/42) are ribosomal proteins, 2 belong to tubulin family (α, β tubulin) and 1 is a subunit of eIF3 protein (eIF3p66), and are representative of the protein hubs identified in our GO enrichment and STRING network analyses (**Figure 1**). Next, to assess their role in *pico*-mediated overexpression, we selected 17 genes with heritable RNAi constructs in flies and measured their effect on adult wing size and morphology alone or in the background of overexpressed *pico* driven by *MS1096-GAL4* (**Figure 7B**). This group of proteins included genes described above, other ribosomal proteins, tubulin proteins, mitochondrial proteins and

chromosome passenger complex proteins. RNAi lines for 7 genes (*VhaM9.7-c*; *CG30382*; *RpL24*; *Grip75*; *SH3PX1*; *Jra*; *γTub37C*) did not show any detectable effect on wing size; 3 (Prosalpha5; NP15.6; RpL6) caused larval lethality; 4 others (RpS3; alphaTub85E; RpS27A; RpS17) induced a wing dysmorphology phenotype making interpretation of effects on growth difficult. RNAi for two genes (RpS9 and deterin) showed a significant reduction ($P<0.05$) on the size of *MS1096>pico* wings but not *MS1096-GAL4* controls (**Figure 7B, C**).

Deterin is required for pico-mediated tissue overgrowth

Since *deterin* knockdown had the strongest effect on *pico*-mediated growth we focused our attention on this genetic interactor. *deterin* encodes *Drosophila* Survivin, a member of the inhibitor of apoptosis (IAP) gene family that has been implicated in apoptosis, chromosome segregation and cytokinesis (Jiang et al., 2001, Jones et al., 2000). Firstly, to determine how specific the effects of *deterin* were, we examined whether knockdown of other apoptosis inhibitors, *diap2* and *bruce*, was similarly able to suppress pico-mediated growth. Notably, although both *diap2* and *bruce* knockdown were able to reduce adult wing size, this effect was independent of *pico* overexpression, suggesting that overgrowth driven by *MS1096>pico* was particularly sensitive to the levels of *deterin* and not these other apoptosis regulators (**Figure 7B**).

Human Mrtf and SRF have been shown to associate with the Survivin/BIRC5 promoter in fibroblasts, prompting us to examine whether this is conserved in flies. To establish whether *deterin* is direct target of SRF, we searched the presence of CarG boxes in the *deterin* promoter and found three sites at -1091, -598 and +63 from the transcription start site (TSS). To test SRF binding experimentally we expressed FLAG-tagged SRF in larvae with *da-GAL4*, precipitated tagged SRF from extracts by ChIP and analysed chromatin recovery using qPCR (**Figure 8A**). The site at -598 showed

significant enrichment following ChIP with anti-Flag antibody compared to controls (IgM ChIP in *da>FLAG-SRF* and FLAG ChIP in *da-GAL4* extracts). A comparison with the Mrtf ChIP-Seq dataset (Salvany et al., 2014) revealed a Mrtf-binding site corresponding to the SRF-binding site at -598, suggesting both SRF and Mrtf are capable of associating at this site.

Studies of other growth drivers, such as the miRNA bantam, have demonstrated that genes stimulating cell proliferation can simultaneously suppress apoptosis (Brennecke et al., 2003). Therefore we wondered whether *pico* only drives net proliferation when apoptosis is simultaneously prevented in a *deterin*-dependent manner. To test this, we examined the effect of overexpressing *pico* in wing imaginal discs with or without *deterin* RNAi knockdown (*deterin*^{IR}) using *MS1096-GAL4*. The line of *deterin*^{IR} that we used for these experiments (det$^{TRiP.GL00572}$) is a 21 bp hairpin line with no predicted off-targets with matches greater than or equal to 15 bp (Hu et al., 2013). Cells undergoing apoptosis were identified by activated Caspase 3 staining (**Figure 8B**). As we had previously observed, stimulation of growth by *pico* was not associated with an increase in apoptosis. Similarly *deterin*^{IR} had little effect on its own, but in discs coexpressing *pico* we observed a dramatic increase in the number of cells undergoing cell death (**Figure 8B,C**).

Discussion

MRL proteins are key molecules that modulate the actin cytoskeleton in response to guidance cues to effect changes in cell morphology and migration. Additionally to this role, several lines of evidence suggest that MRL proteins play also an important role in cell growth in normal and pathological conditions (Colo et al., 2012, Bae et al., 2014). This role in growth was highlighted in *Drosophila* where *pico* overexpression resulted in a coordinated increase in cell proliferation and growth (Lyulcheva et al., 2008). Here we have analysed global RNA expression to help delineate pathways linking the regulation of actin dynamics to tissue overgrowth.

Genetic data previously implicated Mrtf/SRF in the ability of *pico* overexpression to drive wing overgrowth. Here, using a genetic reporter, we found that *pico* is capable of activating SRF-responsive gene expression in the *Drosophila* wing imaginal disc. However, although SRF targets in mammalian cells include growth-promoting genes (Sun et al., 2006), the response to Mrtf/SRF activation, at least over short time periods, predominantly involves the induction of genes involved in actin filament dynamics, cell adhesion and extracellular matrix (ECM) synthesis (Esnault et al., 2014). Given this, how does excessive Mrtf/SRF signalling induce hyperplastic overgrowth? Our transcriptome analysis sheds light on this question. Cytoskeletal genes were not identified in our ontology enrichment analysis as being induced either by *mrtf* or *pico* overexpression in the *Drosophila* wing. Instead, the genes belonging to the common *pico*/*mrtf* response are ontologically-related to, and in some cases are direct orthologues of genes associated with mammalian Mrtf/SRF, including mitochondrial and ribosomal protein genes. These genes are potent growth promoters in flies and humans, and our functional analysis provided evidence that at least one of these genes (Rps9) haves a role in *pico*-mediated growth, although it is likely that multiple genes are involved. One such gene is *deterin*, which we propose enables *pico* to overcome proliferation-induced apoptosis and facilitate net tissue overgrowth.

Despite significant overlap in transcriptional responses to *pico* and *mrtf* overexpression, there was also significant divergence in the response, as identified by our principal component analysis. There could be several reasons for this. For instance, although *mrtf* and *pico* overexpression may increase nuclear accumulation of Mrtf by a G-actin titration mechanism, Mrtf dynamics may not be equivalent under the two conditions. Furthermore, differences in actin levels and/or actin dynamics may have additional effects. For instance, nuclear actin, which is constantly exchanging with a cytoplasmic pool (Skarp and Vartiainen, 2013), associates with the basal transcription machinery and chromatin modifying complexes to regulate

chromatin remodelling, epigenetic programming and gene expression (reviewed (Rajakyla and Vartiainen, 2014)). Consequently, although both *mrtf* and *pico* are capable of activating SRF-mediated transcription as measured by our *in vivo* reporter, there are likely to be differences in the chromatin environment, and consequently Mrtf/SRF occupancy, at different native target sites that may influence target response.

Why has a growth signature not been observed to date in mammalian cells following induction of Mrtf signalling? The deterin/survivin homologue BIRC5, as well as counterparts of mitochondrial and ribosomal genes that we identified, show no difference in expression level in mammalian cells upon acute (30 min) serum-induced Rho-actin signalling (Esnault et al., 2014). However, promoters of all these genes are associated with SRF and Mrtf. One possibility is that the differences in transcriptional response may reflect the difference between short versus long-term exposure to Mal/SRF induction. The fact their *Drosophila* counterparts could be induced in wing discs with persistent overexpression of *pico* or *mrtf* might therefore reflect a difference between acute and chronic changes in actin dynamics. Although we did not identify an induction of other transcriptional regulators acting upstream of ribosome biogenesis genes, such as *Dref* (Killip and Grewal, 2012), in response to *pico* overexpression, we cannot rule out the possibility that some of the transcriptional responses are indirect. This issue will require careful dissection of the promoter regions of candidate targets to monitor the chromatin environment, SRF/Mrtf occupancy and identify *cis* acting sequences that might confer temporal control of their expression under conditions of altered actin dynamics. It will be interesting to determine whether “constitutively expressed” genes, which were initially refractory to Mrtf signalling in mammalian cells, become responsive after chronic induction and whether this similarly promotes a proliferative phenotype. Models of increased extracellular matrix (ECM) rigidity might be starting point for this analysis since ECM rigidity has been linked to chronic changes in actin dynamics and nuclear MRTF accumulation (O'Connor et al., 2015) as well as Rac and Lpd-dependent proliferation (Bae et al., 2014). Furthermore,

it will be interesting to examine whether changes in responsiveness to altered actin dynamics over the long term are associated with alterations to chromatin structure and local activity states.

What is the involvement of the Hippo pathway in *pico*-mediated overgrowth? The transcriptome obtained from wing discs overexpressing *pico* yields little evidence of Yorkie target gene activation, suggesting that F-actin levels, subcellular location and/or structures induced by *pico* do not modify Hippo pathway activity. Lack of interaction with Hippo signalling is supported by studies in S2 cells indicating that knockdown of *pico* has little effect on expression of Yorkie-dependent gene expression (Sansores-Garcia et al., 2011). These data are also consistent with other studies that have suggested that YAP-TAZ and MRTF-SRF signalling are independent of one another (Calvo et al., 2013, Dupont et al., 2011). Nevertheless, it will be interesting to examine whether regulators of F-actin that activate Hippo also activate SRF and whether Mrtf/SRF-dependent gene expression contributes to Hippo-mediated overgrowth, since Mrtf activation would be anticipated under conditions of elevated F-actin. Our *in vivo* reporter will be of use in helping to dissect these questions.

In summary, our work provides additional insight into the molecular mechanisms by which actin remodelling acts as a growth promoting feature. Since the experimental conditions we have examined focus on the effects of overexpression, our findings are likely to have most relevance to abnormal states associated with excessive MRL activity or Mrtf/SRF signalling. Indeed, the transcriptome analysis we report here identifies features of human cancer found in hyperplastic *Drosophila* cells. The association between excessive ribosome biogenesis, translation capacity and proliferation of cancer cells in particular has been well documented (Teng et al., 2013, Johnson et al., 1976, Ruggero and Pandolfi, 2003).

Material and Methods

Fly husbandry and genetics

Flies were reared at 25°C under standard conditions. For overexpression of Flag-tagged SRF, full-length SRF cDNA from 1-3 hr Drosophila embryos was subcloned into pPFMW (Drosophila Genome Resource Center [DGRC]) to introduce an N-terminal Myc-Flag tag (pUAS-SRF-Flag); transgenic flies were generated by *P* element mediated insertion into a w^{1118} strain. To make the SRF Response Element (SRE)-mCherry reporter strain, a synthetic DNA sequence containing 9 consensus CArG boxes (Fig.S1, Text S1), was inserted into the *Not*I/*Kpn*I sites in pRedRabbit (Housden et al., 2012); transgenic flies were generated by φC31 Integrase-mediated transgenesis, with insertion into the *attP18* landing site.

Genotypes

RNA-Seq

w, MS1096-GAL4/w^{1118} (*MS1096*)

w, MS1096-GAL4/w^{1118}*;; UAS-HM-pico/+* (*MS1096>pico*)

w, MS1096-GAL4/w^{1118}*; UAS-Mal-d/+* (*MS1096>mal*)

SRE-mCherry reporter experiments

w, SRE-mCherry; hh-GAL4, UAS-GFP/+ (*SRE-mCherry, hh>GFP*)

w, SRE-mCherry; hh-GAL4, UAS-GFP/UAS-mal (*SRE-mCherry, hh>GFP, mal*)

w, SRE-mCherry; hh-GAL4, UAS-GFP/+; UAS-HM-pico/+ (*SRE-mCherry, hh>GFP, pico*)

ChIP

da-GAL4/+ (*da*)

da-GAL4/+; UAS-FLAG-SRF (*da>SRF*)

Analysis of adult wing size

MS1096>UAS-pico with *UAS-gene*^{IR} *(on 2 or 3)/Tft ; /MKRS*

MS1096>UAS-pico with *Tft and MKRS*

Details of inverted repeat lines used for RNAi are provided in **Text S1**

Caspase staining

w, MS1096-GAL4/w^{1118};; UAS-Venus-pico/+

w, MS1096-GAL4/w^{1118};; UAS-Venus-pico/UAS-det^{IR}

w, MS1096-GAL4/w^{1118};; +/UAS-det^{IR}

RNA-seq and bioinformatics

3rd instar larval imaginal tissues were dissected in cold Phosphate Buffered Saline buffer, put in RNAlater (Invitrogen), quickly frozen in liquid nitrogen and stored at −80°C until isolation of RNA. 4 pools of imaginal discs were made for each condition tested (*MS1096-GAL4* alone, *MS1096>pico* and *MS1096>mal*) corresponding to at least 300 imaginal discs/pool. RNA extractions were performed using the Ambion RNAqueous-Micro Kit (Invitrogen). RNA concentrations were measured at 260 nm with NanoDrop1000 spectrophotometer (Thermofisher) and RNA integrity was assessed with Agilent 2100 Bioanalyser. mRNA was enriched from total RNA samples, using the Dynabeads® mRNA Purification Kit for mRNA Purification from Total RNA Preps (Invitrogen). The libraries were prepared according to the ScriptSeq v2 RNA-Seq Library Preparation Kit protocol (Epicentre). The indexed and multiplexed mRNA libraries were sequenced on an Illumina HiSeq 2000, using paired-end chemistry with 2 x 100 bp read lengths (Illumina). More than 40M reads were generated for each sample. Reads were filtered for quality and mapped onto the *D.melanogaster* reference genome version dm5.39 (Adams et al., 2000) using TopHat 2.0 (Kim et al., 2013). The number of reads mapping to each gene were calculated using HTSeq-count (Anders et al., 2014), and the count data were further analysed using EdgeR (Robinson et al., 2010). The data were normalised to account for differences in library size, and a generalised linear model (GLM) was applied, using *MS1906-GAL4* alone as the reference and contrasting this with *MS1096>pico* and *MS1096>mal*. P-values were obtained using t-tests, and adjusted using the Benjamini and Hochberg (Benjamini and Hochberg, 1995) multiple testing procedure to control the

false discovery rate (FDR). An FDR cut-off of 0.05 was applied to identify differentially expressed genes. RNA-Seq data has been deposited in the NCBI Sequence Read Archive, accession no. SRP068408.

Gene Ontology Analysis

To analyse the enrichment of the genes belonging to specific biological processes, significantly down or up-regulated genes were analysed by Database for Annotation, Visualization and Integrated Discovery (DAVID) (Huang et al., 2009) against *D. melanogaster* database (*P*-value, 0.05; min genes, 5) or using Flymine http://www.flymine.org/ (Lyne et al., 2007). The protein-protein interactions were obtained using STRING http://www.webcitation.org/query.php?url=http://string-db.org/&refdoi=10.1186/1471-2164-14-573(Franceschini et al., 2013). Active prediction methods were experiments, databases & textmining and a medium confidence score (String global scores: 0.4) was applied to identified the predicted interactome, which was based on experimental evidence, database association and co-citations.

Principal Component Analysis

Principal component analysis was carried out using the open source statistical package R and the prcomp function. The loadings of the first 2 components were extracted, and the top 10% of the most positive and most negative loading genes were subject to DAVID Gene-annotation enrichment and functional annotation cluster analysis (Huang et al., 2009). Each annotation cluster was summarised into a single term, taking the most significant term from each cluster, using an FDR cut-off of 10%. These terms were displayed in a bar plot using values of -10 x log10 of the Benjamini and Hochburg adjusted p-values. Literature mining was performed using Flymine (Lyne et al., 2007).

qRT-PCR

qRT-PCR procedures were described previously (Jonchere and Bennett, 2013b). Briefly, 1 ug of total RNA samples were subjected to reverse-transcription using High capacity RNA-to-cDNA kit (Applied biosystems/Invitrogen). Primer design was performed using Primer3 online software (Koressaar and Remm, 2007). cDNA were amplified in real time using the qPCR Master mix plus for power SYBR Green I assay (Invitrogen) and analysed with the StepOnePlus Real-Time PCR System (Applied Biosystems). The level of gene expression in extracts from *MS1096>UAS-pico*, and *MS1096>Mal-d* was compared to controls (*MS1096-GAL4* alone) and expressed as a ratio. Primers used for qPCR are given in **Text S1**.

CarG predictions

The promoting sequences of each selected genes were retrieved (positions -4000 to 100 with respect to the transcriptional start site) with removing sequences shared with neighbouring genes. Using the matrix of SRF binding sites experimentally validated in mammals (Sun et al., 2006b) and our promoter sequences, a positional weight matrix were applied using the Matrix-scan software (Turatsinze et al., 2008). The parameters used for the analysis were those given by default by the software. Binding sites with a *P*-value of $\leq e10^{-4}$ & a weight up to 5 were considered significant.

Chromatin Immunoprecipitation-qPCR

ChIP experiments were performed from wandering L3 larvae, as described previously (Zsindely et al., 2009). For the immunoprecipitations, 25 µg of chromatin was incubated overnight with antibody and another 4 hrs the next day with protein G coated magnetic beads (Diagenode or Millipore). The antibodies used in the IP were: mouse anti-FLAG (F3165, Sigma) and mouse IgM. The DNA was recovery with Ipure Kit (Diagenode). A minimum of 3 biological replicates was done for each genotype. For the qPCR analysis, reactions were done in duplicates and the quantity of DNA bound by specific antibodies was calculated by % Input. Primers used for qPCR are given in **Text S1**.

Immunofluorescence

Tissues were dissected from 3rd instar larvae were fixed and stained as (Ciurciu et al., 2013) with primary antibodies: rabbit anti-cleaved caspase-3 (Cell Signalling Technology, 1:100), rat anti-RFP (Chromotek, 1:1000). Secondary antibody conjugated to Alexa-Fluor 555 (1:500) for 2 hours at room temperature in the dark. TO-PRO-3 Iodide (Invitrogen, 1:1000) or Hoescht (1:1000) was used to visualise DNA. Tissues were mounted in Vectashield mounting medium (Vector Laboratories) and imaged on a Zeiss LSM780 or LSM880 microscope equipped with 405nm, 488nm, 568nm and 633nm lasers using a 20x objective or Plan Apochromat 40x/1.3NA oil immersion objective. Images were imported into Omero (Allan et al., 2012) and adjusted for brightness and contrast uniformly across entire fields where appropriate. Figures were constructed in Adobe Photoshop.

Image analysis

For measurements of SRE-mCherry, image analysis was conducted using Bitplane Imaris version 8.2.0 (Oxford Instruments). The GFP channel was segmented into a single 3D volume (5μm surface grain size) by absolute intensity using an automatically-selected intensity threshold. Small unattached objects were removed using a volume filter. This segmented volume was used to mask the red channel into two new channels by zeroing all voxels inside or outside the volume. These new channels were used to segment the data into spots (estimated diameter of 5μm, using background subtraction). Spots were subjected to an automatically-thresholded intensity filter, which was visually inspected and adjusted if necessary. The mean intensity of each spot was recorded for each sample. The GFP positive fraction was calculated as the number of GFP +ve spots divided by the total number of spots. Intensity Bias was calculated as the mean intensity of GFP positive spots divided by the mean intensity of GFP negative spots. Using the data above, the individual mean spot intensities were scaled to 8-bit values and histograms were produced using MATLAB 2015a (Mathworks). Data were binned into 13 bins spread evenly across the 8-bit range for all conditions. The histograms were then normalised by dividing all frequency

values by the maximum frequency value within that dataset. Data were plotted in Graphpad, along with non-linear regression curve assuming a Gaussian distribution.

For quantitation of cleaved Caspase 3 staining, data were segmented into spots as described above using Imaris. Spots outside the wing pouch (as observed in the transmitted channel) were removed manually, and the remaining spots were counted and their mean intensity measured.

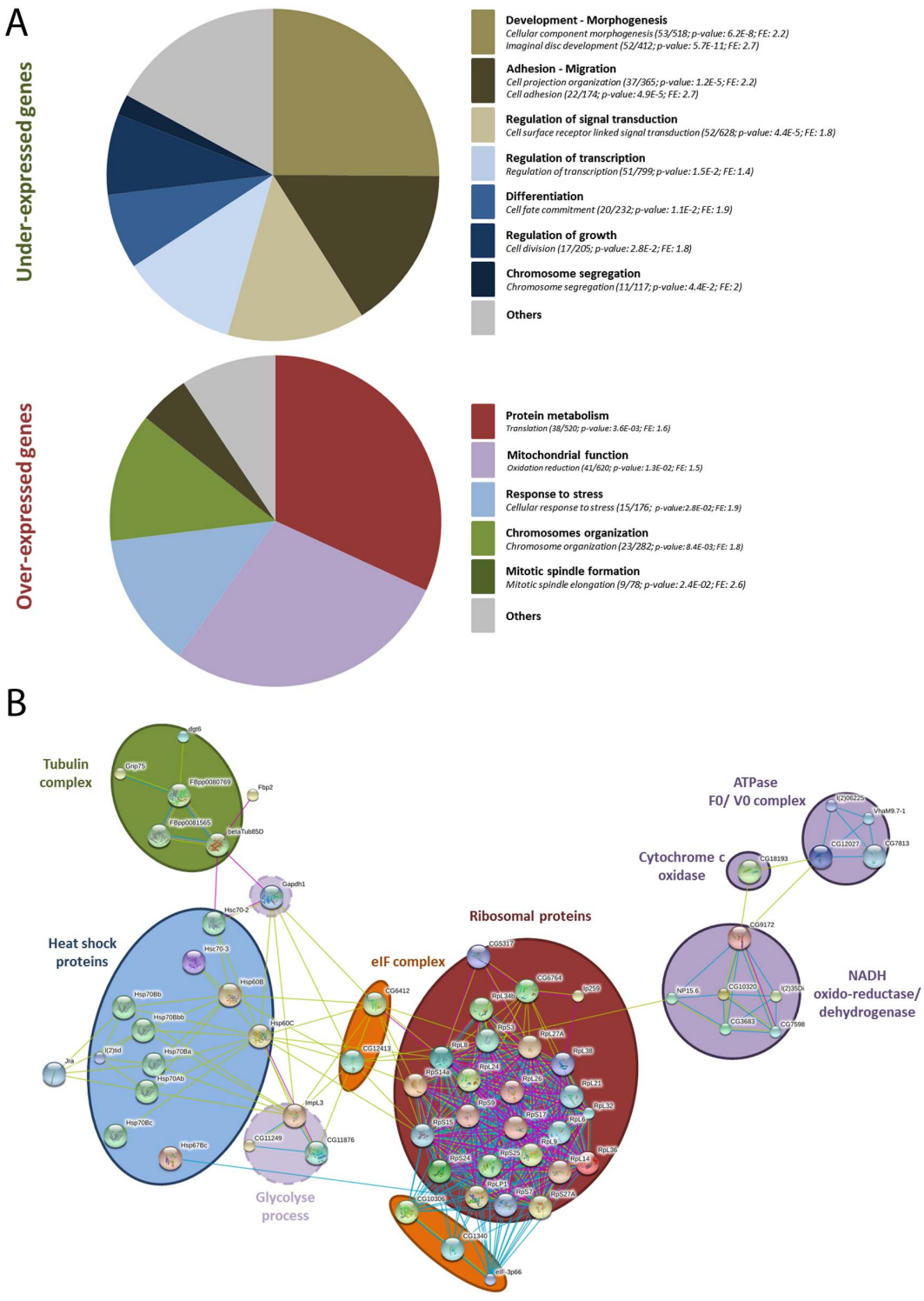

Figure 1. Transcriptome analysis of wing discs overexpressing pico. A, Pie chart showing relative abundance of gene ontology (GO) term enrichment in genes under-expressed and over-expressed in wing imaginal discs of *MS1096>pico* 3rd instar larvae relative to abundance of GO terms for all genes in the genome as determined by DAVID. For each category of

functional group (in bold), the most prominent biological function (in italic) has been annotated with the number of genes affected in that category, the total number of genes in that category, the statistical significance (*P* value) of the match and fold enrichment (FE). The most prominent GO categories amongst those up-regulated in response to *pico* overexpression are related to protein biosynthesis, including initiation of translation, ribosomal function, and protein maturation. There is also an enrichment in proteins localised to mitochondria. **B**, Predicted interacting network for genes over-represented in response to *pico* overexpression, visualised using STRING. Potential associations are indicated by the links in the graph and colour coded by type: co-citation from the abstract of scientific literature (green), proteins related in curated databases (blue) and physical protein-protein for interaction databases (pink).

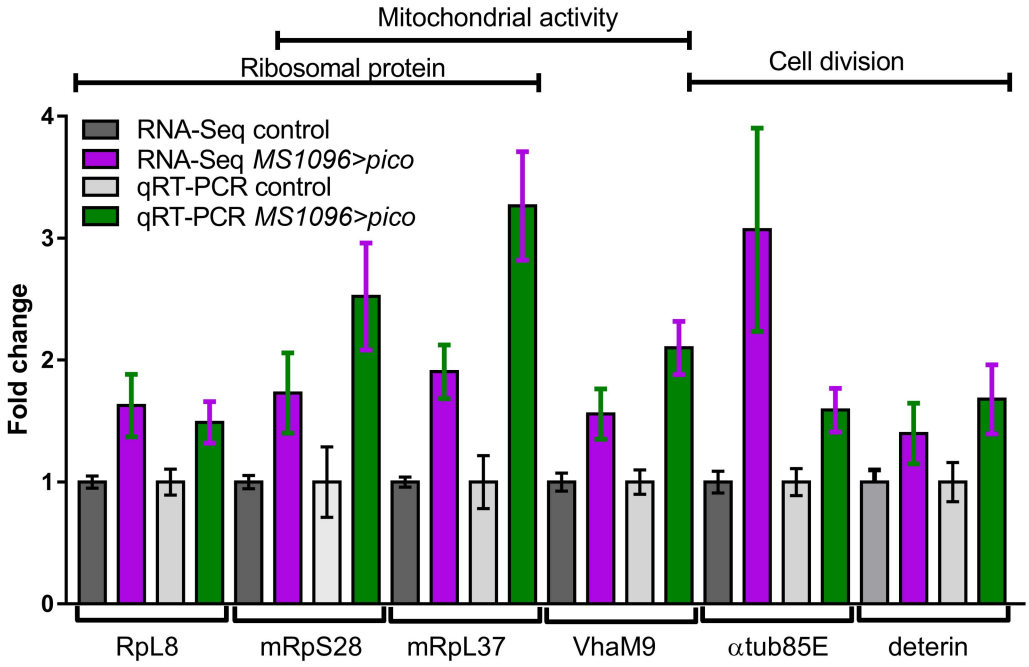

Figure 2 Validation of RNA-Seq by qRT-PCR. Expression levels of selected genes from *MS1096>pico* wing discs from third instar larvae, relative to control, determined by qRT-PCR and by RNA-seq. Error bars represent the SEM of at least 3 biological replicates. The GO categories to which the genes belong are shown at the top. Individual *t*-tests without adjustment for multiple comparisons showed a significant difference ($P<0.05$) in each case between transcript levels in *MS1096>pico* and control discs.

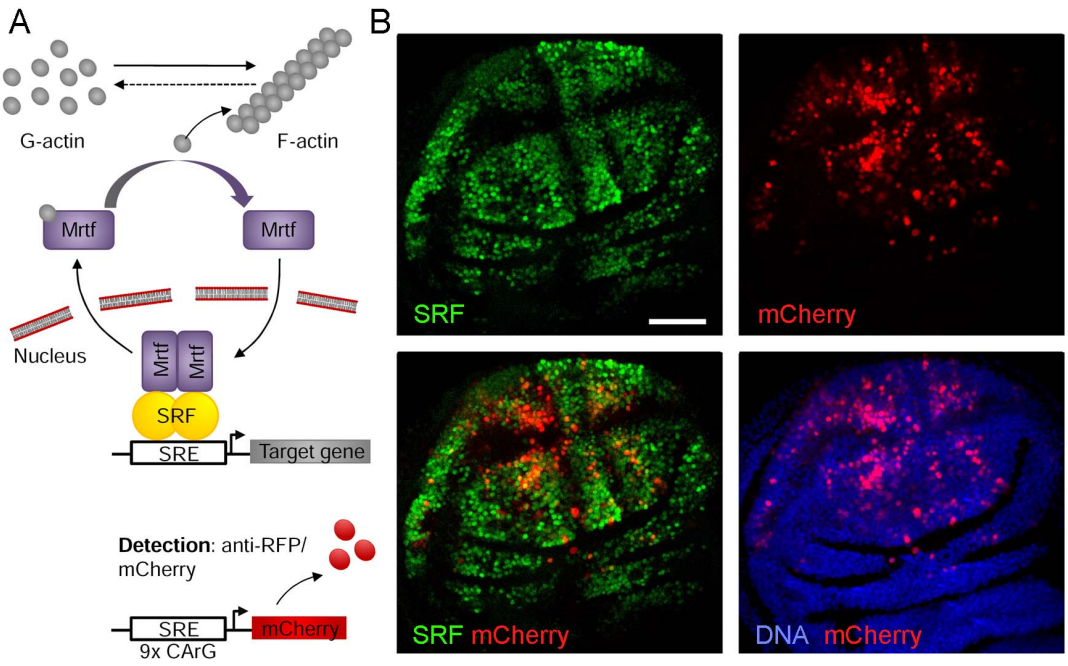

Figure 3. Distribution of an *in vivo* SRF-responsive reporter gene in wing discs. **A**, Model for Mrtf/SRF activation by Pico overexpression. Increased F-actin formation leads to sequestration of G-actin, relieving inhibition of Mrtf, which translocates to the nucleus and complexes with SRF to drive transcription of genes containing SRF-Responsive enhancer Elements (SRE). SRF activation can be monitored using an SRE-mCherry reporter. **B**, Confocal images of wing discs harbouring SRE-mCherry transgenic reporter, stained with anti-SRF antibody. The distribution of the SRE-mcherry reporter closely matches the distribution of SRF protein in presumptive intervein cells.

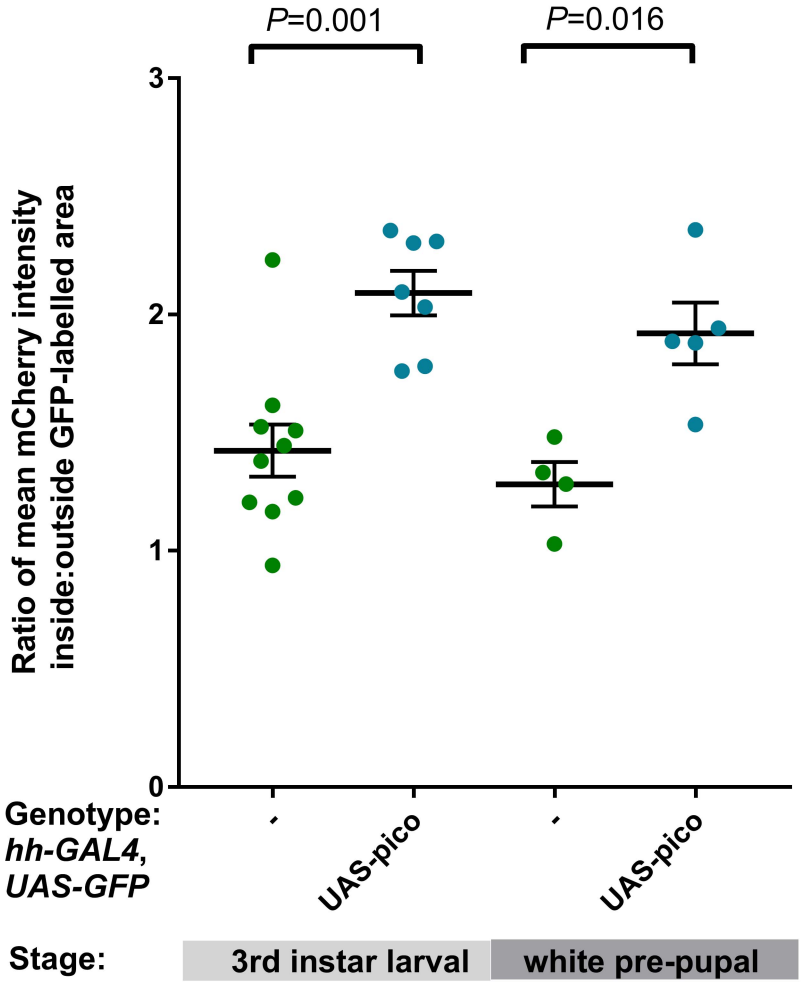

Figure 4. Overexpression of *pico* induces SRE-mCherry expression in larval and pupal wing discs. Scatterplot shows measurements from different wing imaginal discs of the ratio of mean mCherry intensity in cells inside:outside the GFP-labelled posterior half of each disc (from z-stacks of at least 4 wing discs per genotype). Mean values ±SE for each genotype are indicated with a line. The genotype and developmental stage are as indicated ("-" corresponds to *hh-GAL4*, *UAS-GFP* alone). The results of *t*-tests comparing mCherry levels between discs with or without overexpressed *pico* at each stage are indicated.

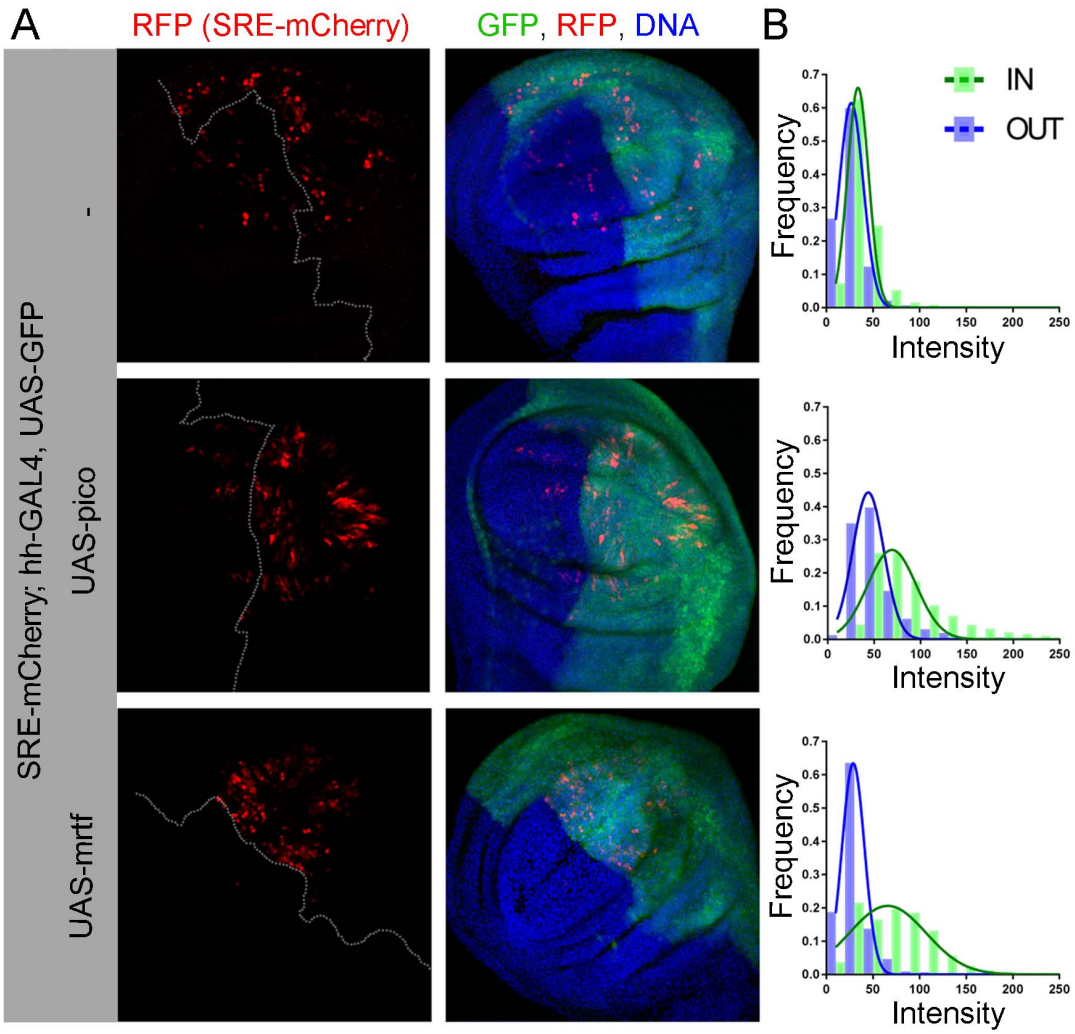

Figure 5. **Overexpression of *mrtf* or *pico* induces SRE-mCherry expression**

A, Shown are representative images of an apical view of wing discs overexpressing *mrtf* or *pico* in the posterior compartment of 3rd instar wing imaginal discs (marked with GFP) using *hh-GAL4*. GFP labels *hh-GAL4* expressing cells (in green), anti-RFP antibody staining reveals SRE-mCherry distribution (in red), TOPRO-3 staining reveals DNA (in blue). For clarity, a dotted line in the images showing SRE-mCherry alone indicates the position of the anterior/posterior boundary. **B**, *mrtf* and *pico* induce SRE-mCherry expression *in vivo*. Shown are graphs of the distribution of SRE-mCherry signal intensities inside (IN) or outside (OUT) GFP-labelled compartments (from z-stacks of at least 10 wing discs). Levels of SRE-mCherry were noticeably elevated in the posterior half of discs expressing *mrtf* or *pico.*

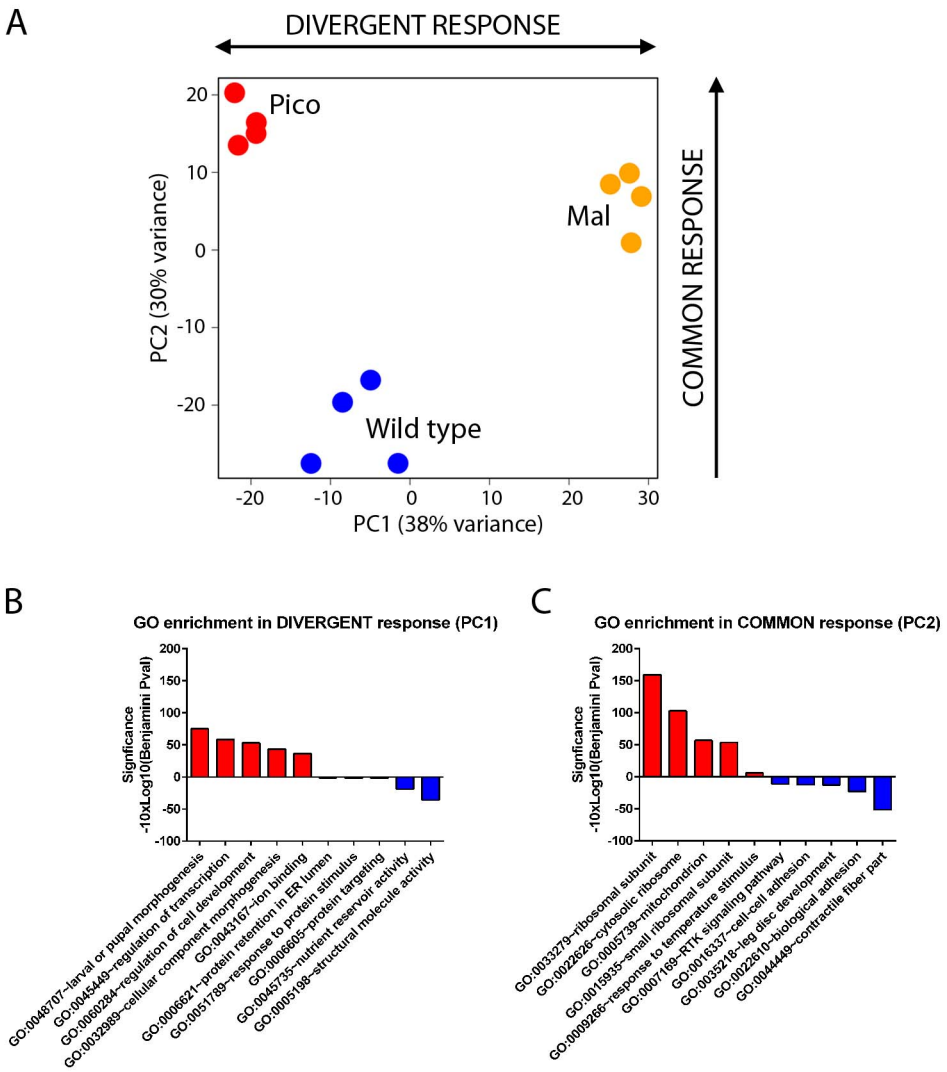

Figure 6. Divergent and common responses to *mal-d* and *pico* overexpression

A, Principal component analysis showing divergent (PC1) and common (PC2) response to overexpressed *pico* and *mrtf*, respectively, which together explain approximately 70% of the variance in gene expression. Data points are 4 independent biological repeats for each condition (*MS1096>pico*, red; *MS1096>mrtf*, yellow, *MS1096-GAL4* alone, blue). **B-C**, GO enrichment for the top (red) and bottom (blue) 10% of loadings from divergent and common responses. The 5 most significant GO categories for each grouping are shown. Both *pico* and *mrtf* overexpression stimulate ribosome protein genes belonging to the GO category “ribosome subunit”

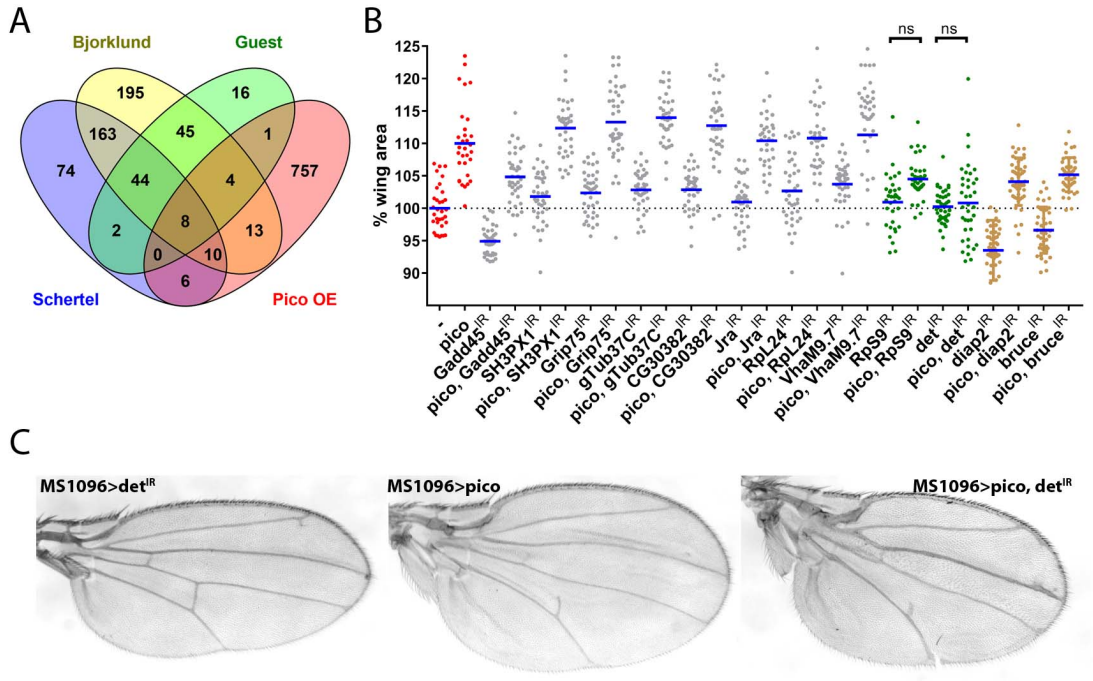

Figure 7. Genes induced by *pico* overexpression are required for *pico*-mediated tissue growth. A, Venn diagram showing overlap between genes significantly overexpressed by *pico* (identified in this study) and genes identified for their role in the cell cycle or growth control in high-throughput functional genetic studies (Guest et al., 2011, Bjorklund et al., 2006, Schertel et al., 2013). **B**, Results of genetic screen showing effect of inverted repeat (IR) contructs for 12 genes on adult male wing size, with or without overexpressed *pico*, expressed as a percentage of control (-, first column; *MS1096-GAL4* alone). All strains contained *MS1096-GAL4* to drive expression in the developing wing disc. Data are shown as scatterplot and mean values indicated with a line (n≥30). Overexpression of *pico* induced approximately a 10% increase in wing size compared to the control (red data points). Most IR constructs had little effect although *UAS-Gadd45^{IR}* had a modest effect on wing size in both the presence and absence of overexpressed *pico*. Notably, *UAS-RpS9^{IR}* and *UAS-det^{IR}* significantly suppressed pico-mediated overgrowth but had little effect in an otherwise wildtype background (ns, not significant $P>0.05$ *t*-test) **C**, Knockdown of *deterin* (*det*) suppressed *pico*-mediated tissue overgrowth, but not an alteration to wing shape. Flies carrying a UAS-inverted repeat for *deterin*

under the control of *MS1096-GAL4* (*MS1096>det^{IR}*) resembled wild type wings (not shown).

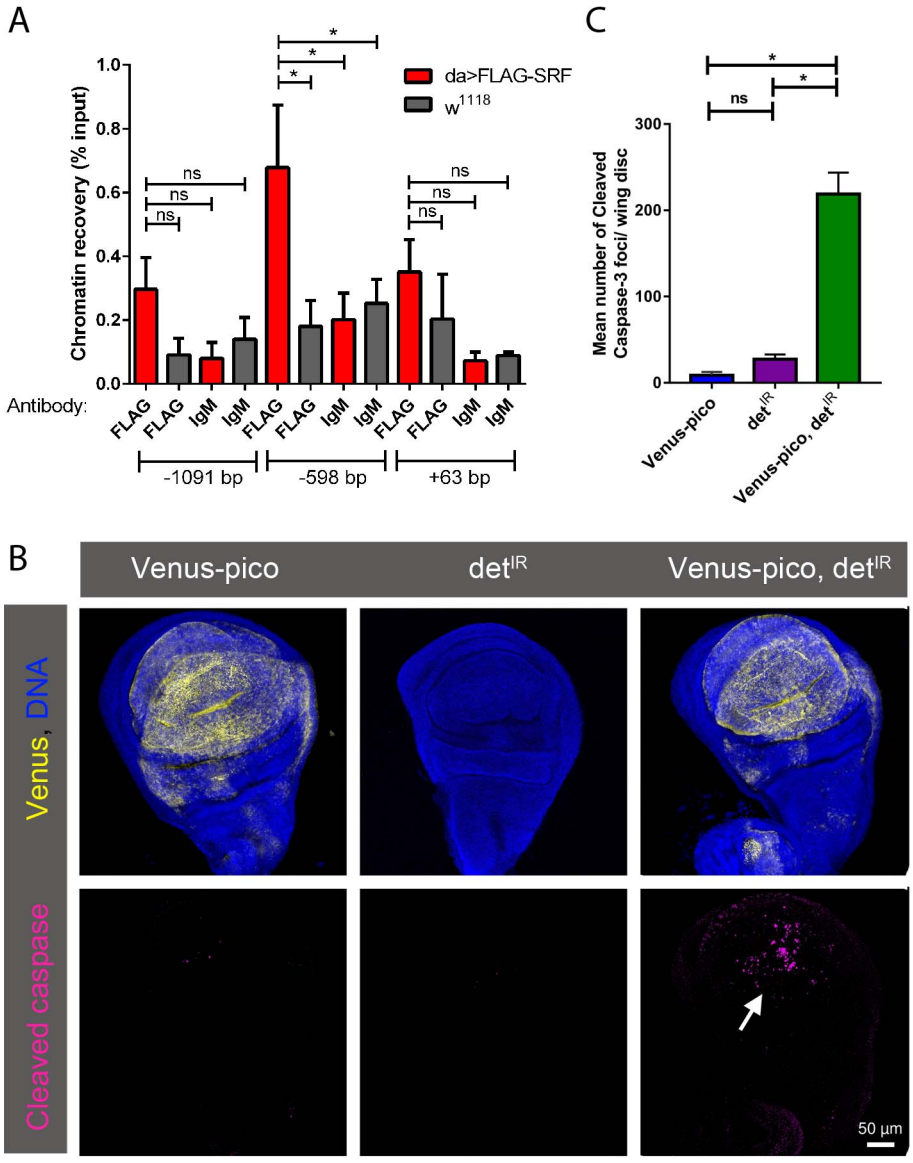

Figure 8. Deterin is a Mrtf/SRF target and suppresses apoptosis during *pico*-mediated tissue overgrowth. A, A site 5' of the transcription start site (TSS) of *deterin* binds FLAG-SRF. Chromatin immunoprecipitation (ChIP) analyses of 3 sites at the 5' end of *deterin* containing a potential CArG box. Position of the CArG box relative to the TSS is indicated at the bottom. ChIP from 3rd instar larval *da>Flag-SRF* and control larvae (*da-GAL4* alone) was

performed using monoclonal anti-FLAG and mouse IgM antibodies. Immunoprecipitated DNA was quantified by qPCR. For each genotype, percent input is the amount of precipitated DNA relative to input DNA. Results are mean ±SEM from three independent experiments. One-way ANOVA: *, *P*<0.05; ns, not significant. Distance of sites from the TSS is indicated on the X axis. **B**, *det*^{IR} induces cell death in wing discs co-overexpressing *pico*. Discs overexpressing Venus-pico (in yellow) are overgrown and show little cleaved Caspase-3 staining (in red); coexpression of detIR reduced tissue size and induced cleaved Caspase-3 in the centre of the wing pouch (arrow). C, Quantitation of number of Caspase-3 positive foci in wing discs expressing *Venus-pico* or *det*^{IR}, alone or in combination (mean ±SEM from z-stacks of at least 3 wing discs). *t*-test: *, P<0.05, ns, not significant.

Supporting Information

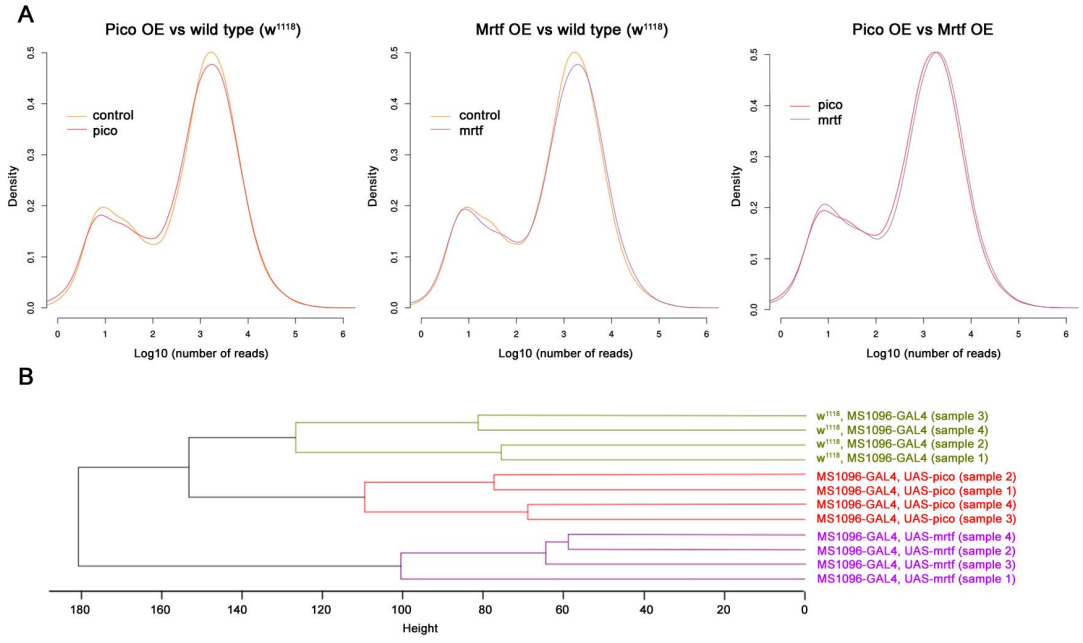

Fig. S1 Comparison of global RNA-Seq gene expression profiles. **A**, When control (*MS1096-GAL4*), *MS1096>pico* and *MS1096>mrtf* samples are grouped together, very little difference in the global gene expression profiles can be seen between conditions. **B**, Nevertheless, dendrograms

show close hierarchical clustering between the different replicates for each genotype, suggesting there are consistent changes in gene expression in response to *pico* and *mrtf* overexpression.

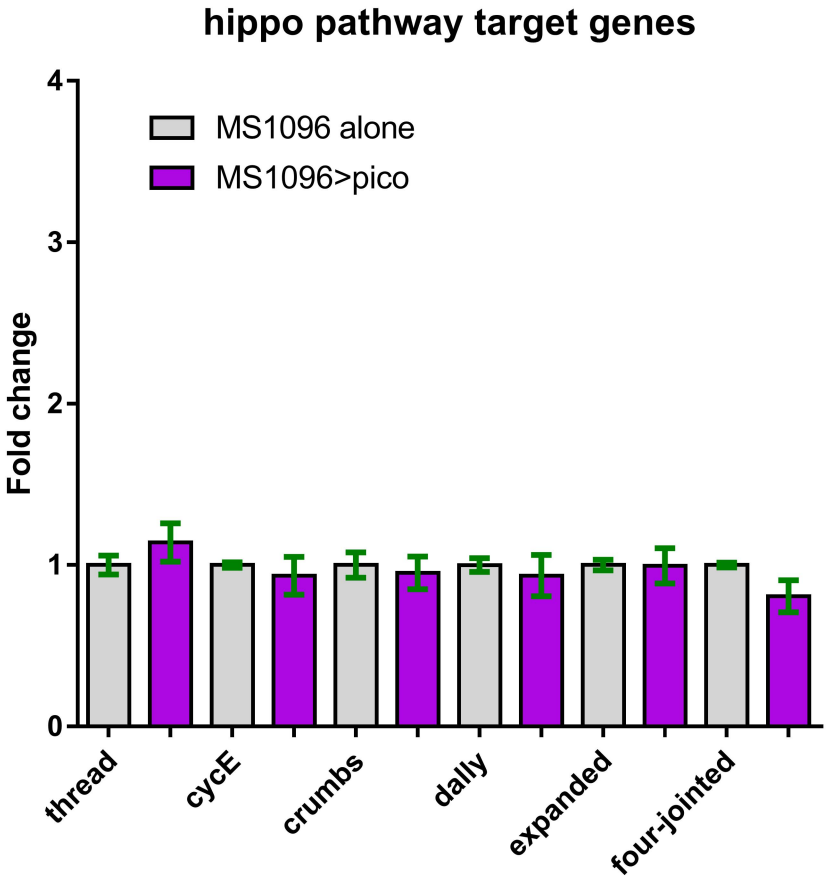

Fig. S2 Levels of Yorkie target genes in wing discs overexpressing *pico*. Fold change in mRNA expression for selected genes based on RNA-Seq data for control (*MS1096-GAL4*) and *MS1096>pico* wing discs (n=4). No significant difference in the level of expression between conditions was detected.

Table S1. Comparison of gene level expression in wings imaginal disks of *pico* to control by RNA-sequencing. mRNA from wings imaginal disks of *MS1096>pico* and *MS1096-GAL4* alone were sequenced on illumina Hi-seq 2000 (40 M reads each repeat) and statistically compared by t-test where *P* value were adjusted by Benjamini-Hochberg (FDR<0.05; (Benjamini and Hochberg, 1995)) multiple testing procedure (allDataset worksheet). Genes significantly under- or over-expressed in *pico* are displayed in separated worksheets.

Table S2. Biological Process Ontology (BP-GO) term enrichment in genes showing their expression affected by *pico*. Gene Ontology (GO) enrichment was determined using DAVID (Huang et al., 2009). Biological process categories from GO analysis that are significantly overrepresented among the genes for which the expression were either decreased (downregulated worksheet) or increased (upregulated worksheet) in response to *pico* overexpression. BP-GO were grouped into categories sharing similar function and used to produce the pie chart (Figure 1A). Only the categories with a minimum of 5 genes per category and an EASE score ≤0.05 were considered.

Text S1. Details of RNAi lines and primer sequences used in this paper.

Acknowledgments

We thank the Bloomington Stock Center and Pernille Rorth for *Drosophila* strains, the *Drosophila* Genome Resource Centre and Sarah Bray for plasmids, Genetic Services Inc. for generation of transgenic lines, Wei Du and Christian Lehner for antibodies, Pernille Rorth for supplementary ChIP-Seq data, Marco Marcello, Centre for Cell Imaging University of Liverpool for assistance with image acquisition, Roy Chaudhuri, Xuan Liu and the Centre for Genomics Research, University of Liverpool for RNA-Seq and bioinformatic analysis, Mirel Lucaci and Simon Fredeval for technical assistance.

Funding

This work was funded by Cancer Research UK (grant C20691/A11834) and Medical Research Council UK (grant MR/K015931/1). NA was supported by the Saudi Arabian Ministry of Higher Education; LD was supported by an MRC Capacity Building studentship. The funders had no role in study design, data collection and analysis, decision to publish, or preparation of the manuscript.

Competing Interests:

The authors have declared that no competing interests exist.

Author Contributions

Conceived and designed the experiments: VJ, DB. Performed the experiments: VJ, NA, EL, LD, GM, DB. Analysed the data: VJ, JH, DM, NA, GM, FF, DB. Contributed to the writing: DB, VJ, NA, JH, DM, FF, EL, LD, GM.

References

Abruzzi, K.C., Rodriguez, J., Menet, J.S., Desrochers, J., Zadina, A., Luo, W., Tkachev, S., and Rosbash, M. (2011). Drosophila CLOCK target gene characterization: implications for circadian tissue-specific gene expression. Genes & development *25*, 2374-2386.

Adams, M.D., Celniker, S.E., Holt, R.A., Evans, C.A., Gocayne, J.D., Amanatides, P.G., Scherer, S.E., Li, P.W., Hoskins, R.A., Galle, R.F.*, et al.* (2000). The genome sequence of Drosophila melanogaster. Science *287*, 2185-2195.

Allan, C., Burel, J.M., Moore, J., Blackburn, C., Linkert, M., Loynton, S., Macdonald, D., Moore, W.J., Neves, C., Patterson, A.*, et al.* (2012). OMERO: flexible, model-driven data management for experimental biology. Nature methods *9*, 245-253.

Anders, S., Pyl, P.T., and Huber, W. (2014). http://www-huber.embl.de/users/anders/HTSeq/doc/overview.html.

Aragona, M., Panciera, T., Manfrin, A., Giulitti, S., Michielin, F., Elvassore, N., Dupont, S., and Piccolo, S. (2013). A mechanical checkpoint controls multicellular growth through YAP/TAZ regulation by actin-processing factors. Cell *154*, 1047-1059.

Bae, Y.H., Mui, K.L., Hsu, B.Y., Liu, S.L., Cretu, A., Razinia, Z., Xu, T., Pure, E., and Assoian, R.K. (2014). A FAK-Cas-Rac-lamellipodin signaling module transduces extracellular matrix stiffness into mechanosensitive cell cycling. Science signaling *7*, ra57.

Benjamini, Y., and Hochberg, Y. (1995). CONTROLLING THE FALSE DISCOVERY RATE - A PRACTICAL AND POWERFUL APPROACH TO MULTIPLE TESTING. J R Stat Soc Ser B-Methodol *57*, 289-300.

Bjorklund, M., Taipale, M., Varjosalo, M., Saharinen, J., Lahdenpera, J., and Taipale, J. (2006). Identification of pathways regulating cell size and cell-cycle progression by RNAi. Nature *439*, 1009-1013.

Calvo, F., Ege, N., Grande-Garcia, A., Hooper, S., Jenkins, R.P., Chaudhry, S.I., Harrington, K., Williamson, P., Moeendarbary, E., Charras, G.*, et al.* (2013). Mechanotransduction and YAP-dependent matrix remodelling is required for the generation and maintenance of cancer-associated fibroblasts. Nat Cell Biol *15*, 637-646.

Cenik, B.K., Liu, N., Chen, B., Bezprozvannaya, S., Olson, E.N., and Bassel-Duby, R. (2016). Myocardin-related transcription factors are required for skeletal muscle development. Development *143*, 2853-2861.

Ciurciu, A., Duncalf, L., Jonchere, V., Lansdale, N., Vasieva, O., Glenday, P., Rudenko, A., Vissi, E., Cobbe, N., Alphey, L.*, et al.* (2013). PNUTS/PP1 regulates RNAPII-mediated gene expression and is necessary for developmental growth. PLoS genetics *9*, e1003885.

Dupont, S., Morsut, L., Aragona, M., Enzo, E., Giulitti, S., Cordenonsi, M., Zanconato, F., Le Digabel, J., Forcato, M., Bicciato, S.*, et al.* (2011). Role of YAP/TAZ in mechanotransduction. Nature *474*, 179-183.

Fernandez, B.G., Gaspar, P., Bras-Pereira, C., Jezowska, B., Rebelo, S.R., and Janody, F. (2011). Actin-Capping Protein and the Hippo pathway regulate F-actin and tissue growth in Drosophila. Development *138*, 2337-2346.

Franceschini, A., Szklarczyk, D., Frankild, S., Kuhn, M., Simonovic, M., Roth, A., Lin, J., Minguez, P., Bork, P., von Mering, C.*, et al.* (2013). STRING v9.1: protein-protein interaction networks, with increased coverage and integration. Nucleic Acids Research *41*, D808-D815.

Grosse, R., Copeland, J.W., Newsome, T.P., Way, M., and Treisman, R. (2003). A role for VASP in RhoA-Diaphanous signalling to actin dynamics and SRF activity. The EMBO journal *22*, 3050-3061.

Guest, S.T., Yu, J., Liu, D., Hines, J.A., Kashat, M.A., and Finley, R.L., Jr. (2011). A protein network-guided screen for cell cycle regulators in Drosophila. Bmc Systems Biology *5*.

Han, Z., Li, X., Wu, J., and Olson, E.N. (2004). A myocardin-related transcription factor regulates activity of serum response factor in Drosophila. Proc Natl Acad Sci U S A *101*, 12567-12572.

Housden, B.E., Millen, K., and Bray, S.J. (2012). Drosophila Reporter Vectors Compatible with PhiC31 Integrase Transgenesis Techniques and Their Use to Generate New Notch Reporter Fly Lines. G3 (Bethesda) *2*, 79-82.

Hu, Y., Roesel, C., Flockhart, I., Perkins, L., Perrimon, N., and Mohr, S.E. (2013). UP-TORR: online tool for accurate and Up-to-Date annotation of RNAi Reagents. Genetics *195*, 37-45.

Huang, D.W., Sherman, B.T., and Lempicki, R.A. (2009). Systematic and integrative analysis of large gene lists using DAVID bioinformatics resources. Nature Protocols *4*, 44-57.

Jiang, X., Wilford, C., Duensing, S., Munger, K., Jones, G., and Jones, D. (2001). Participation of Survivin in mitotic and apoptotic activities of normal and tumor-derived cells. Journal of cellular biochemistry *83*, 342-354.

Johnson, L.F., Levis, R., Abelson, H.T., Green, H., and Penman, S. (1976). Changes in RNA in relation to growth of fibroblast. Journal of Cell Biology *71*, 933-938.

Jones, G., Jones, D., Zhou, L., Steller, H., and Chu, Y.X. (2000). Deterin, a new inhibitor of apoptosis from Drosophila melanogaster. Journal of Biological Chemistry *275*, 22157-22165.

Killip, L.E., and Grewal, S.S. (2012). DREF is required for cell and organismal growth in Drosophila and functions downstream of the nutrition/TOR pathway. Developmental biology *371*, 191-202.

Kim, D., Pertea, G., Trapnell, C., Pimentel, H., Kelley, R., and Salzberg, S.L. (2013). TopHat2: accurate alignment of transcriptomes in the presence of insertions, deletions and gene fusions. Genome Biology *14*, 13.

Koressaar, T., and Remm, M. (2007). Enhancements and modifications of primer design program Primer3. Bioinformatics *23*, 1289-1291.

Lyne, R., Smith, R., Rutherford, K., Wakeling, M., Varley, A., Guillier, F., Janssens, H., Ji, W., McLaren, P., North, P.*, et al.* (2007). FlyMine: an integrated database for Drosophila and Anopheles genomics. Genome Biol *8*, R129.

O'Connor, J.W., Riley, P.N., Nalluri, S.M., Ashar, P.K., and Gomez, E.W. (2015). Matrix Rigidity Mediates TGFbeta1-Induced Epithelial-Myofibroblast Transition by Controlling Cytoskeletal Organization and MRTF-A Localization. Journal of cellular physiology *230*, 1829-1839.

Posern, G., Sotiropoulos, A., and Treisman, R. (2002). Mutant actins demonstrate a role for unpolymerized actin in control of transcription by serum response factor. Molecular biology of the cell *13*, 4167-4178.

Rajakyla, E.K., and Vartiainen, M.K. (2014). Rho, nuclear actin, and actin-binding proteins in the regulation of transcription and gene expression. Small GTPases *5*, e27539.

Robinson, M.D., McCarthy, D.J., and Smyth, G.K. (2010). edgeR: a Bioconductor package for differential expression analysis of digital gene expression data. Bioinformatics *26*, 139-140.

Ruggero, D., and Pandolfi, P.P. (2003). Does the ribosome translate cancer? Nature Reviews Cancer *3*, 179-192.

Salvany, L., Muller, J., Guccione, E., and Rorth, P. (2014). The core and conserved role of MAL is homeostatic regulation of actin levels. Genes & development *28*, 1048-1053.

Sansores-Garcia, L., Bossuyt, W., Wada, K., Yonemura, S., Tao, C., Sasaki, H., and Halder, G. (2011). Modulating F-actin organization induces organ growth by affecting the Hippo pathway. The EMBO journal *30*, 2325-2335.

Schertel, C., Huang, D., Bjorklund, M., Bischof, J., Yin, D., Li, R., Wu, Y., Zeng, R., Wu, J., Taipale, J.*, et al.* (2013). Systematic Screening of a Drosophila ORF Library In Vivo Uncovers Wnt/Wg Pathway Components. Developmental Cell *25*, 207-219.

Skarp, K.P., and Vartiainen, M.K. (2013). Actin as a model for the study of nucleocytoplasmic shuttling and nuclear dynamics. Methods in molecular biology *1042*, 245-255.

Teng, T., Thomas, G., and Mercer, C.A. (2013). Growth control and ribosomopathies. Current Opinion in Genetics & Development *23*, 63-71.

Turatsinze, J.V., Thomas-Chollier, M., Defrance, M., and van Helden, J. (2008). Using RSAT to scan genome sequences for transcription factor binding sites and cis-regulatory modules. Nature Protocols *3*, 1578-1588.

Vartiainen, M.K., Guettler, S., Larijani, B., and Treisman, R. (2007). Nuclear actin regulates dynamic subcellular localization and activity of the SRF cofactor MAL. Science *316*, 1749-1752.

Wada, K., Itoga, K., Okano, T., Yonemura, S., and Sasaki, H. (2011). Hippo pathway regulation by cell morphology and stress fibers. Development *138*, 3907-3914.

Zsindely, N., Pankotai, T., Ujfaludi, Z., Lakatos, D., Komonyi, O., Bodai, L., Tora, L., and Boros, I.M. (2009). The loss of histone H3 lysine 9 acetylation due to dSAGA-specific dAda2b mutation influences the expression of only a small subset of genes. Nucleic Acids Res *37*, 6665-6680.

3.2.3 Investigating the effects of reduced SRF signalling on the SRE-mCherry reporter

Data described in the paper above (section 3.2.2) confirmed that the reporter faithfully replicates the endogenous pattern of SRF expression and exhibits developmental-dependent changes in the level of expression. The reporter is responsive to changes in actin dynamics, which is to be expected since SRF can be activated by the changes in G-actin: F-actin ratios, via the cofactor mal. Although the expression level of mCherry from the reporter was quite weak in larval wing discs it could be robustly detected by using LSM 780 confocal microscope, containing 32 channel ultra-sensitive GaAsP detectors that allow visualisation of weak fluorescent signals with lower photo bleaching and photo toxicity. Notably, although a degree of transcriptional noise was observed, expression of the reporter was restricted to intervein cells, thereby faithfully matching the endogenous SRF expression. In the pupal wing, the expression was much stronger showing there are stage-dependent changes in levels of the reporter.

To further validate the reporter, I examined whether expression was diminished in cells lacking SRF. This was done by examining SRF mutant clones using *bs14*, which is a nonsense mutation in codon 102 that has been predicted to give rise to a shortened protein lacking the MADS domain Figure 3.4. (Montagne et al., 1996). The expectation was that the level of the reporter would be reduced in cells lacking SRF protein, and this would demonstrate the dependence of the SRE-mCherry reporter on SRF.

A

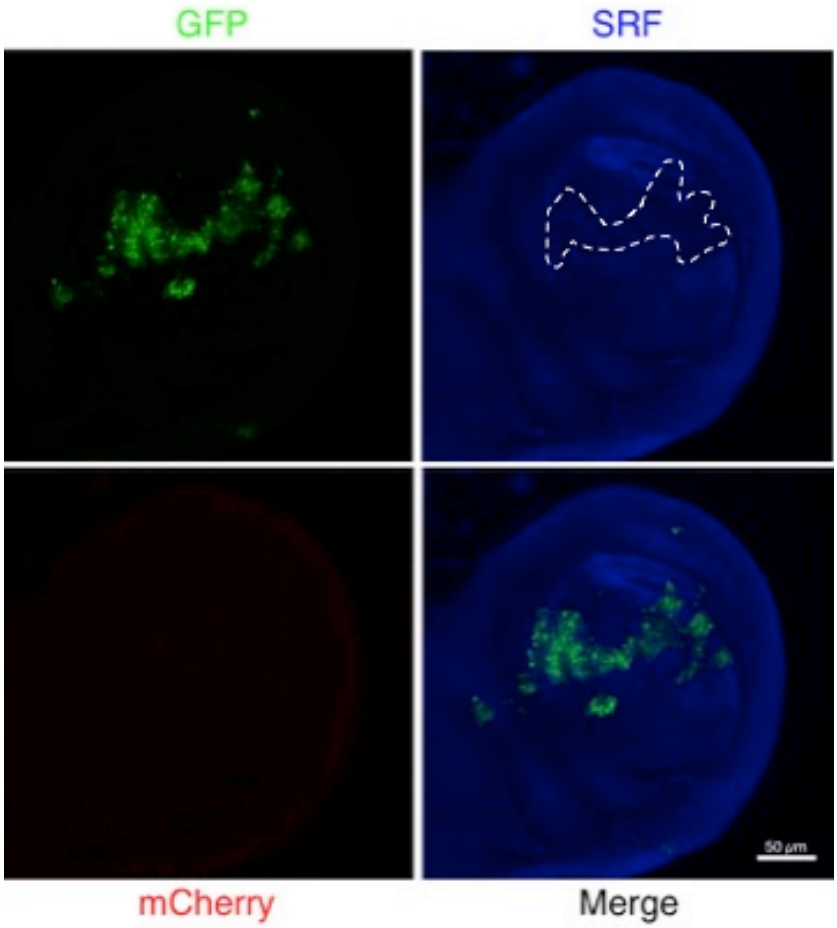
GFP
SRF
50 µm
mCherry
Merge

B

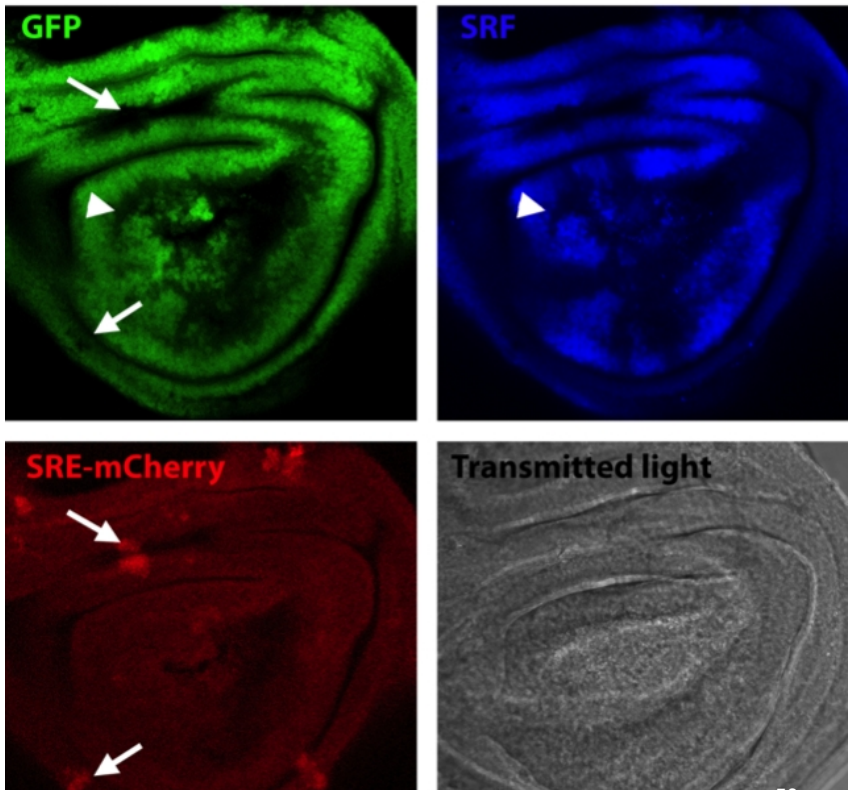
GFP
SRF
SRE-mCherry
Transmitted light

Figure 3.3. Effect of SRF mutant clones on SRE-mCherry expression in the wing imaginal disc. A) Wing disc from third instar larva harbouring positively-marked (GFP-labelled) bs^{14} homozygous mutant clone (in green). SRF antibody staining (in blue) confirmed loss of the epitope recognised by the SRF antibody. mCherry reporter (in red) was below the level of detection. B) Wing disc from third instar larva harbouring negatively-marked bs^{14} homozygous mutant clone (+/+ cells are marked with two copies of GFP in green; +/ bs^{14} cells are marked with one copy of GFP; bs^{14}/bs^{14} mutant cells lack GFP). The developmentally-controlled pattern of SRF expression (in blue) is clearly visible in intervein cells, except where staining is lost in SRF-mutant clones. SRE-mCherry expression, detected with an anti-RFP antibody, is also visible (in red). SRE-mCherry expression in SRF-mutant clones in the wing pouch is reduced somewhat but, notably, there is an elevated level in SRF-mutant clones located outside of this region.

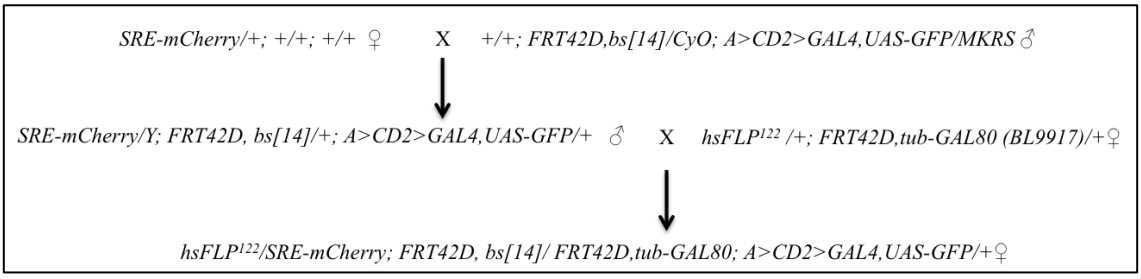

Figure3.4. Genetic scheme used to create SRF mutant clone in wing discs. Virgin females of *SRE- mCherry* crossed to males of *FRT42D, bs[14]/ CyO; A>CD2>GAL4, UAS-GFP/MKRS*. Males from this cross have been crossed to virgin females of $hsFLP^{122}$*; FRT42, tub-GAL80/+* Crosses have been heat chocked at L2, and then GFP+ve wing discs were dissected from female third instar larvae and stained for anti-SRF and anti- RFP.

A) Positive selection of somatic clones

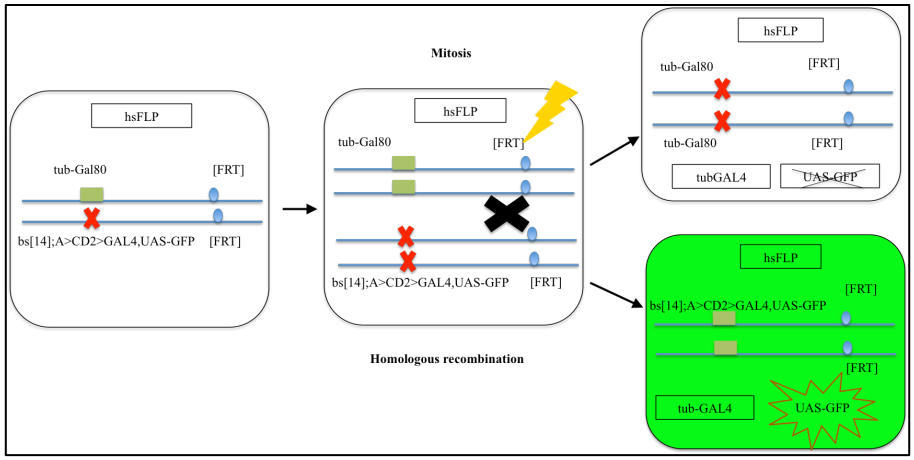

B) Negative selection of somatic clones

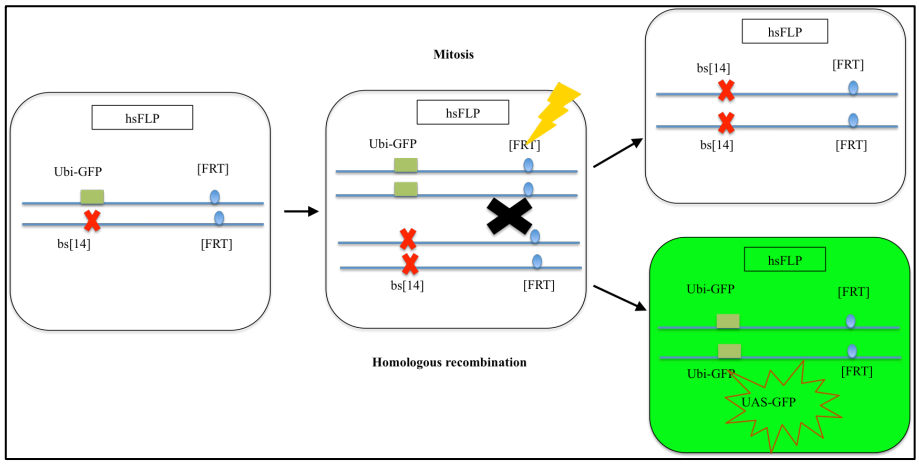

Figure 3.5. The use of FLP/FRT to produce homozygous mutants for mosaic analysis. Female larvae were heat shocked at 37 °C for an hour to induce homologous recombination between FRT sites using a heat shock inducible FLP recombinase during mitosis. (A) Approach to generate positively marked clones. In heterozygous or homozygous wildtype cells, GAL80 is expressed under the control of a ubiquitous tubulin promoter (tub-GAL80), which suppresses the expression of tub-GAL4 UAS-GFP. Of the two daughter cells produced following mitotic recombination, one is a homozygous mutant, in which tub-GAL80 is lost. This leads to derepression of GAL4 in these cells, triggering expression of UAS-GFP. (B) Approach to generate negatively marked clones. Mitotic recombination is induced as in A, except the non-mutant chromosome is marked with Ubi-GFP, which encodes GFP under the control of a ubiquitin promoter. Of the two daughter cells produced by recombination, one is homozygous mutant that is marked by the absence of this element, and does not express GFP, Image adapted from (Xu and Rubin, 1993)

mCherry expression could not be readily detected in these experiments either by staining with anti–RFP antibody or visualising mCherry directly (Figure 3.3.A)., most likely because there was only one copy of the transgene in these female flies. Previous experiments had utilised males carrying an X-chromosome insertion, which would have been hyperactivated due to dosage compensation. Consequently, it was hard to confirm whether SRF mutant clones lose the ability to induce the SRF reporter. Interestingly however, in mutant clones around outside of the wing pouch, elevated RFP expression was detected, suggesting that SRF may be a transcriptional repressor in this region of the wing disc (Figure 3.3.B).

In mammalian cells, a small number of target genes of SRF and MRTF were shown to be downregulated in response to SRF induction (Esnault et al., 2014). Taking this work forward, it may be interesting to determine whether these are evolutionary conserved and respond similarly in the wing disc where patterns of repression could also be detected.

4 Cooperation of Pico and Ras^{V12} during invasive cell migration

4.1 Introduction

Cell migration is essential for many biological processes such as wound healing, gastrulation during embryo development as well as for the generation of an effective immune response (Trepat et al., 2012). However, if migration occurs in cells that are considered as non-motile or at inappropriate times there can be severe consequences. Indeed, the active migration of tumour cells typically results in the invasion of neighboring tissues and the subsequent formation of secondary tumours, metastases, at ectopic sites, which are recognized as the leading cause of cancer-related fatalities. Unfortunately, the genetic and biochemical changes that are required in non-invasive tumour cells to facilitate the acquisition of motile cell behaviours are not fully understood due to the complex nature of the transformation process. In addition, interactions between the tumour cells and surrounding wild type cells have also been shown to play an important role in tumour cell progression (Sahai, 2005).

It is difficult to artificially create such a complex genetic environment in a mammalian model system. In contrast, *Drosophila* has provided a sophisticated and genetically tractable model (Brumby and Richardson, 2003, Pagliarini and Xu, 2003).

The generation of genetically-defined tumour cells in *Drosophila* typically employs the MARCM (Mosaic analysis with a repressible cell marker) technique, which utilizes the *GAL4-UAS* expression system (Brand and Perrimon, 1993, Duffy, 2002),

the FLP/*FRT* site-specific recombination system (Golic, 1991), as well as a repressible cell marker. Non-invasive tumour cells result from the overexpression of a constitutively active form of the oncogene *Ras* (Ras^{v12}) and they are genetically tagged with green fluorescent protein (GFP). Overexpression of Ras^{v12} in clones that are homozygous mutant for metastasis-suppressor gene or by co-overexpressing Ras^{v12} with a metastasis-promoting gene under UAS control can lead to cell invasion, which can be identified by the spread of GFP-labelled cells to more distant sites (Miles et al., 2011). Importantly, the ability to generate multiple genetic mutations in a small subset of cells in an otherwise wild type tissue, make it possible to model the events that take place during tumour development in humans.

Previous studies using this model have shown that loss-of-function mutations in the cell polarity gene *scribble* (*scrib*) could cooperate with Ras^{v12} to drive metastasis (Brumby and Richardson, 2003, Pagliarini and Xu, 2003). Clones were generated in the eye-antennal imaginal disc/optic lobe region using the *eyeless* promoter to express the FLP recombinase (eyFLP). Clonal cells, homozygous mutant for *scrib* and overexpressing with Ras^{v12}, were GFP-labelled (Figure 4.1.). When third instar *ey*> Ras^{v12}, $scrib^{-/-}$ larvae were examined, it was found that the GFP-labelled tumour cells were no longer limited to the eye-antennal imaginal disc region, with secondary tumours observed in the hemolymph. By dissecting these larvae, it was found that tumour cells were capable of spreading from the primary tumours into neighboring tissues. Importantly, neither loss of *scrib* function *nor* Ras^{v12} overexpression could induce metastasis individually.

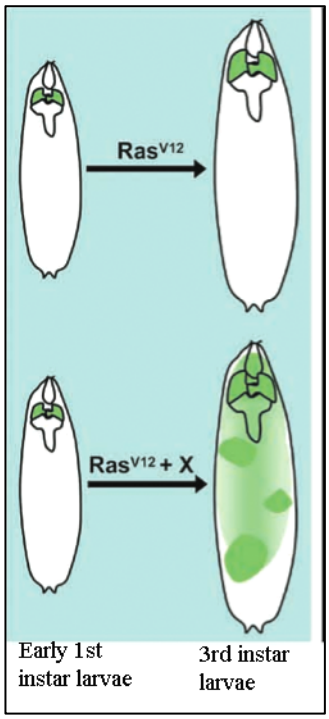

Figure 4.1. *Drosophila* cell invasion model. Shown are schematic drawings of larvae expressing GFP (in green) and other genes in the eye imaginal tissues. Expression of oncogenic *Ras^{V12}* in 1st instar larvae results in the production of benign tumours by the 3rd instar stage (top). When additional genetic changes (X) are present (bottom), GFP-labelled tumours can disseminate to neighbouring or distant tissues (Bennett et al., 2015).

This study revealed that the cell polarity genes *scrib*, *lgl* and *dlg* have a critical role in inhibiting tumour progression and metastasis (Pagliarini and Xu, 2003, Brumby and Richardson, 2003). Furthermore, it has been found that activation of JNK, interclonal cooperation, extracellular matrix remodeling and the immune system also have a role in invasion and metastasis in

this model (Miles et al., 2011). Insights such as these into epithelial cancer biology have helped guide studies of cancer in more advanced model organisms (Vieira et al., 2008).

Previous studies investigating the function of the MRL family members have implicated these proteins in the regulation of cell migration. It has been shown that overexpressing the two-mammalian MRL proteins; Lpd or RIAM in fibroblast cells can induce lamellipodia formation. In contrast, knocking-down the expression of

Lpd in mouse melanoma cells led to impaired lamellipodia formation and a reduction in F-actin levels (Krause et al., 2004, Lafuente et al., 2004). In addition, studies in *C. elegans* indicated that the successful long-range migration of embryonic neurons requires Mig-10, the worm MRL homologue (Chang et al., 2006, Manser et al., 1997, Manser and Wood, 1990). Since all MRL family proteins members share a highly conserved domain structure and regulate cell migration, it is likely that Pico shares this functional property. Indeed, initial studies in the context of border cell migration in *Drosophila* suggest this is the case (Law et al., 2013).

Migration of the *Drosophila* border cell clusters occurs in two phases through the fly egg chamber. The fly PDGF receptor (PVR) predominantly regulates the front extension that characterise the early phase. Behaviour of the dynamic collective "tumbling" characterise the late phase (Bianco et al., 2007, Poukkula et al., 2011). Previous studies have found that overexpression of dominant-negative PVR (PVR-DN) results in the appearance of a higher proportion of rear facing extensions (Prasad and Montell, 2007), causing premature tumbling of the border cell cluster. Overexpression or knockdown of *pico* abrogated migration with *pico* phenocopying the effect of PVR-DN by eliciting a premature tumbling phenotype (Law et al., 2013). This observation suggests that tight control of *pico* function is critical for directed migration through its effects on actin-based protrusions (Law et al., 2013).

4.1.1 Aims

In addition to its role in developmentally-controlled cell migration (Law et al., 2013), overexpressed *pico* was previously shown to be capable of promoting the dissemination of Ras^{V12}-induced tumours by others in the Bennett laboratory

(Lyulcheva, 2006, Taylor, 2010). In these studies (Lyulcheva, 2006, Taylor, 2010), *pico* and Ras^{V12} were expressed in all cells in which the *eyeless*-driven FLP recombinase (eyFLP) was expressed, 'flipping out' a cassette separating the *Actin5C* promoter from the GAL4 ORF, creating a functional driver that could express UAS-transgenes in an *eyeless*-specific pattern.

Utilising this system, co-expression of Ras^{V12} and *pico* produced a noticeable increase in the size of the eye-antennal disc region and in some larvae led to the presence of the GFP-labelled cells at secondary locations. These phenotypes were not observed when either gene was overexpressed alone. The matrix metalloprotease, MMP1, was shown to be overexpressed in some but not all Ras^{V12}*/pico* cells (Lyulcheva, 2006, Taylor, 2010). Subsequent studies indicated that this was not due to stochastic effects of the immune response, a phenomenon that had been reported during studies of Ras^{V12}*, scrib* tumours (Vidal, 2010). This raised the possibility that cell types arising from *eyFLP* progenitors may behave differently to Ras^{V12}*/pico* overexpression. The purpose of work presented in this chapter was to explore this possibility, leading to the observation that *pico* cooperates with oncogenic Ras in glia to drive distinct oncogenic outcomes. SRF signalling had been implicated in the effects of *pico*/Ras^{V12} cooverexpression; mal and various actin-binding proteins had also been shown to cooperate with Ras^{V12} (Lyulcheva, 2006, Taylor, 2010). Using the *SRE-mCherry* reporter reported in Chapter 3, the ability of these actin regulators to activate SRF was also determined.

4.2 Results.

4.2.1 Paper summary

Taylor. E., Alqadri. N., Dodgson. L., Mason. D., Lyulcheva. E., Messina. G., Bennett. D. (2016). MRL proteins cooperate with activated Ras in glia to drive distinct oncogenic outcomes.

Contributions of Authors:

Taylor. E. Performed experiments to quantify effects of overexpressed *pico* and *hLpd* on oncogenic *Ras*-induced tumours (Fig. 1D-E). Performed experiments to demonstrate the effect of Ras^{V12} /*pico* on extracellular matrix breakdown (Fig. 2, 3 A, C, D, F). Performed experiments to quantify the effect of co-overexpressing *mal*, *chic*, *ena* with Ras^{V12} ± *pico* on invasion (Fig. 7C-E). Analysed the data. Contributed to writing and editing the paper.

Alqadri. N. Performed experiments to demonstrate *pico* cooperates with oncogenic *Ras* in glia to drive distinct oncogenic outcomes (Fig. 5). Performed experiments to quantify the effect of co-expressing *Repo-GAL80* on Ras^{V12} /*pico* invasion (Fig. 6). Performed experiments to analyse the distribution of SRF in optic lobes (Fig. 7A-B). Analysed the data. Contributed to writing and editing the paper.

Dodgson. L. Performed experiments to test the role of *egr* mutations on Ras^{V12}/*pico*-mediated invasion (Fig. 4). Analysed the data. Contributed to writing and editing the paper.

Lyulcheva. E. Performed initial experiments showing that overexpression of pico promotes invasion of Ras^{V12}-induced tumours (Fig.1A-B). Contributed to writing and editing the paper.

Bennett. D. Conceived and designed the experiments; secured funding for the work; analysed the data; contributed to writing and editing the paper.

4.2.2 Submitted manuscript

MRL proteins cooperate with activated Ras in glia to drive distinct oncogenic outcomes

Authors:

Eleanor Taylor[1,3,§], Nada Alqadri[1,§], Lauren Dodgson[1,2,4], David Mason[2], Ekaterina Lyulcheva[1,4], Giovanni Messina[1], Daimark Bennett[1,2,*]

Affiliations:

[1]Department of Biochemistry, Institute of Integrative Biology, University of Liverpool, Crown Street, Liverpool, L69 7ZB, UK

[2]Centre for Cell Imaging, Biosciences Building, University of Liverpool, Crown Street, Liverpool, L69 7ZB, UK

[3]Current address: Liverpool Women's NHS Foundation Trust, Crown Street, Liverpool, L8 7SS, UK

[4]Current address: North Western Deanery, Salford Royal NHS Foundation Trust, Salford, M6 8HD, UK

[§]These authors contributed equally

*Corresponding author:

Postal address: Department of Biochemistry, Institute of Integrative Biology, University of Liverpool, Crown Street, Liverpool, L69 7ZB, UK

Email: daimark.bennett@liverpool.ac.uk

Telephone: ++44 151 795-4568

Running title: MRL proteins drive distinct oncogenic outcomes

Word count (excluding abstract, references and figure legends): 4,500

Conflict of Interest statement: There is no conflict of interest to disclose

Abstract

The Mig10/RIAM/Lpd (MRL) adapter protein Lpd regulates actin dynamics through interactions with Scar/WAVE and Ena/VASP proteins to promote the formation of cellular protrusions and to stimulate invasive migration. However, the ability of MRL proteins to interact with multiple actin regulators and to promote SRF signalling has raised the question of whether MRL proteins employ alternative downstream mechanisms to drive oncogenic processes in a context-dependent manner. Here, using a *Drosophila* model, we show that overexpression of either human Lpd or its *Drosophila* orthologue Pico can promote growth and invasion of Ras^{V12}-induced cell tumours in the brain. Notably, effects were restricted to two populations of Repo-positive glial cells: an invasive population, characterised by JNK-dependent elevation of Mmp1 expression, and a hyperproliferative population lacking elevated JNK signalling. JNK activation was not triggered by reactive immune cell signalling, implicating the involvement of an intrinsic stress response. The ability to promote dissemination of Ras^{V12}-induced tumours was shared by a subset of actin regulators, including, most prominently, Chicadee/Profilin, which directly interacts with Pico, and, Mal, a cofactor for SRF that responds to changes in G:F actin dynamics. Suppression of Mal activity partially abrogated the ability of *pico* to promote invasion of Ras^{V12} tumours. Furthermore, we found that larval glia are enriched for SRF expression, explaining the apparent sensitivity of glial cells to $Pico/Ras^{V12}$ overexpression. Taken together, our findings indicate that MRL proteins cooperate with oncogenic Ras to promote formation of glial tumours, and that, in this context, Mal/SRF activation is rate-limiting for tumour dissemination.

Introduction

Regulation of actin-based structures is critical for normal cell adhesion, morphology and motility. Correspondingly, aberrant cytoskeletal dynamics are implicated in the motility and dissemination of cancer cells. In addition to the direct effects of actin reorganisation, for example on lamellipodia-like structures at the leading edge of invasive cells, regulators of cytoplasmic actin also control the localisation and activity of myocardin-related transcription factors (MRTF/Mal), which are transcriptional coactivators of SRF, by regulating the availability of monomeric (G-)actin. Depletion of nuclear and cytoplasmic G-actin in response to increased actin polymerization increases the rate of MRTF/Mal translocation to the nucleus, reduces the rate of nuclear export of MRTF/Mal and derepresses the expression of genes that require MRTF/Mal for transcription, leading to SRF-dependent transcription(Grosse et al., 2003, Sotiropoulos et al., 1999, Vartiainen et al., 2007).

The Mig-10/RIAM/Lamellipodin (MRL) family of adapter proteins transduce signals derived from growth factor receptors, via interactions with Ras-like GTPases and/or phospholipids, to changes in the actin cytoskeleton, increased lamellipodia protrusion, cell motility and altered cell adhesion(Krause et al., 2004, Lafuente et al., 2004). Effects on the actin cytoskeleton are mediated by direct interactions with various actin regulatory proteins, including Ena/VASP, Scar/WAVE and Profilin(Krause et al., 2004, Lafuente et al., 2004, Law et al., 2013). MRL proteins are also capable of activating SRF signalling by altering the ratio of G:F actin(Lyulcheva et al., 2008). MRL proteins are therefore good candidates for genes that drive tumour cell invasion and metastasis. Indeed, in breast cancer, Lpd is upregulated in tumours with lymph node metastases compared to lymph node-negative tumours(Ginestier et al., 2006) and also in highly invasive MDA-MB231 breast cancer cells compared to non-invasive MCF7 breast cancer cells or normal breast tissue(Ross et al., 2000). Furthermore, increased expression and membrane localization correlate with reduced

metastasis-free survival and poor prognosis in breast cancer patients(Carmona et al., 2016). Mechanistically, MRL proteins promote invasive 3D breast cancer cell migration via interactions with the actin regulators Scar/Wave and Ena/VASP(Carmona et al., 2016). Lpd is also part of the “Ras cancer signature” as it is upregulated in human breast epithelial cells transformed with oncogenic Ras(Bild et al., 2006). The “Ras signature” reflects the activation status of the Ras pathway and has been successfully used to identify patterns of pathway deregulation in human tumours and to identify clinically relevant associations with disease outcomes(Bild et al., 2006). An understanding of the functional consequences of MRL-Ras interactions in cancer development is however currently lacking.

Drosophila encodes only one MRL protein, called Pico, enabling the dissection of conserved cancer promoting effects of the MRL gene family in an animal model, with the potential to help guide studies in mammalian systems(Bennett et al., 2015). Many biological processes related to tumourigenesis and metastasis are well conserved in flies and nearly all of the genes linked to cancer progression in humans are present in the *Drosophila* genome (Brumby and Richardson, 2005, Bennett et al., 2015). Here we have tested the prediction that MRL proteins might cooperate with oncogenic Ras by promoting invasiveness of Ras^{V12}-induced tumours in the larval eye disc and brain. Notably, we observed tumour overgrowth and invasion, but these cooperative effects were restricted to cells expressing the pan-glial marker Repo; loss of overexpression in glia, and not in other cell types, completely suppressed oncogenic cooperation. Notably, SRF is strongly enriched in glia providing an explanation for why glia were specifically affected. Moreover, overexpression of *mal*, a cofactor for SRF, or *chickadee, Drosophila* profilin, also cooperated strongly with oncogenic Ras to drive glial invasion. Taken together, our findings provide experimental evidence for the role of MRL proteins in the hyperproliferation and transformation of glial tumours *in vivo*. Furthermore, Profilin and downstream SRF signalling predominantly drive this process rather than other MRL-interactors, Ena/VASP and Scar/WAVE, as is the case in other contexts.

Results

Pico co-operates with oncogenic Ras to promote tumour dissemination

Oncogenic mutations in Ras are frequent events early stages of cancer development, driving proliferative overgrowth and contributing to tumour formation. The Ras pathway also modulates cytoskeleton organisation, cell motility and expression of metastasis signature genes (Choi and Helfman, 2014), but cooperation between oncogenic Ras and its downstream targets are poorly understood. To test the interaction between Pico and Ras, we used a cancer model in *Drosophila* in which genetically-defined tumours can be induced in the developing eye disc and brain(Brumby and Richardson, 2003, Pagliarini and Xu, 2003). First we examined the effect of overexpressing *pico* or Ras^{V12} alone or together in GFP-labelled cells in the eye imaginal discs and optic lobes of wandering third instar larvae. Notably, coexpression of *pico* and Ras^{V12} led to an accumulation of GFP-labelled cells and redistribution to more distant sites. This effect was not observed whether either gene was overexpressed in isolation (**Fig.1A**). To quantify the effects on tissue overgrowth we captured images of optical sections through brains dissected from the different genotypes and measured the volume occupied by GFP-labelled cells. There was no significant difference in volume of GFP-labelled cells expressing *pico* or Ras^{V12} alone compared to controls (**Fig.1B, C**). In contrast, *pico* and Ras^{V12} co-overexpression resulted in a 1.9 fold increase in volume of GFP-labelled cells in the optic lobes compared to GFP alone controls, $P<0.001$ (**Fig.1C**).

Inspection of the distribution of GFP-labelled cells in the brain revealed that GFP-labelled *pico*/Ras^{V12} tumour cells had invaded into the ventral nerve cord (VNC) in the majority (82/100) of cases (**Fig.1B**), whereas cells expressing *pico* or Ras^{V12} alone never extended beyond the optic lobe. To quantitate the tumour cell invasion phenotypes produced for each of the genotypes, brains were assigned to one of four categories based on the degree of VNC invasion observed: Type 0, no invasion of the VNC; Type I,

tumour cell invasion occurring down one side of the VNC only; Type II, tumour cells invading both sides of the VNC; Type III, significant tumour cell invasion of the VNC combined with fusion of the optic lobes (**Fig.1D**). Cephalic complexes dissected from animals expressing *pico* and Ras^{V12} were entirely composed of Type 0 brains, whereas only 18% of Ras^{V12}*/pico* brains were found to exhibit no VNC invasion. 53% of Ras^{V12}*/pico* brains were found to have mild Type I invasion, and 21% and 8% of brains were assigned to Type II and Type III categories, respectively (**Fig.1E**). To test functional conservation, we examined the effect of ectopic overexpression of human Lpd (hLpd) in this system. Brains expressing hLpd showed no evidence of invasion, but, like *pico*, hLpd was able to drive invasion of Ras^{V12}-induced tumours, which occurred in 64/100 of cases (**Fig.1E**).

We previously showed that *pico* promotes coordinated growth and proliferation in the wing imaginal discs prompting us to wonder whether the presence of GFP-positive tumour cells in the VNC could be simply explained by expansion of the population of tumour cells rather than by cell invasion. To address this, we tested the effects of co-overexpressing *Drosophila cyclin-D* (*cycD*) and *cyclin-dependent kinase-4* (*cdk4*) in our assay. Cells overexpressing Ras^{V12}, *cycD* and *cdk4*, showed extensive levels of proliferation but were never located outside of the eye-antennal discs/optic lobe region. This is in agreement with previous reports that excessive proliferation does not account for presence of tumour cells in the VNC (Pagliarini and Xu, 2003). Together these data suggest that ectopic *pico*, can drive the dissemination of otherwise benign Ras^{V12} tumour cells into neighbouring tissues.

Invasive Pico/Ras^{V12} tumours are characterised by elevation of MMP1 and extracellular matrix remodelling

Degradation of the extracellular matrix by matrix metalloproteases (MMPs) is required during tissue remodelling and during the progression of many types of cancer (Coussens and Werb, 2002, Srivastava et al., 2007). To investigate integrity of the extracellular matrix, we examined the distribution of Laminin,

which is a major component both of the basement membrane underpinning the basal side of epithelial cells and of the gliovascular basal lamina of the blood brain barrier. In brains ectopically expressing either *pico* or Ras^{V12}, Laminin staining of the optic lobes was found to be smooth and uninterrupted. In contrast, discontinuous Laminin staining was observed around the optic lobes of Ras^{V12}/*pico* brains, consistent with degradation of the extracellular matrix (**Fig.2A**). When we examined MMP expression we found that Mmp1 was found to be largely absent in brains overexpressing either *pico* or Ras^{V12}. In contrast, a marked increase in Mmp1 levels was observed in cephalic complexes expressing both *pico* and Ras^{V12} (**Fig.2B**). Interestingly, Mmp1 expression was not detected in all Ras^{V12}, *pico* cells; Mmp1 staining was mainly observed in the marginal regions of the optic lobes and in the tumour cells that had invaded the VNC (**Fig.2B**).

JNK activation is required for Pico/Ras^{V12}-mediated MMP expression and tumour cell spreading

Studies of Ras^{V12} tumours with impaired cell polarity (e.g. due to mutations in the tumour suppressor gene *scrib*) have revealed that JNK activation is critical for Mmp1 upregulation and tumour cell invasion of the VNC(Uhlirova and Bohmann, 2006). To assess the state of JNK signalling in Ras^{V12}/*pico brains*, we monitored the levels of *puckered*, a downstream target of JNK (Martin-Blanco et al., 1998) using a *lacZ* enhancer trap (*puc-lacZ*). We observed limited *puc-lacZ* staining in brains expressing Ras^{V12} or *pico* alone, but in Ras^{V12}/*pico* brains we observed a significant increase in the number of *puc-lacZ*-positive nuclei ($P<0.01$) indicative of elevated JNK activation in these cells (**Fig.3A,B**). Not every cell showed *puc-lacZ*-positive nuclei indicating that JNK activation was not a necessary outcome of Ras^{V12}/*pico* overexpression (**Fig.3A**).

To determine the requirement for JNK signalling in Ras^{V12}/*pico*-mediated metastasis we tested the effect of coexpressing a dominant-negative form of the *Drosophila* JNK, encoded by *basket* (bsk^{DN}). Ectopic overexpression of bsk^{DN} strongly suppressed JNK activation as monitored with *puc-lacZ*

(**Fig.3B,C**). Strikingly, overexpression of *bsk*^{DN} also reduced Mmp1 levels 4.1 fold (P<0.01) in GFP-labelled tumour cells (**Fig.3D,E**) and also almost completely blocked *Ras*^{V12}*/pico*-mediated tumour cell invasion of the VNC (**Fig.3F**). In the absence of *bsk*^{DN}, evidence of spreading was observed in 80/100 cases of *Ras*^{V12}*/pico* tumours, whereas in siblings co-expressing *bsk*^{DN}, invasion was only evident in 6/100 cases (Fisher's exact test, *P*<0.0001). Using our scale of the extent of invasion (**Fig.1D**) the average stage score of invasion (ASI) in *Ras*^{V12}*/pico* larvae was 1.16 ±0.08 (mean ±SEM), but this was significantly reduced by coexpression of *bsk*^{DN} to 0.06 ±0.02, (student's t-test, *P*<0.001). Taken together, these data indicate that *pico* cooperates with oncogenic Ras to promote JNK activation, and that JNK activation is essential for invasion of *Ras*^{V12}*/pico* tumours.

Haemocyte-mediated immune responses are not required for pico-mediated invasion

Accumulating evidence suggests that diversion of host immunity can contribute to the acquisition of invasive behaviour. In *Drosophila*, inflammatory responses, mediated by Eiger/TNF-producing haemocytes, trigger JNK activation leading to invasive behaviour of Ras^{V12}-induced tumours (Cordero et al., 2010) (**Fig.4A**). The mechanism of haemocyte recruitment to tumours is not well understood. To test the involvement of the immune response in *Ras*^{V12}*/pico* brains, we examined whether there was accumulation of haemocytes at sites of tumour invasion. Although we observed haemocyte recruitment to a proportion of *Ras*^{V12}*/pico* brains, haemocyte number was not correlated with presence or severity of cellular invasion; some invasive tumours lacked associated haemocytes (**Fig.4B**). To test whether *pico*-mediated metastasis is driven by diversion of the host immune response mediated byTNF/eiger, we tested the effect of *Ras*^{V12} *pico* overexpression in an *eiger* null genetic background. Loss of *eiger* modestly suppressed invasion in *Ras*^{V12}*/pico* brains (**Fig.4C**); whereas 80/100 *Ras*^{V12}*/pico* animals showed GFP-labelled cells in the VNC, invasion was observed in 67/100 *Ras*^{V12}*/pico* animals lacking *eiger* (*eiger*^{3}*/eiger*^{3}), which was at the borderline of significance (Fisher's exact test, *P*=0.054). However,

there was little effect on the average stage of invasion, which reduced from 1.16 ±0.08 to 1.14 ±0.10 (student's t-test, *P*=0.88) when *eiger* was absent. Taken together this indicates that *pico* does not primarily promote invasive behaviour through diversion of a TNF-mediated immune response.

Pico cooperates with activated Ras to drive distinct oncogenic outcomes in glia

When we looked at distribution of JNK activation more closely in *Ras^{V12} pico* brains it was apparent that many puc-lacZ positive cells decorated the surface of the optic lobes. This non-random distribution made us wonder whether JNK activation was restricted to specific cell types. Indeed, we found the combination of *eyFLP* with *AyGAL4* was capable of driving expression in a range of cells in the larval optic lobes (**Fig.5A**), consistent with previous reports showing expression in neuroblasts, lamina and medulla neurons, neurophils and medulla cortex glia (Chotard et al., 2005). When we looked at the distribution of neuronal and glial markers in GFP-labelled *Ras^{V12} pico* tumours we found that almost all cells that were positive for puc-lacZ also stained for the pan-glial marker Repo. GFP-labelled cells invading into the VNC were of this type (**Fig.5B**, arrow); puc-lacZ staining in these cells is consistent with our genetic data indicating a requirement for JNK to mediate Mmp1 expression and extracellular matrix breakdown (see **Fig.3**). Although rare, we did observe a few Repo-negative GFP-labelled cells with puc-lacZ staining, although interestingly these were typically juxtaposed directly next to Repo-positive glial cells (**Fig.5B**, white arrowhead and inset, see Discussion). We also observed a distinct Repo-positive population consisting of many small cells that were puc-lacZ negative, located in a region of the optic lobe that had appeared to have overproliferated (**Fig.5B**, yellow arrowhead; **Fig.5C**). When we counted the number of Repo-positive cells in GFP-labelled tumours within the optic lobes (**Fig.5C,D**), we found that *Ras^{V12}* overexpression led to a 1.6 fold increase in glial number in GFP-labelled regions compared to GFP only controls ($P<0.01$). The increase in glial number was not matched by a significant increase in GFP-labelled tumour volume (**Fig.1**), most likely because many *Ras^{V12}*-overexpressing cells were small (Read et al., 2009). Co-overexpression of *pico* significantly enhanced the effect of *Ras^{V12}* (**Fig.5D**), leading to a 2.3 fold increase in glial number compared to GFP alone controls ($P<0.05$). Taken together, the data above indicate that ectopic *Ras^{V12}* and *pico* cooperate to promote overproliferation of one glial cell population in the developing optic lobe without the activation

of JNK, whilst promoting JNK activation and cell invasion in another glial population.

Overexpression of Ras^{V12} Pico in glia is necessary for an increase in tumour volume and cell invasion

To test if the tumour overgrowth and invasion phenotypes we had observed in the optic lobe were due to ectopic expression of Ras^{V12} and *pico* in *eyFLP*-expressing $Repo^{+}$ glia, we repeated our experiments in a *repo-GAL80* background to block GAL4-mediated expression specifically in *repo*-positive glia but not in other cell types (**Fig.6A**). When we measured the volume of GFP-labelled tumours in Ras^{V12}*/pico* optic lobes from animals with (n=8) or without *repo-GAL80* (n=16), we found that *repo-GAL80* reduced the mean tumour volume 2.9 fold (P<0.001) (**Fig.6C**). The mean intensity of Mmp1 staining in GFP-labelled tumours was also reduced 5.1 fold (P<0.001) (**Fig.6D**). Correspondingly, there was a significant reduction in the instances of invasion into the VNC to 5/100 of cases (Fisher's exact test, *P*<0.0001) and a corresponding reduction in the ASI to 0.05 ±0.02 (*P*<0.0001) (**Fig.6E**). As an additional test, we further validated these findings by using a more restricted *eyeless*-driven FLPase, *ey(3.5)FLP*, which does not drive expression in the optic lobes of the brain (Bazigou et al., 2007). Overexpression of Ras^{V12} *pico* with *ey(3.5)FLP* did not replicate the growth and invasion phenotypes observed with *eyFLP*, consistent with our observations that overexpression in glia was required. Expression of Ras^{V12} specifically in GFP-labelled glia with *repo-GAL4* was pupal lethal but led to overgrowth and extension of the larval VNC (mean VNC length 130% of control, Student's t-test P<0.05, n=10). Co-expression of Ras^{V12} with *pico*, led to lethality at the wandering larval stage and extension of the VNC was significantly enhanced (to 187% of control, P<0.01, n=9), again consistent with a co-operative interaction in glia.

SRF is enriched in larval glia in the CNS

Why should glia be particularly sensitive to coexpression of ectopic *pico* and Ras^{V12}? We recently demonstrated that overexpression of *pico* reduces the

ratio of G:F-actin and is capable of inducing activation of SRF signalling *in vitro* (Lyulcheva et al., 2008). This prompted us to question whether the cooperation between *pico* and Ras^{V12} was mediated by SRF signalling. Although SRF is expressed throughout the adult brain (Donlea et al., 2009), where it plays roles in sleep and visual memory (Donlea et al., 2009, Thran et al., 2013), we wondered whether SRF expression is spatially regulated in the CNS earlier in development, as it is in other tissues such as the wing imaginal disc (data not shown). Notably, we detected strong anti-SRF antibody staining in glia from third instar optic lobes (**Fig.7A-B**). SRF staining was evident both in Repo positive surface glia (**Fig.7A**) and in other glial types (**Fig.7B**).

The ability of Pico to promote tumour invasion is shared by selected actin regulatory genes

To further examine the contribution of actin dynamics and SRF to the development of invasive cell behaviours, we tested the effect of co-overexpressing oncogenic Ras^{V12} together with Profilin/*chic*, which has multiple roles in the augmentation of F-actin dynamics, or with regulatory proteins that bind Pico and are known to control actin polymerisation by affecting the number of free barbed ends: Enabled/*ena* (anti-capping factor) and SCAR (actin nucleation) (Shekhar et al., 2016). We also tested the effect of ectopic *mal*, which encodes a cofactor for SRF and responds to changes in actin dynamics to induce SRF-dependent gene expression. Overexpression of any of the above factors alone in the absence of Ras^{V12} did not induce invasive behaviour as determined by the lack of GFP-positive cells in the VNC. However, overexpression of *mal*, *chic*, *ena* or *scar* was sufficient to promote the acquisition of invasive behaviour in otherwise benign Ras^{V12}-expressing tumours (**Fig.7C**). Based on the percentage number of larvae showing GFP-labelled cells in the VNC, these proteins can be ranked according to their invasive potential in this system, as follows: *mal* (88%)> *pico* (79%)> *chic* (77%)> *ena* (35%)> *scar* (25%), where percentage of larvae with invasion into the VNC are shown in parenthesis (n=100 in each case). This is also in agreement with the average stage of invasion for Ras^{V12}-

induced tumours co-expressing these regulators: *mal* (1.38 ±0.09)> *pico* (1.16 ±0.09)> *chic* (0.92 ±0.06)> *ena* (0.35 ±0.05)> *scar* (0.25 ±0.04). When we tested the effect of co-expressing Ras^{V12} and *pico* together with either *mal, chic* or *ena* we found the degree of invasion observed was not significantly increased compared to the effect of pairwise combinations of these inducers or pico alone with Ras^{V12} (**Fig.7C-D**). The lack of an additive effect suggests that these proteins may act in the same pathway to induce invasion, albeit to different extents.

MRL proteins interact directly with Profilin, Ena/VASP and the Scar/Wave complex via a number of proline-rich regions present in their C-terminal regions (Hansen and Mullins, 2015, Krause et al., 2004, Lafuente et al., 2004, Law et al., 2013, Lyulcheva et al., 2008). To test whether these regions of Pico might be necessary for promoting invasion of Ras^{V12} tumours, we expressed a truncated version of *pico* encoding only its central RA-PH domain ($pico^{RA\text{-}PH}$). $pico^{RA\text{-}PH}$ failed to promote cell invasion into the VNC alone or together with coexpression of Ras^{V12} (0/100 cases of invasion in each case), suggesting that physical interaction between Pico and its downstream effectors are important for cooperation with oncogenic Ras. Profilin, Ena/VASP and the Scar/Wave complex affect the actin cytoskeleton directly but are also capable of promoting Mal-SRF activity via altered actin dynamics. To assess the likely contribution of direct verses indirect effects on the actin cytoskeleton, we tested the effect of a dominant-negative version of Mal (mal^{DN}), which lacks its C-terminal transcription activation domain (Han et al., 2004). Compared to Ras^{V12}*/pico* control animals, there was a significant reduction in the number of cases of tumour invasion in siblings coexpressing mal^{DN} (82/100 to 52/100 cases, respectively; Fisher's exact test, P<0.0001). There was also a significant reduction in the average stage of invasion, from 1.19 ±0.08 to 0.64 ±0.07 (student's t-test, P<0.0001) when mal^{DN} was present (**Fig.7E**). Taken together this indicates that indirect effects via Mal/SRF signalling is rate-limiting for invasion of Ras^{V12}*/pico* tumours.

Discussion

Here, we find that *pico* overexpression is capable of promoting distinct oncogenic behaviours in Ras^{V12}-induced tumour cells. In particular, we observed an invasive cell population showing elevation of JNK signalling, and a hyperproliferative population lacking JNK activation. These effects were restricted to glia since the affected cell populations labelled positively with the pan-glial marker, Repo, and cooperation between Ras^{V12}*/pico* was lost upon transcriptional repression in glia with *repo-GAL80*. In glia, JNK is likely to act as a proapoptotic signal as it does in epithelia – indeed, subperineurial glial cells possess a cryptic JNK-dependent apoptotic programme (Ohayon et al., 2009). However, any such programme must be suppressed by survival signals from oncogenic Ras as it is in other contexts (Wu et al., 2009). We found that Mmp1 expression was JNK-dependent, supporting the idea that JNK activation is subverted by tumour cells to promote invasion. Invasion of Ras^{V12}*/pico* tumours was not dependent on presence of haemocytes, nor was invasion significantly affected by complete loss of *eiger*/TNF function. One possibility is that transformed glial cells may be resistant to haemocyte attachment and/or signalling. Examination of the cell type specific expression pattern of TNF signalling components, such as the recently identified TNF/Eiger receptor Grindelwald (Andersen et al., 2015) may provide a mechanistic explanation for why glia respond differently from epithelial tumour cells to circulating immune cells. Alternatively, transformed glia may express inhibitory cell surface or secreted molecules making them refractory to the innate immune system, as is the case for human glioma cells (Friese et al., 2004).

Interestingly, a small number of Repo negative cells overexpressing Ras^{V12}*/pico*, adjacent to Repo positive Ras^{V12}*/pico* tumour cells, also displayed elevated JNK activity. In addition to roles in CNS development and function, glia are considered to be primary immune cells of the CNS that survey the CNS for neuronal damage, modulating inflammatory responses and engulfing debris or foreign material (Logan and Freeman, 2007). The JNK pathway mediates glial engulfment activity in *Drosophila* (Shklover et

al., 2015, Macdonald et al., 2013), raising the intriguing possibility that *Ras^{V12}/pico* stimulates glial phagocytosis of tissue damage caused by premalignant tumour cells. Diversion of the glial damage response program by carcinoma cells has previously been reported in murine organotypic brain slice co-cultures (Chuang et al., 2013), stimulating local invasion in tumours resistant to glial-induced apoptosis. It will therefore be interesting to examine whether this phenomenon is JNK-dependent.

Recent work has shown the actin cytoskeleton acts both upstream and downstream of JNK (Rudrapatna et al., 2014, Kulshammer and Uhlirova, 2013, Fernandez et al., 2014) and, conceptually, changes in cell tension resulting from altered actin cytoskeleton may trigger JNK as part of a stress response. We were interested to explore whether actin regulators that associate with Pico could similarly cooperate with *Ras^{V12}*. In breast cancer cells, the ability of Lpd to promote 3D invasion relies on its interactions with both Ena/VASP and Scar/WAVE (Carmona et al., 2016). Although both *ena* and *scar* were capable of cooperating with *Ras^{V12}* in our model, their effect was modest compared to the effect of *chic* (*Drosophila* Profilin). This might be because Ena and Scar are not limiting, or it might reflect a specific requirement for Chic. Interestingly, in this regard, Profilin assists in coordination of actin turnover (Balcer et al., 2003, Didry et al., 1998), which is the driving force for membrane protrusion and spreading of some types of glia in the CNS (Nawaz et al., 2015). Recent work has also demonstrated that changes in actin dynamics driven by MRL proteins and their binding partners can activate SRF signalling (Lyulcheva et al., 2008, Pinheiro et al., 2011). This raised the issue of whether effects we observed were due to direct or indirect effects on the actin cytoskeleton. Several lines of evidence suggest that Mal/SRF signalling is important for *pico*/*Ras^{V12}* cooperation: firstly, SRF expression is enriched in glia; secondly, the effects of overexpression of *mal* were at least as potent as those of *pico*; thirdly, *mal^{DN}* suppressed the *pico*-mediated invasion of *Ras^{V12}*-induced tumours. In mammalian cells the majority of SRF target genes encode cytoskeletal components (Esnault et al., 2014) and recent work in *Drosophila* suggest

that actin itself is a key homeostatic target (Salvany et al., 2014). Control of Mal/SRF activity therefore may provide a mechanism by which cytoskeletal gene expression is coordinated with cytoskeletal regulation. Our data showing that *mal* can similarly cooperate with oncogenic *Ras* suggests that actin-dynamics via Mal/SRF signalling has a rate-limiting role, and could function to facilitate the direct effects on cytoskeletal remodelling.

In summary, our data indicate that overexpression of MRL proteins is capable of driving invasion and overproliferation of Ras^{V12}-induced glial cell tumours in an *in vivo* experimental model. Notably, our findings, in glia, implicate *Drosophila* Profilin and SRF signalling in MRL-mediated tumour dissemination, whereas interactions between Lpd and Ena/VASP and Scar/WAVE have been reported to be critical in the invasion of breast cancer cells. This points to important differences in the mechanism of action of MRL proteins depending on the cellular context. Given that SRF is capable of promoting human glioma cell migration (Ziv-Av et al., 2011) and Lpd overexpression has been detected in glioma samples from patients (Petryszak et al., 2016), investigation into whether Lpd or SRF levels are associated with disease progression and patient outcome is warranted.

Material and Methods

Fly husbandry and genetics

Flies were reared at 25°C under standard conditions. All initial *Drosophila* strains have been previously described. 3rd instar larvae were examined 6 days after egg laying. Genotypes are provided in a supplementary file.

Immunohistochemistry

Tissues were dissected from 3rd instar larvae were fixed and stained as (Ciurciu et al., 2013) with minor modifications. After fixation for 20 min in 4% (w/v) paraformaldehyde in PBS, dissected brains from third instar larvae were washed in PBS with 0.1% Triton-X (PBST), then blocked for 2 h in PBST with 5% FCS (blocking solution). Primary antibody staining was done overnight at 4ºC in blocking solution, washed three times with PBST and incubated with secondary antibody in blocking solution for 2 h at room temperature. After three washes in PBST, brains were mounted in Vectasheild mounting media (Vectorlabs). Primary antibodies were as follows: mouse anti-phospho-Histone H3 (Abcam, 1:500); rabbit anti-Laminin (1:1000); guinea-pig anti-Repo (1:1000); rabbit anti-Repo (1:25,000); mouse anti-NimC1 P1 (Kurucz et al., 2007)(1:30), mouse anti-MMP1 (1:1:1 mix of 3A6B4, 3B8D12, 5H7B11 from DSHB diluted 1:10); mouse anti-β–gal (Promega, 1:100); mouse anti-SRF (Active Motif, 1:100). Secondary antibodies were conjugated to Alexa-Fluor 555 or 633 (Invitrogen, 1:500). TO-PRO-3 Iodide (Invitrogen, 1:1000) or DAPI was used to visualise DNA.

Image acquisition and analysis

Dissected tissues were imaged on Zeiss LSM710, 780 or 880 microscopes equipped with 405nm, 488nm, 568nm and 633nm lasers using either Fluor 20x or Plan Apochromat 40x/1.3NA oil immersion objective. Images were imported into OMERO (Allan et al., 2012) and adjusted for brightness and contrast uniformly across entire fields where appropriate. Figures were constructed in Adobe Photoshop. Quantitative analysis of raw confocal data was conducted using Bitplane Imaris version 8.2.0 (Oxford Instruments). The GFP channel was segmented into 3D volumes (5µm surface grain size) by

absolute intensity using an automatically selected intensity threshold. To remove small unattached objects, only the two largest volumes were kept per experiment (corresponding in all cases to the optic lobes), and their volume measured. To count the number of Repo or puc-lacZ positive cells, the above volumes were used to mask the relevant intensity channel, which was then subject to spot segmentation using an estimated spot diameter of 5µm and background subtraction. Spots were subjected to an automatically-thresholded intensity filter. All automatic thresholding was visually inspected and adjusted if necessary. For quantitation of Mmp1 staining, stacks were projected in 'z' and then background subtracted in the Mmp1 channel. The GFP channel was used to segment, then the selection was measured in the Mmp1 channel. Whole animal micrographs were captured with a ZF10 stereomicroscope (Leica) using LAS software (Leica).

Acknowledgements

We thank the Bloomington Stock Centre, Zhe Han, Julian Ng, Pernille Rorth, Eyal Schejter, Marcos Vidal, Sanjai Patel and the Manchester Fly Facility for *Drosophila* strains, B. Altenhein, I Andó, the Developmental Studies Hybridoma Bank, S. Baumgartner and Manzoor Bhat for antibodies, Marco Marcello in the Liverpool Centre for Cell Imaging for assistance with image acquisition, Chris Lofthouse for artwork, and Mirel Lucaci for technical assistance. This work was supported by grants from BBSRC (BB/L014947/1, BB/M012441/1), MRC (MR/K015931/1) and CRUK (C20691/A11834).

References

1. Grosse, R., J.W. Copeland, T.P. Newsome, M. Way, and R. Treisman, A role for VASP in RhoA-Diaphanous signalling to actin dynamics and SRF activity. Embo J, 2003. 22(12): p. 3050-61.
2. Sotiropoulos, A., D. Gineitis, J. Copeland, and R. Treisman, Signal-regulated activation of serum response factor is mediated by changes in actin dynamics. Cell, 1999. 98(2): p. 159-69.
3. Vartiainen, M.K., S. Guettler, B. Larijani, and R. Treisman, Nuclear actin regulates dynamic subcellular localization and activity of the SRF cofactor MAL. Science, 2007. 316(5832): p. 1749-52.
4. Krause, M., J.D. Leslie, M. Stewart, E.M. Lafuente, F. Valderrama, R. Jagannathan, et al., Lamellipodin, an Ena/VASP ligand, is implicated

in the regulation of lamellipodial dynamics. Dev Cell, 2004. 7(4): p. 571-83.

5. Lafuente, E.M., A.A. van Puijenbroek, M. Krause, C.V. Carman, G.J. Freeman, A. Berezovskaya, et al., RIAM, an Ena/VASP and Profilin ligand, interacts with Rap1-GTP and mediates Rap1-induced adhesion. Dev Cell, 2004. 7(4): p. 585-95.

6. Law, A.L., A. Vehlow, M. Kotini, L. Dodgson, D. Soong, E. Theveneau, et al., Lamellipodin and the Scar/WAVE complex cooperate to promote cell migration in vivo. J Cell Biol, 2013. 203(4): p. 673-89.

7. Lyulcheva, E., E. Taylor, M. Michael, A. Vehlow, S. Tan, A. Fletcher, et al., Drosophila pico and its mammalian ortholog lamellipodin activate serum response factor and promote cell proliferation. Dev Cell, 2008. 15(5): p. 680-90.

8. Ginestier, C., N. Cervera, P. Finetti, S. Esteyries, B. Esterni, J. Adelaide, et al., Prognosis and gene expression profiling of 20q13-amplified breast cancers. Clin Cancer Res, 2006. 12(15): p. 4533-44.

9. Ross, D.T., U. Scherf, M.B. Eisen, C.M. Perou, C. Rees, P. Spellman, et al., Systematic variation in gene expression patterns in human cancer cell lines. Nat Genet, 2000. 24(3): p. 227-35.

10. Carmona, G., U. Perera, C. Gillett, A. Naba, A.L. Law, V.P. Sharma, et al., Lamellipodin promotes invasive 3D cancer cell migration via regulated interactions with Ena/VASP and SCAR/WAVE. Oncogene, 2016.

11. Bild, A.H., G. Yao, J.T. Chang, Q. Wang, A. Potti, D. Chasse, et al., Oncogenic pathway signatures in human cancers as a guide to targeted therapies. Nature, 2006. 439(7074): p. 353-7.

12. Bennett, D., E. Lyulcheva, and N. Cobbe, Drosophila as a Potential Model for Ocular Tumors. Ocul Oncol Pathol, 2015. 1(3): p. 190-9.

13. Brumby, A.M. and H.E. Richardson, Using Drosophila melanogaster to map human cancer pathways. Nat Rev Cancer, 2005. 5(8): p. 626-39.

14. Choi, C. and D.M. Helfman, The Ras-ERK pathway modulates cytoskeleton organization, cell motility and lung metastasis signature genes in MDA-MB-231 LM2. Oncogene, 2014. 33(28): p. 3668-76.

15. Brumby, A.M. and H.E. Richardson, scribble mutants cooperate with oncogenic Ras or Notch to cause neoplastic overgrowth in Drosophila. EMBO J, 2003. 22(21): p. 5769-79.

16. Pagliarini, R.A. and T. Xu, A genetic screen in Drosophila for metastatic behavior. Science, 2003. 302(5648): p. 1227-31.

17. Coussens, L.M. and Z. Werb, Inflammation and cancer. Nature, 2002. 420(6917): p. 860-7.

18. Srivastava, A., J.C. Pastor-Pareja, T. Igaki, R. Pagliarini, and T. Xu, Basement membrane remodeling is essential for Drosophila disc

eversion and tumor invasion. Proceedings of the National Academy of Sciences of the United States of America, 2007. 104(8): p. 2721-2726.

19. Uhlirova, M. and D. Bohmann, JNK- and Fos-regulated Mmp1 expression cooperates with Ras to induce invasive tumors in Drosophila. EMBO J, 2006. 25(22): p. 5294-304.

20. Cordero, J.B., J.P. Macagno, R.K. Stefanatos, K.E. Strathdee, R.L. Cagan, and M. Vidal, Oncogenic Ras diverts a host TNF tumor suppressor activity into tumor promoter. Dev Cell, 2010. 18(6): p. 999-1011.

21. Chotard, C., W. Leung, and I. Salecker, glial cells missing and gcm2 cell autonomously regulate both glial and neuronal development in the visual system of Drosophila. Neuron, 2005. 48(2): p. 237-51.

22. Read, R.D., W.K. Cavenee, F.B. Furnari, and J.B. Thomas, A drosophila model for EGFR-Ras and PI3K-dependent human glioma. PLoS Genet, 2009. 5(2): p. e1000374.

23. Bazigou, E., H. Apitz, J. Johansson, C.E. Loren, E.M. Hirst, P.L. Chen, et al., Anterograde Jelly belly and Alk receptor tyrosine kinase signaling mediates retinal axon targeting in Drosophila. Cell, 2007. 128(5): p. 961-75.

24. Donlea, J.M., N. Ramanan, and P.J. Shaw, Use-dependent plasticity in clock neurons regulates sleep need in Drosophila. Science, 2009. 324(5923): p. 105-8.

25. Thran, J., B. Poeck, and R. Strauss, Serum response factor-mediated gene regulation in a Drosophila visual working memory. Curr Biol, 2013. 23(18): p. 1756-63.

26. Shekhar, S., J. Pernier, and M.F. Carlier, Regulators of actin filament barbed ends at a glance. J Cell Sci, 2016.

27. Hansen, S.D. and R.D. Mullins, Lamellipodin promotes actin assembly by clustering Ena/VASP proteins and tethering them to actin filaments. Elife, 2015. 4.

28. Han, Z., X. Li, J. Wu, and E.N. Olson, A myocardin-related transcription factor regulates activity of serum response factor in Drosophila. Proc Natl Acad Sci U S A, 2004. 101(34): p. 12567-72.

29. Miles, W.O., N.J. Dyson, and J.A. Walker, Modeling tumor invasion and metastasis in Drosophila. Dis Model Mech, 2011. 4(6): p. 753-61.

30. Rudrapatna, V.A., R.L. Cagan, and T.K. Das, Drosophila cancer models. Dev Dyn, 2012. 241(1): p. 107-18.

31. Ohayon, D., A. Pattyn, S. Venteo, J. Valmier, P. Carroll, and A. Garces, Zfh1 promotes survival of a peripheral glia subtype by antagonizing a Jun N-terminal kinase-dependent apoptotic pathway. EMBO J, 2009. 28(20): p. 3228-43.

32. Wu, Y., Y. Zhuang, M. Han, T. Xu, and K. Deng, Ras promotes cell survival by antagonizing both JNK and Hid signals in the Drosophila eye. BMC Dev Biol, 2009. 9: p. 53.

33. Andersen, D.S., J. Colombani, V. Palmerini, K. Chakrabandhu, E. Boone, M. Rothlisberger, et al., The Drosophila TNF receptor Grindelwald couples loss of cell polarity and neoplastic growth. Nature, 2015. 522(7557): p. 482-6.

34. Friese, M.A., A. Steinle, and M. Weller, The innate immune response in the central nervous system and its role in glioma immune surveillance. Onkologie, 2004. 27(5): p. 487-91.

35. Logan, M.A. and M.R. Freeman, The scoop on the fly brain: glial engulfment functions in Drosophila. Neuron Glia Biol, 2007. 3(1): p. 63-74.

36. Shklover, J., K. Mishnaevski, F. Levy-Adam, and E. Kurant, JNK pathway activation is able to synchronize neuronal death and glial phagocytosis in Drosophila. Cell Death Dis, 2015. 6: p. e1649.

37. Macdonald, J.M., J. Doherty, R. Hackett, and M.R. Freeman, The c-Jun kinase signaling cascade promotes glial engulfment activity through activation of draper and phagocytic function. Cell Death Differ, 2013. 20(9): p. 1140-8.

38. Chuang, H.N., D. van Rossum, D. Sieger, L. Siam, F. Klemm, A. Bleckmann, et al., Carcinoma cells misuse the host tissue damage response to invade the brain. Glia, 2013. 61(8): p. 1331-46.

39. Rudrapatna, V.A., E. Bangi, and R.L. Cagan, A Jnk-Rho-Actin remodeling positive feedback network directs Src-driven invasion. Oncogene, 2014. 33(21): p. 2801-6.

40. Kulshammer, E. and M. Uhlirova, The actin cross-linker Filamin/Cheerio mediates tumor malignancy downstream of JNK signaling. J Cell Sci, 2013. 126(Pt 4): p. 927-38.

41. Fernandez, B.G., B. Jezowska, and F. Janody, Drosophila actin-Capping Protein limits JNK activation by the Src proto-oncogene. Oncogene, 2014. 33(16): p. 2027-39.

42. Balcer, H.I., A.L. Goodman, A.A. Rodal, E. Smith, J. Kugler, J.E. Heuser, et al., Coordinated regulation of actin filament turnover by a high-molecular-weight Srv2/CAP complex, cofilin, profilin, and Aip1. Curr Biol, 2003. 13(24): p. 2159-69.

43. Didry, D., M.F. Carlier, and D. Pantaloni, Synergy between actin depolymerizing factor/cofilin and profilin in increasing actin filament turnover. J Biol Chem, 1998. 273(40): p. 25602-11.

44. Nawaz, S., P. Sanchez, S. Schmitt, N. Snaidero, M. Mitkovski, C. Velte, et al., Actin filament turnover drives leading edge growth during myelin sheath formation in the central nervous system. Dev Cell, 2015. 34(2): p. 139-51.

45. Pinheiro, E.M., Z. Xie, A.L. Norovich, M. Vidaki, L.H. Tsai, and F.B. Gertler, Lpd depletion reveals that SRF specifies radial versus tangential migration of pyramidal neurons. Nat Cell Biol, 2011. 13(8): p. 989-95.

46. Esnault, C., A. Stewart, F. Gualdrini, P. East, S. Horswell, N. Matthews, et al., Rho-actin signaling to the MRTF coactivators dominates the immediate transcriptional response to serum in fibroblasts. Genes Dev, 2014. 28(9): p. 943-58.

47. Salvany, L., J. Muller, E. Guccione, and P. Rorth, The core and conserved role of MAL is homeostatic regulation of actin levels. Genes Dev, 2014. 28(10): p. 1048-53.

48. Ziv-Av, A., D. Taller, M. Attia, C. Xiang, H.K. Lee, S. Cazacu, et al., RTVP-1 expression is regulated by SRF downstream of protein kinase C and contributes to the effect of SRF on glioma cell migration. Cell Signal, 2011. 23(12): p. 1936-43.

49. Petryszak, R., M. Keays, Y.A. Tang, N.A. Fonseca, E. Barrera, T. Burdett, et al., Expression Atlas update-an integrated database of gene and protein expression in humans, animals and plants. Nucleic Acids Res, 2016. 44(D1): p. D746-52.

50. Ciurciu, A., L. Duncalf, V. Jonchere, N. Lansdale, O. Vasieva, P. Glenday, et al., PNUTS/PP1 regulates RNAPII-mediated gene expression and is necessary for developmental growth. PLoS Genet, 2013. 9(10): p. e1003885.

51. Kurucz, E., R. Markus, J. Zsamboki, K. Folkl-Medzihradszky, Z. Darula, P. Vilmos, et al., Nimrod, a putative phagocytosis receptor with EGF repeats in Drosophila plasmatocytes. Curr Biol, 2007. 17(7): p. 649-54.

52. Allan, C., J.M. Burel, J. Moore, C. Blackburn, M. Linkert, S. Loynton, et al., OMERO: flexible, model-driven data management for experimental biology. Nat Methods, 2012. 9(3): p. 245-53.

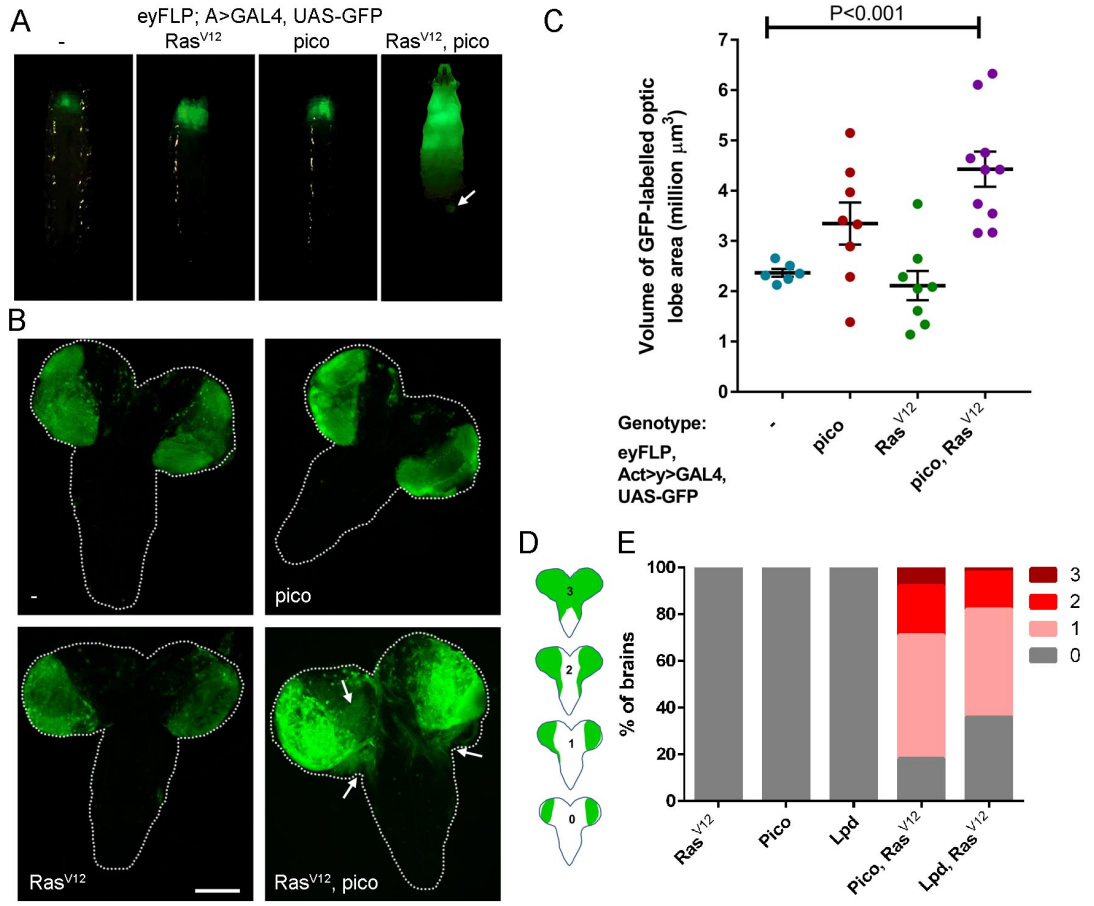

Figure 1. Pico promotes spreading of Ras^{V12}-induced tumours. A, Images of whole larvae showing distribution of GFP expression induced in the eye- discs and optic lobes of larva of different genotypes, as indicated. Expression of GFP alone or together with the transgenes indicated, was driven by flipping-out an FRT-flanked linker from an Act>GAL4 element using eyFLP (eyFLP, Act>GAL4). Overexpression of *Ras^{V12}* with *pico* resulted in a dramatic increase in GFP-marked tissue sometimes leading to the formation of GFP foci at more distant sites (arrow). **B**, Distribution of GFP expression in dissected brains showing overgrowth of the optic lobe and invasion of GFP-labelled cells into the ventral nerve cord in *Ras^{V12}, pico* brains (VNC, arrows). Scale bar 100μM. **C**, Quantification of the volume of GFP-labelled cells in the optic lobes of the indicated genotypes, based on optical sections taken throughout the entire brain. **D-E**, Quantification of the invasion

phenotype. **D**, Individual cephalic complexes were assigned to one of four categories, depicted, based on the degree of VNC invasion observed: Type 0, no invasion of the VNC, Type I, tumour cell invasion occurring down one side of the VNC, Type II, tumour cells invading both sides of the VNC; and, Type III, significant tumour cell invasion of the VNC combined with overgrowth/fusion of the optic lobes. **E**, Stacked bar chart showing the percentage of brains expressing either *Ras^{V12}*, *pico, hLpd, pico/Ras^{V12}* or *hLpd/Ras^{V12}*, classified into each of the four categories (n=100 brains/genotype).

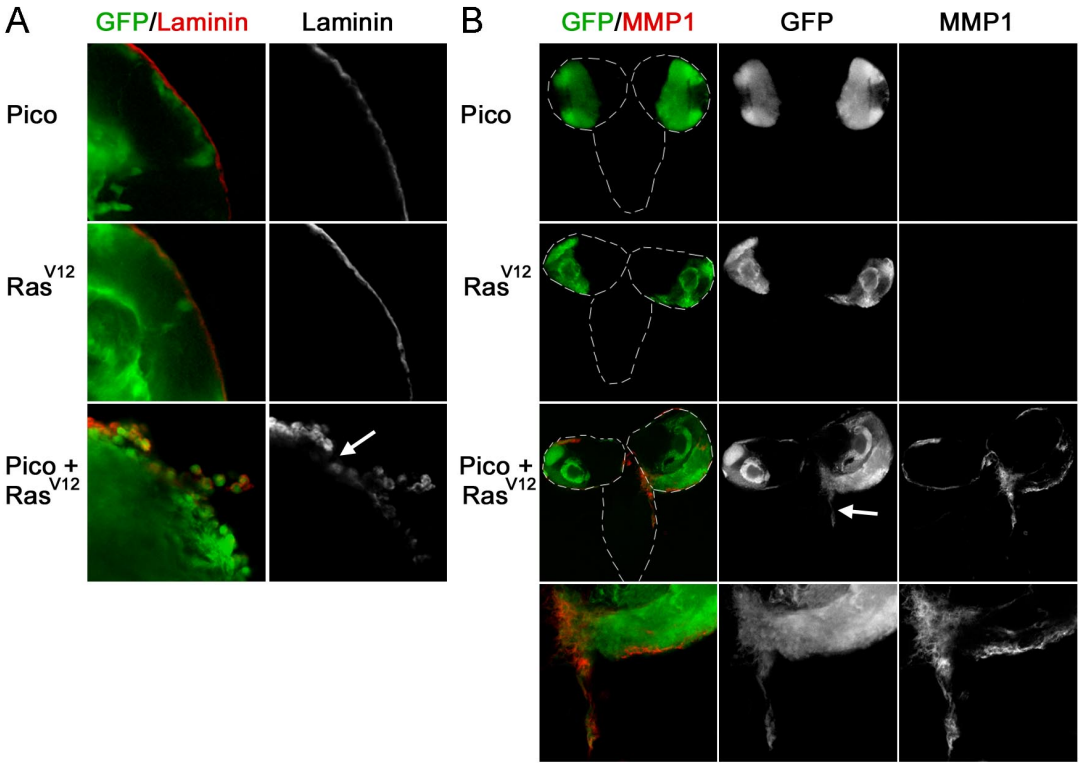

Figure 2. Brains co-expressing *Ras^{V12}* and *pico* display extracellular matrix degradation and ectopic expression of Mmp1. A, Optic lobes from larvae overexpressing *pico*, *Ras^{V12}* or *Ras^{V12}, pico* under the control of eyFLP, Act>GAL4, stained with anti-Laminin antibody, which labels the surface of the optic lobes. Laminin staining was found to be severely interrupted in brains co-expressing *Ras^{V12}* and *pico* but not from brains

expressing *pico* or Ras^{V12} alone. **B**, Distribution of the metalloproteinase Mmp1. Little or no Mmp1 staining was observed in animals expressing Ras^{V12} or *pico* alone. In contrast, animals co-overexpressing Ras^{V12} and *pico* had elevated MMP1 around the edges of the optic lobes and at sites of invasion into the VNC (arrow).

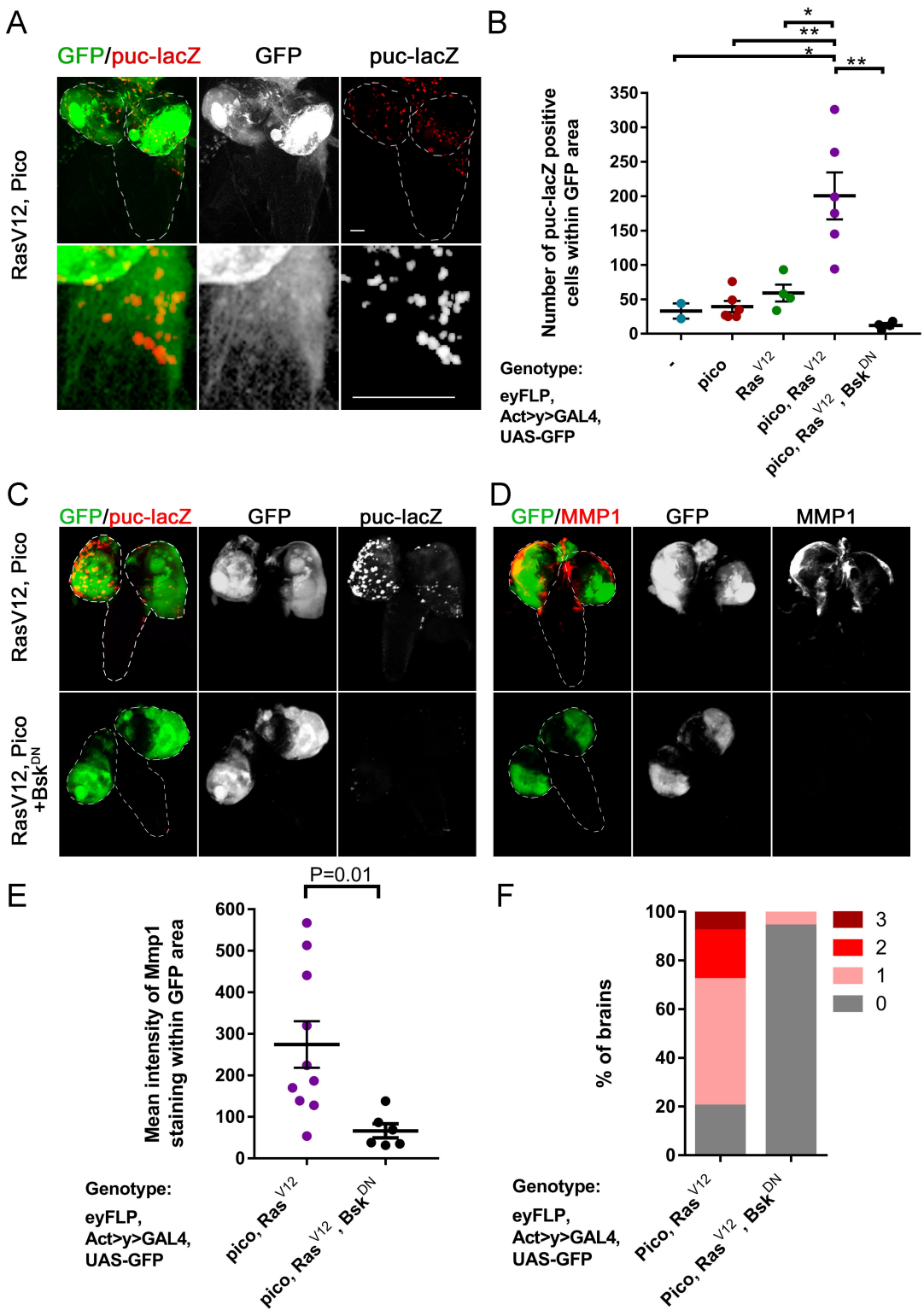

Figure 3. Mmp1 accumulation and invasion into VNC is dependent on JNK activation. A, Co-overexpression of *Ras*^{V12} and *pico* in GFP-labelled tumours (green) leads to JNK activation in some tumour cells, based on β-galactosidase staining to detect *puc-lacZ* (red). Top panels show low

magnification images of brains, lower panels show magnified images of tumours invading into VNC, which are enriched in puc-lacZ staining. Scale bars, 100 μm.

B, Quantitation of number of puc-lacZ positive foci in GFP-labelled areas of the optic lobes from the indicated genotypes. **B,C** Blockade of JNK activation with dominant-negative Bsk/JNK (*Bsk^{DN}*) suppresses activation of the JNK pathway. **C**, Representative images showing puc-lacZ induction in *Ras^{V12} pico* tumours and suppression of this effect by *Bsk^{DN}*: the top row of images were taken from representative *Ras^{V12} pico* larval brains; the bottom row were taken from siblings coexpressing *Bsk^{DN}.* **D,E** Blockade of JNK activation with dominant-negative Bsk/JNK (*Bsk^{DN}*) suppresses the induction of Mmp1. **D**, Representative images of *Ras^{V12} pico* tumours with or without *Bsk^{DN}*. **E**, Quantitation of mean intensity of Mmp1 within GFP-labelled *Ras^{V12} pico* tumours in the presence or absence of *Bsk^{DN}*. **F**, *Bsk^{DN}* suppresses *Ras^{V12}/pico*-mediated invasion into the VNC. Graph summarising extent of invasion in the different genotypes (n=100 brains of each type) according to the scale introduced in Figure 1, with 3 being the most severe and 0 corresponding to no invasion.

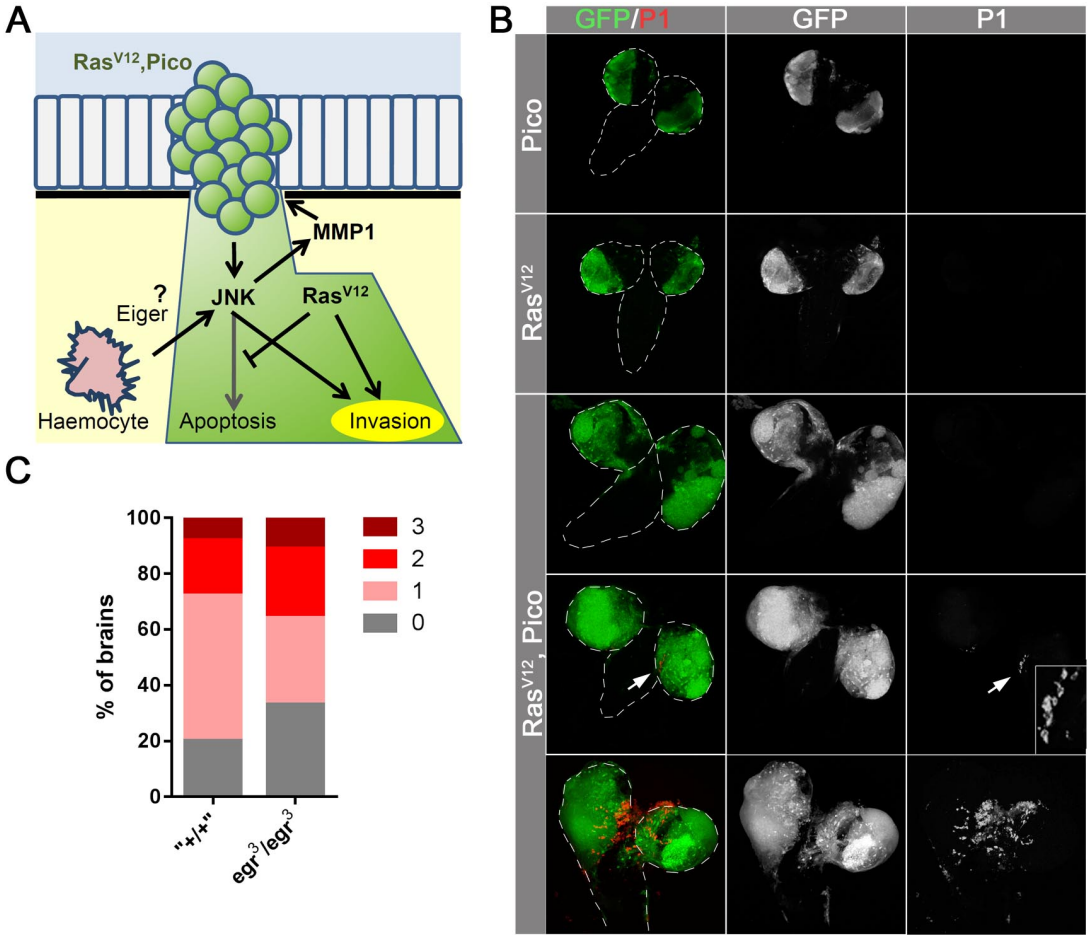

Figure 4. Invasion is not driven by haemocyte recruitment and TNF/Eiger-dependent signalling. A, Possible model of extrinsic signalling from haemocytes to JNK activation in tumours. In the absence of *Ras^{V12}*, activated JNK leads to cell death, whereas in its presence, JNK promotes Mmp1 expression and cellular invasion. **B,** Images of dissected brains showing distribution of haemocytes, as detected with an anti-NimC1 P1 antibody. Haemocytes were not detected in brains expressing *pico* or *Ras^{V12}* alone. In *pico* or *Ras^{V12}* brains, haemocytes were sometimes observed at sites of invasion, but this was not a necessary outcome. **C,** Graph summarising extent of invasion in the different genotypes (n=100 brains of each type).

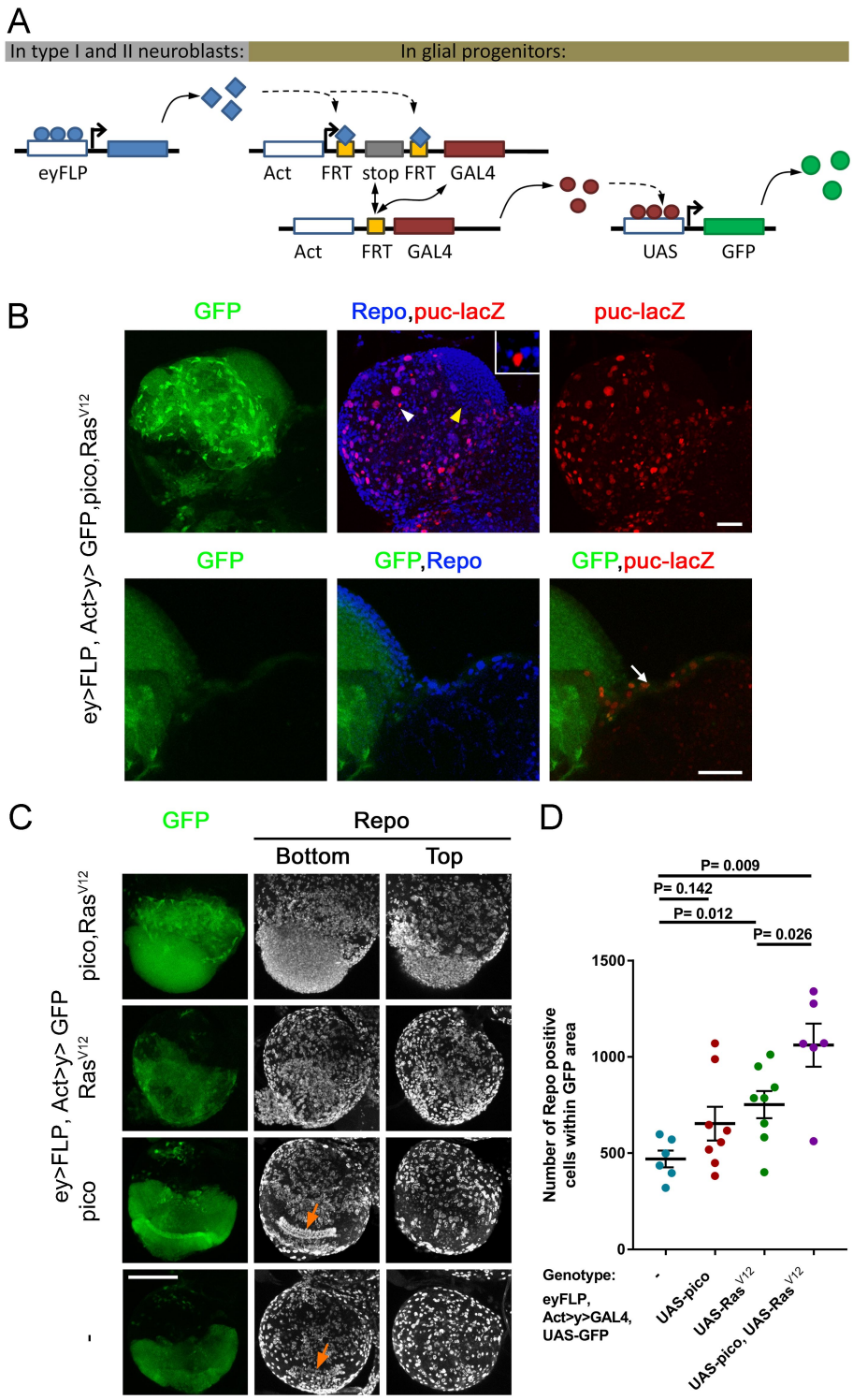

Figure 5. Distinct oncogenic effects in glial populations. A, Schematic outlining heritable overexpression in glial lineages following expression of eyFLP in glial progenitors and removal of an FRT-flanked linker from Act>GAL4 reconstituting the Act-GAL4 driver. This then constitutively drives

expression of UAS-GFP and other UAS constructs in daughter cells. **B**, (Top panels) Optic lobe from third instar larvae, with start of the VNC to the right of the image, showing the effect of co-expressing Ras^{V12} and *pico* with this system. In particular, two distinct effects are observable in glia (Repo +ve, in blue): activation of JNK, marked with *puc-lacZ* (red) and accumulation of glial cells in a region proximal to the ventral nerve cord (yellow arrowhead). Inset is a magnified image of a Repo -ve cell staining positive for *puc-lacZ* (white arrowhead). Magnified images (bottom) show the GFP and *puc-lacZ* labelled population that has invaded into the VNC (arrow). Scale bars, 50 μm. **C**, Anti-Repo staining showing the effect of Ras^{V12} and *pico* co-overexpression on glial distribution and number in optic lobes. Repo-stained images are 2D projections of confocal z-stacks from the bottom and top of the same optic lobe. Bottom sections reveal stereotypical arrangement of glia (arrows) in control optic lobes and those overexpressing *pico*, which is lost upon expression of Ras^{V12}. Scale bar, 100 μm. **D**, Graph showing quantification of number of Repo-positive glia in GFP-labelled areas of the optic lobes from the indicated genotypes.

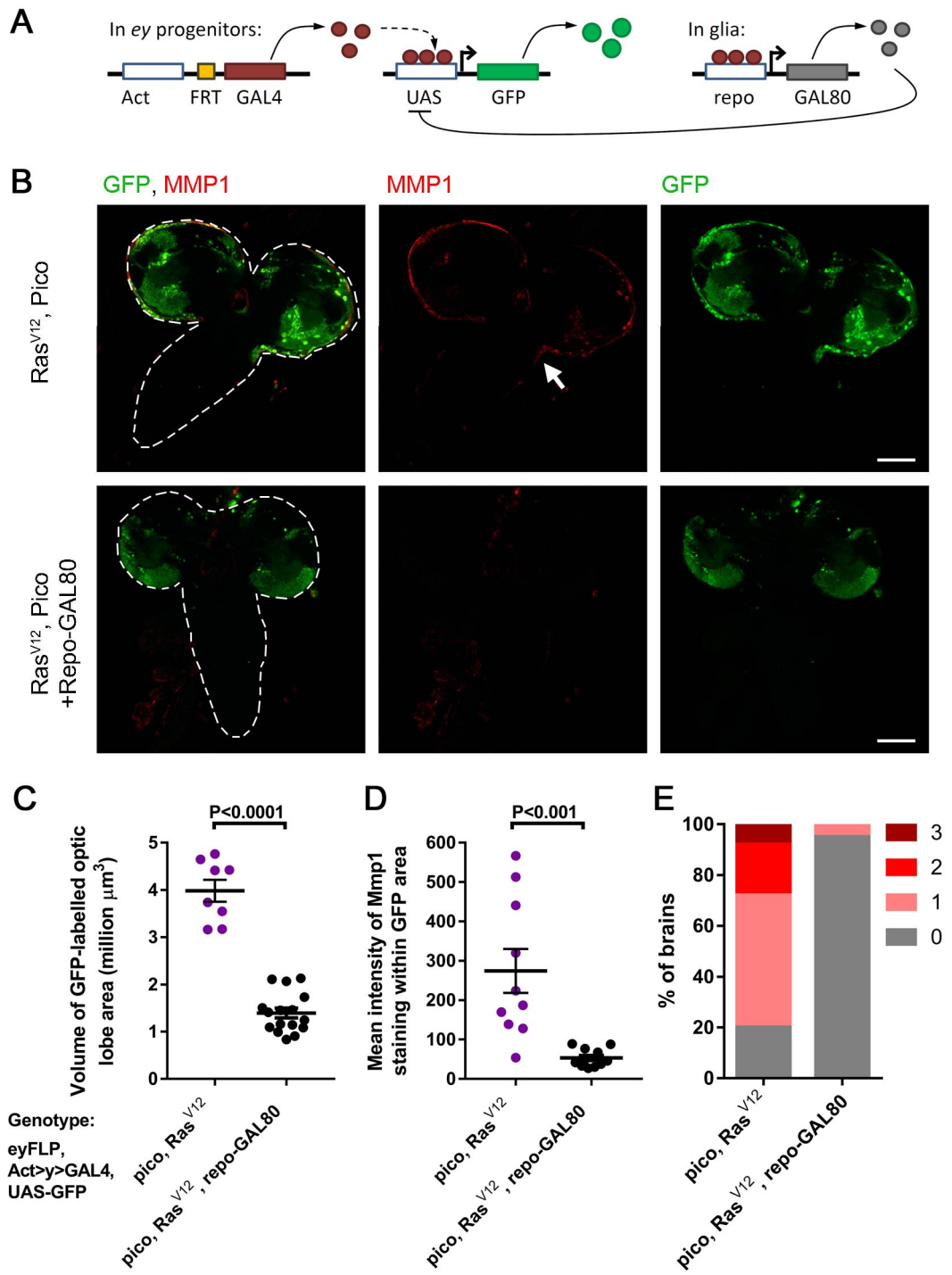

Figure 6. Transcriptional blockade in glia blocks cooperation between *Ras^{V12}* and *pico*. A, Schematic showing suppression of GAL4-mediated overexpression in glia using *repo-GAL80*. **B,** Brains (outlined with dashed line in first set of panels) overexpressing *Ras^{V12}*, *pico* with or without *repo-GAL80*, showing distribution of GFP-labelled cells (green) and Mmp1 (red). Animals co-overexpressing *Ras^{V12}*, *pico* displayed invasion of Mmp1-

expressing cells into the VNC (arrow). Mmp1 staining and invasion were suppressed in siblings containing *repo-GAL80*; optic lobes of these animals were also reduced in size. Scale bars, 100 μm. **C**, Measurements of the volume of GFP-labelled Ras^{V12}, *pico* optic lobe tumours with or without *repo-GAL80*. **D**, measurements of mean intensity of Mmp1 staining in Ras^{V12}, *pico* tumours with or without *repo-GAL80*. **E**, Stacked bar chart summarising extent of invasion in the different genotypes (n=100 brains of each type).

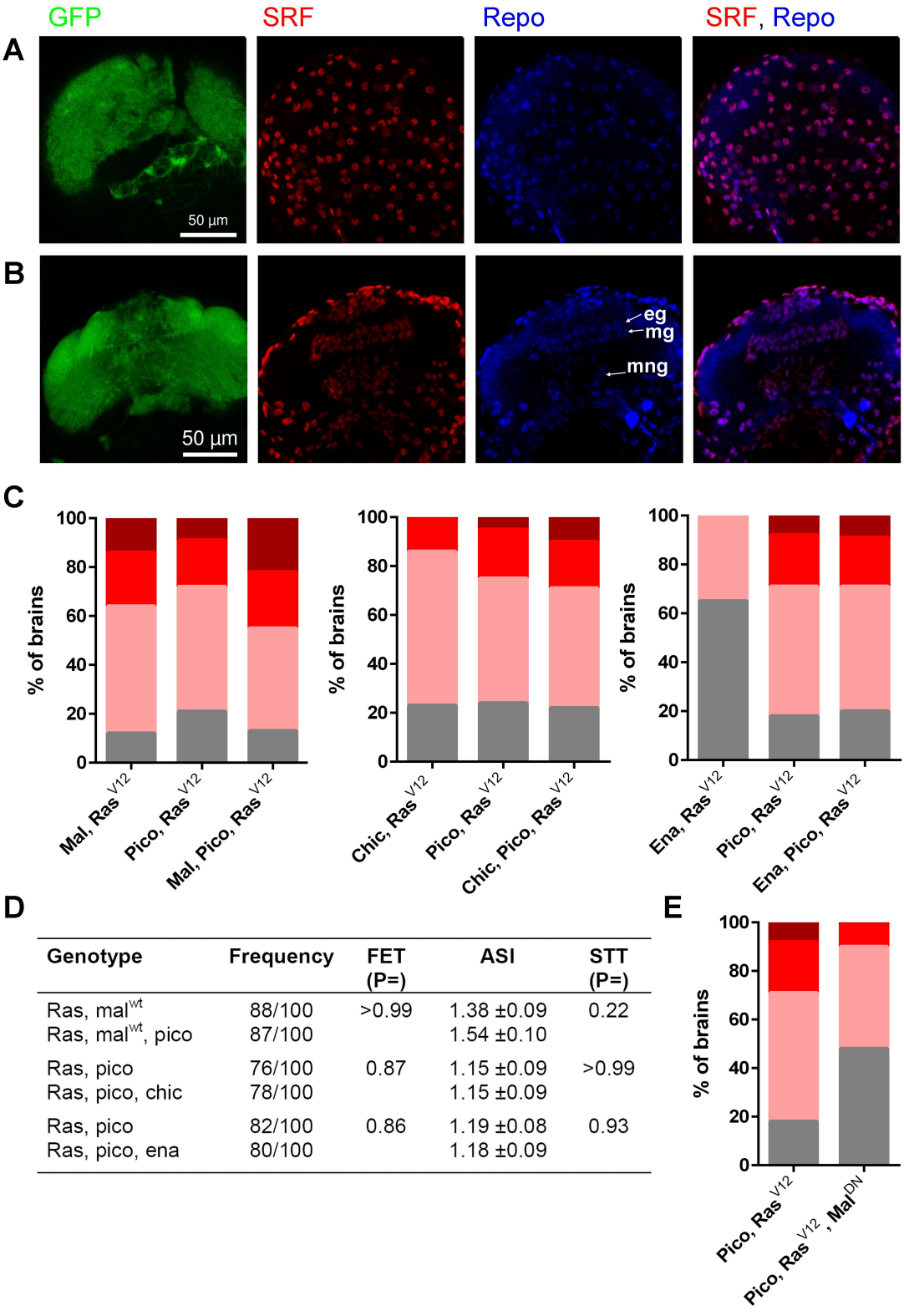

Genotype	Frequency	FET (P=)	ASI	STT (P=)
Ras, mal^{wt}	88/100	>0.99	1.38 ±0.09	0.22
Ras, mal^{wt}, pico	87/100		1.54 ±0.10	
Ras, pico	76/100	0.87	1.15 ±0.09	>0.99
Ras, pico, chic	78/100		1.15 ±0.09	
Ras, pico	82/100	0.86	1.19 ±0.08	0.93
Ras, pico, ena	80/100		1.18 ±0.09	

Figure 7. Mal is rate limiting for tumour dissemination. A-B, Distribution of SRF in the third instar larval optic lobes. SRF antibody staining (red) overlaps that of Repo (blue) both at the surface (A) of the optic lobes and in

cross-section (B). In cross-section, staining in epithelial (eg), marginal (mg) and medulla neurophil (mng) glia is evident. **C,** Cooperation between *Ras*^{V12} and cytoskeletal regulators resulting in cancer cell invasion into the VNC. Graph summarising extent of invasion in the different genotypes (n=100 brains of each type) according to the scale introduced in Figure 1, with 3 being the most severe and 0 corresponding to no invasion. **D**, Summary of statistical tests for results of (C), showing pairwise combinations in each experiment; frequency, number of brains showing invasion/total number; FET, fisher's exact test; ASI, average stage score of invasion; STT, Student's t-test. **E**, *mal*^{DN} partially suppresses the effect of *Ras*^{V12}*, pico* cooverexpression. Graph summarises extent of invasion in the different genotypes (n=100 brains of each type).

4.2.3 Actin regulators modulate the SRE-mCherry expression

In the paper presented above, we propose that *pico* promotes cellular invasion, at least in part, through the activation of SRF signalling. SRF signalling is induced by changes in actin dynamics (Miralles et al., 2003), specifically by a change in the ratio of G:F actin sensed by the SRF cofactor Mal. It is thought that Pico regulates actin dynamics through its interaction with actin regulators, such as Chic, Ena, Scar/Wave, leading to an increase in filamentous actin (F) levels (Small et al., 2002) and reduction of monomeric actin (G) (Taylor, 2010). Reduction in the inhibitory binding of G-actin to the SRF cofactor MAL, enables translocation of MAL to the nucleus where it complexes with SRF to facilitate in the transcription of SRE-containing genes. In Chapter 3, we made use of an SRE-mCherry reporter to monitor SRF activation in the wing disc; both *pico* and *mal* induced SRE-mCherry expression. However, the effects of *chic*, *ena* and *scar* had not been determined. With respect to the paper described above, it would be useful to fill this knowledge gap because it is possible that *chic*, *ena* and *scar* do not have an equal ability to promote SRF activation, which might be correlated with their ability to promote cellular invasion.

To test this, *chic*, *ena* and *scar* were overexpressed in the posterior compartment of the wing imaginal disc using *hh-GAL4* in the presence of the SRE-mCherry reporter (Crossing scheme in figure 4.3.).

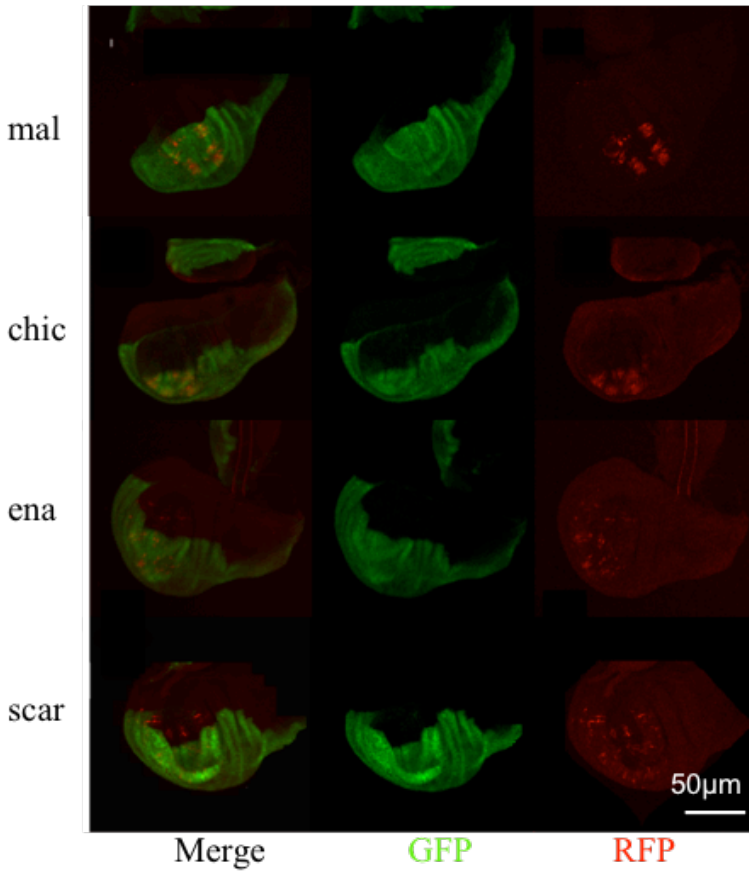

Figure 4.2. Dissected wing discs from wandering males third instar larvae, showing the level of SRE-mCherry reporter expression (in red, detected with anti-RFP antibody staining) in response to overexpression of different actin cytoskeleton regulators (*mal, chickadee, ena* and *scar,*) under the control of *hh-GAL4* in the posterior half of the disc, which is marked with GFP (in green). Genotypes are ordered according to the qualitative strength of response from top (highest induction of mCherry) to bottom (lowest induction). Discs overexpressing *mal* and *chic* are at a slightly earlier stage when basal expression (apparent in the anterior half of the disc) is below the level of detection. Discs with *ena* and *scar,* which are visibly larger, are at a later stage and basal reporter gene activation can be observed in the anterior half, albeit at a lower level or in fewer cells than the posterior half. 15 wing discs were dissected and stained, the reporter has been observed in 12 discs out of 15.

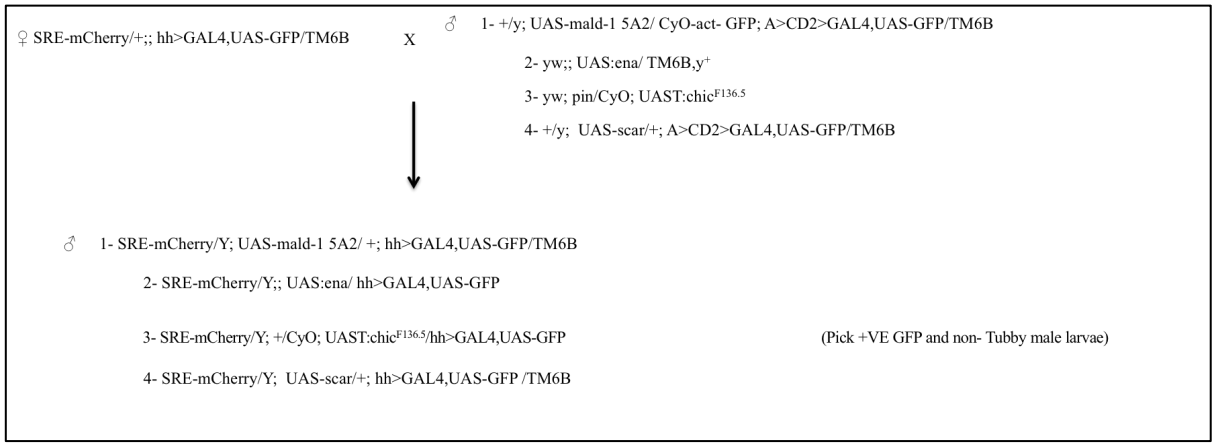

Figure 4.3. Genetic scheme used examine the effect of overexpressing different actin regulators under the control of *hh>GAL4*. Virgin females expressing *hh>GAL4* crossed to males expressing actin regulators (*mal, ena, chickadee and scar).* Then GFP+ve wing discs were dissected from third instar larvae and stained for anti- RFP.

Wing discs were dissected and stained with anti-RFP antibody prior to being imaged by confocal microscopy. A clear increase in the expression level of mCherry was detected in response to *mal* or *chic* overexpression. A lower level of reporter gene induction was detected in response to *ena* or *scar* overexpression.

4.3 Discussion

As outlined in the draft manuscript above, several lines of evidence suggest that Mal-SRF signaling is limiting for the effects of Ras^{V12}/*pico* on tumour invasion. Additional analysis of SRF activity, using the SRE-mCherry reporter, in wing imaginal discs supports the notion that extent of invasion may be correlated to degree of SRF induction; *mal* and *chic* had more pronounced effects than *ena* and *scar* on Ras^{V12}-induced tumours and also induced SRF most strongly. Attempts (not

shown) were made to examine SRE-mCherry expression in the brain, but measurements were unsatisfactory because of a high signal to noise ratio.

A key piece of evidence showing the requirement for Mal/SRF signaling in cellular invasion has come from testing the effect of a dominant negative version of Mal (*DN-Mal*) on the ability of Ras^{V12}/*pico* tumours to become disseminated (Taylor, 2010). Partial suppression of the invasion phenotype was observed, but the efficacy of *DN-Mal* has been hard to determine and so the full extent of Mal/SRF involvement still remains somewhat open to question. Attempts were made to assess the effect of *DN-Mal* on *SRE-mCherry* expressionin the wing imaginal disc, but this could not be readily determined because of low and somewhat variable basal levels of *SRE-mCherry* expression.

An alternative approach to testing the role of Mal/SRF might be to examine proliferation and invasion in null *mal* or *bs*/SRF mutant clones expressing Ras^{V12}/*pico*. For practical reasons, this will be hard to do for *mal* mutants, which reside on the same chromosome as *UAS-*Ras^{V12} and *UAS-pico*, but could be achieved more easily for *bs*/SRF mutants. However, clone production will be hard for glial lineages with low proliferation rates; for astrocyte-like glia or subperineurial glia, mutant clones will have to be induced in the embryo when these glia are still mitotically active.

It would be interesting to explore which glia subtypes hyperproliferate in response to *pico/*Ras^{V12} and which subtypes undergo invasion. Based on their location and morphology, *Drosophila* glia have been classified into different subtypes (Figure

4.4): perineurial glia (II) and subperineurial glia of the surface glia (I), the cortex glia (III), ensheathing glia (V) and astrocyte-like glia of the neuropile subtype (VI) (Freeman and Doherty, 2006, Edwards and Meinertzhagen, 2010, Awasaki et al., 2008). In adult flies, **Perineural glia** have been shown to function in the formation of Blood Brain Barrier (BBB). While this subtype does not express *repo*, the pan-glial cell marker, during early larval development (Nassif et al., 1998), repo does become evident during early pupal stages (Awasaki et al., 2008, Stork et al., 2008). **Subperineurial glia** help in septate junctions formation, as are considered a major component of BBB in larvae. **Cortex glia** enwrap neuronal cell bodies, forming a mesh in the bran cortex region (Freeman and Doherty, 2006, Awasaki et al., 2008). Finally, it is thought that neuronal survival is promoted by **Neuropile glia** through providing trophic support based on the morphology of the Neuropile glia (Awasaki et al., 2006). Neuropile glia can be categorised as ensheathing or astrocyte-like.

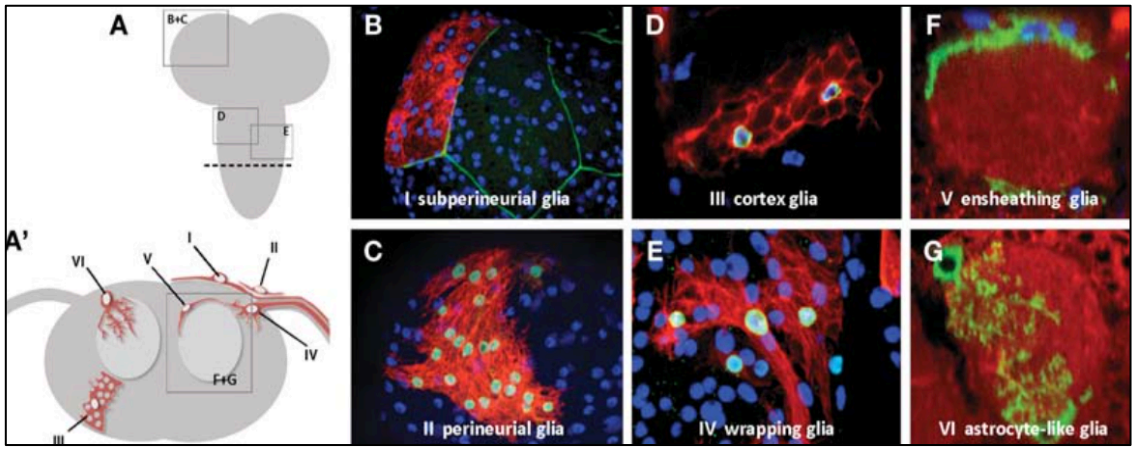

Figure 4.4. Main morphological subclasses of glial cells in *Drosophila*. (A) Schematic overview of the central neuronal system (CNS) of the *Drosophila* third-instar larvae. Optic lobes and ventral nerve cord shown in grey. (A') dark grey represent the cortex, the region of cell bodies and the synaptic neuropil shown in light grey. I- VI represent the different subtypes of glial cells. B-G are the confocal images of glial subtypes morphology. Figure reproduced from(Stork et al., 2012).

The shortage of tools makes testing the glial subtypes quite difficult. There are not that many antibodies to stain different glia subtypes in larval brain. The only glial subtype that can be distinguished by antibody staining is the subperineurial glia, using anti-Moody antibodies (Stork et al., 2012). However, an alternative approach would be to express *pico* with glial-specific GAL4 drivers that are expressed in different subtypes, e.g.: *spg-GAL4* for subperineurial glia, *alrm-GAL4* for Astrocyte-like glia and *nrv2-GAL4* for Cortex glia (Stork et al., 2012). Dissected brains could then be examined for effects on proliferation or cellular invasion as described above.

5 Physical and functional interactions between MAPK and Pico

5.1 Introduction

Pico is capable of interacting with multiple proteins (Lofthouse, 2013), many of which are implicated in its role in hyperplastic growth and invasion, either through direct effects on the actin cytoskeleton or indirectly via downstream SRF activation, as discussed in the previous chapters. Multiple lines of evidence suggest that MRL proteins also associate with kinases and phosphatases, which are enzymes that regulate the phosphorylation state of proteins (Lofthouse, 2013). Reversible protein phosphorylation is an important mechanism of post-translational regulation, since the addition or removal of phosphatase groups can affect the ability of proteins to interact with one another, or affect their sub-cellular localisation and activity. MRL-associated kinases and phosphatases are therefore well placed to regulate dynamics of MRL function and render them sensitive to upstream signals acting on the associated kinase and phosphatases. For instance, Lpd associates with and is phosphorylated by Abl and this interaction positively regulates binding of Lpd to Ena/VASP proteins (Michael et al., 2010). Since Ena/VASP-binding sites in Lpd are not directly phosphorylated by Abl kinases, it is possible that Lpd's tertiary structure is altered by the phosphorylation of Lpd, thus unmasking the Ena/VASP-binding sites (Michael et al., 2010). An intriguing possibility is that differential formation of trimolecular complexes between Lpd, c-Abl, and individual Ena/VASP proteins might allow for fine-tuning of signalling responses.

Drosophila pico was originally identified in a yeast two-hybrid screen for serine/threonine protein phosphatase 1 (PP1) binding proteins (Bennett et al., 2006).

Binding of PP1 to Pico was found to be mediated by a canonical PP1-binding motif in Pico (Bennett et al., 2006); mutation of the critical Phe residue in this motif (F816A) is sufficient to abolish binding (Lyulcheva, 2006). More recently, bioinformatics analysis also revealed a highly conserved MAPK-binding motif adjacent to the N-terminus of the RA domain, which mediates an interaction with MAPK in S2 cell extracts (Lofthouse, 2013). Mutation of either the PP1-binding or MAPK-binding motifs enhances *pico*-mediated overgrowth of the wing, suggesting that MAPK and PP1 normally limit the effects of overexpressed *pico* (Lofthouse, 2013, Lyulcheva, 2006). The substrates of Pico-bound PP1 and MAPK are not known, but Pico itself is known to be a phosphoprotein, having been shown to be phosphorylated at Ser819 in a large proteomics study of embryo extracts (Bodenmiller et al., 2007). A "phospho-mimetic" mutation of this site (S819D) abolished the effect of overexpressed *pico* on wing overgrowth, whereas a non-phosphorylatable mutation (S819A) recapitulated the effect of disrupting MAPK binding. Additionally, $Pico^{S819D}$, but not $Pico^{\Delta MAPK}$ or $Pico^{S819A}$, was able to bind PP1 in cell extracts, suggesting the existence of a potential phosphorylation cascade (MAPK binding → pico phosphorylation at S819 → PP1 binding) involving MAPK and PP1 which deactivates the Pico complex.

The functional effects of the various site-directed mutants and their ability to bind PP1 and MAPK are summarised in Figure 5.1.

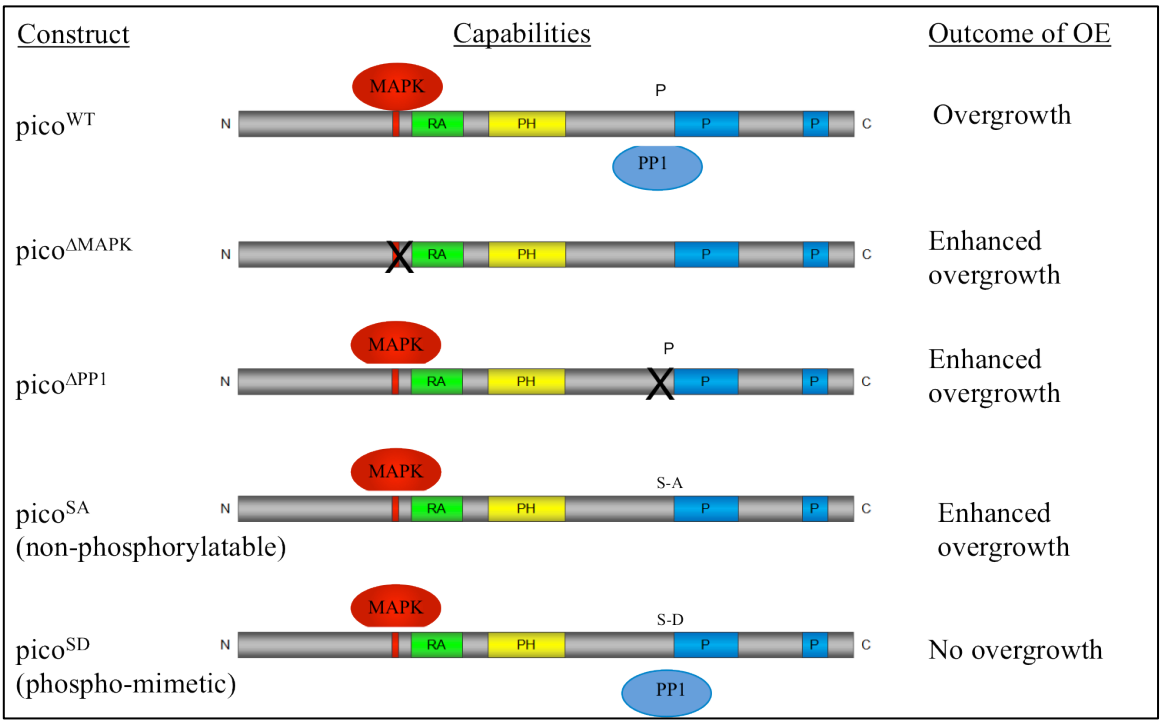

Figure 5.1. Functional effects of the site-directed mutants in Pico and the ability of wild type and Pico variants to bind PP1 and MAPK. The domain structure of the Pico protein is shown together with that of the Pico variants listed on the left of the figure. RA = Ras-association domain, PH = Pleckstrin homology domain, P = Proline rich regions. The ability of the proteins to bind MAPK and PP1 is illustrated. X indicates the position of the site-directed mutant in the respective constructs. To the right of the figure is a summary of the effects of overexpression (OE) in the developing wing.

5.2 Aims

The main aim of the work presented in this chapter was to test a model put forward by Lofthouse (Lofthouse, 2013), based on the analysis of site-directed mutations described above, which proposed that MAPK binding leads to phosphorylation of Pico and the recruitment of PP1, resulting in the suppression of Pico activity in hyperplastic tissue overgrowth (see Chapter 4). This was assessed by determining the possible epistatic relationships between PP1-binding, MAPK-binding and Pico phosphorylation using double mutant *pico* constructs engineered to possess F816A or ΔMAPK (K221A; K224A; L229A) mutations in the presence of a second-site S819D mutation.

The second aim of this chapter was to determine the importance of this putative regulatory mechanism in contexts other than wing overgrowth. To address this, the ability of $pico^{\Delta MAPK}$ to cooperate with oncogenic Ras was compared to that of $pico^{wt}$ in the cell invasion model described in Chapter 4.

5.3 Confirmation of loss of MAPK-binding to Pico

Previous work performed in the Bennett lab had indicated that mutation of three conserved residues in a putative MAPK-binding motif in Pico (K221A; K224A; L229A) abolished the ability of Pico to interact with MAPK (Lofthouse 2013). To confirm this interaction, S2 cell extracts expressing Venus-tagged $Pico^{WT}$, $Pico^{\Delta MAPK}$, $Pico^{\Delta PP1}$, $Pico^{S819A}$ and $Pico^{S819D}$ variants were subjected to GFP-Trap pull-down and precipitates were examined for the presence of endogenous MAPK.

Unlike the other Pico variants, Pico$^{\Delta MAPK}$ was unable to bind MAPK, confirming the importance of K221, K224 and L229 for MAPK-binding.

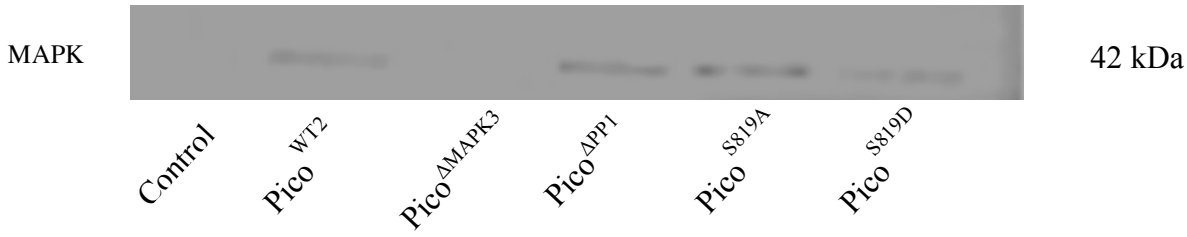

Figure 5.2. Blots showing presence of MAPK in precipitates from S2 cells expressing Pico wild type and variants. Pull-downs were carried out on S2 cells expressing Venus-tagged Pico^{WT}, Pico$^{\Delta MAPK}$, Pico$^{\Delta PP1}$, Pico^{S819A} and Pico^{S819D} constructs using GFP-Trap. Non-transfected S2 cell extracts were employed as a negative control. The samples were examined by western blot for the presence of MAPK. The result indicates that the Pico$^{\Delta MAPK}$ was unable to bind MAPK. This blot is representative of 3 experimental repeats.

5.4 Rationale for making double mutations in pico

Based on preliminary binding data from fly extracts (Lofthouse, 2013), loss of MAPK binding to Pico, or mutation of Ser 819 to Ala, blocked binding of Pico to PP1 (Figure 5.1). This suggests there may be a cascade whereby MAPK phosphorylation of S819 promotes the recruitment of PP1, which in turn acts to limit Pico function. To test this idea further, the following double mutants of Pico were generated; 1) S819D and MAPK-binding mutant; 2) S819D and PP1-binding mutant. (Figure 5.3). The rationale for making these constructs was as follows. If PP1-binding, and suppression of *pico* function, depends on the phosphorylation of

S819 by MAPK then the S819D mutation should compensate for the loss of MAPK binding in Pico$^{\Delta MAPK}$, bind to PP1 and limit tissue overgrowth. Conversely, because S819 phosphorylation is upstream of PP1-binding, the S819D and PP1-binding double mutant should still fail to bind PP1 and promote enhanced tissue overgrowth.

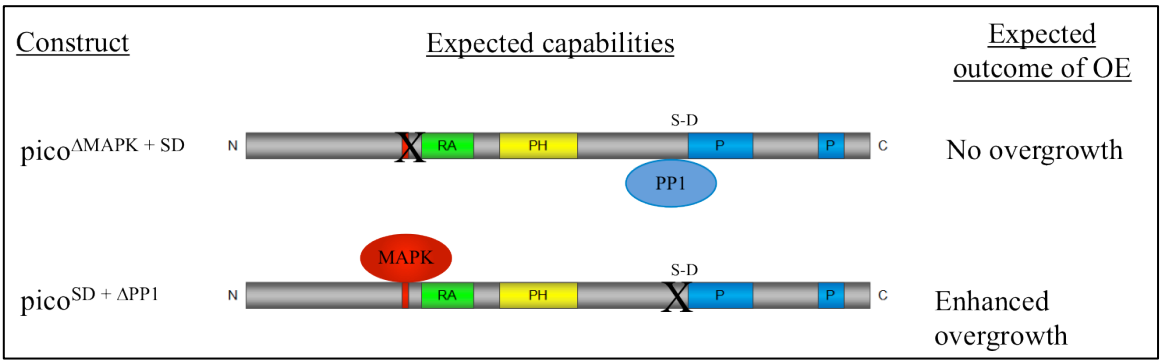

Figure 5.3. Expected capabilities of double mutants of *pico*; S819D (SD) and MAPK-binding mutant, and the S819D and PP1-binding mutant. SD and MAPK double mutant should suppress the effect of MAPK mutant; bind to PP1 and suppress overgrowth. SD and PP1 double mutant should not bind to PP1, and should therefore promote overgrowth.

5.4.1 Generation of *pico* double mutant constructs

First, generating Pico$^{SD\text{-}MAPK}$ double mutant. Pico^{S819D} construct and Pico$^{\Delta MAPK}$ had previously been cloned into a Gateway pDONR221 entry vector to enable simple shuttling of the gene into appropriate destination vectors via LR recombination. Since the MAPK-binding site resides in a unique restriction fragment (*Sac*I/*Sal*I) in this vector, the MAPK-binding mutation could be combined with the S819D mutation by subcloning. For this, both pDONR221 Pico$^{\Delta MAPK}$ and pDONR221 Pico^{S819D} were digested with *Sac*I and *Sal*I (Figure 5.4). Products were run on a low melting agarose gel to separate the products. The resultant ≈ 500bp and

≈ 5000bp bands were cut from the pDONR221 Pico$^{\Delta MAPK}$ and pDONR221 Pico^{S819D} lanes, respectively, before being purified with a gel extraction kit. Following gel purification of the DNA fragments, ligation was performed to insert the short fragment of pDONR221 Pico$^{\Delta MAPK}$ ≈ 500bp into the vector pDONR221 Pico^{S819D} using T4 DNA ligase and the products transformed into competent cells. These cells were subsequently plated onto selective media and single colonies picked. Sequencing was then employed to validate the newly formed constructs (data not shown).

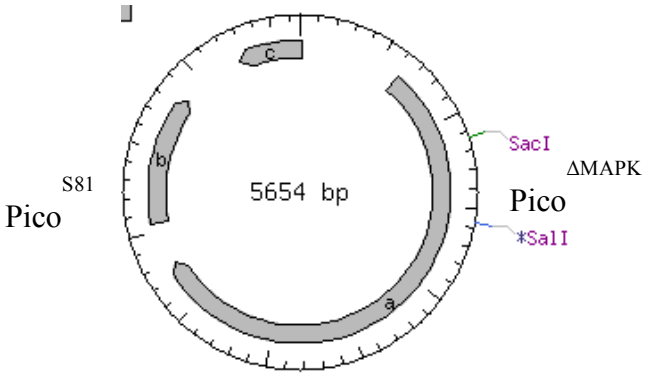

Figure 5.4. *Sac*I-*Sal*I restriction sites. Schematic diagram showing *Sac*I-*Sal*I restriction sites within the Pico$^{\Delta MAPK}$ mutant and pDONR221 Pico^{S819D} vectors.

Second, generating Pico$^{SD\text{-}F816A}$ double mutant. PCR-based site-directed mutagenesis was used to create the Pico$^{SD\text{-}F816A}$ double mutant constructs. Briefly, overlapping primers complementary to the proposed mutational sites, but possessing specific changes required for each construct, were synthesised. A high-fidelity DNA polymerase was used to amplify the complete pDONR221 Pico^{S819D} vector via PCR, before the resultant products were exposed to the endonuclease *Dpn*I. *Dpn*I

specifically cleaves methylated DNA created by DNA methyltransferases (DNMTs) present within the host cell of the parental Pico^{S819D} strand, but not the PCR reaction mix. Consequently, only the DNA of pDONR221 Pico^{S819D} vector was digested, where as the new mutants was not digested to be able to be transformed into chemically competent cells and end joining by the host cells. These cells were subsequently plated onto selective media and single colonies picked. To ensure that the cloning worked, three colonies were picked and digested with *Sac*I-*Sal*I to confirm that there is a 500bp insert and with *StuI* to check whether the wild type fragment has been replaced with the mutant because *StuI* able to cut the wild type but not the mutant (Figure 5.5). Sequencing was then employed to validate the newly formed constructs.

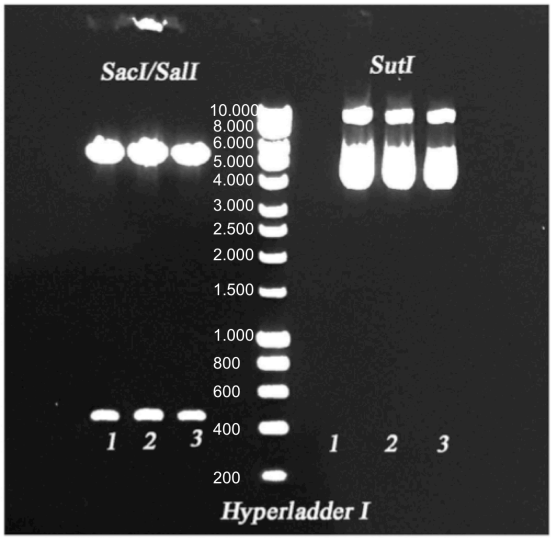

Figure 5.5. Agarose gel electrophoresis to validate the cloning. Three colonies were picked from the plates then *SacI-Sal*I and *StuI* restriction digests were performed. The resulting products were run on an agarose gel, which confirmed the correct orientation of the inserted constructs.

5.4.2 Insertion of constructs into flies

Following generation of *pico* double mutation constructs within the pDONR221 entry vector, an appropriate destination vector needed to be selected to enable their expression within flies using the *Drosophila GAL4-UAS* system. The pTVW vector (#1091) was selected from the *Drosophila* Genomics Resource Centre (DGRC). pTVW possesses a *UASt* promoter to enable somatic expression under the direction of GAL4, and an N-terminal Venus tag. Venus is an enhanced Yellow Fluorescent Protein (YFP) fluorophore derived from Green Fluorescent Protein (GFP) following the addition of several mutations (Rekas et al., 2002).

Shuttling the constructs from the pDONR entry clones into *pTVW* destination vectors was performed using the LR recombination. The resultant products were transformed into competent cells that were selected on the presence of amp^r and the absence of the toxic *ccdB* gene, which is present in unrecombined destination vectors. The accuracy of the insertion and the orientation of the *pico* double mutants constructs within the *pTVW* vectors were verifying using X*hol* and *Sac*II restriction digestion enzymes. The results confirming correct incorporation by gel electrophoresis of the restriction products is shown in (Figure 5.6).

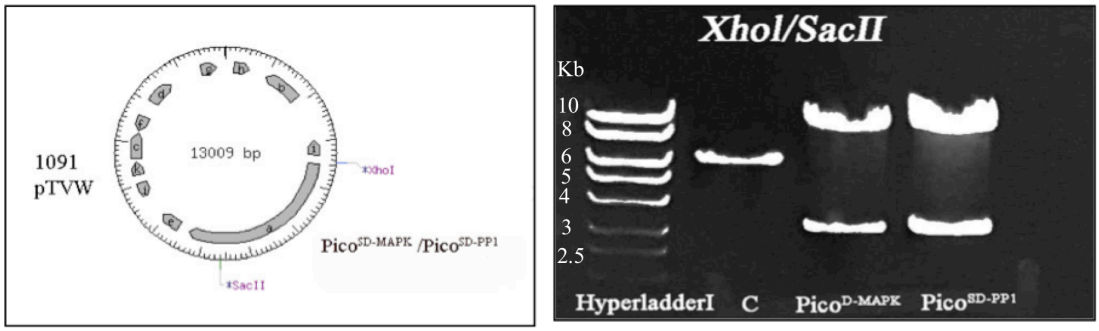

Figure 5.6. Agarose gel electrophoresis to validate *pTVW* Pico vectors following LR recombination. *Xho*l-*Sac*II restriction digests were performed on *pTVW* Pico vectors following LR recombination. The resulting products were run on an agarose gel and confirmed correct orientation of the inserted constructs.

Following validation of the destination vectors, *P*-element mediated germline transformation was used to generate transgenic flies possessing copies of the *UAS*-controlled Venus tagged Pico constructs by Genetic Services, Inc (USA). Briefly, the *pico* double mutant constructs, positioned between *P*-element ends and alongside a *white*$^{+}$ minigene marker within the *pTVW* vectors, were injected into w^{1118} embryos along with the helper vector pUC*hs*Delta2-3 to provide a source of *P*-element transposase. Afterward, the *P*-element with *UASt-Venus Pico* as its cargo was randomly transposed to an indiscriminate chromosomal site (Spradling and Rubin, 1982). The resulting flies were then returned for further analysis.

5.4.3 Determination of Venus-Pico expression levels in fly extracts

Constructs could be located in regions of generally high (euchromatin) or low (heterochromatin) gene expression because of the random nature of *P*-element insertion, dictating in turn the expression levels of the construct itself. As such, the relative Venus-Pico expression level was assessed for each line. Male flies expressing the *pico* double mutant constructs were crossed to virgin females

containing *da-GAL4* driver, then progeny were collected. Visualisation of fluorescent Venus in flies carrying the *da-Gal4* driver and one copy of the transgene of interest was first carried out for verification and analysis of ectopic protein expression. Following attempts to confirm expression levels through Western blot analysis using anti-GFP (Life technologies) proved successful to enable appropriate lines for each construct to be selected for future use (Figure 5.7, 5.8 and Table 5.1).

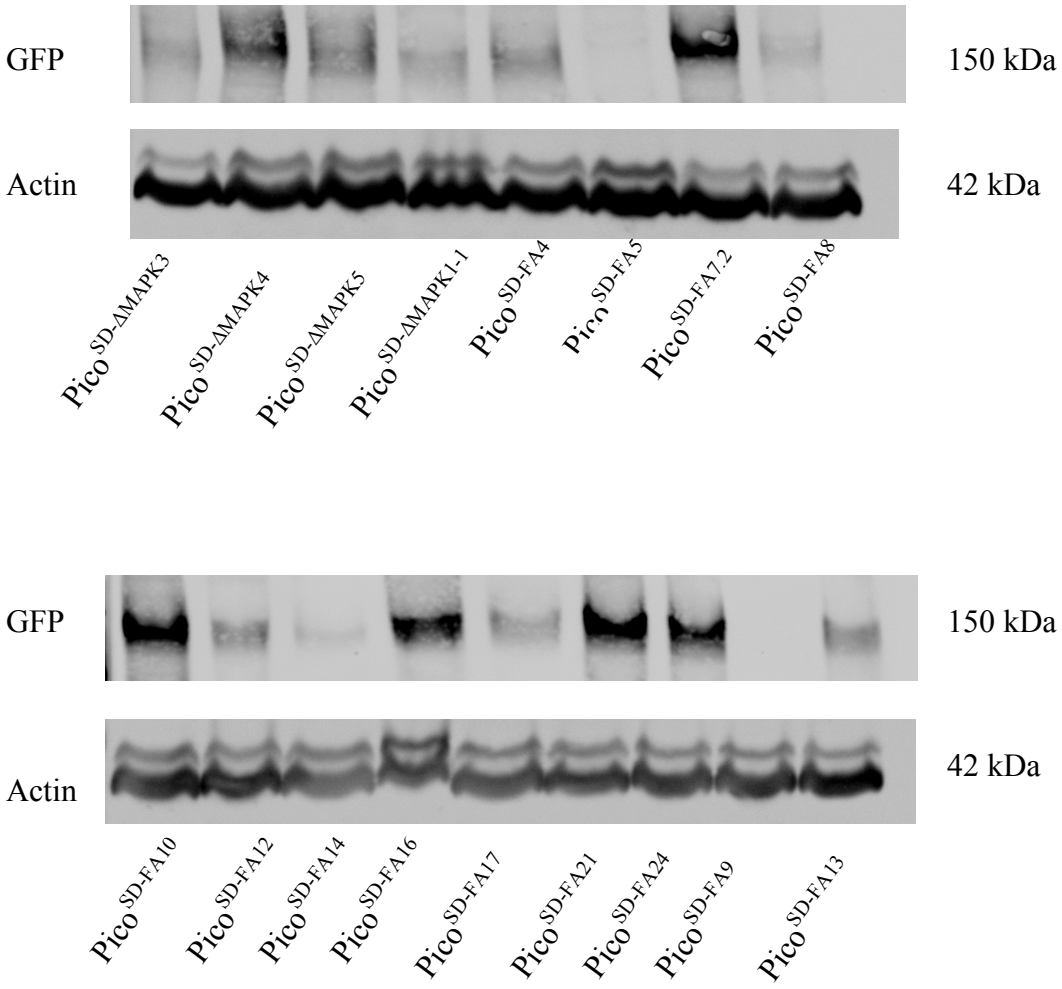

Figure 5.7. Examination of the *pico* double mutant expression level under the control of *da-GAL4*. Western blots were carried out to assess the relative expression levels of Pico double mutants using anti-GFP antibody. Further control blots were carried out using anti-Actin antibody to control for total protein in the samples.

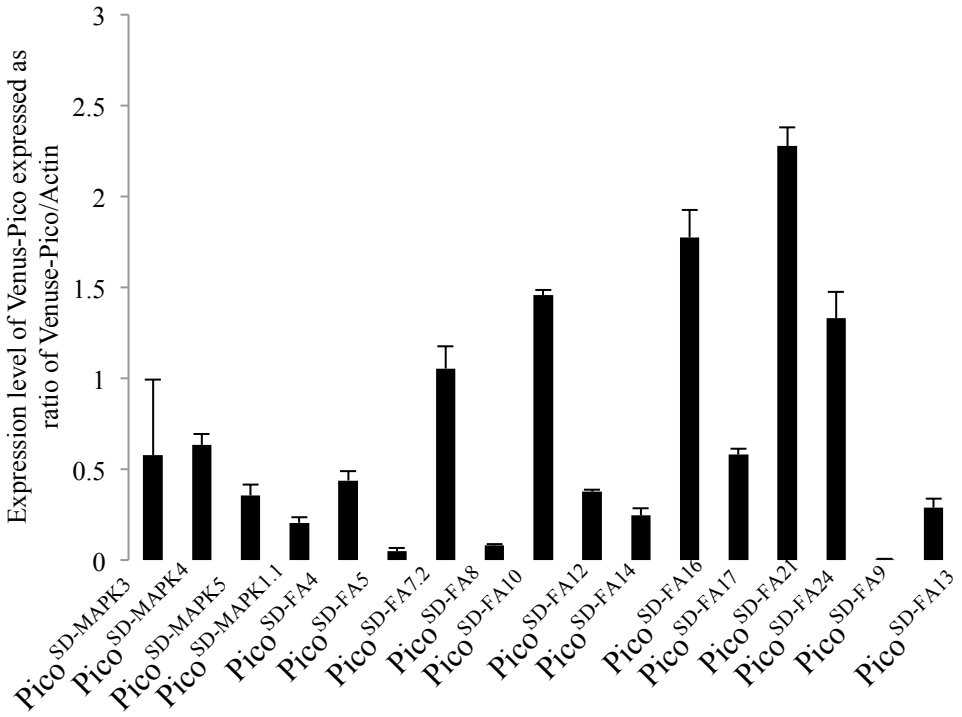

Figure 5.8. Average expression level of Pico double mutations. Expression level of Venus-Pico in different transgenic *Drosophila* lines normalized to the level of β-Actin. Results are expressed as mean ± SE for the different genotypes (n=3).

Table 5.1. Quantification of Westerns blot of different *Drosophila* lines. 10 adult flies were collected from different *Drosophila* lines presented in (A) and (B). The resultant gels were blotted with anti-GFP antibody and anti-β-actin as a loading control. The blots were separately scanned by densitometry and the area under the peak corresponding to each protein was first normalised to that of actin.

(A)

Antibody GFP/Actin	$Pico^{SD-\Delta MAPK3}$	$Pico^{SD-\Delta MAPK4}$	$Pico^{SD-\Delta MAPK5}$	$Pico^{SD-\Delta MAPK1.1}$	$Pico^{SD-FA4}$	$Pico^{SD-FA5}$	$Pico^{SD-FA7.2}$	$Pico^{SD-FA8}$
Mean	0.58	0.63	0.36	0.20	0.44	0.05	1.05	0.08
STDEV	0.72	0.10	0.10	0.05	0.09	0.03	0.03	0.01
SE	0.42	0.06	0.06	0.03	0.05	0.02	0.12	0.01
Ratio	0.58 ± 0.42	0.63 ± 0.06	0.36 ± 0.06	0.20 ± 0.03	0.44 ± 0.05	0.05 ± 0.02	1.05 ± 0.12	0.08 ± 0.01

(B)

Antibody GFP/Actin	$Pico^{SD-FA10}$	$Pico^{SD-FA12}$	$Pico^{SD-FA14}$	$Pico^{SD-FA16}$	$Pico^{SD-FA17}$	$Pico^{SD-FA21}$	$Pico^{SD-FA24}$	$Pico^{SD-FA9}$	$Pico^{SD-FA13}$
Mean	1.46	0.38	0.25	1.78	0.58	2.28	1.33	0	0.29
STDEV	0.05	0.02	0.06	0.26	0.06	0.18	0.25	0	0.09
SE	0.03	0.01	0.04	0.15	0.03	0.10	0.14	0	0.05
Ratio	1.46 ± 0.03	0.38 ± 0.01	0.25 ± 0.04	1.78 ± 0.15	0.58 ± 0.03	2.28 ± 0.10	1.33 ± 0.14	0	0.2 ± 0.05

Once characterisation was completed, appropriate lines were selected from each construct for use in future experiments. Choices of transgenic lines were made based on their relative expression levels, characterised as either high (e.g. Pico$^{SD\text{-}FA21}$), moderate (e.g Pico$^{SD\text{-}FA7.2}$), or low (e.g. Pico$^{SD\text{-}FA5}$).

5.5 Quantification of the effect of single site-directed mutations in *pico* on wing overgrowth

To assess the effect of the double mutants on *pico* function, their ability to promote tissue overgrowth when overexpressed under the control of *MS1096-GAL4* was determined. For comparison, a panel of UAS-Venus-tagged *pico* transgenic flies carrying single site-directed mutations were first analysed: Pico^{WT}, Pico$^{\Delta MAPK3}$, Pico$^{\Delta PP1}$, Pico^{S819A} and Pico^{S819D}. It had previously been demonstrated that the presence of an N-terminal Venus-tag did not affect *pico*'s ability to promote wing overgrowth (Jonchere and Bennett, 2013). Wings from 30 male adult flies were examined from each genotype and compared to sibling *MS1096-GAL4* control flies grown in the same vials to ensure identical genetic and environmental backgrounds.

5.5.1 The ability of Pico to induce growth and proliferation

To determine the effect of *pico* transgenes on tissue growth, adult wings were dissected from flies expressing the Venus-tagged *pico* variants and the surface area was measured using ImageJ. Wings from Venus-Pico^{WT2} were 6% bigger than the *MS1096-GAL4* control (Figure 5.10A). Ectopic expression of the Pico^{MAPK3} and

Pico^{F816A} mutants resulted in significantly enhanced wing overgrowth compared to their controls ($p<0.001$), with increases in wing size of 15% and 19% observed, respectively (Figure 5.10B, C). This effect was considerably higher than that observed in flies expressing Venus-Pico^{WT}. These data indicate that disruption of the PP1 and MAPK binding motifs potentiates the effect of ectopic Pico.

Flies expressing the non-phosphorylatable Pico^{S819A} and phosphomimetic Pico^{S819D} constructs using the *MS1096-GAL4* driver were assessed to determine the role of phosphorylation in regulating the function of Pico. Ectopic Pico^{S819A} caused 20% increase in wing size. Contrastingly, overexpression of Pico^{S819D} led to a minor 2% increase in wing size, suggesting that phosphorylation at serine 819 may disrupt the ability of Pico to induce tissue overgrowth.

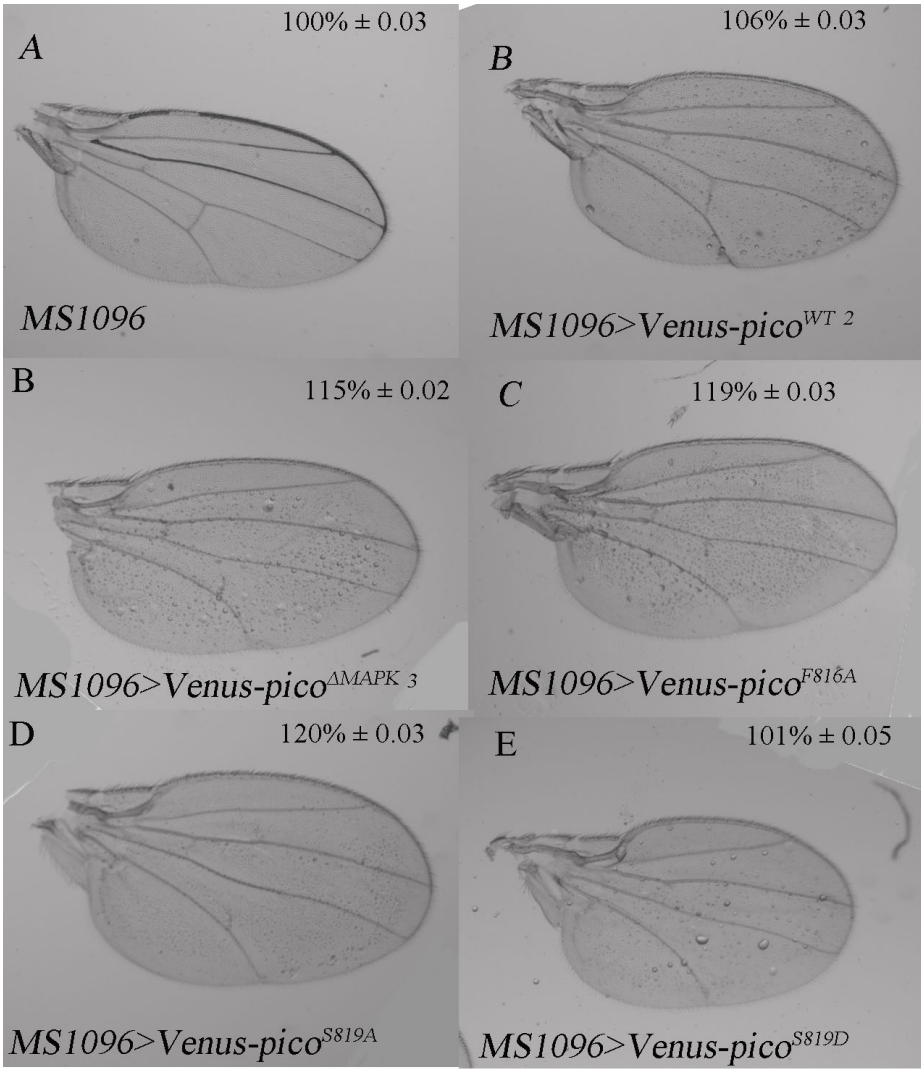

Figure 5.10. Ectopic expression of *pico*$^{\Delta MAPK3}$, *pico*^{F816A} and *pico*^{S819A} mutants display significant overgrowth compared to *Venus-pico*^{WT2}. A-E, Representative adult wings from male *MS1096-GAL4* flies with and without *UAS-Venus-pico* variants. **(A)** Wings from flies containing the *MS1096-GAL4* driver only were used as a comparative control in each cross. A representative example is shown here. **(B)** Flies expressing *Venus-Pico*$^{\Delta MAPK3}$ under the control of the *MS1096-GAL4* driver yielded a 15% increase in wing size while ectopic **(C)** flies expressing *Venus-pico*^{F816A} and **(D)** flies expressing non-phosphorylatable *Venus-pico*^{S819A} caused significant overgrowth, with increases in wing size of 19% and 20%, respectively. **(E)** Overexpression of phosphomimetic *Venus-pico*^{S819D} showed only a slight increase compared to the control. Wing area is expressed as a percentage of control (mean ±SD, n=40).

5.5.2 Ability of *pico* double mutants to induce growth and proliferation

Having established the effect of single mutants in *pico*, the double mutants generated in this chapter were then analysed. As shown in Figure 5.11. below, ectopic Pico$^{SD-\Delta MAPK4}$ caused a very slight increase in wing size 3%. This is significantly reduced compared to the effect of Pico$^{\Delta MAPK3}$ alone ($p<0.001$), suggesting that the S819D mutation is capable of compensating for the loss of MAPK binding, consistent with the model of Lofthouse (Lofthouse, 2013)., Also in keeping with our expectations, Pico$^{SD-FA(16)}$ and Pico$^{SD-FA(10)}$ led to a considerable increase in wing size of 15% and 8%, respectively, comparable to the effect of Pico^{F816A} alone. This would be expected if loss of PP1 binding was epistatic to S819 phophorylation, which is mimicked in these experiments by the S819D mutation.

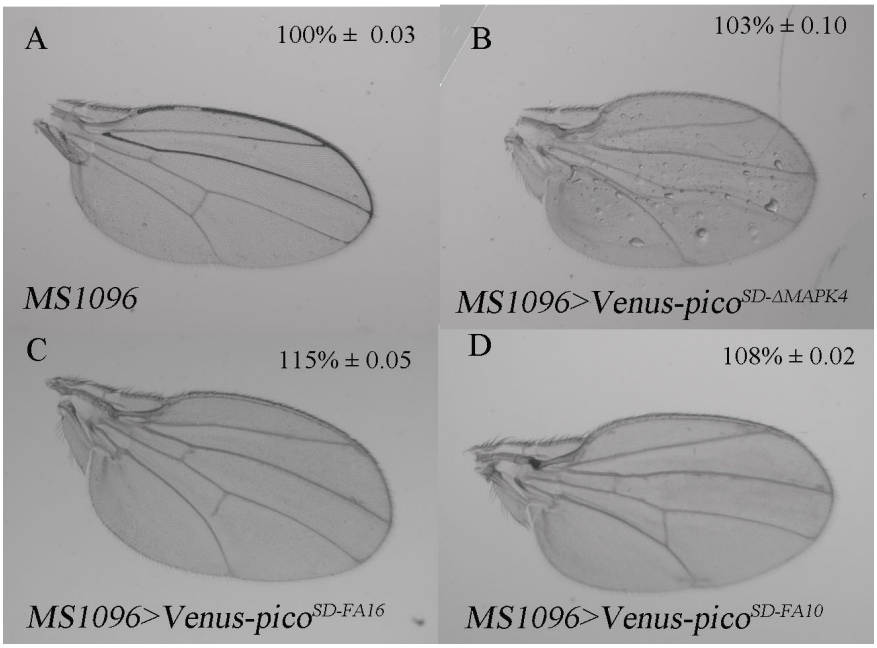

Figure 5.11. Substitution of Serine 819 modulates the effect of other site-directed mutations on *pico*-mediated overgrowth. (A) Flies containing only the *MS1096-GAL4* driver were utilised as a comparative control and exhibited wing sizes comparable to w^{1118}. **(B)** Flies expressing $pico^{SD\text{-}\Delta MAPK4}$ only caused a negligible 3% wing overgrowth, whereas **(C)** overexpression of $pico^{SD\text{-}FA16}$ and **(D)** $pico^{SD\text{-}FA10}$ were found to possess wings displaying a considerable 15% and 8% increase in wing size. Wing area is expressed as a percentage of control (mean ±SD, n=40).

5.5.3 Western blot using anti-GFP

An important caveat to the interpretation of the experiments performed above is that the expression level of Venus-Pico constructs might not be equivalent to one another. Consequently, the phenotypic effect of overexpression might not be a function of the site-directed mutations harboured by each *pico* variant.

To examine this, 20 wing discs were dissected from flies expressing $Venus\text{-}pico^{WT}$ *and mutants* and extracts were examined by immunoblotting with an anti-GFP

antibody. Blotting with anti-Actin antibody was used to control for total protein. Notably, the levels of $Pico^{\Delta MAPK3}$, $Pico^{F816A}$, and $Pico^{S819A}$, which promote exaggerated overgrowth were expressed at higher levels than $Pico^{WT2}$, whereas $Pico^{S189D}$ and $Pico^{SD\text{-}\Delta MAPK4}$, which display reduced overgrowth compared to $Pico^{WT2}$ were expressed at lower levels. One must therefore caution the interpretation of the growth studies reported above and in Lofthouse (Lofthouse, 2013) since the differing effects of site-directed mutants might reflect their level of expression rather than effects on *pico* function.

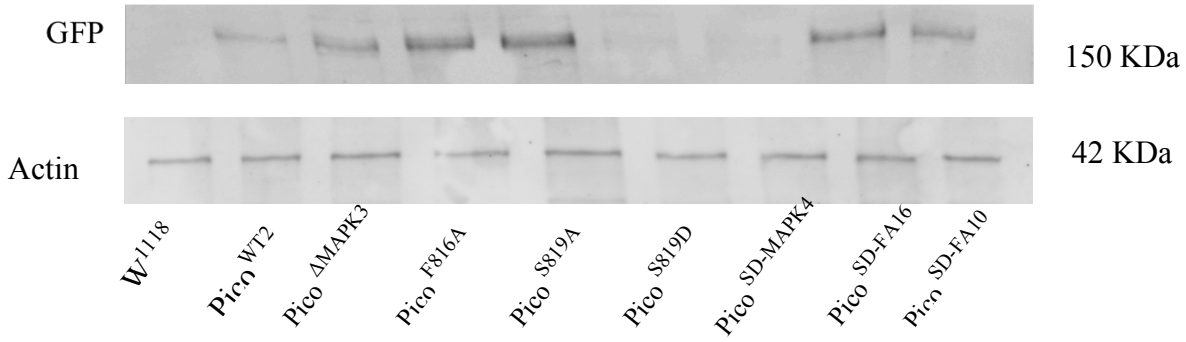

Figure 5.12. *pico* level of production in different *Drosophila* lines. Total extracts from w^{1118}, MS1096-GAL4 UAS-$pico^{WT2}$, MS1096-GAL4 UAS-$pico^{\Delta MAPK3}$, MS1096-GAL4 UAS-$pico^{F816A}$, MS1096-GAL4 UAS-$pico^{S819A}$, MS1096-GAL4 UAS-$pico^{S189D}$, MS1096-GAL4 UAS-$pico^{SD-\Delta MAPK4}$, MS1096-GAL4 UAS-$pico^{SD-FA16}$ and MS1096-GAL4 UAS-$pico^{SD-FA10}$ wing discs were analysed by Western blotting to ascertain the levels of Venus-Pico using anti-GFP antibody and anti-Actin as a control. The results showed that the MS1096-GAL4 $Pico^{S189D}$ and MS1096-GAL4 $Pico^{SD-\Delta MAPK4}$ displayed very little apparent of Pico compared to the other.

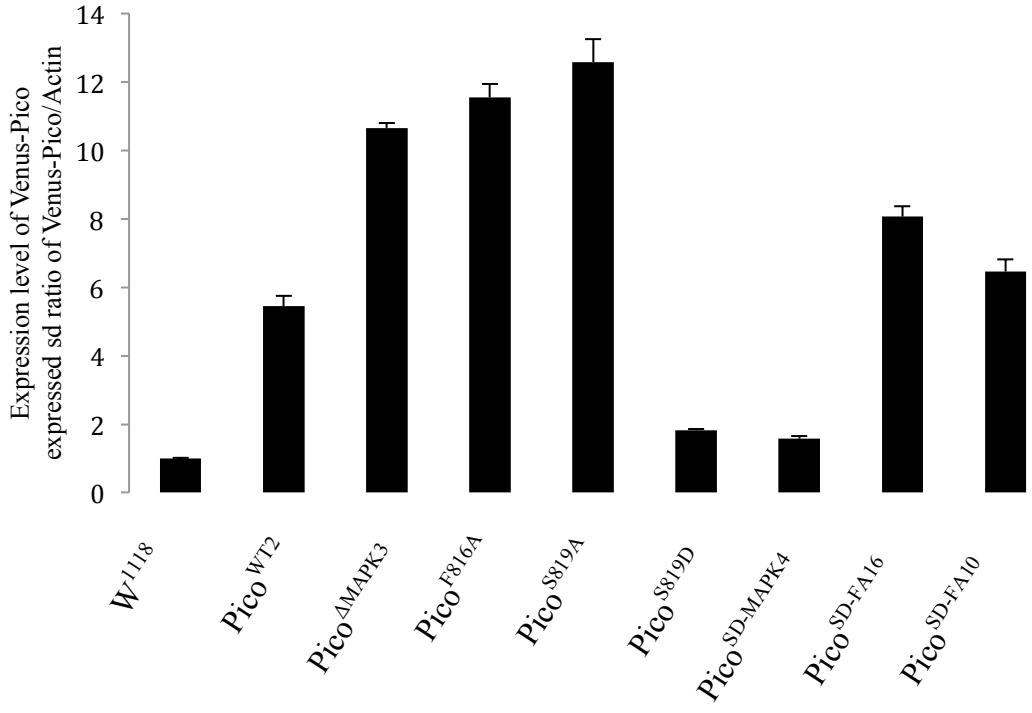

Figure 5.13. Expression level of Venus-tagged Pico in fly extracts as determined by anti-GFP Western blotting. The graph shows the expression level of Pico in different *Drosophila* lines. Flies expressing $Pico^{S819A}$ have the highest level of protein. While flies expressing $Pico^{SD-\Delta MAPK4}$ have the lowest level of the protein. Results are expressed as mean ± SE for the different genotypes (n=3).

Table 5.2. Quantification of Venus-Pico protein levels in *Drosophila* extracts. 20 wing discs were collected from different *Drosophila* lines then 4 win discs were loaded per lane. The resultant gels were blotted with anti-GFP antibody and anti-β-actin as a loading control. The blots were separately scanned by densitometry and the area under the peak corresponding to each protein was first normalised to that of actin and then ratioed to the level of that protein
found in w^{1118} flies. The mean relative abundance mean ± SE form three separate experiments is shown.

Antibody GFP/Actin	**w^{1118}**	**MS1096-GAL4 Pico^{WT2}**	**MS1096-GAL4 Pico$^{\Delta MAPK3}$**	**MS1096-GAL4 Pico^{F816A}**	**MS1096-GAL4 Pico^{S819A}**	**MS1096-GAL4 Pico^{S189D}**	***MS1096-GAL4* Pico$^{SD-\Delta MAPK4}$**	**MS1096-GAL4 Pico$^{SD-FA16}$**	**MS1096-GAL4 Pico$^{SD-FA10}$**
Mean	1	5.46	10.66	11.55	12.59	1.82	1.57	8.07	6.46
STDEV	0.02	0.52	0.26	0.6	1.17	0.08	0.16	0.53	0.64
SE	0.01	0.29	0.15	0.39	0.68	0.05	0.09	0.30	0.37
Ratio	1 ± 0.01	5.46 ± 0.29	10.66 ± 0.15	11.55 ± 0.39	12.59 ± 0.68	1.82 ± 0.05	1.57 ± 0.09	8.07 ± 0.30	6.46 ± 0.37

5.6 Characterisation of wild type and mutant *pico* transgenes

A second aim of this chapter was to test the ability of $pico^{\Delta MAPK3}$ to cooperate with oncogenic *Ras* compared to that of $pico^{WT}$ in the cell invasion model described in Chapter 4. Given the findings reported above, we reanalysed expression levels of the available $pico^{\Delta MAPK3}$ and $pico^{WT}$ transgenic lines to ensure we could make robust inferences about the functional effects of the site-directed mutations. This was done using an alternative approach to Western blotting; in brief, the Venus-tagged proteins were expressed in a segmented fashion using *engrailed-GAL4*, which is expressed in a few cells along segment boundaries, and intensity of Venus fluorescence measured by densitometry. Images were captured with equivalent settings in order to compare relative expression levels. $pico^{WT}$ line 2 and $pico^{\Delta MAPK}$ line 3 had the highest expression level, with $pico^{\Delta MAPK3}$ being approximately twice the level of $pico^{WT2}$, consistent with the measurement of protein levels by Western Blotting (Figure 5.13). $pico^{WT}$ lines 4 and 6, and $pico^{\Delta MAPK}$ lines 8 had lower levels of expression. (Figure 5.14. and 5.15).

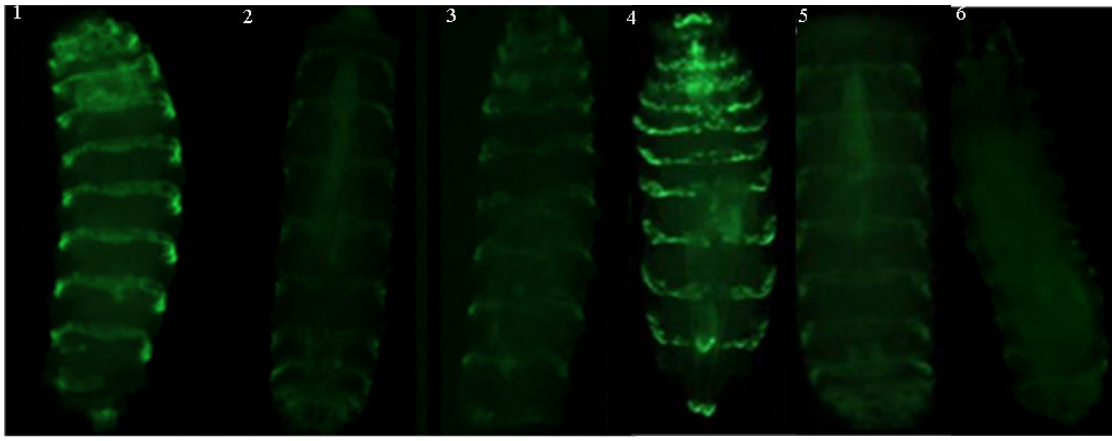

Figure 5.14. Representative images of larvae expressing different transgenic lines of *Venus-pico* wild type, and MAPK mutant under the control of an *engrailed-Gal4* driver. Images (1,2 and 3) represent *Venus-pico* wild type line 2, 4 and 6. Images (4,5 and 6) represent *Venus-pico* MAPK mutant line (3,5 and 8). These show fluorescence of the Venus-tagged protein in the different lines, which can be used to measure of the relative abundance of the ectopic protein.

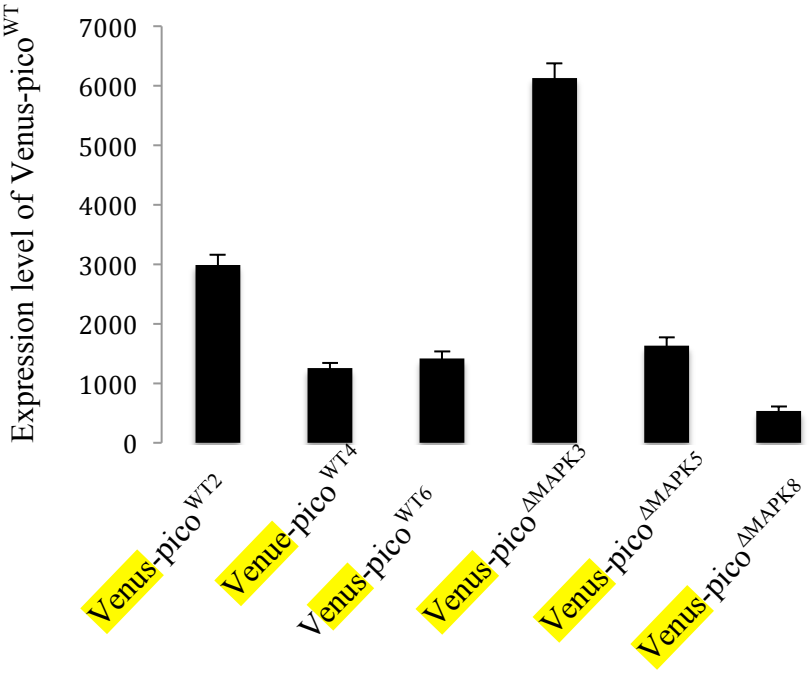

Figure 5.15. Expression level of Venus-tagged Pico in larvae as determined fluorescence level. The graph shows the expression level in different lines of *Venus-pico*$^{WT\ o\ r\ \Delta MAPK}$. Expressing level of *Venus-pico*$^{\Delta MAPK3}$ is almost twice the level of Venus-*pico*^{WT2}.

5.7 Disruption of MAPK-binding to Pico promotes metastasis of Ras^{V12} -induced tumours

Previous work, described in Chapter 4, showed that overexpression of *pico*, under the control of *eyFLP* is capable of promoting the invasion of Ras^{V12}-induced tumours in the larval CNS. The *eyeless* promoter that was utilised drives expression throughout the eye-antennal imaginal discs as well as in a number of defined regions of the optic lobes, but not in the VNC. Therefore it is possible to determine if tumour cells have migrated from their original location by examining the localisation of GFP-labelled cells in the cephalic complex, which consists of -antennal discs (ED), optic lobes (OL), and ventral nerve cord (VNC).

To compare the effect of $pico^{WT2\ or4}$ and $pico^{\Delta MAPK3}$ on Ras^{V12}-induced tumours, larvae of the following four genotypes were generated (crossing scheme presented in Figure 5.16.)

1- eyFLP/Y; $\frac{\text{UAS}-\text{Rasv12}}{+}$; $\frac{\text{A}>CD2>GAL4,UAS-GFP}{+}$

2- eyFLP/Y; $\frac{\text{UAS}-\text{Rasv12}}{+}$; $\frac{\text{A}>CD2>GAL4,UAS-GFP}{\text{UAS}-\text{Venus}-\text{pico wt2}}$

3- eyFLP/Y; $\frac{\text{UAS}-\text{Rasv12}}{\text{UAS}-\text{Venus}-\text{pico wt4}}$; $\frac{\text{A}>CD2>GAL4,UAS-GFP}{+}$

4- eyFLP/Y; $\frac{\text{UAS}-\text{Rasv12}}{+}$; $\frac{\text{A}>CD2>GAL4,UAS-GFP}{\text{UAS}-\text{Venus}-\text{pico }\Delta\text{MAPK3}}$

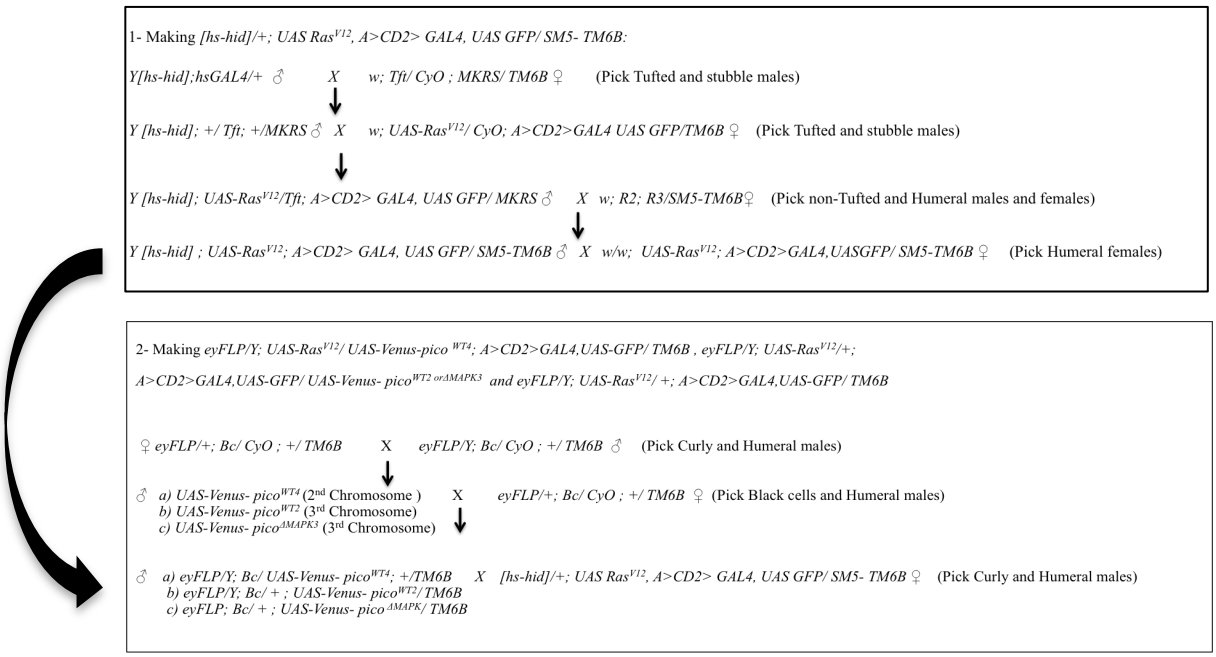

Figure 5.16. Crossing scheme used to generate *ey> Ras^{V12}*, *ey>pico$^{WT2\ and\ 4}$*, *ey>pico$^{\Delta MAPK3}$* larvae to examine the effect of pico MAPK binding mutation. The first scheme was to generate a virginiser tester strain and the second scheme was to generate the larvae harbouring *Ras^{V12}* induced tumours with or without *pico*.

50 brains were dissected from third instar larvae overexpressing *Ras^{V12}* alone, *Ras^{V12}* and *pico^{WT2}* or *Ras^{V12}* and *pico^{WT4}*. 20 brains were dissected from larvae coexpressing *Ras^{V12}* and *pico*$^{\Delta MAPK3}$. Fewer brains were dissected of this genotype because the cephalic complex from its attachments without damaging the underlying structures. The brains were examined using a fluorescence stereomicroscope. *Ras^{V12}* overexpression resulted in an increase in the eye-antennal discs size and exhibited a loss of morphology, however, no cell migration was observed (Figure 5.17). Overexpression of *Ras^{V12}/ pico^{WT}* resulted in significant overproliferation of the eye-antennal imaginal discs and an accompanying loss of morphology. Furthermore, GFP-tagged tumour cells were no longer exclusively found in the eye discs and optic lobes, with invasion of the VNC clearly visible (Figure 5.17). Two independent insertions of the wild type *pico* transgene showed similar effects with *Ras^{V12}* despite

being expressed at different levels (Figure 5.17). However, overexpression of a version of *pico* lacking its MAPK binding site (*pico*$^{\Delta MAPK3}$) showed an enhanced effect with *Ras*^{V12} relative to wild type *pico*; larvae exhibited massive growth in the eye disc and loss of morphology in the optic lobes (Figure 5.17).

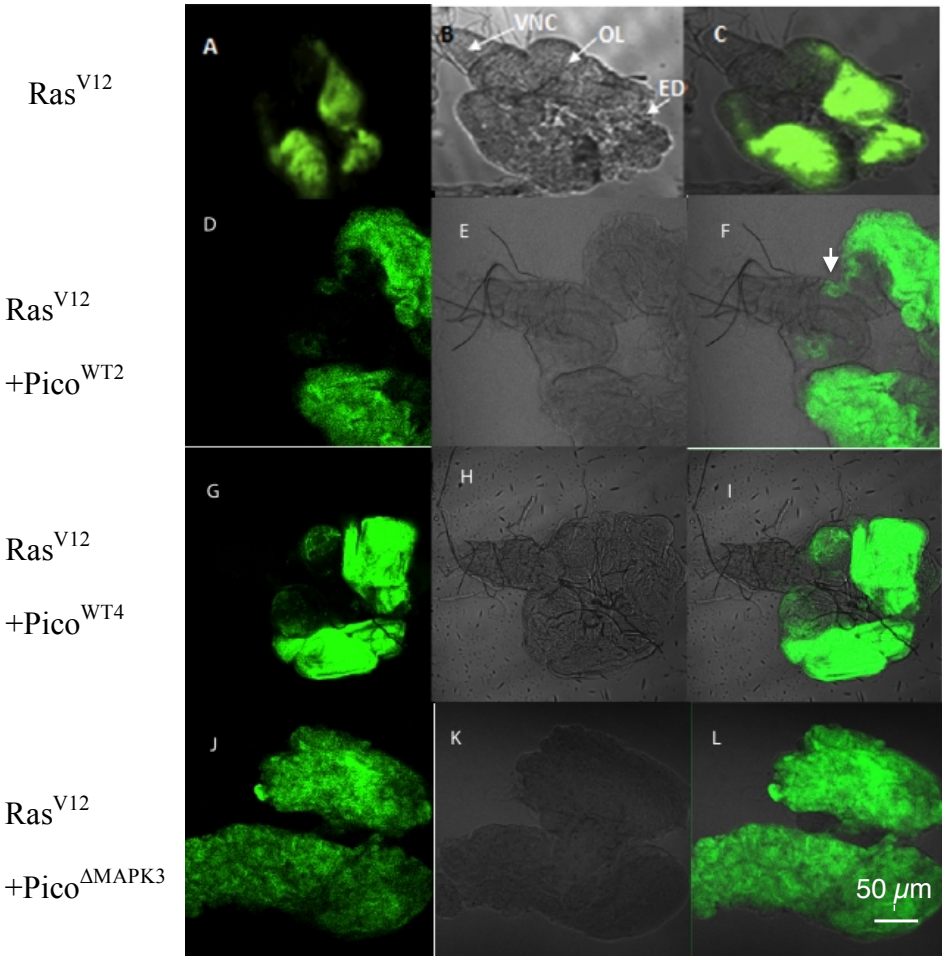

Figure 5.17. Overexpression of *pico* in conjunction with oncogenic *Ras*^{V12} promotes tumour cell migration. The figure shows representative cephalic complexes. Image (A, B and C) illustrates the effect of *Ras*^{V12} alone; (D, E, F, G, H and I) show the effect of *Ras*^{V12} and Wild type Pico;(J, K and L) show the effect of *Ras*^{V12} and mutant Pico in MAPK binding site. 50 brains were dissected from third instar larvae.

The tumour cell invasions produced from each of the phenotypes (*pico*^{WT} line 2 &4) were quantified (Figure 5.18). The degree of invasion was assigned one of four categories based on the degree of the invasion into the ventral nerve cord. Type 0 corresponded to no invasion to the VNC; type I corresponded to tumour cell invasion occurring down one side of the VNC; type II corresponded to tumour cell invasion from both side of the VNC; type III corresponded to significant tumour cell invasion to the VNC as well as overgrowth of the optic lobes. The two WT overexpression lines (line 2 and 4) caused a similar degree of overgrowth in the eye disc and invasion of the tumour cells to the ventral nerve cord when expressed with *Ras*^{V12} (0.98± 0.12) and (0.98± 0.11) respectively. 28% of the *Ras*^{V12}and *pico*^{WT} (line 2) and 26% of the *Ras*^{V12}and *pico*^{WT} (line 4) brains were found to exhibit no VNC invasion (Figure 5.18). 54% of the brains of the *Ras*^{V12}and *pico* WT (line 2) and 56% brains of the *Ras*^{V12} and *pico*^{WT} (line 4) were found to have type I invasion (Figure 5.18). 10% and 12% of brains of the *Ras*^{V12}and *pico*^{WT} (line 2&4) were assigned to type II invasion respectively, and 8% and 6% of brains of the *Ras*^{V12}and *pico*^{WT} (line 2&4) were assigned to type III categories respectively (Figure 5.18). Brains dissected from larvae expressing *Ras*^{V12}alone were entirely composed of type 0 (Figure 5.18).

The tumour cell invasions produced from *Ras*^{V12} *pico*$^{\Delta MAPK3}$ could not be quantified as a result of the enormous growth of the eye disc, which made it impossible to discriminate between the optic lobes and ventral nerve cord. Larvae of *Ras*^{V12} *pico*$^{\Delta MAPK5 \text{and } 8}$ also have abnormal brains, similar to *Ras*^{V12} *pico*$^{\Delta MAPK3}$ brains, which make it difficult to dissect without damaging the underlying structures.

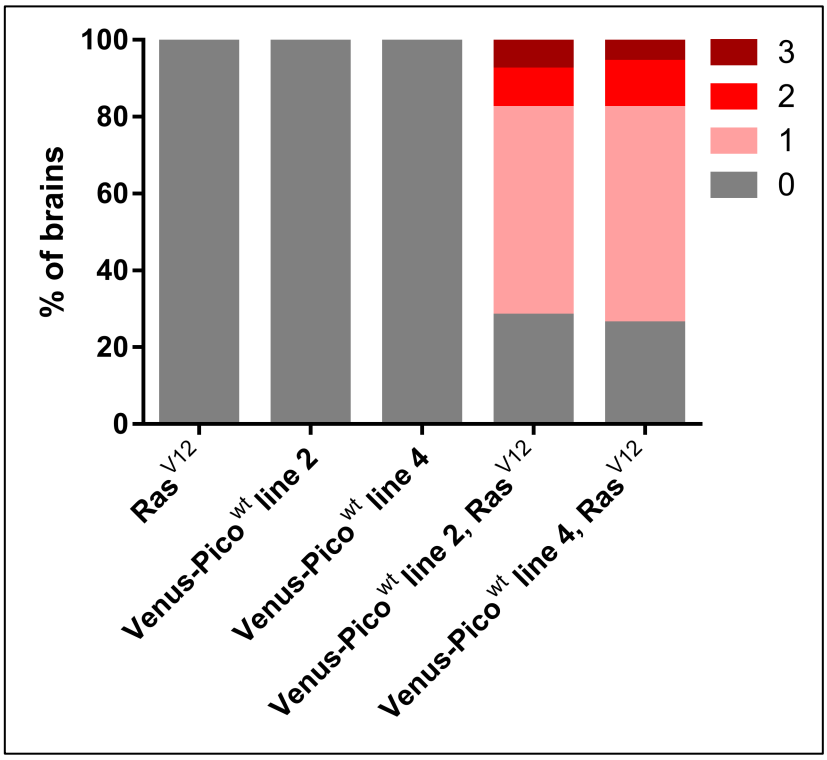

Figure 5.18. Quantification of the severity of metastasis observed in *ey>Ras^{V12}* and *ey>Ras^{V12}, pico^{WT2}* and 4 brains. A) Type 0 corresponded to no invasion to the VNC; type 1 corresponded to tumour cell invasion occurring down one side of the VNC; type 2 corresponded to tumour cell invasion from both side of the VNC; type 3 corresponded to significant tumour cell invasion to the VNC as well as overgrowth of the optic lobes. 50 brains were dissected for each genotype.

5.8 Discussion

Previous work presented in the literature had identified the Ser 819 as a site of phosphorylation within Pico (Bodenmiller et al., 2007). Studies utilising Pico$^{\Delta MAPK}$, which disrupts binding to MAPK, implicated MAPK in the phosphorylation of Serine 819 (Lofthouse, 2013), a residue situated next to the PP1-binding motif.

The investigations also indicated that Pico mediates growth. Previous work within the Bennett laboratory has developed a series of site-directed mutants of *pico* such as Protein Phosphatase 1 binding site mutation (Pico^{F816A}), non-phosphorylatable

(Pico^{S819A}) and phosphomimetic mutations of S819 (Pico^{S819D}) and mutation in the MAPK binding site (Pico$^{\Delta MAPK3}$), which affect on Pico functions (Loufthouse, 2013). These mutations have been examined for their effect on *pico*-mediated growth by measuring effects on adult wing size. Wings expressing *pico*^{F816A} and *pico*$^{\Delta MAPK3}$ mutants showed significant overgrowth compared to wild type *pico* indicating that disruption of the PP1- and MAPK-binding motifs potentiates the effect of ectopic *pico*. This finding identifies potential roles for PP1 and MAPK as negative regulators of *pico* function. In addition, the importance of the phosphorylation in regulating *pico*'s activity was examined by using flies expressing the non-phosphorylatable *pico*^{S819A} and phosphomimetic *pico*^{S819D} constructs, although it should be noted that substitution of Ser819 for an Asp residue may not fully replicate the effects of covalent addition of a phosphate group to Ser. Wing measurements showed that there was a significant increase in wing size in flies expressing *pico*^{S819A}, that was comparable to expression of *pico*^{WT2}. Contrastingly, overexpression of *pico*^{S819D} caused a slight increase in wing size, suggesting that phosphorylation at serine 819 may disrupt the ability of *pico* to induce tissue overgrowth. These findings were examined further by generating double mutant constructs: Pico$^{SD\text{-}\Delta MAPK}$ and Pico$^{SD\text{-}FA}$. Flies expressing *pico*$^{SD\text{-}\Delta MAPK}$ showed a reduction in wing size compared the wing produced from flies expressing the *pico*$^{\Delta MAPK}$ mutant, confirming that the ability of *pico* to promote tissue overgrowth can be disturbed by the phosphorylation at Ser 819, whilst *pico*$^{SD\text{-}FA}$ retained the ability of *pico*^{F816A} to produce exaggerated overgrowth.

An important caveat to the findings above however is that the expression level of the Venus-pico transgenic lines used in these experiments was not equivalent. This

problem is most likely caused by different position effects associated with each of the transgenes, which were inserted randomly into the *Drosophila* genome using *P*-element transposition (Spradling and Rubin, 1982). A highly efficient site-specific transposition system has been reported that makes use of the *Streptomyces* φC31 integrase (Groth et al., 2004). Studies have been shown that φ C31 used for either simple insertion plasmids or for larger constructs (Venken et al., 2010), via a single *attP* site (integrated) and *attB* sites (vector) recombination (Cherbas et al., 2015). Two new sequences, *attL* and *attR*, are produced from this recombination, that occurs at a core TTG common to both site (Kuhstoss and Rao, 1991, Rausch and Lehmann, 1991)(Figure 5.20). Now that well-characterised *Drosophila* strains containing *attP* landing sites are widely available, it would be desirable in the future to use this system to compare the effects of *UAS-pico* variants and will help to confirm their functional effects.

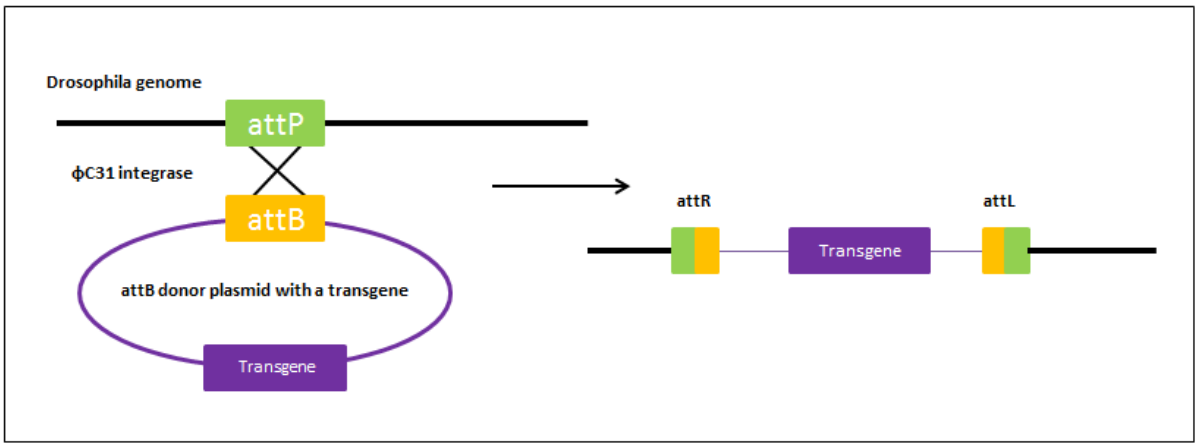

Figure 5.19. φC31-mediated integration of DNA into the Drosophila genome. An attP in the *Drosophila* genome acts as the recipient site. A pUAST plasmid containing attB is coinjected with φC31integrase mRNA into attP-containing recipient embryos, leading to insertion of the transgene into attP site. Two new sequences attL and attR are formed resulting in preventing further integrase-catalysed movement of the integrated transgene. Figure adapted from (Fish et al., 2007).

In the last part of this chapter, disruption of the MAPK binding site was examined for its ability to promote cellular invasion compared to a wild type *pico* transgene. Data showed that co-overexpression of Ras^{V12} and *pico* had a greater effect on tumour growth than overexpression of Ras^{V12} on its own, in keeping with the findings reported in Chapter 4. It is useful to note that the presence of an N-terminal Venus tag did not obviously interfere with *pico*'s ability to promote invasion in this context. Disruption of the MAPK binding site in *pico* caused significant overgrowth in the eye disc compared to wild type *pico.* This suggests that MAPK binding may negatively regulate *pico's* activity in the eye disc as it does in the wing. However, the effects of $pico^{\Delta MAPK3}$ on the invasion of Ras^{V12}-induced tumours was hard to assess because brains coexpressing these proteins were morphologically abnormal. One way to address this issue might be to make clones of cells co-expressing $pico^{\Delta MAPK3}$ and Ras^{V12}, to limit the amount of tissue affected. Alternatively, it would be interesting to test the effect of overexpression with glial-specific drivers, which also may limit the morphological defects but reveal effects on e.g. proliferation and invasion of the different glial subtypes.

6 General discussion

6.1 A novel tool for monitoring SRF activity

This thesis has employed the model organism, *Drosophila melanogaster* to examine the role of the MRL protein in promoting tissue growth and cell migration. It has been proposed that members of this family facilitate the transduction of signals derived from membrane receptors to changes in the actin cytoskeleton allowing regulation of actin dynamics, cell adhesion, migration and growth (Krause et al., 2004, Lafuente et al., 2004, Lyulcheva et al., 2008, Colo et al., 2012b). In addition, MRL proteins have been reported to have the ability to activate serum response factor (SRF) *in vitro* (Pinheiro et al., 2011), but *in vivo* evidence for MRL-induced SRF signalling had been lacking. To address this we generated an SRF responsive reporter gene that faithfully replicates the endogenous pattern of SRF expression and reveals developmental-dependent changes in the level of expression (Chapter 3.2.2). In Chapter 3 we demonstrate that *pico* is capable of inducing the expression of this reporter in developing wing imaginal discs. The reporter is also responsive to overexpression of the SRF cofactor Mal and other actin regulators, including Ena, Chic, Scar that can alter actin dynamics (Chapter 4.3). These findings are consistent with a model, proposed by Lyulcheva that Pico induces SRF activation via its association with actin regulators (Lyulcheva, 2006, Lyulcheva et al., 2008). It would be interesting to test this explicitly using site-directed mutagenesis of the Ena and Scar binding sites in Pico.

Although several lines of evidence suggest that the SRF reporter described in Chapter 3 is induced in response to changes in actin dynamics and developmental cues, it has not yet been demonstrated that expression is diminished in cells lacking SRF. However, the difficulty of detecting basal mCherry expression made it hard to confirm whether *bs*/SRF mutant clones lose the ability to induce the SRF reporter (Chapter 3.2.3). Analysis of the effect of clones in the pupal wing, where expression is strongest, might help to address this issue. Of note, however, was the observation that mutant clones in the periphery of the wing disc showed elevated reporter activity, indicating that *bs*/SRF negatively regulates the reporter in a spatially-dependent manner.

A prerequisite to understanding mechanisms of transcriptional activation and inhibition mediated by SRF in the wing disc is the identification of SRF-target genes, which are not yet fully determined. In the ovary, actin itself has been proposed to be a key SRF target (Muehlich et al., 2016). Another potential target, uncovered by transcriptomics analysis performed by Vincent Jonchere (see Chapter 3) is *deterin,* which encodes *Drosophila* Survivin. To test the importance of deterin, we examined the effect of overexpressing *pico* in wing imaginal discs with or without *deterin* RNAi knockdown (*deterin*^{IR}), using activated Caspase 3 antibody to identify cells undergoing apoptosis. A dramatic increase in the number of cells undergoing cell death were observed when coexpressing *pico,* particularly in the wing pouch where SRF and SRF-dependent gene expressed (Chapter 3.2.2). These data suggest that *pico*-induced *deterin* expression is necessary to suppress proliferation induced apoptosis.

6.2 The role of MRL proteins in hyperplastic growth and cell invasion

Previous studies in the Bennett laboratory demonstrated that Pico, in addition to its role as a growth regulator, possesses the capacity to regulate cell spreading in model of cancer metastasis (Taylor, 2010). Using the *Drosophila* Ras^{V12} model of metastasis it was found that co- expression of Ras^{V12} and *pico* promoted the breakdown of extracellular matrix and tumour dissemination (Chapter 4.2.2). In Chapter 4, we report the results of genetic experiments revealing that the effects of coexpressing Ras^{V12} and *pico* are restricted to glial cells in the CNS, which are enriched in SRF. SRF signalling is therefore also implicated in the cooperative phenotypes in the larval brain that we have described. These studies could potentially be extended by looking at the levels of the SRE-mCherry reporter in metastatic brains. Preliminary experiments were performed along these lines (not shown) but the level of mCherry fluorescence was very weak, though detectible in glia, but the signal to noise ratio was low making quantitation impossible. One way to address this in the future might be to make use of multiple transgenic insertions of the SRE-mCherry construct.

It would be also interesting to use the reporter in studying cell invasion in other contexts. *pico* and *mal* have independently been reported to play a role in invasive border cell migration in the *Drosophila* ovary (Law et al., 2013, Somogyi and Rørth, 2004). Ectopic overexpression of *pico* was found to promote migration of the border cell cluster towards the oocyte, while depletion of *pico* by RNAi resulted in retarded migration of the cluster relative to wild type (Law et al., 2013). Scar may be an important mediator of *pico*'s affects on the actin cytoskeleton in border cells, but whether indirect effects via Mal-SRF are involved is not clear (Law et al., 2013).

Analysis of the SRE-mCherry reporter in this context might help to clarify this matter.

6.3 Regulation of MRL protein function by reversible phosphorylation

Reversible phosphorylation is a key mechanism that provides temporal and spatial control to cellular processes and the organisation of cellular structures, including the actin cytoskeleton, which is dynamically regulated. It is perhaps not surprising therefore to find MRL proteins associated with kinases and phosphatases. The Ser 819 has been identified as a site of phosphorylation within Pico (Bodenmiller et al., 2007).

Previous studies indicated that phosphorylation of Serine 819 modulates binding of PP1 to Pico at residues 813-816 and that phosphorylation and PP1-binding was dependent on binding of MAPK to Pico at a more N-terminal site (Lofthouse, 2013). Here we found that $Pico^{\Delta MAPK}$, $Pico^{F816A}$ and $Pico^{S819A}$, which all prevent binding to PP1, enhanced proliferative effects compared to $Pico^{WT}$ suggesting that PP1-binding negatively regulates *pico* function (Chapter 5.4.1). These findings were examined further by generating double mutant constructs: $Pico^{SD\text{-}\Delta MAPK}$ and $Pico^{SD\text{-}FA}$. Reduction in wing size was observed in flies expressing $Pico^{SD\text{-}\Delta MAPK}$, which would be predicted to allow binding to PP1, compared to wings produced from flies expressing the $Pico^{\Delta MAPK}$, inhibits PP1-binding (Chapter 5.4.2). These data indicate that the ability of *pico* to promote tissue overgrowth can be disturbed by the phosphorylation at Ser 819 and are consistent with a functional interaction between Pico-associated MAPK and PP1. In contrast, $pico^{SD\text{-}FA}$ showed a similar ability to

promote wing overgrowth to *pico*^{F816A}, which would be expected if this double mutant prevents binding to PP1 (Chapter 5.4.2). In addition, data in this report suggests that Pico's activity is negatively regulated by MAPK binding in the eye disc as it does in the wing, as disruption of the MAPK binding site in *pico* caused significant overgrowth in the eye disc compared to wild type *pico* (Chapter 5.6). Clearly, it will be necessary to confirm the predictions of this model biochemically, e.g. to show that the double mutants display the expected PP1-binding characteristics. It would also be useful to test genetic interactions between *pico*, *MAPK* and *PP1* mutants to provide further evidence of the functional interactions. An outstanding question is what are the targets of Pico-associated PP1? If MAPK phosphorylates Pico to regulate PP1 binding, then what does PP1 dephosphorylate? One possibility is that PP1 dephosphorylates a Pico-associated protein, such as Ena or Chic/Profilin, or another actin-associated protein to fine tune the effects on the actin cytoskeleton.

Finally, it should be said that the work in this thesis focusses on the analysis of *pico* gain-of-function. This is particularly relevant to understanding the roles of *pico* in aberrant situations, such as cancer, where MRL proteins are overexpressed. However, future work should also assess the effect of disrupting physical interactions between endogenous Pico and its binding partners, which will provide insights into the importance of regulatory mechanisms during normal development. This could be achieved by expressing the *pico* transgenes reported in this thesis in a mutant background or by using gene-editing approaches to engineer the site-directed mutations into the native locus. Given the homology between Pico and its human

orthologues, it will also be interesting to test whether regulation of MRL function by serine/threonine phosphorylation is conserved in human cells.

7 References

ABRUZZI, K. C., RODRIGUEZ, J., MENET, J. S., DESROCHERS, J., ZADINA, A., LUO, W., TKACHEV, S. & ROSBASH, M. 2011. Drosophila CLOCK target gene characterization: implications for circadian tissue-specific gene expression. *Genes Dev,* 25**,** 2374-86.

ADAMS, M. D., CELNIKER, S. E., HOLT, R. A., EVANS, C. A., GOCAYNE, J. D., AMANATIDES, P. G., SCHERER, S. E., LI, P. W., HOSKINS, R. A., GALLE, R. F., GEORGE, R. A., LEWIS, S. E., RICHARDS, S., ASHBURNER, M., HENDERSON, S. N., SUTTON, G. G., WORTMAN, J. R., YANDELL, M. D., ZHANG, Q., CHEN, L. X., BRANDON, R. C., ROGERS, Y. H. C., BLAZEJ, R. G., CHAMPE, M., PFEIFFER, B. D., WAN, K. H., DOYLE, C., BAXTER, E. G., HELT, G., NELSON, C. R., MIKLOS, G. L. G., ABRIL, J. F., AGBAYANI, A., AN, H. J., ANDREWS-PFANNKOCH, C., BALDWIN, D., BALLEW, R. M., BASU, A., BAXENDALE, J., BAYRAKTAROGLU, L., BEASLEY, E. M., BEESON, K. Y., BENOS, P. V., BERMAN, B. P., BHANDARI, D., BOLSHAKOV, S., BORKOVA, D., BOTCHAN, M. R., BOUCK, J., BROKSTEIN, P., BROTTIER, P., BURTIS, K. C., BUSAM, D. A., BUTLER, H., CADIEU, E., CENTER, A., CHANDRA, I., CHERRY, J. M., CAWLEY, S., DAHLKE, C., DAVENPORT, L. B., DAVIES, A., DE PABLOS, B., DELCHER, A., DENG, Z. M., MAYS, A. D., DEW, I., DIETZ, S. M., DODSON, K., DOUP, L. E., DOWNES, M., DUGAN-ROCHA, S., DUNKOV, B. C., DUNN, P., DURBIN, K. J., EVANGELISTA, C. C., FERRAZ, C., FERRIERA, S., FLEISCHMANN, W., FOSLER, C., GABRIELIAN, A. E., GARG, N. S., GELBART, W. M., GLASSER, K., GLODEK, A., GONG, F. C., GORRELL, J. H., GU, Z. P., GUAN, P., HARRIS, M., HARRIS, N. L., HARVEY, D., HEIMAN, T. J., HERNANDEZ, J. R., HOUCK, J., HOSTIN, D., HOUSTON, D. A., HOWLAND, T. J., WEI, M. H., IBEGWAM, C., et al. 2000. The genome sequence of Drosophila melanogaster. *Science,* 287**,** 2185-2195.

ADAMS, M. D. & SEKELSKY, J. J. 2002. From sequence to phenotype: reverse genetics in Drosophila melanogaster. *Nature Reviews Genetics,* 3**,** 189-198.

AJIRO, M., NISHIDATE, T., KATAGIRI, T. & NAKAMURA, Y. 2010. Critical involvement of RQCD1 in the EGFR-Akt pathway in mammary carcinogenesis. *International journal of oncology,* 37**,** 1085-1093.

ALAM, J. & COOK, J. L. 1990. Reporter genes: Application to the study of mammalian gene transcription. *Analytical biochemistry,* 188**,** 245.

ALLAN, C., BUREL, J. M., MOORE, J., BLACKBURN, C., LINKERT, M., LOYNTON, S., MACDONALD, D., MOORE, W. J., NEVES, C., PATTERSON, A., PORTER, M., TARKOWSKA, A., LORANGER, B., AVONDO, J., LAGERSTEDT, I., LIANAS, L., LEO, S., HANDS, K., HAY, R. T., PATWARDHAN, A., BEST, C., KLEYWEGT, G. J., ZANETTI, G. & SWEDLOW, J. R. 2012. OMERO: flexible, model-driven data management for experimental biology. *Nat Methods,* 9**,** 245-53.

ANDERS, S., PYL, P. T. & HUBER, W. 2014. http://www-huber.embl.de/users/anders/HTSeq/doc/overview.html.

ANDERSEN, D. S., COLOMBANI, J., PALMERINI, V., CHAKRABANDHU, K., BOONE, E., ROTHLISBERGER, M., TOGGWEILER, J., BASLER, K., MAPELLI, M., HUEBER, A. O. & LEOPOLD, P. 2015. The Drosophila TNF receptor Grindelwald couples loss of cell polarity and neoplastic growth. *Nature,* 522**,** 482-6.

ARAGONA, M., PANCIERA, T., MANFRIN, A., GIULITTI, S., MICHIELIN, F., ELVASSORE, N., DUPONT, S. & PICCOLO, S. 2013. A mechanical checkpoint controls multicellular growth through YAP/TAZ regulation by actin-processing factors. *Cell,* 154**,** 1047-59.

AWASAKI, T., LAI, S.-L., ITO, K. & LEE, T. 2008. Organization and postembryonic development of glial cells in the adult central brain of Drosophila. *The Journal of Neuroscience,* 28**,** 13742-13753.

AWASAKI, T., TATSUMI, R., TAKAHASHI, K., ARAI, K., NAKANISHI, Y., UEDA, R. & ITO, K. 2006. Essential role of the apoptotic cell engulfment genes draper and ced-6 in programmed axon pruning during Drosophila metamorphosis. *Neuron,* 50**,** 855-867.

BAE, Y. H., MUI, K. L., HSU, B. Y., LIU, S. L., CRETU, A., RAZINIA, Z., XU, T., PURE, E. & ASSOIAN, R. K. 2014. A FAK-Cas-Rac-lamellipodin signaling module transduces extracellular matrix stiffness into mechanosensitive cell cycling. *Sci Signal,* 7**,** ra57.

BALCER, H. I., GOODMAN, A. L., RODAL, A. A., SMITH, E., KUGLER, J., HEUSER, J. E. & GOODE, B. L. 2003. Coordinated regulation of actin filament turnover by a high-molecular-weight Srv2/CAP complex, cofilin, profilin, and Aip1. *Curr Biol,* 13**,** 2159-69.

BALZA, R. O. & MISRA, R. P. 2006. Role of the Serum Response Factor in Regulating Contractile Apparatus Gene Expression and Sarcomeric Integrity in Cardiomyocytes. *Journal of Biological Chemistry,* 281**,** 6498-6510.

BANGE, J., ZWICK, E. & ULLRICH, A. 2001. Molecular targets for breast cancer therapy and prevention. *Nature medicine,* 7.

BAZIGOU, E., APITZ, H., JOHANSSON, J., LOREN, C. E., HIRST, E. M., CHEN, P. L., PALMER, R. H. & SALECKER, I. 2007. Anterograde Jelly belly and Alk receptor tyrosine kinase signaling mediates retinal axon targeting in Drosophila. *Cell,* 128**,** 961-75.

BEAR, J. E., SVITKINA, T. M., KRAUSE, M., SCHAFER, D. A., LOUREIRO, J. J., STRASSER, G. A., MALY, I. V., CHAGA, O. Y., COOPER, J. A. & BORISY, G. G. 2002. Antagonism between Ena/VASP proteins and actin filament capping regulates fibroblast motility. *Cell,* 109**,** 509-521.

BENJAMINI, Y. & HOCHBERG, Y. 1995. CONTROLLING THE FALSE DISCOVERY RATE - A PRACTICAL AND POWERFUL APPROACH TO MULTIPLE TESTING. *Journal of the Royal Statistical Society Series B-Methodological,* 57**,** 289-300.

BENNETT, D., LYULCHEVA, E. & ALPHEY, L. 2006. Towards a comprehensive analysis of the protein phosphatase 1 interactome in Drosophila. *Journal of molecular biology,* 364**,** 196-212.

BENNETT, D., LYULCHEVA, E. & COBBE, N. 2015. Drosophila as a potential model for ocular tumors. *Ocular Oncology and Pathology,* 1**,** 190-199.

BÉRÉZIAT, V., KASUS-JACOBI, A., PERDEREAU, D., CARIOU, B., GIRARD, J. & BURNOL, A.-F. 2002. Inhibition of insulin receptor catalytic activity by the molecular adapter Grb14. *Journal of Biological Chemistry,* 277**,** 4845-4852.

BIANCO, A., POUKKULA, M., CLIFFE, A., MATHIEU, J., LUQUE, C. M., FULGA, T. A. & RØRTH, P. 2007. Two distinct modes of guidance signalling during collective migration of border cells. *Nature,* 448**,** 362-365.

BILD, A. H., POTTI, A. & NEVINS, J. R. 2006a. Linking oncogenic pathways with therapeutic opportunities. *Nature reviews cancer,* 6**,** 735-741.

BILD, A. H., YAO, G., CHANG, J. T., WANG, Q., POTTI, A., CHASSE, D., JOSHI, M.-B., HARPOLE, D., LANCASTER, J. M. & BERCHUCK, A. 2006b. Oncogenic pathway signatures in human cancers as a guide to targeted therapies. *Nature,* 439**,** 353-357.

BJORKLUND, M., TAIPALE, M., VARJOSALO, M., SAHARINEN, J., LAHDENPERA, J. & TAIPALE, J. 2006. Identification of pathways regulating cell size and cell-cycle progression by RNAi. *Nature,* 439**,** 1009-1013.

BODENMILLER, B., MALMSTROM, J., GERRITS, B., CAMPBELL, D., LAM, H., SCHMIDT, A., RINNER, O., MUELLER, L. N., SHANNON, P. T., PEDRIOLI, P. G., PANSE, C., LEE, H. K., SCHLAPBACH, R. & AEBERSOLD, R. 2007. PhosphoPep—a phosphoproteome resource for systems biology research in Drosophila Kc167 cells. *Molecular Systems Biology,* 3.

BOS, J. L. 1989. Ras oncogenes in human cancer: a review. *Cancer research,* 49**,** 4682-4689.

BOS, J. L. 2005. Linking Rap to cell adhesion. *Current opinion in cell biology,* 17**,** 123-128.

BOURNE, H. R., SANDERS, D. A. & MCCORMICK, F. 1990. The GTPase superfamily: a conserved switch for diverse cell functions. *Nature,* 348**,** 125-132.

BRAND, A. H. & PERRIMON, N. 1993. Targeted gene expression as a means of altering cell fates and generating dominant phenotypes. *development,* 118**,** 401-415.

BRONSTEIN, I., FORTIN, J., STANLEY, P. E., STEWART, G. S. A. B., KRICKA, L. J., BRONSTEIN, I., FORTIN, J., STANLEY, P. E., STEWART, G. S. A. B. & KRICKA, L. J. 1994. Chemiluminescent and Bioluminescent Reporter Gene Assays. *Analytical biochemistry,* 219**,** 169.

BRUMBY, A. M. & RICHARDSON, H. E. 2003. scribble mutants cooperate with oncogenic Ras or Notch to cause neoplastic overgrowth in Drosophila. *The EMBO journal,* 22**,** 5769-5779.

BRUMBY, A. M. & RICHARDSON, H. E. 2005. Using Drosophila melanogaster to map human cancer pathways. *Nature Reviews Cancer,* 5**,** 626-639.

CALVO, F., EGE, N., GRANDE-GARCIA, A., HOOPER, S., JENKINS, R. P., CHAUDHRY, S. I., HARRINGTON, K., WILLIAMSON, P., MOEENDARBARY, E., CHARRAS, G. & SAHAI, E. 2013. Mechanotransduction and YAP-dependent matrix remodelling is required for the generation and maintenance of cancer-associated fibroblasts. *Nat Cell Biol,* 15**,** 637-46.

CARMONA, G., PERERA, U., GILLETT, C., NABA, A., LAW, A. L., SHARMA, V. P., WANG, J., WYCKOFF, J., BALSAMO, M., MOSIS, F., DE PIANO, M., MONYPENNY, J., WOODMAN, N., MCCONNELL, R. E., MOUNEIMNE, G.,

VAN HEMELRIJCK, M., CAO, Y., CONDEELIS, J., HYNES, R. O., GERTLER, F. B. & KRAUSE, M. 2016. Lamellipodin promotes invasive 3D cancer cell migration via regulated interactions with Ena/VASP and SCAR/WAVE. *Oncogene*.

CENIK, B. K., LIU, N., CHEN, B., BEZPROZVANNAYA, S., OLSON, E. N. & BASSEL-DUBY, R. 2016. Myocardin-related transcription factors are required for skeletal muscle development. *Development,* 143**,** 2853-61.

CHANG, A. E. 2006. *Oncology. [electronic book] : an evidence-based approach*, New York : Springer, ©2006.

CHANG, C., ADLER, C. E., KRAUSE, M., CLARK, S. G., GERTLER, F. B., TESSIER-LAVIGNE, M. & BARGMANN, C. I. 2006. MIG-10/lamellipodin and AGE-1/PI3K promote axon guidance and outgrowth in response to slit and netrin. *Current biology,* 16**,** 854-862.

CHARALAMBOUS, M., COWLEY, M., GEOGHEGAN, F., SMITH, F. M., RADFORD, E. J., MARLOW, B. P., GRAHAM, C. F., HURST, L. D. & WARD, A. 2010. Maternally-inherited Grb10 reduces placental size and efficiency. *Developmental biology,* 337**,** 1-8.

CHARALAMBOUS, M., SMITH, F. M., BENNETT, W. R., CREW, T. E., MACKENZIE, F. & WARD, A. 2003. Disruption of the imprinted Grb10 gene leads to disproportionate overgrowth by an Igf2-independent mechanism. *Proceedings of the National Academy of Sciences,* 100**,** 8292-8297.

CHERBAS, L., HACKNEY, J. F., GONG, L., SALZER, C., MAUSER, E., ZHANG, D. & CHERBAS, P. 2015. Targeted insertion in well-characterized Drosophila cell lines using φC31 integrase. *bioRxiv*.

CHOI, C. & HELFMAN, D. M. 2014. The Ras-ERK pathway modulates cytoskeleton organization, cell motility and lung metastasis signature genes in MDA-MB-231 LM2. *Oncogene,* 33**,** 3668-76.

CHOTARD, C., LEUNG, W. & SALECKER, I. 2005. glial cells missing and gcm2 cell autonomously regulate both glial and neuronal development in the visual system of Drosophila. *Neuron,* 48**,** 237-51.

CHUANG, H. N., VAN ROSSUM, D., SIEGER, D., SIAM, L., KLEMM, F., BLECKMANN, A., BAYERLOVA, M., FARHAT, K., SCHEFFEL, J., SCHULZ, M., DEHGHANI, F., STADELMANN, C., HANISCH, U. K., BINDER, C. & PUKROP, T. 2013. Carcinoma cells misuse the host tissue damage response to invade the brain. *Glia,* 61**,** 1331-46.

CIURCIU, A., DUNCALF, L., JONCHERE, V., LANSDALE, N., VASIEVA, O., GLENDAY, P., RUDENKO, A., VISSI, E., COBBE, N., ALPHEY, L. & BENNETT, D. 2013. PNUTS/PP1 regulates RNAPII-mediated gene expression and is necessary for developmental growth. *PLoS Genet,* 9**,** e1003885.

CLARK, W. 1991. Tumour progression and the nature of cancer. *British journal of cancer,* 64**,** 631.

CODY, C. W., PRASHER, D. C., WESTLER, W. M., PRENDERGAST, F. G. & WARD, W. W. 1993. Chemical structure of the hexapeptide chromophore of the Aequorea green-fluorescent protein. *Biochemistry (ACS),* 32**,** 1212.

COLÓ, G. P., HERNÁNDEZ-VARAS, P., LOCK, J., BARTOLOMÉ, R. A., ARELLANO-SÁNCHEZ, N., STRÖMBLAD, S. & TEIXIDÓ, J. 2012a. Focal adhesion disassembly is regulated by a RIAM to MEK-1 pathway. *Journal of cell science,* 125**,** 5338-5352.

COLO, G. P., LAFUENTE, E. M. & TEIXIDO, J. 2012b. The MRL proteins: Adapting cell adhesion, migration and growth. *European Journal of Cell Biology,* 91**,** 861-868.

COOPER 2000. The cell a molecular approach.

COOPER, S. J., TRINKLEIN, N. D., NGUYEN, L. & MYERS, R. M. 2007. Serum response factor binding sites differ in three human cell types. *Genome Res,* 17**,** 136-44.

CORDERO, J. B., MACAGNO, J. P., STEFANATOS, R. K., STRATHDEE, K. E., CAGAN, R. L. & VIDAL, M. 2010. Oncogenic Ras diverts a host TNF tumor suppressor activity into tumor promoter. *Dev Cell,* 18**,** 999-1011.

COUSSENS, L. M. & WERB, Z. 2002. Inflammation and cancer. *Nature,* 420**,** 860-7.

DEPETRIS, R. S., WU, J. & HUBBARD, S. R. 2009. Structural and functional studies of the Ras-associating and pleckstrin-homology domains of Grb10 and Grb14. *Nature structural & molecular biology,* 16**,** 833-839.

DIDRY, D., CARLIER, M. F. & PANTALONI, D. 1998. Synergy between actin depolymerizing factor/cofilin and profilin in increasing actin filament turnover. *J Biol Chem,* 273**,** 25602-11.

DONLEA, J. M., RAMANAN, N. & SHAW, P. J. 2009. Use-dependent plasticity in clock neurons regulates sleep need in Drosophila. *Science,* 324**,** 105-8.

DREES, F. & GERTLER, F. B. 2008. Ena/VASP: proteins at the tip of the nervous system. *Current opinion in neurobiology,* 18**,** 53-59.

DUFFY, J. B. 2002. GAL4 system in Drosophila: a fly geneticist's Swiss army knife. *genesis,* 34**,** 1-15.

DUPONT, S., MORSUT, L., ARAGONA, M., ENZO, E., GIULITTI, S., CORDENONSI, M., ZANCONATO, F., LE DIGABEL, J., FORCATO, M., BICCIATO, S., ELVASSORE, N. & PICCOLO, S. 2011. Role of YAP/TAZ in mechanotransduction. *Nature,* 474**,** 179-83.

EDWARDS, T. N. & MEINERTZHAGEN, I. A. 2010. The functional organisation of glia in the adult brain of Drosophila and other insects. *Progress in neurobiology,* 90**,** 471-497.

EHRHARDT, A., EHRHARDT, G. R., GUO, X. & SCHRADER, J. W. 2002. Ras and relatives—job sharing and networking keep an old family together. *Experimental hematology,* 30**,** 1089-1106.

ENDRIS, V., HAUSSMANN, L., BUSS, E., BACON, C., BARTSCH, D. & RAPPOLD, G. 2011. SrGAP3 interacts with lamellipodin at the cell membrane and regulates Rac-dependent cellular protrusions. *J Cell Sci,* 124**,** 3941-3955.

ESNAULT, C., STEWART, A., GUALDRINI, F., EAST, P., HORSWELL, S., MATTHEWS, N. & TREISMAN, R. 2014. Rho-actin signaling to the MRTF coactivators dominates the immediate transcriptional response to serum in fibroblasts. *Genes & Development*.

ETTINGER, D., BEPLER, G., BUENO, R., CHANG, A., CHANG, J., CHIRIEAC, L., D'AMICO, T., DEMMY, T., FEIGENBERG, S. & GRANNIS JR, F. 2006. Non-small cell lung cancer clinical practice guidelines in oncology. *Journal of the National Comprehensive Cancer Network: JNCCN,* 4**,** 548.

FERNANDEZ, B. G., GASPAR, P., BRAS-PEREIRA, C., JEZOWSKA, B., REBELO, S. R. & JANODY, F. 2011. Actin-Capping Protein and the Hippo pathway

regulate F-actin and tissue growth in Drosophila. *Development,* 138**,** 2337-46.
FERNANDEZ, B. G., JEZOWSKA, B. & JANODY, F. 2014. Drosophila actin-Capping Protein limits JNK activation by the Src proto-oncogene. *Oncogene,* 33**,** 2027-39.
FISCHER, O. M., STREIT, S., HART, S. & ULLRICH, A. 2003. Beyond herceptin and gleevec. *Current opinion in chemical biology,* 7**,** 490-495.
FISH, M. P., GROTH, A. C., CALOS, M. P. & NUSSE, R. 2007. Creating transgenic Drosophila by microinjecting the site-specific [phi]C31 integrase mRNA and a transgene-containing donor plasmid. *Nat. Protocols,* 2**,** 2325-2331.
FORRESTER, W. C. & GARRIGA, G. 1997. Genes necessary for C. elegans cell and growth cone migrations. *Development,* 124**,** 1831-1843.
FOULDS, L. 1958. The natural history of cancer. *Journal of chronic diseases,* 8**,** 2-37.
FRANCESCHINI, A., SZKLARCZYK, D., FRANKILD, S., KUHN, M., SIMONOVIC, M., ROTH, A., LIN, J., MINGUEZ, P., BORK, P., VON MERING, C. & JENSEN, L. J. 2013. STRING v9.1: protein-protein interaction networks, with increased coverage and integration. *Nucleic Acids Research,* 41**,** D808-D815.
FRANTZ, J. D., GIORGETTI-PERALDI, S., OTTINGER, E. A. & SHOELSON, S. E. 1997. Human GRB-IRβ/GRB10 Splice variants of an insulin and growth factor receptor-binding protein with PH and SH2 domains. *Journal of Biological Chemistry,* 272**,** 2659-2667.
FREEMAN, M. R. & DOHERTY, J. 2006. Glial cell biology in Drosophila and vertebrates. *Trends in neurosciences,* 29**,** 82-90.
FRIEDL, P. & BRÖCKER, E.-B. 2000. The biology of cell locomotion within three-dimensional extracellular matrix. *Cellular and molecular life sciences CMLS,* 57**,** 41-64.
FRIEDL, P. & WOLF, K. 2003. Tumour-cell invasion and migration: diversity and escape mechanisms. *Nature Reviews Cancer,* 3**,** 362-374.
FRIESE, M. A., STEINLE, A. & WELLER, M. 2004. The innate immune response in the central nervous system and its role in glioma immune surveillance. *Onkologie,* 27**,** 487-91.
GARMAN, K. S., NEVINS, J. R. & POTTI, A. 2007. Genomic strategies for personalized cancer therapy. *Human molecular genetics,* 16**,** R226-R232.
GINESTIER, C., CERVERA, N., FINETTI, P., ESTEYRIES, S., ESTERNI, B., ADELAIDE, J., XERRI, L., VIENS, P., JACQUEMIER, J., CHARAFE-JAUFFRET, E., CHAFFANET, M., BIRNBAUM, D. & BERTUCCI, F. 2006. Prognosis and gene expression profiling of 20q13-amplified breast cancers. *Clin Cancer Res,* 12**,** 4533-44.
GIOVANNONE, B., LEE, E., LAVIOLA, L., GIORGINO, F., CLEVELAND, K. A. & SMITH, R. J. 2003. Two novel proteins that are linked to insulin-like growth factor (IGF-I) receptors by the Grb10 adapter and modulate IGF-I signaling. *Journal of Biological Chemistry,* 278**,** 31564-31573.
GOLIC, K. G. 1991. Site-specific recombination between homologous chromosomes in Drosophila. *Science,* 252**,** 958-961.
GREENSPAN, R. J. 2004. Fly pushing: the theory and practice of Drosophila genetics.

GROSSE, R., COPELAND, J. W., NEWSOME, T. P., WAY, M. & TREISMAN, R. 2003. A role for VASP in RhoA-Diaphanous signalling to actin dynamics and SRF activity. *EMBO J,* 22**,** 3050-61.

GROTH, A. C., FISH, M., NUSSE, R. & CALOS, M. P. 2004. Construction of transgenic Drosophila by using the site-specific integrase from phage φC31. *Genetics,* 166**,** 1775-1782.

GUEST, S. T., YU, J., LIU, D., HINES, J. A., KASHAT, M. A. & FINLEY, R. L., JR. 2011. A protein network-guided screen for cell cycle regulators in Drosophila. *Bmc Systems Biology,* 5.

HAN, D. C. & GUAN, J.-L. 1999. Association of focal adhesion kinase with Grb7 and its role in cell migration. *Journal of Biological Chemistry,* 274**,** 24425-24430.

HAN, J., LIM, C. J., WATANABE, N., SORIANI, A., RATNIKOV, B., CALDERWOOD, D. A., PUZON-MCLAUGHLIN, W., LAFUENTE, E. M., BOUSSIOTIS, V. A. & SHATTIL, S. J. 2006. Reconstructing and deconstructing agonist-induced activation of integrin αIIbβ3. *Current Biology,* 16**,** 1796-1806.

HAN, Z., LI, X., WU, J. & OLSON, E. N. 2004. A myocardin-related transcription factor regulates activity of serum response factor in Drosophila. *Proc Natl Acad Sci U S A,* 101**,** 12567-72.

HANAHAN, D. & WEINBERG, R. A. 2000. The hallmarks of cancer. *cell,* 100**,** 57-70.

HANAHAN, D. & WEINBERG, R. A. 2011. Hallmarks of cancer: the next generation. *cell,* 144**,** 646-674.

HANSEN, H., SVENSSON, U., ZHU, J., LAVIOLA, L., GIORGINO, F., WOLF, G., SMITH, R. J. & RIEDEL, H. 1996. Interaction between the Grb10 SH2 domain and the insulin receptor carboxyl terminus. *Journal of Biological Chemistry,* 271**,** 8882-8886.

HANSEN, S. D. & MULLINS, R. D. 2015. Lamellipodin promotes actin assembly by clustering Ena/VASP proteins and tethering them to actin filaments. *Elife,* 4.

HARVEY, J. 1964. An unidentified virus which causes the rapid production of tumours in mice.

HASLAM, R. J., KOIDE, H. B. & HEMMINGS, B. A. 1993. Pleckstrin domain homology. *Nature,* 363**,** 309-310.

HE, W., ROSE, D. W., OLEFSKY, J. M. & GUSTAFSON, T. A. 1998. Grb10 interacts differentially with the insulin receptor, insulin-like growth factor I receptor, and epidermal growth factor receptor via the Grb10 Src homology 2 (SH2) domain and a second novel domain located between the pleckstrin homology and SH2 domains. *Journal of Biological Chemistry,* 273**,** 6860-6867.

HERNÁNDEZ-VARAS, P., COLÓ, G. P., BARTOLOMÉ, R. A., PATERSON, A., MEDRAÑO-FERNÁNDEZ, I., ARELLANO-SÁNCHEZ, N., CABAÑAS, C., SÁNCHEZ-MATEOS, P., LAFUENTE, E. M. & BOUSSIOTIS, V. A. 2011. Rap1-GTP-interacting adaptor molecule (RIAM) protein controls invasion and growth of melanoma cells. *Journal of Biological Chemistry,* 286**,** 18492-18504.

HIRSCH, J. 2006. An anniversary for cancer chemotherapy. *Jama,* 296**,** 1518-1520.

HOLT, L. & SIDDLE, K. 2005. Grb10 and Grb14: enigmatic regulators of insulin action--and more? *The Biochemical journal,* 388**,** 393-406.
HOLT, L. J. & DALY, R. J. 2005. Adapter protein connections: the MRL and Grb7 protein families. *Growth Factors,* 23**,** 193-201.
HOUSDEN, B. E., MILLEN, K. & BRAY, S. J. 2012. Drosophila Reporter Vectors Compatible with PhiC31 Integrase Transgenesis Techniques and Their Use to Generate New Notch Reporter Fly Lines. *G3 (Bethesda),* 2**,** 79-82.
HU, Y., ROESEL, C., FLOCKHART, I., PERKINS, L., PERRIMON, N. & MOHR, S. E. 2013. UP-TORR: online tool for accurate and Up-to-Date annotation of RNAi Reagents. *Genetics,* 195**,** 37-45.
HUANG, D. W., SHERMAN, B. T. & LEMPICKI, R. A. 2009. Systematic and integrative analysis of large gene lists using DAVID bioinformatics resources. *Nature Protocols,* 4**,** 44-57.
HUDIS, C. A. 2007. Trastuzumab—mechanism of action and use in clinical practice. *New England Journal of Medicine,* 357**,** 39-51.
HYNES, R. O. 2002. Integrins: bidirectional, allosteric signaling machines. *Cell,* 110**,** 673-687.
JAHN, T., SEIPEL, P., URSCHEL, S., PESCHEL, C. & DUYSTER, J. 2002. Role for the adaptor protein Grb10 in the activation of Akt. *Molecular and cellular biology,* 22**,** 979-991.
JANES, P. W., LACKMANN, M., CHURCH, W. B., SANDERSON, G. M., SUTHERLAND, R. L. & DALY, R. J. 1997. Structural determinants of the interaction between the erbB2 receptor and the Src homology 2 domain of Grb7. *Journal of Biological Chemistry,* 272**,** 8490-8497.
JANG, A. C.-C., STARZ-GAIANO, M. & MONTELL, D. J. 2007. Modeling migration and metastasis in Drosophila. *Journal of mammary gland biology and neoplasia,* 12**,** 103-114.
JANKNECHT, R., ERNST, W. H., PINGOUD, V. & NORDHEIM, A. 1993. Activation of ternary complex factor Elk-1 by MAP kinases. *Embo j,* 12**,** 5097-104.
JENZORA, A., BEHRENDT, B., SMALL, J. V., WEHLAND, J. & STRADAL, T. E. 2005. PREL1 provides a link from Ras signalling to the actin cytoskeleton via Ena/VASP proteins. *FEBS letters,* 579**,** 455-463.
JIANG, X., WILFORD, C., DUENSING, S., MUNGER, K., JONES, G. & JONES, D. 2001. Participation of Survivin in mitotic and apoptotic activities of normal and tumor-derived cells. *J Cell Biochem,* 83**,** 342-54.
JOHNSON, L. F., LEVIS, R., ABELSON, H. T., GREEN, H. & PENMAN, S. 1976. Changes in RNA in relation to growth of fibroblast. *Journal of Cell Biology,* 71**,** 933-938.
JONCHERE, V. & BENNETT, D. 2013. Validating RNAi phenotypes in Drosophila using a synthetic RNAi-resistant transgene. *PloS one,* 8**,** e70489.
JONES, G., JONES, D., ZHOU, L., STELLER, H. & CHU, Y. X. 2000. Deterin, a new inhibitor of apoptosis from Drosophila melanogaster. *Journal of Biological Chemistry,* 275**,** 22157-22165.
KAIROUZ, R., PARMAR, J., LYONS, R. J., SWARBRICK, A., MUSGROVE, E. A. & DALY, R. J. 2005. Hormonal regulation of the Grb14 signal modulator and its role in cell cycle progression of MCF-7 human breast cancer cells. *Journal of cellular physiology,* 203**,** 85-93.

KARIN, M. 1994. Signal transduction from the cell surface to the nucleus through the phosphorylation of transcription factors. *Current Opinion in Cell Biology,* 6**,** 415.

KASUS-JACOBI, A., BEREZIAT, V., PERDEREAU, D., GIRARD, J. & BURNOL, A.-F. 2000. Evidence for an interaction between the insulin receptor and Grb7. A role for two of its binding domains, PIR and SH2. *Oncogene,* 19**,** 2052-2059.

KASUS-JACOBI, A., PERDEREAU, D., AUZAN, C., CLAUSER, E., VAN OBBERGHEN, E., MAUVAIS-JARVIS, F., GIRARD, J. & BURNOL, A.-F. 1998. Identification of the rat adapter Grb14 as an inhibitor of insulin actions. *Journal of Biological Chemistry,* 273**,** 26026-26035.

KILLIP, L. E. & GREWAL, S. S. 2012. DREF is required for cell and organismal growth in Drosophila and functions downstream of the nutrition/TOR pathway. *Dev Biol,* 371**,** 191-202.

KIM, D., PERTEA, G., TRAPNELL, C., PIMENTEL, H., KELLEY, R. & SALZBERG, S. L. 2013. TopHat2: accurate alignment of transcriptomes in the presence of insertions, deletions and gene fusions. *Genome Biology,* 14**,** 13.

KING, C. C. & NEWTON, A. C. 2004. The adaptor protein Grb14 regulates the localization of 3-phosphoinositide-dependent kinase-1. *Journal of Biological Chemistry,* 279**,** 37518-37527.

KORESSAAR, T. & REMM, M. 2007. Enhancements and modifications of primer design program Primer3. *Bioinformatics,* 23**,** 1289-1291.

KRAUSE, M., LESLIE, J. D., STEWART, M., LAFUENTE, E. M., VALDERRAMA, F., JAGANNATHAN, R., STRASSER, G. A., RUBINSON, D. A., LIU, H. & WAY, M. 2004. Lamellipodin, an Ena/VASP ligand, is implicated in the regulation of lamellipodial dynamics. *Developmental cell,* 7**,** 571-583.

KUHSTOSS, S. & RAO, R. N. 1991. Analysis of the integration function of the streptomycete bacteriophage φC31. *Journal of molecular biology,* 222**,** 897-908.

KULSHAMMER, E. & UHLIROVA, M. 2013. The actin cross-linker Filamin/Cheerio mediates tumor malignancy downstream of JNK signaling. *J Cell Sci,* 126**,** 927-38.

KURUCZ, E., MARKUS, R., ZSAMBOKI, J., FOLKL-MEDZIHRADSZKY, K., DARULA, Z., VILMOS, P., UDVARDY, A., KRAUSZ, I., LUKACSOVICH, T., GATEFF, E., ZETTERVALL, C. J., HULTMARK, D. & ANDO, I. 2007. Nimrod, a putative phagocytosis receptor with EGF repeats in Drosophila plasmatocytes. *Curr Biol,* 17**,** 649-54.

LAFUENTE, E. M., VAN PUIJENBROEK, A., KRAUSE, M., CARMAN, C. V., FREEMAN, G. J., BEREZOVSKAYA, A., CONSTANTINE, E., SPRINGER, T. A., GERTIER, F. B. & BOUSSIOTIS, V. A. 2004. RIAM, an EnaNASP and profilin ligand, interacts with Rap1-GTP and mediates Rap1-induced adhesion. *Developmental Cell,* 7**,** 585-595.

LANGLAIS, P., DONG, L. Q., RAMOS, F. J., HU, D., LI, Y., QUON, M. J. & LIU, F. 2004. Negative regulation of insulin-stimulated mitogen-activated protein kinase signaling by Grb10. *Molecular endocrinology,* 18**,** 350-358.

LANIER, L. M. & GERTLER, F. B. 2000. From Abl to actin: Abl tyrosine kinase and associated proteins in growth cone motility. *Current opinion in neurobiology,* 10**,** 80-87.

LAW, A.-L., VEHLOW, A., KOTINI, M., DODGSON, L., SOONG, D., THEVENEAU, E., BODO, C., TAYLOR, E., NAVARRO, C. & PERERA, U. 2013. Lamellipodin and the Scar/WAVE complex cooperate to promote cell migration in vivo. *The Journal of cell biology,* 203**,** 673-689.

LEE, H.-S., LIM, C. J., PUZON-MCLAUGHLIN, W., SHATTIL, S. J. & GINSBERG, M. H. 2009. RIAM activates integrins by linking talin to ras GTPase membrane-targeting sequences. *Journal of Biological Chemistry,* 284**,** 5119-5127.

LEGG, J. A. & MACHESKY, L. M. 2004. MRL proteins: leading Ena/VASP to Ras GTPases. *Nature cell biology,* 6**,** 1015-1017.

LEMMON, M. & FERGUSON, K. 2000. Signal-dependent membrane targeting by pleckstrin homology (PH) domains. *The Biochemical journal,* 350**,** 1-18.

LEMMON, M. A. 2003. Phosphoinositide recognition domains. *Traffic,* 4**,** 201-213.

LEMMON, M. A. Pleckstrin homology (PH) domains and phosphoinositides. Biochemical Society Symposia, 2007. Portland Press Limited, 81-93.

LEMMON, M. A. 2008. Membrane recognition by phospholipid-binding domains. *Nature reviews Molecular cell biology,* 9**,** 99-111.

LODISH, H., BERK, A., ZIPURSKY, S. L., MATSUDAIRA, P., BALTIMORE, D. & DARNELL, J. 2000. Proto-oncogenes and tumor-suppressor genes.

LOFTHOUSE, C. 2013. *Dissecting the role and regulation of MRL function in Drosophila.* PhD, University of Liverpool.

LOGAN, M. A. & FREEMAN, M. R. 2007. The scoop on the fly brain: glial engulfment functions in Drosophila. *Neuron Glia Biol,* 3**,** 63-74.

LUPAS, A. 1996. Coiled coils: new structures and new functions. *Trends in biochemical sciences,* 21**,** 375-382.

LYNE, R., SMITH, R., RUTHERFORD, K., WAKELING, M., VARLEY, A., GUILLIER, F., JANSSENS, H., JI, W., MCLAREN, P., NORTH, P., RANA, D., RILEY, T., SULLIVAN, J., WATKINS, X., WOODBRIDGE, M., LILLEY, K., RUSSELL, S., ASHBURNER, M., MIZUGUCHI, K. & MICKLEM, G. 2007. FlyMine: an integrated database for Drosophila and Anopheles genomics. *Genome Biol,* 8**,** R129.

LYONS, R. J., DEANE, R. N., LYNCH, D. K., YE, Z.-S. J., SANDERSON, G. M., EYRE, H. J., SUTHERLAND, G. R. & DALY, R. J. 2001. Identification of a novel human tankyrase through its interaction with the adaptor protein Grb14. *Journal of Biological Chemistry,* 276**,** 17172-17180.

LYULCHEVA, E. 2006. *Pico: a novel regulator of cell growth and proliferation.* PhD, University of Oxford.

LYULCHEVA, E., TAYLOR, E., MICHAEL, M., VEHLOW, A., TAN, S., FLETCHER, A., KRAUSE, M. & BENNETT, D. 2008. Drosophila pico and its mammalian ortholog lamellipodin activate serum response factor and promote cell proliferation. *Developmental cell,* 15**,** 680-690.

MACDONALD, J. M., DOHERTY, J., HACKETT, R. & FREEMAN, M. R. 2013. The c-Jun kinase signaling cascade promotes glial engulfment activity through activation of draper and phagocytic function. *Cell Death Differ,* 20**,** 1140-8.

MANSER, J., ROONPRAPUNT, C. & MARGOLIS, B. 1997. C. elegansCell migration genemig-10Shares similarities with a family of SH2 domain proteins and

acts cell nonautonomously in excretory canal development. *Developmental biology,* 184**,** 150-164.
MANSER, J. & WOOD, W. B. 1990. Mutations affecting embryonic cell migrations in Caenorhabditis elegans. *Developmental genetics,* 11**,** 49-64.
MATOZAKI, T., NAKANISHI, H. & TAKAI, Y. 2000. Small G-protein networks:: Their crosstalk and signal cascades. *Cellular signalling,* 12**,** 515-524.
MAYER, B. J., REN, R., CLARK, K. L. & BALTIMORE, D. 1993. A putative modular domain present in diverse signaling proteins. *Cell,* 73**,** 629-630.
MCSHEA, M. A., SCHMIDT, K. L., DUBUKE, M. L., BALDIGA, C. E., SULLENDER, M. E., REIS, A. L., ZHANG, S., O'TOOLE, S. M., JEFFERS, M. C. & WARDEN, R. M. 2013. Abelson interactor-1 (ABI-1) interacts with MRL adaptor protein MIG-10 and is required in guided cell migrations and process outgrowth in C. elegans. *Developmental biology,* 373**,** 1-13.
MIANO, J. M., LONG, X. & FUJIWARA, K. 2007. Serum response factor: master regulator of the actin cytoskeleton and contractile apparatus. *American Journal of Physiology - Cell Physiology,* 292**,** C70-C81.
MICHAEL, M., VEHLOW, A., NAVARRO, C. & KRAUSE, M. 2010. c-Abl, Lamellipodin, and Ena/VASP proteins cooperate in dorsal ruffling of fibroblasts and axonal morphogenesis. *Current Biology,* 20**,** 783-791.
MILES, W. O., DYSON, N. J. & WALKER, J. A. 2011. Modeling tumor invasion and metastasis in Drosophila. *Disease Models and Mechanisms,* 4**,** 753-761.
MIRALLES, F., POSERN, G., ZAROMYTIDOU, A.-I., TREISMAN, R., MIRALLES, F., POSERN, G., ZAROMYTIDOU, A.-I. & TREISMAN, R. 2003. Actin Dynamics Control SRF Activity by Regulation of Its Coactivator MAL. *Cell,* 113**,** 329.
MISTELI, T., SPECTOR, D. L., MISTELI, T. & SPECTOR, D. L. 1997. Applications of the green fluorescent protein in cell biology and biotechnology. *Nature biotechnology,* 15**,** 961.
MONCOQ, K., BROUTIN, I., LARUE, V., PERDEREAU, D., CAILLIAU, K., BROWAEYS-POLY, E., BURNOL, A.-F. & DUCRUIX, A. 2003. The PIR domain of Grb14 is an intrinsically unstructured protein: implication in insulin signaling. *FEBS letters,* 554**,** 240-246.
MONTAGNE, J., GROPPE, J., GUILLEMIN, K., KRASNOW, M. A., GEHRING, W. J. & AFFOLTER, M. 1996. The Drosophila Serum Response Factor gene is required for the formation of intervein tissue of the wing and is allelic to blistered. *Development,* 122**,** 2589-2597.
MUEHLICH, S., HERMANNS, C., MEIER, M. A., KIRCHER, P. & GUDERMANN, T. 2016. Unravelling a new mechanism linking actin polymerization and gene transcription. *Nucleus,* 11**,** 1-5.
NASSIF, C., NOVEEN, A. & HARTENSTEIN, V. 1998. Embryonic development of the Drosophila brain. I. Pattern of pioneer tracts. *Journal of Comparative Neurology,* 402**,** 10-31.
NAWAZ, S., SANCHEZ, P., SCHMITT, S., SNAIDERO, N., MITKOVSKI, M., VELTE, C., BRUCKNER, B. R., ALEXOPOULOS, I., CZOPKA, T., JUNG, S. Y., RHEE, J. S., JANSHOFF, A., WITKE, W., SCHAAP, I. A., LYONS, D. A. & SIMONS, M. 2015. Actin filament turnover drives leading edge growth during myelin sheath formation in the central nervous system. *Dev Cell,* 34**,** 139-51.
NAYLOR, L. H. 1999. Reporter gene technology: the future looks bright. *Biochemical pharmacology,* 58**,** 749.

NELSON, H., PETRELLI, N., CARLIN, A., COUTURE, J., FLESHMAN, J., GUILLEM, J., MIEDEMA, B., OTA, D. & SARGENT, D. 2001. Guidelines 2000 for colon and rectal cancer surgery. *Journal of the National Cancer Institute,* 93**,** 583-596.

NIU, Z., LI, A., ZHANG, S. X., SCHWARTZ, R. J., NIU, Z., LI, A., ZHANG, S. X. & SCHWARTZ, R. J. 2007. Serum response factor micromanaging cardiogenesis. *Current Opinion in Cell Biology,* 19**,** 618.

NOLAN, G. P., FIERING, S., NICOLAS, J. F. & HERZENBERG, L. A. 1988. Fluorescence-activated cell analysis and sorting of viable mammalian cells based on beta-D-galactosidase activity after transduction of Escherichia coli lacZ. *Proc Natl Acad Sci U S A,* 85**,** 2603-7.

NORMAN, C., RUNSWICK, M., POLLOCK, R., TREISMAN, R. & NORMAN, C. 1988. Isolation and properties of cDNA clones encoding SRF, a transcription factor that binds to the c-fos serum response element. *Cell,* 55**,** 989.

O'CONNOR, J. W., RILEY, P. N., NALLURI, S. M., ASHAR, P. K. & GOMEZ, E. W. 2015. Matrix Rigidity Mediates TGFbeta1-Induced Epithelial-Myofibroblast Transition by Controlling Cytoskeletal Organization and MRTF-A Localization. *J Cell Physiol,* 230**,** 1829-39.

OHAYON, D., PATTYN, A., VENTEO, S., VALMIER, J., CARROLL, P. & GARCES, A. 2009. Zfh1 promotes survival of a peripheral glia subtype by antagonizing a Jun N-terminal kinase-dependent apoptotic pathway. *EMBO J,* 28**,** 3228-43.

PAGLIARINI, R. A. & XU, T. 2003. A Genetic Screen in Drosophila for Metastatic Behavior. *Science,* 302**,** 1227-1231.

PATSOUKIS, N., LAFUENTE, E. M., MERANER, P., SUB KIM, J., DOMBKOWSKI, D., LI, L. & BOUSSIOTIS, V. A. 2009. RIAM regulates the cytoskeletal distribution and activation of PLC-γ1 in T cells. *Science signaling,* 2**,** ra79.

PERO, S., SHUKLA, G., COOKSON, M., FLEMER, S. & KRAG, D. 2007. Combination treatment with Grb7 peptide and Doxorubicin or Trastuzumab (Herceptin) results in cooperative cell growth inhibition in breast cancer cells. *British journal of cancer,* 96**,** 1520-1525.

PETRYSZAK, R., KEAYS, M., TANG, Y. A., FONSECA, N. A., BARRERA, E., BURDETT, T., FULLGRABE, A., FUENTES, A. M., JUPP, S., KOSKINEN, S., MANNION, O., HUERTA, L., MEGY, K., SNOW, C., WILLIAMS, E., BARZINE, M., HASTINGS, E., WEISSER, H., WRIGHT, J., JAISWAL, P., HUBER, W., CHOUDHARY, J., PARKINSON, H. E. & BRAZMA, A. 2016. Expression Atlas update-an integrated database of gene and protein expression in humans, animals and plants. *Nucleic Acids Res,* 44**,** D746-52.

PHILIPPAR, U., SCHRATT, G., DIETERICH, C., MU, UML, LLER, J. M., GALGO, ACUTE, CZY, P., ENGEL, F. B., KEATING, M. T., GERTLER, F., SCHU, UML, LE, R., VINGRON, M., NORDHEIM, A., PHILIPPAR, U., SCHRATT, G., DIETERICH, C., UUML, LLER, J. M., GALG, OACUTE, CZY, P., ENGEL, F. B., KEATING, M. T., GERTLER, F., SCH, UUML, LE, R., VINGRON, M. & NORDHEIM, A. 2004. The SRF Target Gene Fhl2 Antagonizes RhoA/MAL-Dependent Activation of SRF. *Molecular Cell,* 16**,** 867.

PINHEIRO, E. M., XIE, Z., NOROVICH, A. L., VIDAKI, M., TSAI, L.-H. & GERTLER, F. B. 2011. Lpd depletion reveals that SRF specifies radial versus tangential migration of pyramidal neurons. *Nature cell biology,* 13**,** 989-995.

PIPES, G. C. T., CREEMERS, E. E. & OLSON, E. N. 2006. The myocardin family of transcriptional coactivators: versatile regulators of cell growth, migration, and myogenesis. *Genes & Development,* 20**,** 1545-1556.
PITOT, H. C. 1993. The molecular biology of carcinogenesis. *Cancer,* 72**,** 962-970.
PITOT, H. C., GOLDSWORTHY, T. & MORAN, S. 1981. The natural history of carcinogenesis: implications of experimental carcinogenesis in the genesis of human cancer. *Journal of supramolecular structure and cellular biochemistry,* 17**,** 133-146.
POLLARD, T. D. & BORISY, G. G. 2003. Cellular motility driven by assembly and disassembly of actin filaments. *Cell,* 112**,** 453-465.
PONTING, C. P. & BENJAMIN, D. R. 1996. A novel family ofras-binding domains. *Trends in biochemical sciences,* 21**,** 422.
POSERN, G., SOTIROPOULOS, A. & TREISMAN, R. 2002. Mutant actins demonstrate a role for unpolymerized actin in control of transcription by serum response factor. *Mol Biol Cell,* 13**,** 4167-78.
POSERN, G. & TREISMAN, R. 2006. Actin' together: serum response factor, its cofactors and the link to signal transduction. *Trends in Cell Biology,* 16**,** 588-596.
POUKKULA, M., CLIFFE, A., CHANGEDE, R. & RØRTH, P. 2011. Cell behaviors regulated by guidance cues in collective migration of border cells. *The Journal of cell biology,* 192**,** 513-524.
PRASAD, M. & MONTELL, D. J. 2007. Cellular and molecular mechanisms of border cell migration analyzed using time-lapse live-cell imaging. *Developmental cell,* 12**,** 997-1005.
PRASHER, D. C., ECKENRODE, V. K., WARD, W. W., PRENDERGAST, F. G. & CORMIER, M. J. 1992. Primary structure of the Aequorea victoria green-fluorescent protein. *Gene,* 111**,** 229-233.
QUINN, C. C., PFEIL, D. S., CHEN, E., STOVALL, E. L., HARDEN, M. V., GAVIN, M. K., FORRESTER, W. C., RYDER, E. F., SOTO, M. C. & WADSWORTH, W. G. 2006. UNC-6/netrin and SLT-1/slit guidance cues orient axon outgrowth mediated by MIG-10/RIAM/lamellipodin. *Current biology,* 16**,** 845-853.
RAFTOPOULOU, M. & HALL, A. 2004. Cell migration: Rho GTPases lead the way. *Developmental biology,* 265**,** 23-32.
RAJAKYLA, E. K. & VARTIAINEN, M. K. 2014. Rho, nuclear actin, and actin-binding proteins in the regulation of transcription and gene expression. *Small GTPases,* 5**,** e27539.
RAMEH, L. E., ARVIDSSON, A.-K., CARRAWAY, K. L., COUVILLON, A. D., RATHBUN, G., CROMPTON, A., VANRENTERGHEM, B., CZECH, M. P., RAVICHANDRAN, K. S. & BURAKOFF, S. J. 1997. A comparative analysis of the phosphoinositide binding specificity of pleckstrin homology domains. *Journal of Biological Chemistry,* 272**,** 22059-22066.
RAUSCH, H. & LEHMANN, M. 1991. Structural analysis of the actinophae ΦC31 attachment site. *Nucleic acids research,* 19**,** 5187-5189.
READ, R. D., CAVENEE, W. K., FURNARI, F. B. & THOMAS, J. B. 2009. A drosophila model for EGFR-Ras and PI3K-dependent human glioma. *PLoS Genet,* 5**,** e1000374.

REKAS, A., ALATTIA, J.-R., NAGAI, T., MIYAWAKI, A. & IKURA, M. 2002. Crystal Structure of Venus, a Yellow Fluorescent Protein with Improved Maturation and Reduced Environmental Sensitivity. *Journal of Biological Chemistry,* 277**,** 50573-50578.

ROBINSON, M. D., MCCARTHY, D. J. & SMYTH, G. K. 2010. edgeR: a Bioconductor package for differential expression analysis of digital gene expression data. *Bioinformatics,* 26**,** 139-140.

RODRIGUEZ-VICIANA, P., SABATIER, C. & MCCORMICK, F. 2004. Signaling specificity by Ras family GTPases is determined by the full spectrum of effectors they regulate. *Molecular and cellular biology,* 24**,** 4943-4954.

ROSS, D. T., SCHERF, U., EISEN, M. B., PEROU, C. M., REES, C., SPELLMAN, P., IYER, V., JEFFREY, S. S., VAN DE RIJN, M., WALTHAM, M., PERGAMENSCHIKOV, A., LEE, J. C., LASHKARI, D., SHALON, D., MYERS, T. G., WEINSTEIN, J. N., BOTSTEIN, D. & BROWN, P. O. 2000. Systematic variation in gene expression patterns in human cancer cell lines. *Nat Genet,* 24**,** 227-35.

ROSSI, F. M., BLAKELY, B. T. & BLAU, H. M. 2000. Interaction blues: protein interactions monitored in live mammalian cells by β-galactosidase complementation. *Trends in cell biology,* 10**,** 119-122.

ROTMAN, B., ZDERIC, J. A. & EDELSTEIN, M. 1963. NATIONAL ACADEMY OF SCIENCES: OFFICERS, COUNCIL, MEMBERS, FORIEGN ASSOCIATES, AND SECTIONS. *Proceedings of the National Academy of Sciences of the United States of America (PNAS),* 50**,** 1.1.

RUDRAPATNA, V. A., BANGI, E. & CAGAN, R. L. 2014. A Jnk-Rho-Actin remodeling positive feedback network directs Src-driven invasion. *Oncogene,* 33**,** 2801-6.

RUGGERO, D. & PANDOLFI, P. P. 2003. Does the ribosome translate cancer? *Nature Reviews Cancer,* 3**,** 179-192.

SAHAI, E. 2005. Mechanisms of cancer cell invasion. *Current opinion in genetics & development,* 15**,** 87-96.

SALVANY, L., MULLER, J., GUCCIONE, E. & RORTH, P. 2014. The core and conserved role of MAL is homeostatic regulation of actin levels. *Genes Dev,* 28**,** 1048-53.

SAMELSON, L. E. 2002. Signal Transduction Mediated by the T Cell Antigen Receptor: The Role of Adapter Proteins*. *Annual review of immunology,* 20**,** 371-394.

SANSORES-GARCIA, L., BOSSUYT, W., WADA, K., YONEMURA, S., TAO, C., SASAKI, H. & HALDER, G. 2011. Modulating F-actin organization induces organ growth by affecting the Hippo pathway. *EMBO J,* 30**,** 2325-35.

SANTOS, A. C. & LEHMANN, R. 2004. Germ cell specification and migration in Drosophila and beyond. *Current biology,* 14**,** R578-R589.

SCHERTEL, C., HUANG, D., BJORKLUND, M., BISCHOF, J., YIN, D., LI, R., WU, Y., ZENG, R., WU, J., TAIPALE, J., SONG, H. & BASLER, K. 2013. Systematic Screening of a Drosophila ORF Library In Vivo Uncovers Wnt/Wg Pathway Components. *Developmental Cell,* 25**,** 207-219.

SCHMIDT, C. 2007. Book Review of" The Molecular Biology of Cancer" by Stella Pelengaris, Michael Khan (Editors). *Molecular Cancer,* 6**,** 72.

SELVARAJ, A. & PRYWES, R. 2004. Expression profiling of serum inducible genes identifies a subset of SRF target genes that are MKL dependent. *BMC Mol Biol,* 5**,** 13.

SHAW, P. E., SCHR, OUML, TER, H., NORDHEIM, A. & SHAW, P. 1989. The ability of a ternary complex to form over the serum response element correlates with serum inducibility of the human c-fos promoter. *Cell,* 56**,** 563.

SHEEHAN, J. P., SHAFFREY, M. E., GUPTA, B., LARNER, J., RICH, J. N. & PARK, D. M. 2010. Improving the radiosensitivity of radioresistant and hypoxic glioblastoma. *Future oncology,* 6**,** 1591-1601.

SHEKHAR, S., PERNIER, J. & CARLIER, M. F. 2016. Regulators of actin filament barbed ends at a glance. *J Cell Sci*.

SHEN, T.-L. & GUAN, J.-L. 2004. Grb7 in intracellular signaling and its role in cell regulation. *Front Biosci,* 9**,** 192-200.

SHEN, T.-L., HAN, D. C. & GUAN, J.-L. 2002. Association of Grb7 with phosphoinositides and its role in the regulation of cell migration. *Journal of Biological Chemistry,* 277**,** 29069-29077.

SHIURA, H., MIYOSHI, N., KONISHI, A., WAKISAKA-SAITO, N., SUZUKI, R., MUGURUMA, K., KOHDA, T., WAKANA, S., YOKOYAMA, M. & ISHINO, F. 2005. Meg1/Grb10 overexpression causes postnatal growth retardation and insulin resistance via negative modulation of the IGF1R and IR cascades. *Biochemical and biophysical research communications,* 329**,** 909-916.

SHKLOVER, J., MISHNAEVSKI, K., LEVY-ADAM, F. & KURANT, E. 2015. JNK pathway activation is able to synchronize neuronal death and glial phagocytosis in Drosophila. *Cell Death Dis,* 6**,** e1649.

SIAMAKPOUR-REIHANI, S., ARGIROS, H. J., WILMETH, L. J., HAAS, L. L., PETERSON, T. A., JOHNSON, D. L., SHUSTER, C. B. & LYONS, B. A. 2009. The cell migration protein Grb7 associates with transcriptional regulator FHL2 in a Grb7 phosphorylation-dependent manner. *Journal of Molecular Recognition,* 22**,** 9-17.

SKARP, K. P. & VARTIAINEN, M. K. 2013. Actin as a model for the study of nucleocytoplasmic shuttling and nuclear dynamics. *Methods Mol Biol,* 1042**,** 245-55.

SMALL, J. V., STRADAL, T., VIGNAL, E. & ROTTNER, K. 2002. The lamellipodium: where motility begins. *Trends in cell biology,* 12**,** 112-120.

SOMOGYI, K. & RØRTH, P. 2004. Evidence for tension-based regulation of Drosophila MAL and SRF during invasive cell migration. *Developmental cell,* 7**,** 85-93.

SOTIROPOULOS, A., GINEITIS, D., COPELAND, J. & TREISMAN, R. 1999. Signal-regulated activation of serum response factor is mediated by changes in actin dynamics. *Cell,* 98**,** 159-69.

SPECK, O., HUGHES, S. C., NOREN, N. K., KULIKAUSKAS, R. M. & FEHON, R. G. 2003. Moesin functions antagonistically to the Rho pathway to maintain epithelial integrity. *Nature,* 421**,** 83-87.

SPRADLING, A. C. & RUBIN, G. M. 1982. Transposition of cloned P elements into Drosophila germ line chromosomes. *Science,* 218**,** 341-347.

SRIVASTAVA, A., PASTOR-PAREJA, J. C., IGAKI, T., PAGLIARINI, R. & XU, T. 2007. Basement membrane remodeling is essential for Drosophila disc eversion and tumor invasion. *Proceedings of the National Academy of Sciences of the United States of America,* 104**,** 2721-2726.

ST JOHNSTON, D. 2002. The art and design of genetic screens: Drosophila melanogaster. *Nature reviews genetics,* 3**,** 176-188.

STEIN, D., WU, J., FUQUA, S., ROONPRAPUNT, C., YAJNIK, V., D'EUSTACHIO, P., MOSKOW, J., BUCHBERG, A., OSBORNE, C. & MARGOLIS, B. 1994. The SH2 domain protein GRB-7 is co-amplified, overexpressed and in a tight complex with HER2 in breast cancer. *The EMBO Journal,* 13**,** 1331.

STEIN, E. G., GUSTAFSON, T. A. & HUBBARD, S. R. 2001. The BPS domain of Grb10 inhibits the catalytic activity of the insulin and IGF1 receptors. *FEBS letters,* 493**,** 106-111.

STORK, T., BERNARDOS, R. & FREEMAN, M. R. 2012. Analysis of glial cell development and function in Drosophila. *Cold Spring Harbor Protocols,* 2012**,** pdb. top067587.

STORK, T., ENGELEN, D., KRUDEWIG, A., SILIES, M., BAINTON, R. J. & KLÄMBT, C. 2008. Organization and function of the blood–brain barrier in Drosophila. *The Journal of Neuroscience,* 28**,** 587-597.

SUN, Q., CHEN, G., STREB, J. W., LONG, X., YANG, Y., STOECKERT, C. J. & MIANO, J. M. 2006. Defining the mammalian CArGome. *Genome Res,* 16**,** 197-207.

SUTO, C., IGNAR, D. & SUTO, C. M. 1997. Selection of an Optimal Reporter Gene for Cell-Based High Throughput Screening Assays. *Journal of Biomolecular Screening,* 2**,** 7.

TANAKA, S., PERO, S. C., TAGUCHI, K., SHIMADA, M., MORI, M., KRAG, D. N. & ARII, S. 2006. Specific peptide ligand for Grb7 signal transduction protein and pancreatic cancer metastasis. *Journal of the National Cancer Institute,* 98**,** 491-498.

TANAKA, S., SUGIMACHI, K., KAWAGUCHI, H., SAEKI, H., OHNO, S., WANDS, J. R. & SUGIMACHI, K. 2000. Grb7 signal transduction protein mediates metastatic progression of esophageal carcinoma. *Journal of cellular physiology,* 183**,** 411-415.

TAYLOR, E. 2010. *Using Drosophila Melanogaster to investigate the conserved roles of MRL proteins in cell growth, cell migration and metastasis.* PhD, University of Oxford.

TENG, T., THOMAS, G. & MERCER, C. A. 2013. Growth control and ribosomopathies. *Current Opinion in Genetics & Development,* 23**,** 63-71.

THEODOSIOU, N. A. & XU, T. 1998. Use of FLP/FRT System to StudyDrosophilaDevelopment. *Methods,* 14**,** 355-365.

THRAN, J., POECK, B. & STRAUSS, R. 2013. Serum response factor-mediated gene regulation in a Drosophila visual working memory. *Curr Biol,* 23**,** 1756-63.

TREISMAN, R. 1986. Identification of a protein-binding site that mediates transcriptional response of the c-fos gene to serum factors. *Cell,* 46**,** 567.

TREPAT, X., CHEN, Z. & JACOBSON, K. A. 2012. Cell migration. *Comprehensive Physiology,* 2**,** 2369-2392.

TROLL, W. & WIESNER, R. 1985. The role of oxygen radicals as a possible mechanism of tumor promotion. *Annual Review of Pharmacology and toxicology,* 25**,** 509-528.

TSIEN, R. Y. 1998. The green fluorescent protein. *Annual Review of Biochemistry,* 67**,** 509-544.

TURATSINZE, J. V., THOMAS-CHOLLIER, M., DEFRANCE, M. & VAN HELDEN, J. 2008. Using RSAT to scan genome sequences for transcription factor binding sites and cis-regulatory modules. *Nature Protocols,* 3**,** 1578-1588.

UHLIROVA, M. & BOHMANN, D. 2006. JNK- and Fos-regulated Mmp1 expression cooperates with Ras to induce invasive tumors in Drosophila. *EMBO J,* 25**,** 5294-304.

VARTIAINEN, M. K., GUETTLER, S., LARIJANI, B. & TREISMAN, R. 2007. Nuclear actin regulates dynamic subcellular localization and activity of the SRF cofactor MAL. *Science,* 316**,** 1749-52.

VENKEN, K. J., POPODI, E., HOLTZMAN, S. L., SCHULZE, K. L., PARK, S., CARLSON, J. W., HOSKINS, R. A., BELLEN, H. J. & KAUFMAN, T. C. 2010. A molecularly defined duplication set for the X chromosome of Drosophila melanogaster. *Genetics,* 186**,** 1111-1125.

VERDONI, A. M., AOYAMA, N., IKEDA, A., IKEDA, S., VERDONI, A. M., AOYAMA, N., IKEDA, A. & IKEDA, S. 2008. Effect of destrin mutations on the gene expression profile in vivo. *Physiological Genomics,* 34**,** 9.

VIDAL, M. 2010. The dark side of fly TNF: an ancient developmental proof reading mechanism turned into tumor promoter. *Cell Cycle,* 9**,** 3851-3856.

VIEIRA, V., DE LA HOUSSAYE, G., LACASSAGNE, E., DUFIER, J., JAIS, J., BEERMANN, F., MENASCHE, M. & ABITBOL, M. 2008. Differential regulation of Dlg1, Scrib, and Lgl1 expression in a transgenic mouse model of ocular cancer.

WADA, K., ITOGA, K., OKANO, T., YONEMURA, S. & SASAKI, H. 2011. Hippo pathway regulation by cell morphology and stress fibers. *Development,* 138**,** 3907-14.

WANG, D.-S., SHAW, R., WINKELMANN, J. C. & SHAW, G. 1994. Binding of PH domains of β-adrenergic-receptor kinase and β-spectrin to WD40/β-transducin repeat containing regions of the β-subunit of trimeric G-proteins. *Biochemical and biophysical research communications,* 203**,** 29-35.

WANG, L., BALAS, B., CHRIST-ROBERTS, C. Y., KIM, R. Y., RAMOS, F. J., KIKANI, C. K., LI, C., DENG, C., REYNA, S. & MUSI, N. 2007. Peripheral disruption of the Grb10 gene enhances insulin signaling and sensitivity in vivo. *Molecular and cellular biology,* 27**,** 6497-6505.

WATANABE, N., BODIN, L., PANDEY, M., KRAUSE, M., COUGHLIN, S., BOUSSIOTIS, V. A., GINSBERG, M. H. & SHATTIL, S. J. 2008. Mechanisms and consequences of agonist-induced talin recruitment to platelet integrin αIIbβ3. *The Journal of cell biology,* 181**,** 1211-1222.

WELSH, S., WELSH, S., WELSH, S. & KAY, S. A. 1997. Reporter gene expression for monitoring gene transfer. *Current opinion in biotechnology,* 8**,** 617.

WENNERBERG, K., ROSSMAN, K. L. & DER, C. J. 2005. The Ras superfamily at a glance. *J Cell Sci,* 118**,** 843-846.

WICK, K. R., WERNER, E. D., LANGLAIS, P., RAMOS, F. J., DONG, L. Q., SHOELSON, S. E. & LIU, F. 2003. Grb10 inhibits insulin-stimulated insulin receptor substrate (IRS)-phosphatidylinositol 3-kinase/Akt signaling pathway by disrupting the association of IRS-1/IRS-2 with the insulin receptor. *Journal of Biological Chemistry,* 278**,** 8460-8467.

WOOD, K., WOOD, K. & WOOD, K. V. 1995. Marker proteins for gene expression. *Current opinion in biotechnology,* 6**,** 50.

WU, Y., ZHUANG, Y., HAN, M., XU, T. & DENG, K. 2009. Ras promotes cell survival by antagonizing both JNK and Hid signals in the Drosophila eye. *BMC Dev Biol,* 9**,** 53.

XU, T. & RUBIN, G. M. 1993. Analysis of genetic mosaics in developing and adult Drosophila tissues. *Development,* 117**,** 1223-1237.

XU, T., WANG, W., ZHANG, S., STEWART, R. A. & YU, W. 1995. Identifying tumor suppressors in genetic mosaics: the Drosophila lats gene encodes a putative protein kinase. *Development,* 121**,** 1053-1063.

YAMAGIWA, K. & ICHIKAWA, K. 1977. Experimental study of the pathogenesis of carcinoma. *CA: a cancer journal for clinicians,* 27**,** 174-181.

YANAGAWA, S.-I., LEE, J.-S. & ISHIMOTO, A. 1998. Identification and Characterization of a Novel Line ofDrosophila Schneider S2 Cells That Respond to Wingless Signaling. *Journal of Biological Chemistry,* 273**,** 32353-32359.

YAO, L., KAWAKAMI, Y. & KAWAKAMI, T. 1994. The pleckstrin homology domain of Bruton tyrosine kinase interacts with protein kinase C. *Proceedings of the National Academy of Sciences,* 91**,** 9175-9179.

ZHANG, S. X., GARCIA-GRAS, E., WYCUFF, D. R., MARRIOT, S. J., KADEER, N., YU, W., OLSON, E. N., GARRY, D. J., PARMACEK, M. S. & SCHWARTZ, R. J. 2005. Identification of Direct Serum-response Factor Gene Targets during Me2SO-induced P19 Cardiac Cell Differentiation. *Journal of Biological Chemistry,* 280**,** 19115-19126.

ZIV-AV, A., TALLER, D., ATTIA, M., XIANG, C., LEE, H. K., CAZACU, S., FINNISS, S., KAZIMIRSKY, G., SARID, R. & BRODIE, C. 2011. RTVP-1 expression is regulated by SRF downstream of protein kinase C and contributes to the effect of SRF on glioma cell migration. *Cell Signal,* 23**,** 1936-43.

ZSINDELY, N., PANKOTAI, T., UJFALUDI, Z., LAKATOS, D., KOMONYI, O., BODAI, L., TORA, L. & BOROS, I. M. 2009. The loss of histone H3 lysine 9 acetylation due to dSAGA-specific dAda2b mutation influences the expression of only a small subset of genes. *Nucleic Acids Res,* 37**,** 6665-80.